

THE UNIVERSITY OF SHEFFIELD



**Ursodeoxycholic Acid as a Putative Treatment for Parkinson's Disease:
In vitro study of the cytoprotective effect**

Mohammed Matoog Karami

Thesis submitted for the degree of Doctor of Philosophy
Faculty of Medicine, Dentistry and Health
Department of Neuroscience

Supervisors:

Prof. Oliver Bandmann

Dr. Heather Mortiboys

October 2018

Abstract

Parkinson's disease (PD) is an incurable neurodegenerative disease of the elderly. Although the precise molecular mechanism is unknown, accumulative evidence suggests the involvement of mitochondrial dysfunction. Accordingly, a previous drug screening study was carried out in our group with the aim of identifying compounds that rescue mitochondrial function in fibroblasts from PD patients with *parkin* mutation. Based on the findings in that study, ursodeoxycholic acid (UDCA) was presented as a putative novel treatment for PD. UDCA is an approved treatment for primary biliary cirrhosis. Therefore, its adoption should require less time and cost than de novo drugs.

The main aim of this project is to investigate the rescue effect of UDCA in the context of PD. Our group previously described increased activity in each of the individual respiratory chain enzymes following treatment with Ursocholic acid (UCA), a structurally similar compound. Therefore, we first hypothesised that the rescue effect of UCA/UDCA involves upregulation in mitochondrial biogenesis. However, upon following the treatment protocol used with *parkin* patient fibroblasts, we were unable to demonstrate an increase in the expression of mitochondrial proteins and mtDNA copy number.

Subsequently, we investigated the ability of UDCA to activate the Nrf2 pathway, which is one of the most important antioxidant pathways in cells and has been reported to mediate the action of UDCA in hepatobiliary-related research. In this project we used a specifically designed reporter cell line to assess Nrf2 activation. As a transcriptional factor, activated Nrf2 binds to a distinct sequence (named antioxidant response element (ARE)) in the promotor of its targeted genes, and drives their transcription. The used reporter cells contain several repeats of the ARE sequence linked to green fluorescent protein (GFP) motif. Thus, the measurement of green fluorescence should correlate with the transcription of the ARE sequences. We found that UDCA increased green fluorescence in a dose-dependent manner. However, this increase was not translated into a reduction in oxidative stress in copper-stressed cells. Moreover, UDCA treatment did not rescue these reporter cells when they were stressed with mitochondrial toxins.

The reporter cells are not ideal for investigating treatments for PD since they are non-human and non-neuronal in nature. Therefore, the human neuroblastoma-derived SH-SY5Y cell line was subsequently used. UDCA significantly reduced cytotoxicity and increased ATP levels in SH-SY5Y cells stressed with the mitochondrial uncoupler, carbonyl cyanide *m*-chlorophenyl hydrazine (CCCP). To investigate whether this rescue effect is mediated via the Nrf2 pathway, we quantified the expression of Nrf2 downstream genes via RT-qPCR; however, no positive results were obtained.

Subsequent experiments showed that the rescue effect was associated with significant activation of the AKT pathway (a cell survival pathway that has been reported to mediate the action of UDCA). Interestingly, the inhibition of AKT abolished the beneficial effect on ATP but not the cytotoxicity, indicating that the mechanism of action of UDCA is not entirely dependent on AKT. The effect of UDCA treatment on the phosphorylation of selected AKT downstream targets was investigated using western blotting and immunocytochemistry; however, no positive results were obtained. More work is needed to identify AKT/non-AKT downstream targets that are activated/inhibited upon UDCA treatment.

Acknowledgment

First and foremost, I would like to thank the one above all of us, the omnipresent God, for giving me the power and the strength to accomplish this work.

I would like to thank my supervisor Prof. Oliver Bandmann for the opportunity to undertake my PhD in his fantastic group and for all the guidance and expert-knowledge I have received over the last four years.

A special thanks to Dr. Phillippa Carling for mentoring me in the lab in the first years of my PhD. She greatly helped me developing my scientific thinking and was always there to help whenever I needed.

My sincere thanks also goes to Dr. Heather Mortiboys for supervising me for the rest of my PhD. Definitely, her role and support was beyond the role of the secondary supervisor. Her guidance helped me in all aspects of my study, in the context of research work, the lab work, and the writing of this thesis.

I am also thankful for all researchers in our group, Dr. Simeon Mihaylov and Dr. Lisa Trollope who had helped me in many occasions during my PhD.

I extend my thanks to everyone who assisted me during my PhD. In my daily work I have been blessed with a friendly and cheerful group of fellow students and SITran tutors who will never be forgotten.

Without doubt, I wouldn't survive through my PhD without my beloved wife, Fatimah Ajzaji, who supported me in my hardest moments and did tremendous effort to give me the best study environment at the expense of her time and comfort. Words cannot express how grateful I am, thank you very much Fatimah.

A special thanks to my parents for all of the sacrifices that they have made on my behalf. Their prayer for me was what sustained me this far. Any achievements in my life have only been possible through the continued love and support I've received from them.

My final thanks goes to King Abdul Aziz University and the Department of Human Physiology for the financial and the academic support, and to my god fathers in this field of science, Prof. Abdel Rahman Fahmy and Dr. Husam Awad.

Contents

1 Introduction.....	19
1.1 Parkinson’s disease	19
1.1.1 History, manifestations and pathology	19
1.1.2 Genetics of Parkinson’s disease	21
1.1.3 Risk factors for Parkinson’s disease	23
1.2 Mitochondria.....	27
1.2.1 Mitochondrial origin and history.....	27
1.2.2 Mitochondrial structure	28
1.2.3 Oxidative phosphorylation and energy production	29
1.2.4 Mitochondrial dynamics.....	31
1.3 Mechanisms of Parkinson’s disease	33
1.3.1 Lessons learned from Parkinson’s genetics.....	33
1.3.2 Mechanisms of environmental toxins.....	37
1.3.3 Role of ageing.....	37
1.3.4 Oxidative stress and neuronal vulnerability.....	38
1.3.5 Cell death in PD	41
1.3.6 The role of mitochondrial dysfunction in Parkinson’s disease.....	42
1.4 Cellular models of PD	45
1.4.1 General advantages and limitations of cellular models	45
1.4.2 Fibroblasts of PD patients	46
1.5 Drug discovery in Parkinson’s disease.....	49
1.6 Bile acids and UDCA	51
1.7 Aims and objectives.....	57
2 Materials and methods	59
2.1 List of materials and reagents used in this project	59
2.2 Cell lines.....	62
2.3 Tissue culture	63
2.3.1 Growing cells	63
2.3.2 Collecting and passaging the cells.....	64
2.3.3 Cryopreservation	64
2.3.4 Pelleting cells.....	64
2.3.5 Counting cells	65
2.3.6 Drugs and toxins.....	65
2.3.7 Differentiation of SH-SY5Y cells.....	65
2.4 Western blotting	66
2.4.1 Cell lysis	66

2.4.2 BSA assay	66
2.4.3 Gel electrophoresis and transfer.....	67
2.4.4 Probing and imaging.....	69
2.4.5 Quantitative analysis	71
2.5 Immunocytochemistry	72
2.5.1 Plating.....	72
2.5.2 Fixation	72
2.5.3 Antibody staining.....	72
2.5.4 Nuclear staining and imaging	74
2.6 Quantitative real-time PCR.....	74
2.6.1 DNA extraction	74
2.6.2 RNA extraction	75
2.6.1 Quality control.....	76
2.6.2 cDNA synthesis	76
2.6.3 qPCR reaction	77
2.7 ARE reporter assay	80
2.8 Oxidative stress assay.....	80
2.9 Cytotoxicity measurement	80
2.9.1 LDH assay.....	80
2.9.1 Trypan blue assay	82
2.10 ATP assay.....	83
2.11 Cellular fractionation.....	84
2.11.1 Mitochondrial isolation	84
2.11.2 Mitochondria purification	84
2.12 Statistical analysis.....	85
3 Investigating the effect of UDCA on mitochondrial biogenesis in patient fibroblasts.....	87
3.1 Introduction.....	87
3.1.1 Parkinson’s disease and mitochondrial biogenesis.....	87
3.1.2 Mechanism of mitochondrial biogenesis	87
3.1.3 Objectives	89
3.2 Experimental design	89
3.3 Quantifying the expression of mitochondrial respiratory complexes via western blotting in patient fibroblasts.....	90
3.4 Positive control testing.....	91
3.5 Assessing the effect of drug treatment on the expression of mitochondrial respiratory complexes in patient fibroblasts	95
3.6 Quantifying mtDNA via qPCR	96

3.7 Assessing the effect of drug treatment on mtDNA copy number in patient fibroblasts	98
3.8 Discussion	99
4 Investigating the beneficial effect of UCA and UDCA on oxidative stress, ATP and cytotoxicity in ARE reporter cell line	102
4.1 Introduction.....	102
4.1.1 Nrf2 pathway.....	102
4.1.2 Nrf2 structure	102
4.1.3 Regulation of Nrf2 activity.....	103
4.1.4 Nrf2 genes and the mechanism of action	106
4.1.5 Objectives	107
4.2 Investigating the effect of UCA and UDCA on the Nrf2 pathway in CHO cells.....	108
4.2.1 Assessing the effects of UCA/UDCA on ARE expression in CHO cells	108
4.2.2 Assessing the effect of the UCA/UDCA on the expression of Nrf2 genes in CHO cells	112
4.3 Assessing the ability of UCA and UDCA to ameliorate oxidative stress in CHO cells	119
4.3.1 Optimising DCF concentrations and assessing the effect of different stressors.....	119
4.3.2 Assessing the effect of UCA/UDCA on CuSO ₄ stressed CHO cells	121
4.3.3 Evaluating the effect of CuSO ₄ using a second stressing method (protocol B).....	122
4.3.4 Assessing the effect of UCA/UDCA on CuSO ₄ -stressed CHO cells (protocol B).....	123
4.3.5 Evaluating the effect of CuSO ₄ using a third stressing method (protocol C)	124
4.3.6 Assessing the effect of UCA/UDCA on CuSO ₄ -stressed CHO cells (protocol C).....	125
4.4 Investigating the ability of UCA/UDCA to rescue mitochondrial function in stressed CHO cells...	126
4.4.1 Optimisation experiments for rotenone treatment.....	126
4.4.2 Assessing the effect of UCA/UDCA on rotenone-stressed CHO cells.....	130
4.4.3 Optimisation experiments for CCCP treatment	133
4.4.4 Assessing the effect of UCA/UDCA on CCCP-stressed CHO cells.....	135
4.5 Discussion	137
5 Investigating the beneficial effect of UDCA on ATP levels and cytotoxicity in SH-SY5Y cells	143
5.1 Introduction.....	143
5.1.1 SH-SY5Y Origin.....	143
5.1.2 SH-SY5Y characteristics	143
5.1.3 SH-SY5Y differentiation	143
5.1.4 Objectives	145
5.2 Assessing the ability of UCA/UDCA to rescue mitochondrial function in stressed undifferentiated SH-SY5Y cells.....	146
5.2.1 Optimisation of culture medium and rotenone concentration	146
5.2.2 Assessing the effect of UCA and UDCA in rotenone-stressed SH-SY5Y cells.....	147
5.2.3 Assessing the effect of UCA and UDCA in CCCP-stressed SH-SY5Y cells	148

5.3 Assessing the ability of UDCA to rescue mitochondrial function in stressed differentiated SH-SY5Y cells.....	150
5.3.1 Characterisation of differentiated SH-SY5Y.....	150
5.3.2 Optimising CCCP concentration	155
5.3.3 Assessing the effect of UDCA in CCCP-stressed differentiated SH-SY5Y.....	161
5.4 Evaluating the effect of UDCA on the expression of Nrf2 genes in stressed undifferentiated SH-SY5Y cells.....	164
5.4.1 Initial testing of the primers.....	164
5.4.2 Assessing the effect of UDCA and BG12 on the expression of Nrf2 downstream genes in undifferentiated SH-SY5Y cells	170
5.5 Discussion.....	171
6 Investigating the effect of UDCA on the AKT pathway	177
6.1 Introduction to the AKT pathway.....	177
6.1.1 Background.....	177
6.1.2 Activation and regulation of the AKT pathway	177
6.1.3 AKT downstream	180
6.1.4 Objectives	182
6.2 Determining the ability of UCA and UDCA to activate AKT in CHO cells.....	183
6.2.1 Testing AKT antibodies and IGF as a positive control in CHO cells	183
6.2.2 Assessing the effect of UCA and UDCA on AKT activation in CHO cells	185
6.3 Determining the ability of UDCA to activate AKT in SH-SY5Y cells.....	186
6.3.1 Optimisation experiments.....	186
6.3.2 Drug treatment experiments	189
6.4 Investigating the role of AKT activation in the UDCA-mediated rescue effect in SH-SY5Y cells....	191
6.5 Investigating AKT translocation into the mitochondria in UDCA-treated SH-SY5Y cells.....	194
6.5.1 Cellular fractionation.....	194
6.5.2 The effect of UDCA on AKT translocation into the mitochondria in SH-SY5Y cells	196
6.6 Investigating the effect of UDCA on AKT downstream targets in SH-SY5Y cells.....	200
6.6.1 Assessing the effect of UDCA on CREB phosphorylation	200
6.6.2 Assessing the effect of UDCA on mTOR phosphorylation.....	203
6.6.3 Assessing the effect of UDCA on FOXO1 phosphorylation.....	206
6.6.4 Assessing the effect of UDCA on the mitochondrial hexokinase level.....	209
6.7 Discussion.....	214
7 Discussion	220
7.1 Mitochondrial biogenesis in <i>parkin</i> patients' fibroblasts.....	220
7.2 Activation of the Nrf2 pathway in ARE reporter cell lines	221
7.3 Beneficial effects in stressed SH-SY5Y cells.....	223
7.4 Mechanism of action of UDCA in SH-SY5Y cells	224

7.5 UDCA doses	226
7.6 Future work	227
7.6.1 Alternative AKT downstream targets	227
7.6.2 Glucocorticoid receptors	228
7.6.3 Mitophagy pathway	228
7.7 Concluding remarks.....	229

List of figures

Figure 1.1 The relationship between the manifestations of PD and the loss of dopaminergic neurons. .	21
Figure 1.2 An overview of mitochondrial structure and respiratory chain complexes.....	31
Figure 1.3 A summary of the proposed mechanisms for neuronal degeneration in PD.....	44
Figure 1.4 Some of the identified drugs in the Bandmann group screening project.....	50
Figure 1.5 An overview of the bile acid pathway in humans.	56
Figure 1.6 A comparison between bile acids in term of hydrophilicity.....	57
Figure 2.1 BSA assay for quantification of protein concentration.	67
Figure 2.2 The principle of the CytoTox Cytotoxicity Assay.	82
Figure 2.3 The principle of the ATP Detection Assay System.....	83
Figure 2.4 Purification of mitochondria by sucrose step density gradient centrifugation.	85
Figure 3.1 Total OXPHOS Human Antibody Cocktail proved to be efficient in detecting its target proteins in each mitochondrial respiratory complex.	90
Figure 3.2 Resveratrol increased the expression of proteins from three mitochondrial respiratory complexes in a pilot test.	93
Figure 3.3 The positive effect of resveratrol on the expression of mitochondrial proteins was not reproducible despite the trial of higher doses.	94
Figure 3.4 Neither UCA nor UDCA treatment altered the expression of mitochondrial respiratory proteins in control and patient fibroblasts.....	95
Figure 3.5 <i>B2M</i> and <i>ND1</i> primers have high efficiency and specificity in qPCR reactions.....	97
Figure 3.6 Neither UCA nor UDCA treatment altered mtDNA copy number in control and patient fibroblasts.....	98
Figure 4.1 Overview of the structure and the regulation of Nrf2.	105
Figure 4.2 BG12 significantly increased ARE expression in CHO reporter cells.	108
Figure 4.3 BG12 and RTA408 induced a dose dependant increase in ARE expression in CHO reporter cells.	109
Figure 4.4 UCA and UDCA induced a dose dependant increase in ARE expression at different time points.	110
Figure 4.5 24 hours of treatment with increasing concentrations of UCA, UDCA, TUDCA and GUDCA induced a small increase in ARE expression.....	111
Figure 4.6 <i>GAPDH</i> primers have high efficiency and specificity in qPCR reactions.....	113
Figure 4.7 <i>NQO1</i> primers have high efficiency and specificity in qPCR reactions.....	114
Figure 4.8 <i>FTH1</i> primers have sub-optimal efficiency and high specificity in qPCR reactions.....	115
Figure 4.9 <i>GCLC</i> primers have high efficiency and specificity in qPCR reactions.	116
Figure 4.10 <i>HMOX1</i> primers have low efficiency and specificity in qPCR reactions.	117
Figure 4.11 UCA and UDCA exert variable effect on the expression of Nrf2 downstream genes.	118
Figure 4.12 DCF readings are significantly increased in CuSO ₄ stressed CHO cells.....	120
Figure 4.13 Initial experiments showed that UCA and UDCA do not decrease DCF readings in CuSO ₄ -stressed cells.	121
Figure 4.14 Testing a second stressing method (protocol B) demonstrated an increase in DCF reading with 24h recovery time.	122
Figure 4.15 UCA and UDCA had no positive effect in CuSO ₄ -stressed cells (protocol B).....	123
Figure 4.16 Testing a third stressing method (protocol C) demonstrated clear dose-dependent increase in DCF reading.	124
Figure 4.17 UCA and UDCA had no positive effect in CuSO ₄ -stressed cells (protocol C).....	125
Figure 4.18 Rotenone and antimycinA did not show a dose-dependant effect on LDH and ATP readings in regular culture medium.....	126
Figure 4.19 The sensitivity toward rotenone was significantly increased in galactose and 2-Deoxy-D-Glucose medium.....	127

Figure 4.20 Low rotenone doses had massive effects on LDH and ATP readings when the cells were culture in galactose medium.	128
Figure 4.21 Assessing the effect of extra low rotenone doses on LDH and ATP readings at different time points in galactose medium.	129
Figure 4.22 Multiple concentrations of UCA and UDCA did not induce a positive effect in unstressed and rotenone-stressed CHO cells (24h rotenone).....	130
Figure 4.23 Multiple concentrations of UCA and UDCA did not induce a positive effect in unstressed and rotenone-stressed CHO cells (48h rotenone).....	131
Figure 4.24 pre-treatment with UCA and UDCA did not induce a positive effect in unstressed and rotenone-stressed CHO cells.	132
Figure 4.25 CCCP did not show a dose-dependant effect on LDH and ATP readings in regular culture medium.	133
Figure 4.26 Wide range of CCCP concentrations induced a clear dose-dependant effect on LDH and ATP readings in galactose medium.....	134
Figure 4.27 UCA and UDCA did not induce a positive effect in unstressed and CCCP-stressed CHO cells (48h CCCP).	135
Figure 4.28 Pre-treatment with UCA and UDCA did not induce a positive effect in unstressed and CCCP-stressed CHO cells.	136
Figure 4.29 An overview of the reactive oxygen species.	141
Figure 5.1 Rotenone induced a dose-dependant effect on cytotoxicity and ATP readings in galactose culture mediums.	146
Figure 5.2 UCA and UDCA did not induce a positive effect in unstressed and rotenone-stressed SH-SY5Y.	147
Figure 5.3 UDCA induced a small non-significant positive effect in CCCP-stressed SH-SY5Y.	148
Figure 5.4 A UDCA dose of 300 μ M induced a significant positive effect on ATP and LDH levels in CCCP-stressed SH-SY5Y.	149
Figure 5.5 Differentiating SH-SY5Y cells have lower growth rate and higher cell death rate in comparison to the undifferentiated cells.....	151
Figure 5.6 Differentiated SH-SY5Y cells exhibited remarkable change in their morphology.....	152
Figure 5.7 The expression of the neuronal marker MAP2 is significantly higher in differentiated SH-SY5Y cells.....	153
Figure 5.8 The expression of the dopaminergic markers is significantly higher in differentiated SH-SY5Y cells.....	154
Figure 5.9 A pilot experiment to optimise CCCP concentration demonstrated high basal toxicity readings in unstressed differentiated SH-SY5Y.....	155
Figure 5.10 Cleaved caspase 3 staining is an efficient approach to assess cytotoxicity in differentiated SH-SY5Y.	156
Figure 5.11 Image analysis software can detect and exclude dead cells co-stained with Hoechst and caspase-3.....	157
Figure 5.12 Multiple CCCP concentrations induced a dose-dependent effect on several parameters of caspase-3 spots analysis (1/2).....	159
Figure 5.13 Multiple CCCP concentrations induced a dose-dependent effect on several parameters of caspase-3 spots analysis (2/2).....	160
Figure 5.14 Assessing the effect of multiple CCCP doses on ATP readings demonstrated comparable responses with 5 μ M and 10 μ M.....	161
Figure 5.15 Multiple doses of UDCA did not induce a positive effect on cleaved caspase 3 staining in CCCP-stressed differentiated SH-SY5Y cells (1/2).....	162
Figure 5.16 Multiple doses of UDCA did not induce a positive effect on cleaved caspase 3 staining in CCCP-stressed differentiated SH-SY5Y cells (2/2).....	163

Figure 5.17 Multiple doses of UDCA did not induce a significant positive effect on ATP levels in CCCP-stressed differentiated SH-SY5Y cells.	164
Figure 5.18 <i>GAPDH</i> primers have high efficiency and specificity in qPCR reactions.	165
Figure 5.19 <i>GST2A</i> primers have high efficiency and specificity in qPCR reactions.	166
Figure 5.20 <i>GCLC</i> primers have high efficiency and specificity in qPCR reactions.	167
Figure 5.21 <i>FTH1</i> primers have high efficiency and specificity in qPCR reactions.	168
Figure 5.22 HMOX1 and NQO1 primers showed secondary peaks in melt peak graphs in qPCR reactions.	169
Figure 5.23 UDCA treatment induced variable effects on the expression of Nrf2 downstream genes in undifferentiated SH-SY5Y cells.	170
Figure 6.1 Overview of the structure and activation of AKT.	179
Figure 6.2 pilot test of AKT antibodies and IGF as a positive control in CHO cells.	184
Figure 6.3 UCA and UDCA treatments did not induce significant effects on AKT phosphorylation in unstressed CHO cells.	185
Figure 6.4 The addition of serum to the culture medium has no effect on IGF-mediated AKT activation.	187
Figure 6.5 The AKT antibodies are usable in western blotting experiments.	188
Figure 6.6 300 μ M UDCA significantly increased AKT phosphorylation in CCCP-stressed SH-SY5Y cells (western blot images).	189
Figure 6.7 300 μ M UDCA significantly increased AKT phosphorylation in CCCP-stressed SH-SY5Y cells (data analysis).	190
Figure 6.8 Triciribine treatment inhibited AKT phosphorylation in UDCA/IGF treated cells.	192
Figure 6.9 AKT inhibition abolished the UDCA-mediated rescue effect on ATP level in CCCP-stressed SH-SY5Y cells.	193
Figure 6.10 The fractionation protocol proved to be efficient in producing mitochondrial enriched extracts.	195
Figure 6.11 Fractionation of treated SH-SY5Y cells (unstressed).	196
Figure 6.12 Fractionation of treated SH-SY5Y cells (CCCP-stressed).	197
Figure 6.13 UDCA treatment did not induce a significant change in the expression of AKT in the mitochondrial fraction of SH-SY5Y cells.	198
Figure 6.14 UDCA treatment did not induce a significant change in the expression of AKT in the cytoplasmic fraction of SH-SY5Y cells.	199
Figure 6.15 UDCA treatment had no significant effect on CREB phosphorylation in CCCP-stressed SH-SY5Y cells (via western blotting).	201
Figure 6.16 Immunocytochemistry images of UDCA-treated SH-SY5Y cells probed with phosphorylated and total CREB antibodies.	202
Figure 6.17 UDCA treatment had no significant effect on CREB phosphorylation in CCCP-stressed SH-SY5Y cells (via immunocytochemistry).	203
Figure 6.18 UDCA treatment had no significant effect on mTOR phosphorylation in CCCP-stressed SH-SY5Y cells (via western blotting).	204
Figure 6.19 Immunocytochemistry images of UDCA-treated SH-SY5Y cells probed with phosphorylated and total mTOR antibodies.	205
Figure 6.20 UDCA treatment had no significant effect on mTOR phosphorylation in CCCP-stressed SH-SY5Y cells (via immunocytochemistry).	206
Figure 6.21 UDCA treatment had no significant effect on FOXO1 phosphorylation in CCCP-stressed SH-SY5Y cells (via western blotting)	207
Figure 6.22 Total FOXO1 antibody is not effective in immunocytochemistry experiments.	208
Figure 6.23 Assessing the effect of UDCA on mitochondrial hexokinase content in CCCP-stressed SH-SY5Y cells by western blotting.	209

Figure 6.24 UDCA treatment did not induce a significant change in the expression of hexokinase in the mitochondrial fraction of SH-SY5Y cells.	210
Figure 6.25 Immunocytochemistry images of UDCA-treated SH-SY5Y cells probed with hexokinase and Tom20 antibodies.....	212
Figure 6.26 UDCA treatment had no significant effect on mitochondrial hexokinase content in CCCP-stressed SH-SY5Y cells (via immunocytochemistry)	213
Figure 7.1 A summary of the main research questions and the main findings in this projects.....	230

List of tables

Table 1.1 The loci of familial PD.	23
Table 1.2 Risk loci identified in a large-scale meta-analysis of genome-wide association data.	25
Table 2.1 Information on patient and control fibroblasts	62
Table 2.2 Contents of the prepared cultured medium for different types of cells	63
Table 2.3 Components of stacking and resolving gel	69
Table 2.4 Buffers used in Western blotting (all made in H ₂ O)	69
Table 2.5 Antibodies used in western blotting	70
Table 2.6 Antibodies used in immunocytochemistry	73
Table 2.7 Primers used in q-PCR.	79
Table 3.1 Resveratrol doses in human fibroblasts.	92
Table 4.1 Examples of Nrf2 target genes	106

List of abbreviations

6-OHDA	6-hydroxydopamine
ADP	Adenosine diphosphate
AKT	Protein kinase B
AMPK	AMP-activated protein kinase
AP1	Activator protein 1
APAF-1	Apoptotic protease activating factor 1
ARE	Antioxidant response element
ARJP	Autosomal recessive juvenile parkinsonism
ATP	Adenosine triphosphate
B2M	Beta-2-microglobulin
BAAT	Bile acid coenzyme-A: amino acid N-acyltransferase
BAD	Bcl-2-associated death promoter
BAG-1	BAG family molecular chaperone regulator 1
BAK	Bcl-2 homologous antagonist-killer protein
BA	Bile acids
BAX	BCL2-associated X protein
BBB	Blood brain barrier
BCL-2	B-cell lymphoma 2
BCL-XL	B-cell lymphoma-extra large
BDNF	Brain-derived neurotrophic factor
BG12	Dimethyl fumarate
BID	BH3 interacting-domain death agonist
BIM	Bcl-2-like protein 11
BMP2	Recombinant bone morphogenetic protein 2
BSA	Bovine serum albumin
CA	Cholic acid
CaMKII	Ca ²⁺ /calmodulin-dependent protein kinase
cAMP	Cyclic adenosine monophosphate
CBP	CREB-binding protein
CCCP	Carbonyl cyanide m-chlorophenyl hydrazone
CDCA	Chenodeoxycholic acid
CHO	Chinese hamster ovary
Chr	Chromosome
Cnc	Cap 'n' Collar
Cnc-bZIP	Cnc-basic leucine zipper
CNS	Central nervous system

CREB	cAMP response element binding
CSF	Cerebrospinal fluid
DA	Dopaminergic
DAT	Dopamine transporter
DAQ	DA-quinone
dbcAMP	Dibutyryl cyclic adenosine monophosphate
DCA	Deoxycholic acid
DCF	6-carboxy-2',7'-dichlorodihydrofluorescein
DMEM	Dulbecco's Modified Eagle Medium
DMSO	Dimethyl sulfoxide
DOPAL	3,4-dihydroxyphenylacetaldehyde
Drp1	Dynammin-related Protein 1
DTT	Dithiothreitol
DUA	Dehydro (11,12) ursolic acid lactone
EDTA	Ethylenediaminetetraacetic acid
Erk2	Mitogen-activated protein kinase 1
FBS	Foetal bovine serum
Fis1	Mitochondrial fission 1 protein
FMN	Flavin mononucleotide
FOXO	Forkhead box O
FTH1	Ferritin Heavy Chain 1
G6P	Glucose-6-phosphate
GAPDH	Glyceraldehyde-3-Phosphate Dehydrogenase
GBA	Glucocerebrosidase
GCLC	Glutamate-Cysteine Ligase Catalytic Subunit
GDF5	Growth/differentiation factor 5
GDNF	Glial cell line-derived neurotrophic factor
GFP	Green fluorescent protein
GRs	Glucocorticoid receptors
GSH	Glutathione
GSK3 β	Glycogen synthase kinase 3 beta
GST	Glutathione S-transferase
GTP	Guanosine Triphosphate
GWASs	Genome wide association studies
HEPES	4-(2-hydroxyethyl)-1-piperazineethanesulfonic acid
HES	Hospital Episode Statistics
HMOX1	Heme Oxygenase 1

HRP	Horseradish peroxidase
HtrA2	High temperature requirement protein A2
IB	Mitochondrial isolation buffer
ICC	Immunocytochemistry
IL-6	Interleukin-6
ILK	Integrin-linked kinase
iNPCs	neuronal progenitor cells
iNs	Induced neurosn
INT	Iodonitrotetrazolium violet
iPSCs	Human induced pluripotent stem cells
JNK	C-Jun N-terminal kinase
K/O	knockout
Keap1	Kelch-like ECH-associated protein 1
KID	Kinase-inducible domain
KIX	KID-interacting domain
LBs	Lewy bodies
LC3	Microtubule-associated protein 1A/1B-light chain 3
LCA	Lithocholic acid
LDH	Lactate dehydrogenase enzyme
L-DOPA	L-tyrosine into L-3,4-dihydroxyphenylalanine
LRRK2	Leucine-rich repeat kinase 2
MAP2	Microtubule-associated protein 2
MAPK	Mitogen-activated protein kinase
MCL-1	Induced myeloid leukaemia cell differentiation
MDM2	Mouse double minute 2 homolog
MEFs	Mouse embryonic fibroblasts
Mff	Mitochondrial fission factor
Mfn1,2	Mitofusin 1,2
MiD49, 51	Mitochondrial dynamics proteins 49, 51
MPP+	1-methyl-4-phenylpyridinium
MPTP	1-methyl-4-phenyl-1,2,3,6-tetrahydropyridine
MTA	Material Transfer Agreement
mtDNA	Mitochondrial DNA
mTORC2	Mechanistic target of rapamycin (mTOR) complex 2
mtSSB	Mitochondrial single-stranded DNA-binding protein
NADH/NAD+	Nicotinamide adenine dinucleotide
ND1	NADH dehydrogenase subunit 1

Neh	Nrf2-ECH homology
NQO1	NAD(P)H:quinone oxidoreductase
Nrf2	Nuclear factor erythroid 2-like 2 or [NFE2L2]
Ns	Not Statistically Significant
NSAIDs	Non-steroidal anti-inflammatory drugs
OPA1	Optic Atrophy 1
OR	Odds ratio
OXPPOS	Oxidative phosphorylation
PARIS	Parkin interacting substrate
PBS	Phosphate-buffered saline
PD	Parkinson's disease
PDK1	Pyruvate dehydrogenase kinase
PFA	Paraformaldehyde
PGC-1 α	Peroxisome proliferator-activated receptor gamma coactivator 1-alpha
PH	Pleckstrin homology
PHLPPs	PH-domain leucine-rich repeat protein phosphatases
PKC	Protein kinase C
PI3	Phosphoinositide 3
PI3K	Phosphoinositide 3-kinase
PIP2	Phosphatidylinositol 4,5-bisphosphate
PIP3	Phosphatidylinositol 3,4,5 trisphosphate
POLRMT	Mitochondrial RNA polymerase
POLG	DNA polymerase subunit gamma-1
PP2A	Protein phosphatase 2A
PTEN	Phosphatase and tensin homologue
PTM	Post-translational modification
PUMA	P53 upregulated modulator of apoptosis
PVDF	Polyvinylidene fluoride
RA	Retinoic acid
RARE	Retinoic acid response element
RHEB	Ras homolog enriched in the brain
ROS	Reactive oxygen species
S6K1	S6 kinase beta-1
SD	Standard deviation
SDS	Sodium dodecyl sulfate
SHIP	Src homology domain 2 (SH2)-containing inositol phosphatase
SMAC	Second mitochondria-derived activator of caspases

SNpc	Substantia nigra pars compacta
SNPs	Single-nucleotide polymorphisms
SOD2	Superoxide dismutase 2
STH	Sheffield Teaching Hospitals
TBST	Tris-buffered saline with Tween 20
TFAM	Mitochondrial transcription factor A
TFB2M	Mitochondrial transcription Factor B2
TGR5	G-protein coupled receptor
TH	Tyrosine hydroxylase
TOM	Translocase of the outer membrane
TPA	12-O-tetradecanoylphorbol-13-acetate
TSC 1, 2	Tuberous sclerosis complexes 1, 2
TUDCA	Tauroursodeoxycholic acid
TuJ1	Neuron-specific class III β -tubulin
UA	Ursolic acid
UCA	Ursocholic acid
UCP1, 2	Uncoupling protein 1, 2
UDCA	Ursodeoxycholic acid
VDAC	Voltage-dependent anion channel
VMAT2	Vesicular monoamine transporter 2
WB	Western blotting

Chapter 1. Introduction

1 Introduction

1.1 Parkinson's disease

Parkinson's disease (PD) is one of the most common neurodegenerative diseases. It has an estimated prevalence of 0.1 to 0.2% in the entire population and affects about 1% of people older than 60 years (Tysnes and Storstein, 2017, Pringsheim et al., 2014).

PD is a chronic progressive motor disease that influences patients' lives significantly. Treatment of PD in the United Kingdom (UK) has an estimated cost of more than £15,000 per patient, per year (Bovolenta et al., 2017). According to a cross-sectional analysis of British hospitals, the total number of PD admissions in the UK was more than 180,000 between 2009 and 2013 (Low et al., 2015). In this study, the Hospital Episode Statistics (HES) database was used to investigate the burden of hospitalisation of PD, in comparison to other admissions (Low et al., 2015). It was found that PD patients have a 1.5 to 2.6 greater chance of suffering serious conditions, such as pneumonia, urinary tract infection and hip fracture (Low et al., 2015). A meta-analysis report, which included more than 80 studies, found an approximate 5% annual decrease in survival rate and a crude mortality ratio of around 1.5 in comparison to healthy controls (Macleod et al., 2014).

1.1.1 History, manifestations and pathology

The history of PD extends back to 1817, when English physician James Parkinson described and grouped the features of the disease as one neurological syndrome. Based on observations of only six cases, he specified all major cardinal manifestations, including bradykinesia (slowness of movement), rest tremor (occurs involuntarily when the muscle is relaxed), rigidity and gait disturbance (walking with steps of little acceleration) (Duvoisin, 1987).

The diagnosis of PD requires detailed patient history and full physical examination. Even when a patient has the primary motor signs, the physician still needs to exclude alternative diagnoses, and might start a trial treatment to assess the response of the patient before giving a definite diagnosis (Poewe et al., 2017). In addition to motor signs, there are various non-motor manifestations that might appear before or after the classical motor features (Pont-Sunyer et al., 2015). Since PD treatment only alleviates motor symptoms, non-motor symptoms can become a major problem for patients (Schapira et al., 2017). These include sensory malfunctions, such as

pain, hyposmia and visual disturbances, or neuropsychiatric features, such as sleep disorders, anxiety, depression, cognitive deficits and dementia (Schapira et al., 2017). PD patients might also have bladder and gastrointestinal dysfunctions.

Motor manifestations of PD are predominantly attributed to the degeneration of dopaminergic (DA) neurons in the substantia nigra pars compacta (SNpc) in the basal ganglia. The degeneration re-shapes the circuitry of the basal ganglia and consequently alters their projection activity and overall functionality (Wichmann et al., 2011). The basal ganglia's primary function is to control motor signals. Nonetheless, the basal ganglia are also connected to various specific areas in the brain, such as orbitofrontal, limbic and association areas, via their projection loops (Ikemoto et al., 2015). This explains, at least in part, the non-motor manifestations in PD (Shulman et al., 2011). Pathological studies have found that a significant portion of DA neurons are already degenerated at the early stages of PD, suggesting that the degeneration and the pathological process may start years before clinical recognition of the disease (Dijkstra et al., 2014) [Figure 1.1].

Another characteristic pathological feature in PD is the presence of intra-cytoplasmic eosinophilic inclusions, called Lewy bodies (LBs) (Poewe et al., 2017). LBs are protein aggregates that are mainly composed of α -synuclein protein (Baba et al., 1998). They are often found in various areas in the central and peripheral nervous system. Non-basal LBs have been linked to the non-motor features of PD and to the symptoms that precede the clinical recognition of PD (Halliday et al., 2011).

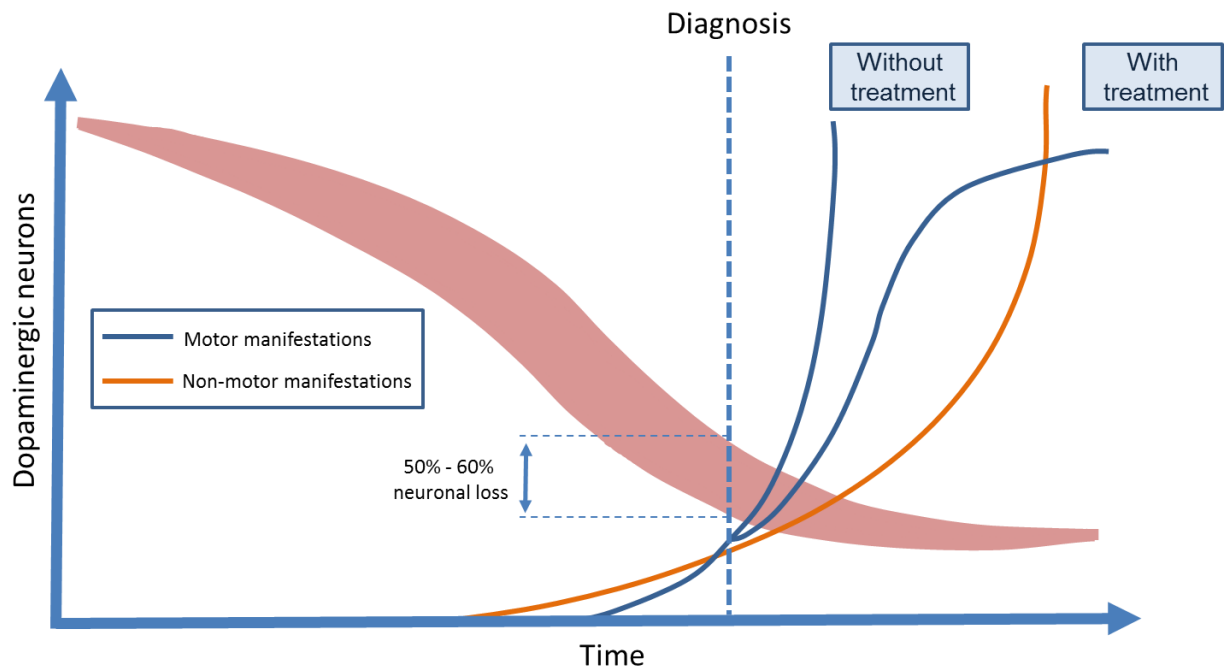


Figure 1.1 The relationship between the manifestations of PD and the loss of dopaminergic neurons.

By the time clinical manifestations appear, significant DA neuronal loss has already occurred. Dopamine replacement therapy only alleviates motor manifestations, but does not modulate the rate of degeneration. Re-produced with permission from Schapira (2017).

1.1.2 Genetics of Parkinson's disease

PD can be classified into familial and sporadic. There are currently 21 chromosomal loci (PARK loci) that segregate with the familial form of the disease. Yet, the causative genes and mutations in some of these loci still await confirmation (Kumaran and Cookson, 2015). Monogenic PD, which is caused by a single mutation in a dominantly or recessively inherited gene, accounts only for 5 to 10% of all cases (Poewe et al., 2017). PD loci, as well as their inheritance pattern and associated form of the disease, are listed in Table 1.1.

The first identified mutation in PD gene was the α -synuclein gene *SNCA* in 1987 (Polymeropoulos et al., 1997). The identified missense mutation, Ala53Thr, in this gene, was associated with a relatively high progression autosomal dominant early onset PD (Polymeropoulos et al., 1997). To date, only five more mutations have been discovered: Ala30Pro, Glu46Lys, Gly51Asp, His50Gln and Ala53Glu. The pathogenicity of His50Gln has been disputed (Blauwendraat et al., 2018). In addition to point mutations, α -synuclein duplication/triplication has also been linked to familial PD (Chartier-Harlin et al., 2004, Singleton et al., 2003). In these conditions, the amount of α -synuclein

has been found to positively correlate with the severity of the disease, and to negatively correlate with the age of onset. Despite these interesting findings, α -synuclein mutations are rare and account only for 1 to 2% of all cases of autosomal dominant PD (Kalinderi et al., 2016).

Leucine-rich repeat kinase 2 (*LRRK2*) mutations are more common than α -synuclein mutations and represent 10% of all familial PD cases (Kalinderi et al., 2016). Dozens of *LRRK2* mutations have been identified. However, only seven of these have a high degree of association with PD. The most common is Gly2019Ser, followed by Arg1441His, Arg1441Gly, Arg1441Cys, Y1699Cys, Ile2020Thr and Asn1437His (Abdullah et al., 2015). The prevalence of the Gly2019Ser mutation in PD patients vary across populations. The highest percentage is found in northern African Arab populations (37 to 41% of both familial and sporadic PD) (Lesage et al., 2006), followed by Ashkenazi Jewish populations (10 to 20% of both familial and sporadic PD) (Ozelius et al., 2006). The penetrance of this mutation increases with age, as the risk increases from around 30% at age 60 up to 74% at age 80 (Healy et al., 2008). While clinically indistinguishable from sporadic PD, pathological examination showed tauopathy and neurofibrillary tangles, as well as LB (Kalinderi et al., 2016).

The *parkin* gene was identified one year after the discovery of an α -synuclein mutation in a family with autosomal recessive juvenile parkinsonism (ARJP) (Kitada et al., 1998). Generally, this class of PD has some atypical signs, such as psychiatric manifestations and dystonia, but the major feature is the early age of onset (Kalinderi et al., 2016). *Parkin* mutations are the most common cause for ARJP, with a prevalence of approximately 50% in PD patients aged under 25 (Kalinderi et al., 2016). Dozens of *parkin* mutations have been identified. Notably, LB pathology was not found in all *parkin* cases (Kalinderi et al., 2016). However, a significant generalised degeneration of DA neurons in the SN was present in all examined cases (Kalinderi et al., 2016).

Table 1.1 The loci of familial PD.

Loci	Gene	Inheritance	Phenotype	Reference
PARK1	<i>SNCA</i>	AD	Early onset	(Polymeropoulos et al., 1997)
PARK2	<i>parkin</i>	AR	Early onset	(Kitada et al., 1998)
PARK3	Unknown	AD	Classical	(Gasser et al., 1998)
PARK4	<i>SNCA</i>	AD	Early onset	(Singleton et al., 2003)
PARK5	<i>UCHL1</i>	AD	Classical	(Leroy et al., 1998)
PARK6	<i>PINK1</i>	AR	Early onset	(Valente et al., 2004)
PARK7	<i>DJ-1</i>	AR	Early onset	(Bonifati et al., 2003)
PARK8	<i>LRRK2</i>	AD	Classical	(Paisán-Ruiz et al., 2004)
PARK9	<i>ATP13A2</i>	AR	Atypical PD	(Ramirez et al., 2006)
PARK10	Unknown	Risk factor	Classical	(Hicks et al., 2002)
PARK11	Unknown	AD	Late onset	(Pankratz et al., 2003b)
PARK12	Unknown	Risk factor	Classical	(Pankratz et al., 2003a)
PARK13	<i>HTRA2</i>	AD / Risk factor	Classical	(Strauss et al., 2005)
PARK14	<i>PLA2G6</i>	AR	Early onset	(Paisan - Ruiz et al., 2009)
PARK15	<i>FBX07</i>	AR	Early onset	(Di Fonzo et al., 2009)
PARK16	Unknown	Risk factor	Classical	(Satake et al., 2009)
PARK17	<i>VPS35</i>	AD	Classical	(Zimprich et al., 2011)
PARK18	<i>EIF4G1</i>	AD	Classical	(Chartier-Harlin et al., 2011)
PARK19	<i>DNAJC6</i>	AR	Juvenile atypical PD	(Edvardson et al., 2012)
PARK20	<i>SYNJ1</i>	AR	Juvenile atypical PD	(Krebs et al., 2013)
PARK21	<i>DNAJC13</i>	AD	Late onset	(Vilariño-Güell et al., 2013)

A list of PD loci showing the affected genes (if identified), the mode of inheritance and the associated phenotype. The term PARKs is used to denote chromosomal loci that have been associated with PD and they are numbered in chronological order. (AD): autosomal dominant, (AR): autosomal recessive.

1.1.3 Risk factors for Parkinson's disease

While the majority of PD cases are sporadic, with no definitive cause, epidemiological investigations have shown that there are environmental, behavioural and genetic factors that increase or, occasionally, decrease the risk of the disease. It is important to point out that in comparison to these factors, ageing is still the most important risk factor. However, studying these risk factors has significantly enhanced our understanding of PD.

Environmental risk factors

The discovery of 1-methyl-4-phenyl-1,2,3,6-tetrahydropyridine (MPTP) - induced Parkinsonism in drug abusers led to the assumption that environmental toxins may contribute to the aetiology of PD (Langston et al., 1983). There are numerous epidemiological studies investigating the link between environmental or industrial toxins and PD, driven by the fact that MPTP is structurally similar to pesticides. Additionally, researchers have investigated the effect of metals such as iron,

zinc, lead and copper. While many studies showed controversy with regard to metal exposure and the risk of PD (Goldman, 2014), the results were more consistent with regard to pesticide exposure. A worldwide meta-analysis of more than 40 studies showed an increased risk ratio of about 1.6 (95% confidence interval: 1.4 to 1.9) for those who have been exposed to pesticides (Mark et al., 2012). A large case control study that involved 767 patients with PD around Europe concluded that pesticide exposure was statistically associated with PD (attributable risk: 8.1%, odds ratio: 3.22, p-value: 0.002, confidence interval: 1.56 to 6.65) (Gorell et al., 2004). The same study found that exposure to metals (copper, iron, lead and manganese) did not increase the risk of PD. In a longitudinal agricultural health study that lasted for 10 years, the risk of PD was positively correlated with the number of days of pesticide exposure (Ascherio and Schwarzschild, 2016). The association was higher with pesticides that compromise mitochondria, such as rotenone and paraquat (Ascherio and Schwarzschild, 2016). Since pesticides are widely used in agriculture, it is not surprising that many studies have suggested a link between PD and farming, rural living and well-water drinking (Das et al., 2010, Moisan et al., 2011).

Genetic risk factors

Gaucher disease is an autosomal recessive storage disorder caused by bi-allelic mutations in the glucocerebrosidase gene (GBA) (Ferreira and Massano, 2017). Clinicians have noted that patients and their relatives have a higher incidence rate of PD. Initial studies in the Ashkenazi Jewish population revealed that GBA mutations increased the risk of PD up to seven fold (Chen et al., 2007b). A subsequent worldwide study also found that GBA mutations are consistently associated with an increased risk of PD disease (odds ratio: 5.43, 95% confidence interval: 3.89 to 7.57) (Sidransky et al., 2009). To date, GBA mutations are the most common genetic risk factors for PD (Ferreira and Massano, 2017).

A leap forward in PD research has been accomplished following the advent of genome-wide association studies (GWAS), which allow researchers to identify novel associations in genes that may not have been strong priori candidates for PD. The largest GWAS was performed in 2014 and investigated over seven million variants across 13,708 cases and 95,282 controls, identifying

more than 20 independent risk variants for PD (Nalls et al., 2014). The identified single-nucleotide polymorphisms (SNPs) are listed in Table 1.2.

Table 1.2 Risk loci identified in a large-scale meta-analysis of genome-wide association data.

SNP	Chr.	Closest gene(s)	Effect	Alternate	Joint phase	
			allele	allele	OR	P
rs35749011	1	GBA-SYT11	A	G	1.824	1.37×10^{-29}
rs823118	1	RAB7L1-NUCKS1	T	C	1.122	1.66×10^{-16}
rs10797576	1	SIPA1L2	T	C	1.131	4.87×10^{-10}
rs6430538	2	ACMSD-TMEM163	T	C	0.875	9.13×10^{-20}
rs1474055	2	STK39	T	C	1.214	1.15×10^{-20}
rs115185635	3	KRT8P25-APOOP2	C	G	1.142	0.022
rs12637471	3	MCCC1	A	G	0.842	2.14×10^{-21}
rs34016896	3	NMD3	T	C	1.067	1.08×10^{-5}
rs34311866	4	TMEM175-GAK-DGKQ	T	C	0.786	1.02×10^{-43}
rs11724635	4	BST1	A	C	1.126	9.44×10^{-18}
rs6812193	4	FAM47E-SCARB2	T	C	0.907	2.95×10^{-11}
rs356182	4	SNCA	A	G	0.76	4.16×10^{-73}
rs9275326	6	HLA-DQB1	T	C	0.826	1.19×10^{-12}
rs199347	7	GPNMB	A	G	1.11	1.18×10^{-12}
rs591323	8	FGF20	A	G	0.916	6.68×10^{-8}
rs60298754	8	MMP16	T	C	1.078	0.181
rs117896735	10	INPP5F	A	G	1.624	4.34×10^{-13}
rs7077361	10	ITGA8	T	C	1.092	4.16×10^{-5}
rs3793947a	11	DLG2	A	G	0.929	3.96×10^{-7}
rs329648	11	MIR4697	T	C	1.105	9.83×10^{-12}
rs76904798	12	LRRK2	T	C	1.155	5.24×10^{-14}
rs11060180	12	CCDC62	A	G	1.105	6.02×10^{-12}
rs11158026	14	GCH1	T	C	0.904	5.85×10^{-11}
rs1555399	14	TMEM229B	A	T	0.897	6.63×10^{-14}
rs2414739	15	VPS13C	A	G	1.113	1.23×10^{-11}
rs14235	16	BCKDK-STX1B	A	G	1.103	2.43×10^{-12}
rs17649553	17	MAPT	T	C	0.769	2.37×10^{-48}
rs11868035	17	SREBF1-RAI1	A	G	0.939	5.98×10^{-5}
rs12456492	18	RIT2	A	G	0.904	7.74×10^{-12}
rs62120679	19	SPPL2B	T	C	1.097	5.57×10^{-7}
rs8118008	20	DDRGK1	A	G	1.111	3.04×10^{-11}
rs2823357	21	USP25	A	G	1.031	0.027

A list of SNPs identified in the meta-analysis of a genome-wide association study. The joint phase represents the combination of the cases from the discovery phase and the replication phase. The replication phase was conducted to identify which of the putatively associated loci were truly relevant to the disease, via the addition of independent sample series. (SNP): Single-nucleotide polymorphism, (Chr.): chromosome, (OR): odds ratio. Re-used with permission from Nalls (2014).

Interestingly, variants of known familial PD genes are present in this list. A complex polymorphic microsatellite repeat named Rep1, which is located in the promotor region of the *SNCA* gene, is the best example. The 261bp variant increases the risk for PD, while the 259bp variant is protective, arguably via modulating the gene expression level (Maraganore et al., 2006, Mata et al., 2010, Kalinderi et al., 2016). In addition, variants in *LRRK2*, such as Gly2385Arg and Arg1628Pro polymorphisms, have been linked to increased PD risk in the Asian population (Kalinderi et al., 2016). These findings suggest that sporadic PD is mechanistically related to inherited disease. Thus, studying the underlying pathological pathways in familial PD may be relevant to the sporadic form as well. The evidence of genetic involvement in the disease has led researchers to propose that Mendelian and sporadic forms of PD can be considered as two extremes of one spectrum, where a single mutation causes the disease, whereas others contribute to increasing the risk to different degrees (Spataro et al., 2015).

Other risk factors

Identifying novel risk factors for PD has been an objective of a vast number of researchers. While some have found statistically significant results, others have either failed to do so, or have reached conclusions that are inconsistent with other studies. The investigated risk factors include body mass index, diabetes, cholesterol level, hypertension, antioxidant vitamins such as vitamin C and E, intake of vitamin D and calcium, iron intake, oral contraceptives and pregnancy (Ascherio and Schwarzschild, 2016). The inconsistency between results does not necessarily mean a lack of association, as there might be unidentified factors that modulate the association. Amongst confirmed associations, overconsumption of milk and dairy products have consistently been shown to increase the risk of PD in several papers (Chen et al., 2007b, Jiang et al., 2014). Another well-established association is observed between PD and melanoma, where the presence of either of them increases the risk of the other (Wirdefeldt et al., 2013, Constantinescu et al., 2014). In contrast to milk consumption and melanoma, the risk of PD is reduced amongst smokers (Li et al., 2015). The decrease in risk is positively correlated with the duration of smoking and negatively correlated with the number of years passed after quitting smoking (Thacker et al., 2007). Other protective factors include caffeine and non-steroidal anti-inflammatory drugs (NSAIDs) (Ascherio

and Schwarzschild, 2016). Alcohol intake was also associated with a small decrease in PD risk, unless overconsumption of alcohol took place (Ascherio and Schwarzschild, 2016).

1.2 Mitochondria

Impairment of different molecular biological pathways has been suggested as an underlying cause of the neuronal degeneration in PD, such as altered proteolysis, inflammatory changes and excitotoxicity (Celardo et al., 2014). However, numerous discoveries in genetically-based studies have placed mitochondrial dysfunction as a central part of the disease pathology. This is not a novel finding since the first link between mitochondrial dysfunction and PD was suggested decades before the genetic breakthrough (Lin and Beal, 2006). The MPTP-induced Parkinsonism in drug abusers was found to be associated with mitochondrial respiratory complex I inhibition. A similar finding was also reported in different brain regions of PD patients, as well as in fibroblasts, lymphocytes and blood platelets (Yoshino et al., 1992, Krige et al., 1992, Mytilineou et al., 1994). Genetic studies of PD have shown that other elements in the mitochondria can also be affected. Hence, understanding mitochondrial biology is important in PD research.

1.2.1 Mitochondrial origin and history

Mitochondria generate the energy-storing molecule adenosine triphosphate (ATP), which is the main source of energy in all human cells. ATP is also crucial for various cellular functions, such as biosynthesis, protein folding and degradation, cellular migration, neuronal cell signalling and muscle contraction (Kühlbrandt, 2015). In the course of evolution of eukaryotic cells, the emergence of the mitochondria is considered as one of the most critical stages. It is believed that an interaction between primogenitor oxidative bacteria and glycolytic cells led to the development of a syntrophic relationship, which eventually resulted in the engulfment of the live bacteria by the cells (endosymbiosis). The endosymbiosis occurred one and a half billion years ago. With time, the bacteria became what we now know as mitochondria (Ettema, 2016). This endosymbiosis process was remarkably beneficial to the eukaryotic cells, as it provided a superfluous amount of energy that facilitated the emergence of more complex cellular components and pathways. In the current time, Mitochondria still have their own genetic system and protein translation machinery

(Dennerlein et al., 2017). However, they have become heavily integrated into the biology of the cells (Couvillion et al., 2016). The current mitochondria rely mostly on nuclear genes for protein synthesis (Couvillion et al., 2016).

1.2.2 Mitochondrial structure

The gross structure of mitochondria was revealed by light more than 100 years ago (Ernster and Schatz, 1981, Kühlbrandt, 2015). However, the visualisation of their detailed structure was not possible until the invention of the high-resolution electron microscope in 1952 (Ernster and Schatz, 1981, Kühlbrandt, 2015). The advance in imaging technology allowed a more in-depth study of mitochondrial structure. For example, the use of electron tomography revealed the structure of the inner membrane in three-dimensional space, while the use of Cryo-EM revealed mitochondrial macromolecular components at nanometre scales (Perkins and Frey, 2000).

The mitochondrion is composed of outer and inner membranes [Figure 1.2], which correspond to the cellular membrane-derived vesicle and the bacterial membrane, according to the endosymbiosis theory (Ettema, 2016). The outer membrane has channels that are made by distinct proteins (porins), such as the voltage-dependent anion channel (VDAC), which makes it permeable to ions and small uncharged molecules (Prasai, 2017). There are also specific transporters for larger proteins (Prasai, 2017). On the other hand, the inner membrane only allows the passage of certain molecules by highly sophisticated transporters (Prasai, 2017). The innermost compartment of the mitochondria [Figure 1.2], the mitochondrial matrix, has a high pH (7.9) and protein concentration, and it is the site for mitochondrial transcription and translation (Prasai, 2017). All mitochondrial genes are present in this compartment (Kühlbrandt, 2015). The inner membrane form cristae that extend deep into the matrix (Cogliati et al., 2016). Since the inner membrane is the site of oxidative phosphorylation, these invaginations significantly increase the surface area of the inner membrane and, consequently, increase the efficiency of ATP production. Most of the inner membrane contributes to the cristae, particularly in cells that require a high energy supply, such as myocytes (Kühlbrandt, 2015). The cristae region of the inner membrane contains all of the respiratory chain protein complexes. The remaining parts of the

inner membrane are separated from the outer membrane by the intermembrane space (approximately 20nm) [Figure 1.2] (Prasai, 2017).

1.2.3 Oxidative phosphorylation and energy production

Oxidative phosphorylation (OXPHOS) is the process through which cells produce ATP via the use of the five respiratory chain complexes. In this process, four of the complexes pump protons from the matrix into the intermembrane space, leading to an increase in the electrochemical gradient across the inner membrane (Lemarie and Grimm, 2011). Concentrated protons can only pass through the fifth respiratory chain complex, the ATP synthase complex, resulting in the phosphorylation of the low energy molecule adenosine diphosphate (ADP) into ATP (Lemarie and Grimm, 2011).

Complex I (Nicotinamide adenine dinucleotide (NADH) dehydrogenase) is a large complex that is composed of more than 40 proteins (Zhu et al., 2016). The functions of most of its subunits are not yet understood. Complex I oxidises a molecule of NADH into NAD⁺. In this process, two electrons are released and transported via the flavin mononucleotide (FMN) and several iron sulphur centres within complex I, and bind to coenzyme Q10 (also known as ubiquinone) (Efremov et al., 2010). In addition, two hydrogen ions (H⁺) from the matrix bind ubiquinone and reduce it to ubiquinol (Efremov et al., 2010). In contrast to the stationary respiratory complexes, ubiquinone/ubiquinol are electron acceptors/donors, which move freely between the complexes, facilitating electron transfer. Following the reduction, ubiquinol travels through the inner membrane and associates with respiratory complex III (Chaban et al., 2014). The NADH oxidation also results in pumping four hydrogen ions from the matrix to the intermembrane space (Chaban et al., 2014).

Complex III (cytochrome c oxidoreductase) extracts the two electrons from the ubiquinol via cytochrome b and c1 subunits (Chaban et al., 2014). Consequently, the two electrons are transferred into two cytochrome c molecules, another mobile protein that is usually associated with complex III. A further four hydrogen ions are pumped into the intermembrane space as a result of this event (Chaban et al., 2014). Then, cytochrome c delivers the electrons to complex IV.

Complex IV (cytochrome c oxidase) uses the two electrons to reduce oxygen into one water molecule. Therefore, oxygen is the final electron acceptor in the respiratory chain. This step is associated with pumping two hydrogen ions into the intermembrane space (Chaban et al., 2014).

The hydrogen ions pass through the F₀ part (the transmembrane part) of Complex V (ATP synthase) in compliance with their electrochemical gradient, and rotate the C subunits (belong to the F₁ part which presents in the matrix) (Koopman et al., 2013). This rotation drives the conversion of ADP into ATP at the matrix side of the inner mitochondrial membrane (Koopman et al., 2013). The passage of three to four hydrogen ions is required to generate one ATP molecule (Hattori and Gouaux, 2012). Accordingly, oxidative phosphorylation of one NADH molecule results in the generation of 2.5 - 3 ATP molecules, theoretically.

Complex II (succinate oxidoreductase) is an alternate electron entry point from complex I (Chaban et al., 2014). Complex II facilitates the conversion of succinate into fumarate within the citric acid (Krebs) cycle, and concomitantly reduces FAD into FADH₂ (Chaban et al., 2014). FADH₂ provides the electrons that will be transported through the electron chain. Complex II transfers the two electrons via its iron centres into ubiquinone and reduces it to ubiquinol, which translocates to complex III as described above (Chaban et al., 2014). This process is not associated with pumping of hydrogen ions from the matrix to the intermembrane space. Notably, the total number of pumped hydrogen ions associated with the FADH₂ molecule is six, because it does not pass through complex I. Therefore, oxidative phosphorylation of one FADH₂ molecule generates 1.5 – 2 ATP molecules, theoretically.

It is important to note that energy production is not the only function of the mitochondria. Through the course of evolution, the mitochondria developed multiple roles to support the survival of organisms. For example, in mammals, mitochondria can maintain body temperature by generating heat instead of ATP (Cedikova et al., 2016). This phenomenon is attributed to a mitochondrial inner membrane channel protein named thermogenin or uncoupling protein 1 (UCP1), which leaks protons and causes mitochondrial uncoupling (Cedikova et al., 2016). In addition, mitochondria have a pivotal role in determining cell fate, as they can initiate apoptotic signalling. Via the production of reactive oxygen species (ROS), mitochondria are involved in

homeostatic pathways and contribute to adaptive stress signalling pathways (Hamanaka and Chandel, 2010). Moreover, mitochondria can modulate the levels of amino acids, metabolites and numerous regulatory enzymes, such as histone deacetylases, and play an important role in iron metabolism, which is a vital component in haemoglobin and respiratory chain complexes (Nunnari and Suomalainen, 2012). With regard to neurons, mitochondria play a role in lipid acid synthesis, which is particularly important for neuronal physiology (Mayr et al., 2011). Moreover, the ability of the mitochondria to regulate Ca^{+2} flux from the plasma membrane and endoplasmic reticulum is critical for neurogenesis, neuronal plasticity and neurotransmitter release (Nunnari and Suomalainen, 2012).

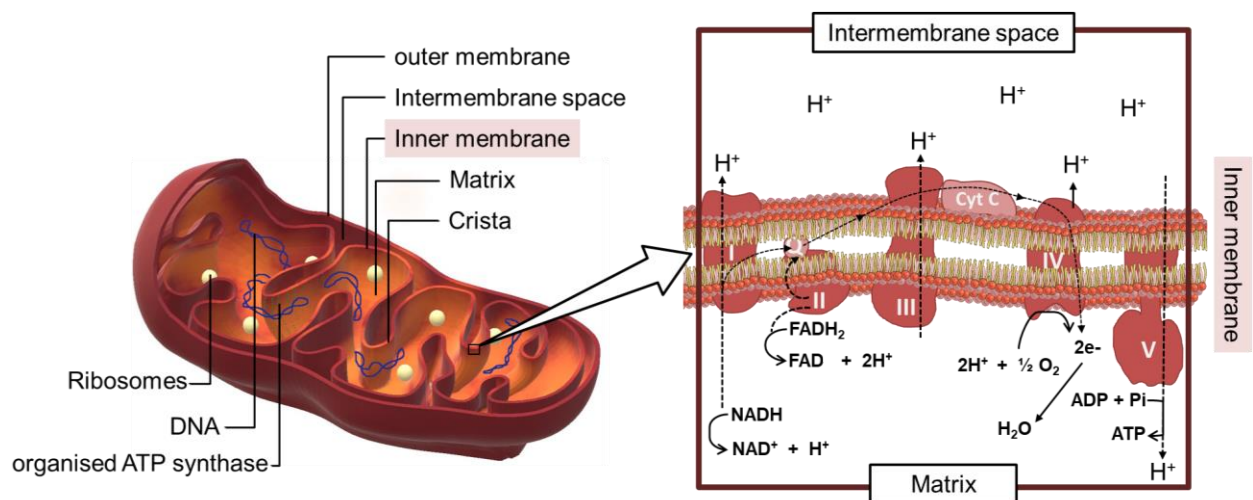


Figure 1.2 An overview of mitochondrial structure and respiratory chain complexes.

Mitochondria are double-membrane organelles that contain three separate compartments. All respiratory protein complexes are distributed along the inner membrane, and are organised to pump hydrogen ions into the intermembrane space (Adam-Vizi and Chinopoulos, 2006).

1.2.4 Mitochondrial dynamics

Mitochondrial morphology varies depending on a number of factors, including cell type and metabolic/nutrient status (Mishra and Chan, 2016). Mitochondria undergo two main dynamic processes that regulate their morphology: fission and fusion. The net balance between these two processes determines whether the mitochondria look fragmented or elongated (Mishra and Chan, 2016).

Fission

Mitochondrial fission is mainly regulated by dynamin-related protein 1 (Drp1) (Youle and Van Der Bliek, 2012). The process involves the accumulation of Drp1 as a ring around the outer mitochondrial membrane, via binding to a group of receptors such as mitochondrial fission factor (Mff), mitochondrial fission 1 protein (Fis1) and mitochondrial dynamics proteins (MiD49), and (MiD51) (van der Bliek et al., 2013). Then, the Drp1 ring incises the mitochondria in a guanosine triphosphate (GTP)-dependent manner (van der Bliek et al., 2013). In humans, Drp1 mutation has been linked to microencephaly, refractory epilepsy and neonatal death (Vanstone et al., 2016, Waterham et al., 2007).

Drp1 activity is mainly regulated via phosphorylation, but other post-translational modifications (PTM) such as SUMOylation and ubiquitination are also reported (Chang and Blackstone, 2010). Various kinases and phosphorylation sites have been identified (Dickey and Strack, 2011) (Kashatus et al., 2015). The response of Drp1 to either phosphorylation or dephosphorylation is site dependant. For example, phosphorylation at ser637 by protein kinase A supresses Drp1 activity and increases mitochondrial length (Chang and Blackstone, 2007). Similarly, phosphorylation at ser637 as a result of mTOR inhibition diminishes Drp1 activity (Gomes et al., 2011). On the other hand, mitogen-activated protein kinase 1 (Erk2) and Ca²⁺/calmodulin-dependent protein kinase (CaMKII) phosphorylate Drp1 at ser616 and enhance its activity (Kashatus et al., 2015, Bo et al., 2018). Mitochondrial uncouplers, such as carbonyl cyanide m-chlorophenyl hydrazone CCCP, which classically induce mitochondrial fragmentation, also activate Drp1. The activation is achieved via dephosphorylating ser637 through the action of Ca²⁺-dependent phosphatase calcineurin (Cereghetti et al., 2008). Moreover, CCCP stimulates the mitochondrial metalloprotease Oma1 to increase the amount of the short form of optic atrophy 1 (Opa1), which indirectly promotes fission by downregulating fusion (Mishra and Chan, 2016).

Fusion

Mitochondrial fusion is mainly regulated by the outer membrane proteins, Mitofusin 1 (Mfn1) and Mitofusin 2 (Mfn2), and the inner membrane protein, Opa1 (Westermann, 2012). The deletion of fusion proteins results in significant mitochondrial fragmentation and eliminates the free

movement of mitochondrial content within the mitochondria (Mishra and Chan, 2016). Mitochondrial fusion has a positive correlation with OXPHOS. Mitochondria tend to elongate in conditions that require more energy via OXPHOS, such as culturing cells in a galactose medium (Ren et al., 2017). In contrast, fragmented mitochondria are less efficient in energy production (Liesa and Shirihi, 2013). Evidence suggests that the response to reduced fusion is cell dependant. Embryonic fibroblasts can tolerate deletion of a single Mfn protein, while neurons show a significant decrease in survival, which has been attributed to a decline in mitochondrial DNA (mtDNA) content and compromised respiratory chain activity (Chen et al., 2007a). Therefore, it is not surprising that mutations in those proteins result in neuron-related diseases, such as Charcot-Marie-Tooth disease type 2A (Mfn2 mutation) (Hikiami et al., 2018) and dominant optic atrophy (Opa1 mutation) (Millet et al., 2016).

The long-inner membrane bound form of Opa1 can be cleaved into a short soluble form by the metalloproteases Yme1L and Oma1 (MacVicar and Langer, 2016). In contrast to the long Opa1, the cleavage of Opa1, together with the increase in its shorter form, is believed to stimulate mitochondrial fission (MacVicar and Langer, 2016). Evidence suggests that Yme1L and Oma1 regulate inner membrane fusion according to the metabolic state of the cells. As an inner membrane protein, Opa1 also plays a role in stabilising mitochondrial cristae and respiratory chain supercomplex (Cogliati et al., 2013).

1.3 Mechanisms of Parkinson's disease

1.3.1 Lessons learned from Parkinson's genetics

SNCA

α -synuclein is a small protein that is believed to play a role in exocytosis and complex assembly of vesicles (Helley et al., 2017). α -synuclein predominantly presents in the cytoplasm. However, it is capable of interacting with mitochondria via its N-terminus, which has a specific mitochondrial targeting sequence (Helley et al., 2017). Research has revealed that some modified forms of α -synuclein can bind Translocase of the outer membrane (Tom20) and block the import of proteins, leading to mitochondrial dysfunction (Di Maio et al., 2016). Additionally α -synuclein can travel

through VDAC, access the inner mitochondrial compartment and damage respiratory complex proteins and mtDNA (Rostovtseva et al., 2015). α -synuclein also inhibits mitochondrial biogenesis via downregulating PGC1 α , the key transcriptional factor in mitochondrial biogenesis (Rostovtseva et al., 2015).

α -synuclein has a natural capability to aggregate to form oligomers and larger insoluble fibrils (Dehay et al., 2015). Studies have suggested that α -synuclein exists in different conformations that are in dynamic equilibrium (Dehay et al., 2015). When a toxic mutation presents, the balance shifts towards the insoluble fibril that aggregates to form LB. Artificially mutant α -synuclein that is unable to form insoluble fibrils has excessive toxicity in vivo (Winner et al., 2011). This observation indicates that LB body formation might be a protective process that prevents the mutated α -synuclein from reaching the mitochondria. Transferring LB extract from PD patients into mice and monkeys induces progressive DA neuron degeneration and pathological conversion of endogenous α -synuclein, possibly via altering the dynamic of endogenous α -synuclein (Recasens et al., 2014).

LRRK2

LRRK2 is a protein that consists of multiple domains (Cookson, 2015). LRRK2 has a GTPase domain, kinase domain and several other protein interacting domains (Cookson, 2015). Therefore, LRRK2 is believed to have a complex role in cell biology. Research has shown that LRRK2 is involved in many cellular functions, such as cytoskeletal and vesicle dynamics, autophagy and mitochondrial functions (Helley et al., 2017). However, our understanding of LRRK2 is far from complete.

In PD, most of the reported LRRK2 mutations have been associated with an increase in kinase activity which was associated with increased mitochondrial fragmentation (Helley et al., 2017) (Cookson, 2015). Researchers have found a direct interaction between LRRK2 and various mitochondrial dynamic proteins, such as Mfn1, Mfn2 and Opa1 (Kang and Marto, 2017). The expression of Gly2019Ser mutant LRRK2, as well as the overexpression of the wild type, was associated with Drp1-dependent mitochondrial fragmentation (Kang and Marto, 2017). These

findings are consistent with a previous study that reported Drp1 activation upon interaction with LRRK2 via phosphorylation at Thr595 (Su and Qi, 2013).

In addition to abnormal mitochondrial morphology, functional mitochondrial impairments, such as decreased mitochondrial membrane potential and ATP levels, have been observed in patient fibroblasts (Mortiboys et al., 2010, Mortiboys et al., 2015). Increased levels of UCP2 have also been linked to LRRK2 mutations. In human neuroblastoma and mouse fibroblast models of LRRK2 Gly2019Ser mutation, mitochondrial membrane potential was increased upon using UCP activity inhibitors, as well as the LRRK2 kinase inhibitor (Papkovskaia et al., 2012).

In human fibroblasts of Gly2019Ser mutant individuals, fibroblasts of both affected and carrier donors showed a decreased mitochondrial membrane potential (Grünewald et al., 2014b). However, the increase in UCP2 was seen only in cells of affected donors. In addition, not all cells with increased UCP2 showed an increase in oxidative stress levels (Grünewald et al., 2014b). Therefore, the increase in UCP2 expression could be a secondary outcome of LRRK2 pathology. The UCP2 level is known to be elevated in oxidative stress states to eliminate the effect of ROS through mild uncoupling of the respiratory chain (Hass and Barnstable, 2016).

PINK1 and parkin

There are several lines of defence to maintain a healthy mitochondrial pool. For example, mitochondrial chaperones facilitate proper folding of newly synthesised polypeptides (Harbauer et al., 2014). If chaperones fail, mitochondrial proteases can eliminate the misfolded proteins (Quirós et al., 2015). In addition, mitochondrial antioxidant enzymes help to lessen the effect of ROS on mitochondrial DNA and proteins (Sena and Chandel, 2012). When these mechanisms fail and mitochondrial damage occurs, the defective part is removed via a selective autophagy process (mitophagy), to be replaced by a newly synthesised component (Bingol and Sheng, 2016). Mitophagy is vital to the cells since the presence of dysfunctional mitochondria does not only influence energy production, but also Ca buffering and apoptotic signalling (Bingol and Sheng, 2016).

Under normal conditions, PINK1 is continuously imported into the mitochondria, inserted into the inner mitochondrial membrane and cleaved by matrix-processing peptidases (Rüb et al., 2017). Under stressful conditions, PINK1 accumulates on the mitochondrial surface. This occurs as a result of decreased mitochondrial membrane potential, which interferes with PINK1 import into the mitochondrial inner membrane (Rüb et al., 2017). PINK1 recruits and activates Parkin via phosphorylation at ser65 (Rüb et al., 2017). Then, activated Parkin ubiquitinates nearby outer mitochondria membrane proteins, such as porin, mitofusin and Miro proteins (Sarraf et al., 2013). PINK1 also phosphorylates the ubiquitinated domains, which in turn activate more Parkin (Rüb et al., 2017). Adaptor proteins bind both ubiquitinated proteins and Microtubule-associated protein 1A/1B-light chain 3 (LC3), allowing the mitochondria to be targeted by the autophagosomal membranes (Rüb et al., 2017). Ultimately, autophagosomes merge with lysosomes and mitochondrial contents degrade through the action of lysosomal enzymes. Via this mechanism, the PINK1/Parkin system ensures that autophagic membranes target only the defective part of the mitochondria. Interestingly, recent evidence shows that highly metabolic cells (such as neurons) have elevated basal mitophagy rates that occur independently of PINK1. This finding indicates that there might be other pathways involved in mitochondrial quality control (McWilliams et al., 2018).

Other genes

The role of mitochondria in PD pathogenesis has also been suggested through studying genes that increase the risk of PD. In vitro, blocking GBA significantly compromises mitochondrial function and increases mitochondrial fragmentation (Cleeter et al., 2013). Although the mechanism through which this happens is still unclear, it has been suggested that the process involves an impairment in the mitophagy pathway. Interestingly, α -synuclein has a direct reciprocal relationship with GBA. When α -synuclein is overexpressed, GBA activity tends to decrease (Yang et al., 2016). Conversely, in mutant GBA, α -synuclein accumulates in aggregate and promotes lysosomal impairment (Du et al., 2015).

1.3.2 Mechanisms of environmental toxins

Toxins that interfere with mitochondria are associated with a higher risk of PD (Ascherio and Schwarzschild, 2016). Many of these toxins have been used to induce PD in animals for research purposes. Since MPTP is the first toxin known to induce PD, its mechanism of action has been investigated thoroughly. MPTP is capable of crossing the blood brain barrier (BBB) due to its lipophilic nature (Jagmag et al., 2016). When MPTP enters the brain, it is oxidised and converted into its active form, 1-methyl-4-phenylpyridinium (MPP⁺), primarily within astrocytes (Brooks et al., 1989). MPP⁺ has a high affinity to dopamine active transporter (DAT), with comparatively lower affinities to the norepinephrine and serotonin transporters (Javitch et al., 1985). Once transported into the DA neurons, MPP⁺ is concentrated in the mitochondria through energy-dependant mechanisms (Ramsay and Singer, 1986). MPP⁺ possesses an inhibitory effect on complex I of the mitochondrial transport chain, which in turn leads to a decrease in overall ATP production. Blocking the electron transport chain increases the production of ROS and, consequently, oxidative stress levels (Hasegawa et al., 1990). Unlike MPTP, which is only used in labs for research purposes, the structurally similar compound, rotenone, has been used in veterinary medicine to eliminate mites, lice and/or ticks that grow on domestic animals (Rohan et al., 2015). It has also been used in agriculture to control beetles and aphids, and in water to eliminate unwanted fish (Rohan et al., 2015). Paraquat, which is another similar compound to MPTP, is a widely used pesticide in agriculture. Both rotenone and paraquat are widely used in labs for research purposes.

1.3.3 Role of ageing

Ageing is not only the strongest risk factor for PD, but it is also a determinant of the progression rate and the response to the treatment (Rodriguez et al., 2015). Evidence shows that the underlying mechanisms of ageing and PD are shared at some levels. Thus, ageing acts as a factor that increases the baseline threshold of PD susceptibility, so that other factors, such as genetic mutations and environmental toxins, can initiate the pathological process. DA neuron loss has been observed in aged healthy individuals and non-human primates (Rodriguez et al., 2015, Collier et al., 2011). Studies have also shown that the loss occurs autonomously within the

lifespan, at a rate of approximately 7% per decade. In PD, the rate of this process accelerates significantly above that baseline (Stark and Pakkenberg, 2004).

At molecular levels, PD and ageing also share common mechanisms, where mitochondria play a pivotal role. In fact, the mitochondrial theory of ageing proposed that the mitochondria are the pacemaker of ageing (Navarro and Boveris, 2010). ROS, which are produced by dysfunctional mitochondria, are responsible for oxidative damage of various cellular components, as well as DNA mutations with telomere shortening (Hindle, 2010). In the long term, the accumulated damage leads to tissue ageing. Neurons have higher energy demands and are more sensitive to the accumulated effects of ageing. Decreased activity of respiratory complex I and IV, and decreased overall ATP production have been reported in mammalian ageing brains (Boveris and Navarro, 2008). Compensatory mechanisms that alleviate the harmful effects of mitochondrial dysfunction, such as lysosome-mediated autophagy, also decline with ageing (Tai and Schuman, 2008).

1.3.4 Oxidative stress and neuronal vulnerability

Oxidative stress

ROS can be produced as by-products upon metabolising certain compounds and toxins, or upon the exposure to harmful radiation (Liochev, 2013). However, the major source of ROS in cells is the mitochondria (Song and Zou, 2015). The generation of ROS via the respiratory chain consumes about 2% of the O₂ utilised by the mitochondria (Orrenius, 2007). ROS are mainly produced via respiratory complexes I and III, but small amounts are also produced via complex II (Song and Zou, 2015). In the brain, complex I is superior to complex III in ROS production (Kim et al., 2015).

Under healthy conditions, low level of ROS has physiological functions and serve as cellular signalling molecules. Oxidative stress occurs when ROS accumulate and the cellular antioxidant mechanisms fail to neutralise them (Dasuri et al., 2013). The generation of ROS is enhanced in mitochondrial dysfunction, especially when electron transfer is interrupted, such as when the respiratory complexes are blocked (Lushchak, 2015). As a result, electrons leak and reduce molecular oxygen into superoxide anions, which can be transformed into other type of ROS

(Lushchak, 2015). Oxidative stress damages DNA, induces cellular membrane peroxidation and alters the structures and functions of proteins via oxidation (Dasuri et al., 2013). Since the mitochondria are the main producers of ROS, they are at higher risk of ROS-mediated damage, which in turn leads to further increases in ROS production.

One of the important PD-related proteins affected by oxidative stress is α -synuclein. Lipid peroxidation of the cell membrane by ROS produces 4-hydroxy-2-nonenal, which mediates α -synuclein damage and renders it unable to form insoluble fibrils (Bae et al., 2013). As a result, the amount of toxic soluble α -synuclein increases, as well as its toxicity (Bae et al., 2013).

Naturally, there are various mechanisms through which cells protect themselves from the deleterious effect of oxidative stress. The activation of phase II detoxification enzymes via the Nrf2 pathway is considered to be one of the most important mechanisms. This pathway is discussed in detail in the fourth chapter. In addition, Adaptive stress response involve the activation of other pathways such as activator protein 1 (AP-1), resulting in the expression of genes required for the detoxification of oxidizing molecules (Espinosa-Diez et al., 2015). AP-1 is a family of dimeric bZIP transcription factors. This family includes Jun, Fos, CREB and MAF, which usually dimerise and bind to TPA-responsive element or cAMP response elements (Glover and Harrison, 1995). AP-1 is involved in several cellular processes such as cell proliferation, apoptosis, survival, and differentiation (Karin et al., 2001). AP-1 activity is regulated both through the increased synthesis of its components, the Jun and Fos proteins, and through their phosphorylation (Shaulian and Karin, 2001). Two main signaling pathways whose activation leads to upregulation of jun and fos genes are the JNK and MAPK pathways (Silvers et al., 2003). JNK activation is particularly important, as it enhance AP-1 activity post transcriptionally via phosphorylation of the Jun proteins (Musti et al., 1997).

Neuronal vulnerability

In comparison to other types of cells, neurons are more sensitive to oxidative stress. There are many reasons behind this vulnerability. First, the brain has high energy demands, as it is one of the most active organs in the body. The brain's use of oxygen accounts for about 20% of the total body needs, although it represents only 2% of body mass (Bélanger et al., 2011). Second, the

brain contains relatively copious amounts of iron and copper, which are important for the formation of ROS (Scheiber et al., 2014). Third, the brain is enriched with polyunsaturated fatty acids, which are preferable targets for ROS and mediate the formation of secondary reactive species, such as 4-hydroxy-2-nonenal (Wang and Michaelis, 2010). Finally, the capacity of the neurons to neutralise ROS is relatively low in comparison to other types of cells (Kim et al., 2015).

DA neurons lack the myelin sheath around their axons (Haddad and Nakamura, 2015), which is important for energetically efficient impulse propagation (Almeida and Lyons, 2017). Therefore, DA neurons have higher energetic demand, which renders them more vulnerable when mitochondrial dysfunction occurs. In line with this, axons of DA neurons are the sites where pathological α -synuclein accumulates and where neurodegeneration initially starts (Haddad and Nakamura, 2015). The selective DA neuronal loss in the brain also suggests dopamine metabolism as an additional contributing factor in the vulnerability of this subset of neurons. In fact, hydroxylated dopamine, 6-hydroxydopamine (6-OHDA), is a classical toxin used for modelling PD in animals. 6-OHDA treatment results in selective injury to nigrostriatal DA cells (Blesa et al., 2016).

Dopamine synthesis starts with the hydroxylation of L-tyrosine into L-3,4-dihydroxyphenylalanine (L-DOPA), which is converted into dopamine through the action of aromatic acid decarboxylase (Puspita et al., 2017). Within cells, dopamine is stored in vesicles through the action of vesicular monoamine transporter 2 (VMAT2), to protect it from oxidation by cytoplasmic molecules (Puspita et al., 2017). Following dopamine release into the synaptic space, DAT mediates its reuptake into the cells, where it can be either re-stored in vesicles, or degraded by enzymes such as monoamine oxidases and aldehyde dehydrogenase (Puspita et al., 2017). This process generates the ROS, 3,4-dihydroxyphenylacetaldehyde (DOPAL) and H_2O_2 (Goldstein et al., 2013). In addition, cytoplasmic metals, such as iron, can oxidise the reabsorbed dopamine into DA-quinone (DAQ) and the more stable highly reactive compound, aminochrome (Puspita et al., 2017). DAQ interacts with mitochondrial proteins and inhibits respiratory complexes I and IV (Puspita et al., 2017). DAQ also modulates various important proteins, such as α -synuclein, Parkin, DJ-1, DAT and Tyrosine hydroxylase (TH), and exerts a negative effect on lysosomal interaction in autophagy (Blesa et al., 2015).

1.3.5 Cell death in PD

The mitochondria play a key role in determining the fate of the cells by triggering apoptosis. The intrinsic pathway of apoptosis, also referred to as the mitochondrial pathway, is induced by most apoptotic stimuli (Lopez and Tait, 2015). A critical step in this pathway is the permeabilisation of the mitochondrial outer membrane and the leak of the cytochrome c from the intermembrane space (Lopez and Tait, 2015). In the cytoplasm, apoptosomes are formed through the binding of cytochrome c to the apoptotic protease activating factor 1 (APAF-1) (Zhou et al., 2015). Apoptosomes attract and activate pro-caspase 9, which in turn cleaves caspase 3 and caspase 7 into their active forms (Zhou et al., 2015). The activation of the caspases drives apoptosis by consequently cleaving a battery of apoptosis-related proteins. However, it has been shown that mitochondrial outer membrane permeabilisation can initiate apoptosis independently of caspase activation (Tait et al., 2014).

The integrity of the outer mitochondrial membrane is regulated by the balance between pro-apoptotic proteins and anti-apoptotic proteins. Pro-apoptotic proteins Bcl-2-associated X (BAX) and Bcl-2 homologous antagonist killer (BAK) are usually activated upon interaction with pro-apoptotic BH3-only proteins, such as BH3 interacting-domain (BID), Bcl-2-like protein 11 (BIM), Bcl-2-associated death promoter (BAD) and p53 upregulated modulator of apoptosis (PUMA) (Lopez and Tait, 2015). Some of the BH3-only proteins facilitate apoptosis by interfering with the anti-apoptotic proteins. On the other hand, the anti-apoptotic proteins (B-cell lymphoma 2 (BCL-2), BCL-B, B-cell lymphoma-extra large (Bcl-xL) and induced myeloid leukemia cell differentiation protein (MCL-1)) antagonise the activity of BAX and BAK (Lopez and Tait, 2015). Activated BAX and BAK oligomerise with the mitochondrial membrane and disturb its lipid structure to form pores that allow the leakage of cytochrome c (Lopez and Tait, 2015). Other leaked proteins, such as Second mitochondria-derived activator of caspases (SMAC) and High temperature requirement protein A2 (HtrA2) act synergistically and promote apoptosis by neutralising cytoplasmic caspase inhibitors (Lopez and Tait, 2015). Despite the supportive evidence for apoptosis, the exact mechanism of cell death in PD is not fully understood. Other proposed mechanisms include extrinsic apoptosis, autophagic cell death, necroptosis and ferroptosis (Guiney et al., 2017).

1.3.6 The role of mitochondrial dysfunction in Parkinson's disease

The first evidence that linked mitochondrial dysfunction to PD arose from studying MPTP-induced Parkinsonism in drug abusers (Langston et al., 1983). Research showed that MPTP mediates its action via selective inhibition of mitochondrial respiratory complex I (Hasegawa et al., 1990). Subsequently, complex I inhibition was reported in the substantia nigra of PD patients (Mann et al., 1992, Schapira et al., 1990). Common environmental toxins that increased the risk of PD (such as rotenone and paraquat) also interfere with mitochondrial respiratory complexes (Ascherio and Schwarzschild, 2016) [Figure 1.3]. Mitochondrial dysfunction, and in particular, complex I inhibition, leads to increased production of ROS (Li et al., 2003). Oxidative stress is believed to be the driver of the pathological process in PD. Notably; elevated oxidative stress is also a feature of aging which is the strongest risk factor for PD (Hindle, 2010).

The deleterious effect of ROS involves all organelles in the cell including the mitochondria themselves. In addition, ROS may damage the mitochondria indirectly via their interaction with α -synuclein [Figure 1.3]. ROS modify α -synuclein into a misfolded toxic form (Bae et al., 2013), which is similar to the mutated α -synuclein in patients with autosomal dominant PD. Misfolded α -synuclein are known to damage the mitochondria either via interfering with mitochondrial protein import or via inducing mutations in mitochondrial DNA. Thus, the aggregation of α -synuclein in Lewy Bodies is believed to be a protective process as it quarantines the toxic form of α -synuclein.

Although the generation of ATP is the main function of the mitochondria, cell death in PD disease is not attributed to a failure in maintaining cellular energetic demands. Instead, it is attributed to the activation of apoptotic cell death programme, which is highly regulated by the mitochondria, and is typically activated in case of mitochondrial dysfunction (Choudhury et al., 2012) [Figure 1.3]. In post-mortum brain tissue of PD patients, research demonstrated significant increase in the expression of apoptotic related proteins such as p53, CD95 and activated caspase-3 (Hartmann et al., 2000, Sohn et al., 1998).

Research shows that various PD related genes are required for normal mitochondrial function and dynamic. Mitochondrial fission allows the cells to isolate dysfunctional mitochondria and consequently removes them via autophagic degradation (mitophagy), which hinder the

activation the cell death program (Kim et al., 2007). Mutations of PINK1 and Parkin, the most studied mitophagy related proteins, are known causes of familial PD (Rüb et al., 2017). Additionally, *in vitro* study showed that Parkin knock-out mice have reduced activity of complex I and complex IV as well as lower respiratory capacity, indicating that the mitochondrial role of this proteins is not limited to mitophagy (Palacino et al., 2004). Fusion is also required for a normal mitochondria function as it allows the mitochondria to mix their contents, thus enabling protein complementation, mtDNA repair and equal distribution of metabolites (Bose and Beal, 2016). LRRK2, which is linked to 10% of all familial PD cases has been reported to interact with various mitochondrial fission and fusion factors (Kang and Marto, 2017), resulting in the appearance of more fragmented mitochondria. This morphological change is also associated with functional mitochondrial impairments, such as decreased MMP and ATP levels (Mortiboys et al., 2010, Mortiboys et al., 2015).

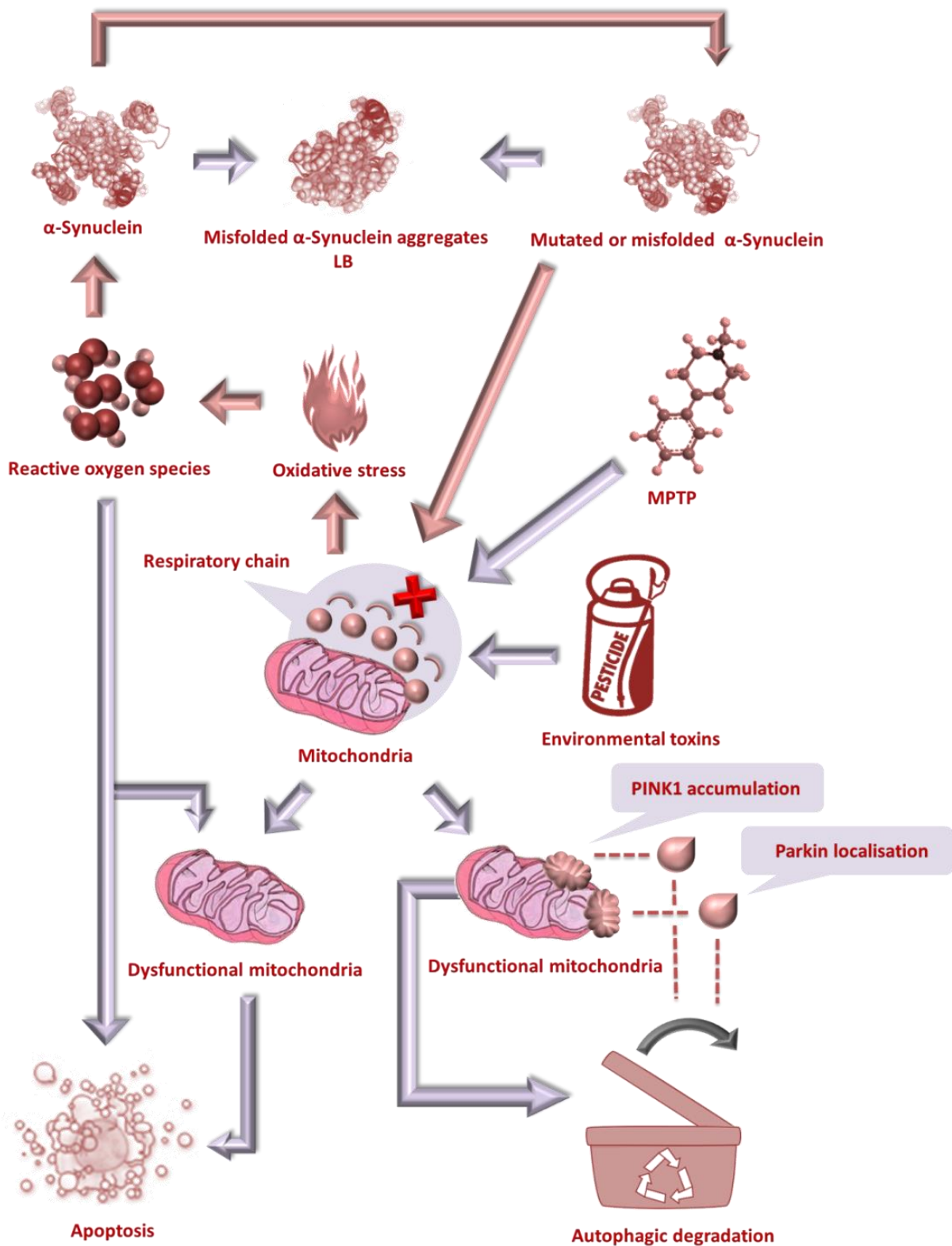


Figure 1.3 A summary of the proposed mechanisms for neuronal degeneration in PD.

Defective mitochondria and oxidative stress are the major drivers of the process. They can develop as a consequent of genetic defects, environmental insults or a mix of both. Misfolded α -synuclein can increase the level of reactive oxygen species by damaging the mitochondrial proteins and/or can be a consequence of the action of reactive oxygen species on its normal form. PINK1 and Parkin play a role in mitochondrial quality control, as they remove the dysfunctional mitochondria from the system. In the end, the accumulative defects force the cells to commence apoptosis.

1.4 Cellular models of PD

1.4.1 General advantages and limitations of cellular models

PD modelling can be applied at the cellular level or at the level of living organisms. The models can be based either on toxins or genetics. The choice of a specific model depends on the experimental question. In drug testing experiments, complex multicellular organisms are useful in studying the effect of the drug on pathophysiology, such as changes in neural network properties or in motor and sensory responses. On the other hand, cellular models are crucial for investigating the molecular mechanisms of a given drug at the level of intracellular organelles.

In comparison to animals, cellular models are more flexible in terms of handling, propagation and storing. Dealing with cells has fewer ethical concerns and require less time and effort. In addition, cells are more practical in high throughput drug screening experiments. In PD, human cells that have been used in research or drug screening can be grouped into three major categories. First, non-patient immortalized human cell lines such as SH-SY5Y and immortalized human embryonic mesencephalic cells, LUHMES. Second, primary patient-derived cells, such as primary skin fibroblasts. Third, stem cell models, such as human embryonic and adult neural stem cells and human induced pluripotent stem cells (iPSCs), which can be transformed into more relevant types of cells (Schüle et al., 2009). Interestingly, patient primary cells, such as skin fibroblasts, can be programmed to produce iPSCs, which can be differentiated into neuronal progenitor cells (iNPCs) and then into neurons (Mertens et al., 2016). Direct conversion of patient fibroblasts into neurons (iNs) is also possible. In this approach, the cells retain the transcriptomic feature of aging (Mertens et al., 2015).

One apparent limitation of the cellular model is the lack of in vivo natural factors and substances that surround the cells, which are replaced by the culture medium. Another limitation is that the development of the connections between the cells occurs in a two-dimensional plane and does not involve other types of cells that might be important in shaping and determining the final biological response in vivo. To tackle this issue, researchers occasionally use co-culture and 3D culture techniques. In the following section, skin-derived fibroblasts will be discussed in detail, due to their relevance to this project.

1.4.2 Fibroblasts of PD patients

Skin fibroblasts carry all of the genetic information of the patient, including the age-related changes that are extremely important, given the fact that aging is the strongest risk factor for PD. The process of obtaining and generating the cell line is relatively simple and straightforward (Burbulla and Krüger, 2012). Crude samples are usually extracted from a 2mm punch skin biopsy, taken from the inner side of the upper arm. Although this procedure is safe, it should be performed by a physician or a nurse under sterile conditions and local anaesthesia. The specimen, which is typically 4×4 mm or 6×6 mm, can be split and seeded into a T25 flask coated with foetal bovine serum (FBS). Then, the flask is placed gently in the incubator after the addition of a mixture of culture medium and FBS (50/50). Over the following few days, the samples are regularly fed by replacing 50% volume of the mixture. Initially, only circular epithelial cells appear. In four to five days, fibroblasts become apparent and are usually fed by the careful addition of drops of the mixture on alternative days. Once an adequate number of fibroblasts are present in the flask (30 to 50 cells around each skin sample), a culture medium with the standard 10% FBS and supplements can be used for feeding. Fibroblasts are cultured in a regular incubator at standard settings (37°C, 5% CO₂). Once confluent, primary fibroblasts can be split into three T75 flasks. Generally, the handling of these cells is not significantly different from other cell lines. The culture specimen initially contains other types of cells, such as keratinocytes (Auburger et al., 2012). However, by the time the third passage is reached, only fibroblasts remain. The sample might also be contaminated with mycoplasma, which can result in an inflammatory process and oxidative stress, and can slow the growth of the cells (Auburger et al., 2012). Therefore, a routine mycoplasma test is necessary. If the test is positive, the cells should be treated with ciprofloxacin.

Skin fibroblasts have many advantages in comparison to other in vitro models. Probably the most important one is that they encompass all the accumulative chronological and biological changes of the patient, as well as the primary genetic abnormality, which make them superior to artificially induced genetic models. Accordingly, skin fibroblasts are probably the best method to model sporadic PD. The fact that they are derived from humans is also an advantage. Although fibroblasts do not extend neurites like neurons, they are capable of making dynamic contacts, a feature that is not evident with other types of patient cells often used in research, such as blood

cells (Auburger et al., 2012). In addition, fibroblasts can be programmed and differentiated into DA neurons (Jang and Jung, 2017). The downside of this path is the practical difficulty, and required time and resources. Yet, it holds significant promise in the field of PD research.

On the other hand, one of the disadvantages of fibroblasts as a model for PD is that they are skin cells and their transcriptional profile is different from that of neurons. For example, the expression of the α -synuclein is extremely low in fibroblasts (Auburger et al., 2012). Fibroblasts are also more resistant to stressors in comparison to neurons (Auburger et al., 2012). When compared to primary fibroblasts, immortalised fibroblasts have a higher growth rate. Yet, it is still behind the average growth rate of other commonly used immortalised cells, such as SHSY5Y and HEK cells (1 to 2 weeks vs. 3 to 5 days). The change in genetics is inevitable with increasing passages. The protein expression profile of passaged fibroblasts has been compared to the primary fibroblasts (Sprenger et al., 2010). Sprenger's study showed that the difference between the two lines is generally minor. However, changes in the expression of proteins involved in the tyrosine kinase pathway and cellular cytoskeleton have been reported (Auburger et al., 2012). Therefore, accurate monitoring of passaging history is important and matched conditions should be at equal passages as possible.

To be able to use fibroblasts as a model for PD, it is crucial to demonstrate that these cells carry molecular defects that are exclusive to the patients. Fibroblasts from sporadic patients have shown an increased sensitivity towards rotenone (Ambrosi et al., 2014) and also have been reported to have a decreased microtubule mass, which was also noticed in *LRRK2* and *parkin* mutant fibroblasts (Cartelli et al., 2012). However, more interesting findings have come from patients with a familial form of PD. *Parkin* mutant fibroblasts have shown a significant mitochondrial defect in terms of function and morphology (Mortiboys et al., 2008). The decrease in ATP levels (around 60%) was mostly attributed to reduced complex I activity in these cells. Increased mitochondrial branching has also been observed in *parkin*-mutant fibroblasts (Mortiboys et al., 2008). Knocking down *parkin* in control fibroblasts produced a similar result, which confirmed that the observed defects were a result of Parkin dysfunction (Mortiboys et al., 2008). In another study, it was reported that the activity of complexes IV was reduced as well

(Pacelli et al., 2011). In contrast to these findings, Haylett and colleagues assessed mitochondrial function via measuring the oxygen consumption rate using the Seahorse XF Cell Mito Stress Test, and found an increase in mitochondrial readings in *parkin* patient fibroblasts (Haylett et al., 2016). Specifically, there was an increase in basal respiration, ATP-coupled respiration and maximal respiratory rate, suggesting elevated oxidative phosphorylation. These conflicting findings were believed to be a result of a compensatory mechanism in the fibroblasts used in the study. Zanellati and colleagues used the same method to assess mitochondrial function in *parkin* fibroblasts and found reduced ATP-coupled respiration and low total ATP levels in patient cells (Zanellati et al., 2015). Other findings include high basal respiration, high maximal respiration and an impairment of mitochondrial membrane potential, which suggests mitochondrial uncoupling (Zanellati et al., 2015). The fact that the fibroblasts in these two studies were obtained from different patients with different *parkin* mutations, and that the cell culture was performed in different types of medium, might contribute to the discrepancy between the findings.

Similarly, investigating fibroblasts from *LRRK2* G2019S patients revealed a decreased ATP level, decreased mitochondrial membrane potential and a specific reduction in the activity of respiratory chain complex IV (Mortiboys et al., 2010, Mortiboys et al., 2015, Papkovskaia et al., 2012). Mitochondrial morphology was changed in the direction of increasing interconnectivity in those fibroblasts (Mortiboys et al., 2010). Grünewald and colleagues reported similar mitochondrial defects, although the mitochondria were more fragmented in patient fibroblasts (Grünewald et al., 2014a). Interestingly, the defect was present in non-manifesting *LRRK2* carriers as well. The study of the autophagy pathway revealed an increase in the LC3-II to LC3-I ratio in the *LRRK2* G2019 patient fibroblasts, as well as an increase in the p62 levels (Grünewald et al., 2014a). Collectively, these findings suggest an increase in the mitophagy process. However, quantifying the mitochondrial protein, glucose-regulated protein 75, to assess the mitochondrial mass did not show a significant change (Grünewald et al., 2014a). Overall, the cumulative evidence confirms the presence of mitochondrial defects in the fibroblasts of familial PD patients. These results have attracted attention towards investigating PD pathology in fibroblasts, as well as using them for drug screening.

1.5 Drug discovery in Parkinson's disease

Regardless of all the discoveries in the field, PD is still an incurable disease. Dopamine replacement therapy with administration of its precursors, such as levodopa, can provide symptomatic relief of the motor deficit. As the disease progresses, the effect of the treatment usually declines. All available treatment options (whether drugs or surgeries) target only symptomatic relief and improving the quality of life of the patient, rather than slowing disease progression. The growing understanding of PD has been accompanied by increasing efforts to find a disease-modifying treatment. Research carried out in our own group demonstrated a systematic stepwise approach in searching the Microsource compound library for compounds that rescue mitochondrial function (Mortiboys et al, 2013). Importantly, the study was performed on PD patients' fibroblasts (with *parkin* mutations). This was the first compound screen performed in patient derived cells in PD. Relying on the accumulative evidence that links mitochondrial impairment to PD, the screening process aimed to identify compounds that improve mitochondrial membrane potential and increase ATP levels. After excluding compounds that showed toxicity and compounds that failed to generate a sigmoidal dose response curve, 29 positive hits remained. The screening was performed on fibroblasts obtained from two PD patients with *parkin* mutation. However, the mitochondrial rescue effect of the remaining 29 compounds was further verified in fibroblasts from two other *parkin* patients. 14 compounds failed to pass this step. Compounds known for their harmful side-effects in humans and others that have shown no neuroprotective effects in previous research were excluded. Two compounds were finally identified, which were pursued further: ursocholic acid (UCA) and dehydro (11,12) ursolic acid lactone (DUA).

Despite the substantial advances in the literature and screening technologies, the process of drug validation and approval is still long and arduous (Ciociola et al., 2014). Besides time and effort, financial impacts cannot be omitted. Establishing a novel treatment can cost up to 800 million pounds (Ciociola et al., 2014). Indeed, these expenses will have an effect on the price of the treatment, which will then be a burden on patients or health care systems. Therefore, identifying a new use for an already approved drug can significantly decrease the cost and facilitate the

availability of the treatment to the patient. With regard to the results in our group screening project (Mortiboys et al, 2013); the identified two compounds have never been used in clinical trials. However, two relatively commonly used compounds were found to be structurally very close to DUA and UCA: ursolic acid (UA) and ursodeoxycholic acid (UDCA) [Figure 1.4]. As expected, both reproduced the rescue effect observed in their corresponding compounds (Mortiboys et al, 2013). UA and UDCA also restored the ATP level in fibroblasts obtained from PD patients with manifesting and non-manifesting *LRRK2* G2019S mutation and Parkin-deficient cortical mouse neurons (Mortiboys et al., 2013, Mortiboys et al., 2015). This indicates that the response is not limited to one form of PD and that the drugs can rescue different relevant types of cells (Mortiboys et al., 2013). UA is a pentacyclic triterpenoid carboxylic acid, which is naturally present in apple peel and other fruits (Zhang et al., 2014b). UDCA, on the other hand, is a bile acid and a drug that has been approved for decades as a treatment for primary biliary cirrhosis (Zhang et al., 2013b). Therefore, the adoption of UDCA as a treatment for PD should require less time and cost in comparison to de novo drugs.

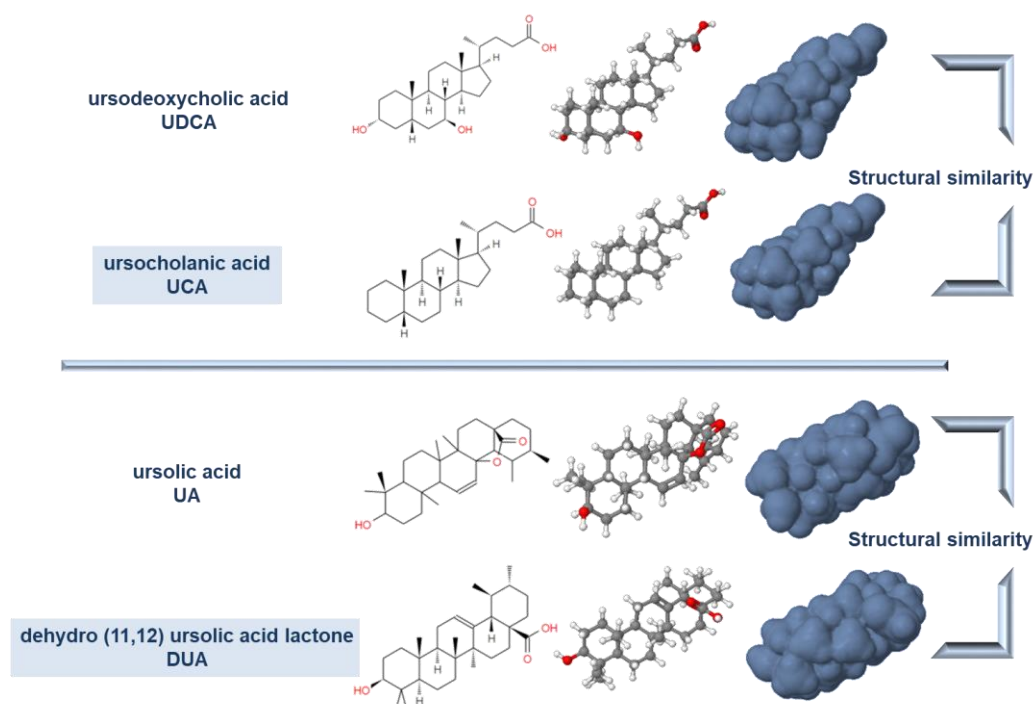


Figure 1.4 Some of the identified drugs in the Bandmann group screening project.

The figure shows the drugs (highlighted in blue) in comparison to similar compounds at structural and conformational levels (Mortiboys et al., 2013).

Abbreviations: UDCA: Ursodeoxycholic acid, UCA: Ursocholic acid, UA: Ursolic acid, DUA: Dehydro (11,12) ursolic acid lactone

1.6 Bile acids and UDCA

Bile acids (BAs) are steroid-based molecules that facilitate the digestion and the absorption of lipids in the gastrointestinal tract. BAs are primarily synthesised in the liver and are stored in the gallbladder in a concentrated form. They are secreted into the duodenum after fatty meal ingestion. The majority of BAs follow the enterohepatic circulation, through which they are absorbed and recycled (Martinot et al., 2017). There are various types of naturally occurring BAs that differ in their chemical structure and characteristics. Nevertheless, all BAs are composed of 24 carbon atoms with a steroid core.

In humans, there are two primary BAs synthesised directly by liver cells: chenodeoxycholic acid (CDCA) and cholic acid (CA) (McMillin and DeMorrow, 2016b). The synthesis starts with cholesterol molecules, which are converted into 7 α -hydroxycholesterol through the action of microsomal cytochrome P-450, CYP7A1 (also called cholesterol 7 α -hydroxylase) (McMillin and DeMorrow, 2016a) [Figure 1.5]. This compound is subsequently hydroxylated by sterol 12 α -hydroxylase or 7 α ,12 α -hydroxylase and modified by other enzymes, resulting in the formation of CDCA and CA. There is an alternative pathway for bile acid synthesis, which is facilitated by CYP27A1 (cholesterol 27-hydroxylase), and leads to the conversion of cholesterol into 27-hydroxycholesterol [Figure 1.5]. Further hydroxylation by CYP7B1 (25-hydroxycholesterol 7- α -hydroxylase), and modification by other enzymes results in the production of primary BAs, mainly CDCA (McMillin and DeMorrow, 2016a). Within the hepatocyte, taurine/glycine conjugated BAs are produced through the action of the peroxisomal enzyme bile acid coenzyme-A: amino acid N-acyltransferase (BAAT) (Martinot et al., 2017). Most of the BAs excreted from the liver are conjugated (98%); two-thirds of them are taurine conjugates, because BAAT has a higher affinity towards taurine (Martinot et al., 2017). Bile acid conjugation is important for their function. It makes the BAs more hydrophilic, which is crucial for the emulsification of lipids. In this process, the hydrophobic side of BAs is inserted into the lipid, while the hydrophilic side stays at the surface. This results in large lipid aggregates being broken down into smaller droplets that have a greater surface area. Thus, this increases the contact with the hydrophilic lipase molecules (Sarkar et al., 2016). Conjugation also ameliorates bile acid toxicity, which will be discussed in

more detail in the next section. Intestinal microbial flora play an important role in modifying BAs through de-conjugation and decarboxylation, resulting in the formation of secondary BAs, such as UDCA, deoxycholic acid (DCA) and lithocholic acid (LCA) (Camilleri and Gores, 2015). All of these can be re-circulated and/or re-conjugated via the enterohepatic circulation (Camilleri and Gores, 2015). This cycle can be repeated up to 12 times per day and, as a result, eliminates the need for daily total replacement of the bile acid pool (Ikegami and Matsuzaki, 2008). In fact, 95% of the bile acid pool is not derived from de novo biosynthesis in the liver (Ikegami and Matsuzaki, 2008).

Bile acid toxicity has been extensively studied in cholestatic diseases. Research shows that the hydrophobicity is the major determinant of the toxicity of a given bile acid. Generally, BAs are amphipathic molecules. Yet, their hydrophobicity varies according to the number, position and orientation of the hydroxyl group [Figure 1.6]. Bile acid molecules are relatively planar, with a convex face that is hydrophobic because of methyl radicals, and a hydrophilic face with hydroxyl radicals (Sarkar et al., 2016). Accordingly, tri-hydroxylated BAs are more hydrophilic than di-hydroxylated BAs. Moreover, conjugation of BAs with taurine or glycine makes them more hydrophilic. Exceptionally, UDCA has a hydroxyl group in the 7β position in an equatorial orientation [Figure 1.6]. This unique structure makes UDCA the most hydrophilic bile acid (Perez and Briz, 2009). The toxicity of hydrophobic BAs is believed to be mediated via interfering with mitochondrial physiology. Toxic BAs decrease the activity of respiratory chain complexes and increase mitochondrial membrane permeability, with consequent mitochondrial uncoupling (Perez and Briz, 2009). These events increase ROS production, which in turn can exaggerate toxicity and trigger the apoptotic pathway. There are other reported mechanisms, such as direct cellular and organelle membrane damage due to the detergent-like properties of hydrophobic BAs (Perez and Briz, 2009). The toxicity is not exclusive to liver cells, as it has been observed in placental, foetal, renal and pulmonary cells (Perez and Briz, 2009, Perez et al., 2006). On the other hand, hydrophilic BAs are cytoprotective. It has been proposed that biliary diseases arise from an imbalance between toxic and protective BAs. In line with this, treatment with the most hydrophilic bile acid, UDCA, is beneficial in biliary diseases. In fact, UDCA is the main FDA-approved

treatment for primary biliary cholangitis and primary biliary cirrhosis (Chascsa et al., 2017, FDA, 2009). Despite its established effectiveness, its main mechanism of action is still under debate.

BAs from dozens of animals have been used as remedies in traditional oriental medicines for centuries (Wang and Carey, 2014). The bile is steroidal in nature and contains different fat-soluble vitamins, which might contribute to the observed beneficial effects. Concentrated bear bile has been used in traditional Chinese medicine as a treatment for liver diseases (Wang and Carey, 2014). Interestingly, UDCA is the most abundant bile acid in bear bile (Wang and Carey, 2014). UDCA-packed tablets were commercially available in Japan in the mid-twentieth century (Hofmann and Hagey, 2014). However, it was offered as a 10mg tablet and the FDA-recommended dose is approximately 1000mg/day (13 to 15mg/kg/day). Therefore, it is most likely that patients did not benefit from the full therapeutic action of UDCA at that time. Currently, UDCA is available as 250 or 500mg tablets (FDA, 2009). Following oral intake, UDCA diffuses passively through the intestinal epithelium. The unabsorbed UDCA is dihydroxylated into LCA and excreted in the faeces. Only 50% of UDCA is uptaken from the blood by hepatocytes in healthy individuals (FDA, 2009). Normally, UDCA constitutes 3% of the bile acid pool in humans (Ikegami and Matsuzaki, 2008). Upon chronic UDCA treatment, the amount increases up to 50% (FDA, 2009). Hepatic conjugation of UDCA into more active hydrophilic BAs is highly efficient, even in cholestasis liver. Therefore, it is unnecessary to prescribe conjugated UDCA for those patients (Poupon, 2012).

UDCA-related clinical studies are mostly concerned with liver disease. Little is known about its bioavailability in the CNS. However, it has been reported that oral UDCA administration has led to an increase in its level in the cerebrospinal fluid (CSF) in a dose-dependent manner. Treating ALS patients with high doses (15mg/kg/day to 50mg/kg/day) eventually led to doubling the concentration in the CSF (140nM to 280nM). Notably, high-dose UDCA treatment was safe and tolerable in those patients (Parry et al., 2010).

The beneficial effect of UDCA has been studied extensively in the context of hepatobiliary diseases. Multiple mechanisms of action have been proposed. These can be divided broadly into two groups: the first is concerned with bile acid homeostasis and the second is concerned with a

cytoprotective effect. Within the gastrointestinal tract, UDCA can decrease the levels of toxic BAs. Conjugated UDCA competes with other endogenous toxic BAs and prevents their absorption at the distal part of the small intestine (Poupon, 2012). In addition, UDCA stimulates bile acid secretion and serves as an anti-cholestatic reagent (Poupon, 2012). Cholestasis is a well-recognised pathology in primary biliary cholangitis and primary sclerosing cholangitis, and is believed to intensify the effect of toxic BAs. UDCA acts at transcriptional and post-transcriptional levels to increase the expression of transporter proteins in the basolateral and canalicular membranes and facilitate the secretion (not synthesis) of BAs (Ikegami and Matsuzaki, 2008). Evidence suggests that UDCA and its conjugates facilitate the trafficking and insertion of transporter proteins by regulating intracellular Ca^{2+} , protein kinase C (PKC) isoforms, and cyclic adenosine monophosphate (cAMP) (Ikegami and Matsuzaki, 2008).

Within cells, evidence suggests that inhibition of apoptosis is one of the main protective effects of UDCA. UDCA and its conjugates inhibit apoptosis by preventing mitochondrial membrane perturbation, pore formation, BAX translocation, cytochrome c release, caspase activation and subsequent substrate cleavage (Amaral et al., 2009). It has also been reported that Tauroursodeoxycholic acid (TUDCA) can ameliorate ER stress by decreasing calcium efflux and caspase-12 activation (Xie et al., 2002). The shared chemical structure between BAs and steroids, as well as the shared associated anti-inflammatory responses, have led to the assumption that they both activate glucocorticoid receptors (GRs). Nuclear translocation of the GR was reported after UDCA treatment. However, several studies have shown that UDCA does not bind to the GR, indicating that there is an indirect mechanism for the activation (Hapgood et al., 2016). In addition, it has been demonstrated that UDCA activates important survival signalling pathways, such as mitogen-activated protein kinase (MAPK) and Phosphoinositide 3-kinase (PI3K) (Amaral et al., 2009). Besides the anti-apoptotic effect, UDCA has also been reported to increase cellular defence against oxidative stress. In iron-stressed HepG2 cells, UDCA treatment elevated Glutathione (GSH) levels and decreased ROS production via the activation of the nuclear factor-like 2 (Nrf2) pathway (Arisawa et al., 2009). Further validation came from experiments on mice liver cells, where UDCA significantly enhanced Nrf2 expression and

translocation into the nucleus. These results suggest that Nrf2 activation plays an important role in the mechanism of action of UDCA (Shin et al., 2013). Besides their ability to activate different signal transduction pathways, BAs bind specifically to a distinct group of receptors, such as the G-protein coupled receptor (TGR5), and nuclear receptors, such as the farnesoid X receptor, vitamin D receptor and pregnane X receptor (Martinot et al., 2017). Therefore, BAs in general are increasingly recognised as signalling molecules. Investigating the mechanism of action mediated through these receptors is currently ongoing.

Independent groups have reported the beneficial effect of UDCA/TUDCA in PD. In a rat rotenone model, UDCA treatment restored striatal dopamine content and significantly improved the behaviour in the open field test (Abdelkader et al., 2016). Pre-treatment with TUDCA also increased DA neurons by 30% in a mouse MPTP model (Castro-Caldas et al., 2012). The increase in neuron numbers was associated with an increase in TH immunofluorescence intensity and a decrease in DA fibre degeneration (Castro-Caldas et al., 2012). The effect of TUDCA on motor disability in the mouse MPTP model was extensively investigated recently (Rosa et al., 2018). The results showed that TUDCA treatment significantly improved gait quality and reduced foot dragging. Moreover, there was a reduction in PD-related manifestations, such as tremors and inability to initiate movement (Rosa et al., 2018). In these animal models, UDCA and TUDCA increased ATP levels and decreased ROS production. Proposed mechanisms of action involved the activation of the protein kinase B (AKT) pathway and the inhibition of intrinsic and extrinsic apoptotic pathways (Abdelkader et al., 2016, Castro-Caldas et al., 2012, Rosa et al., 2018). Rosa and colleagues have recently investigated the rescue effect of TUDCA in a primary culture of mice cortical neurons stressed with MPP⁺ and confirmed the positive effect on ATP, mitochondrial membrane potential, cytotoxicity and oxidative stress (Rosa et al., 2017). The results showed increased expression of peroxisome proliferator-activated receptor gamma coactivator-1alpha (PGC1 α) and Mitochondrial transcription factor A (TFAM), indicating enhanced mitochondrial biogenesis. In addition, the results suggest the involvement of autophagy and mitophagy in the mechanism of action. TUDCA induced an accumulation in mitochondrial PINK1 and Parkin, as well as an increase in LC3 lipidation (Rosa et al., 2017). Importantly, the positive effect on ATP

levels was lessened when the experiment was repeated using *parkin* knock down SH-SY5Y cells, which indicates that Parkin plays a role in the protective action of TUDCA in MPP stressed cells (Rosa et al., 2017). Parkin was also found to play a role in the TUDCA-mediated protective effect observed in CCCP stressed SY-SY5Y cells (Fonseca et al., 2017).

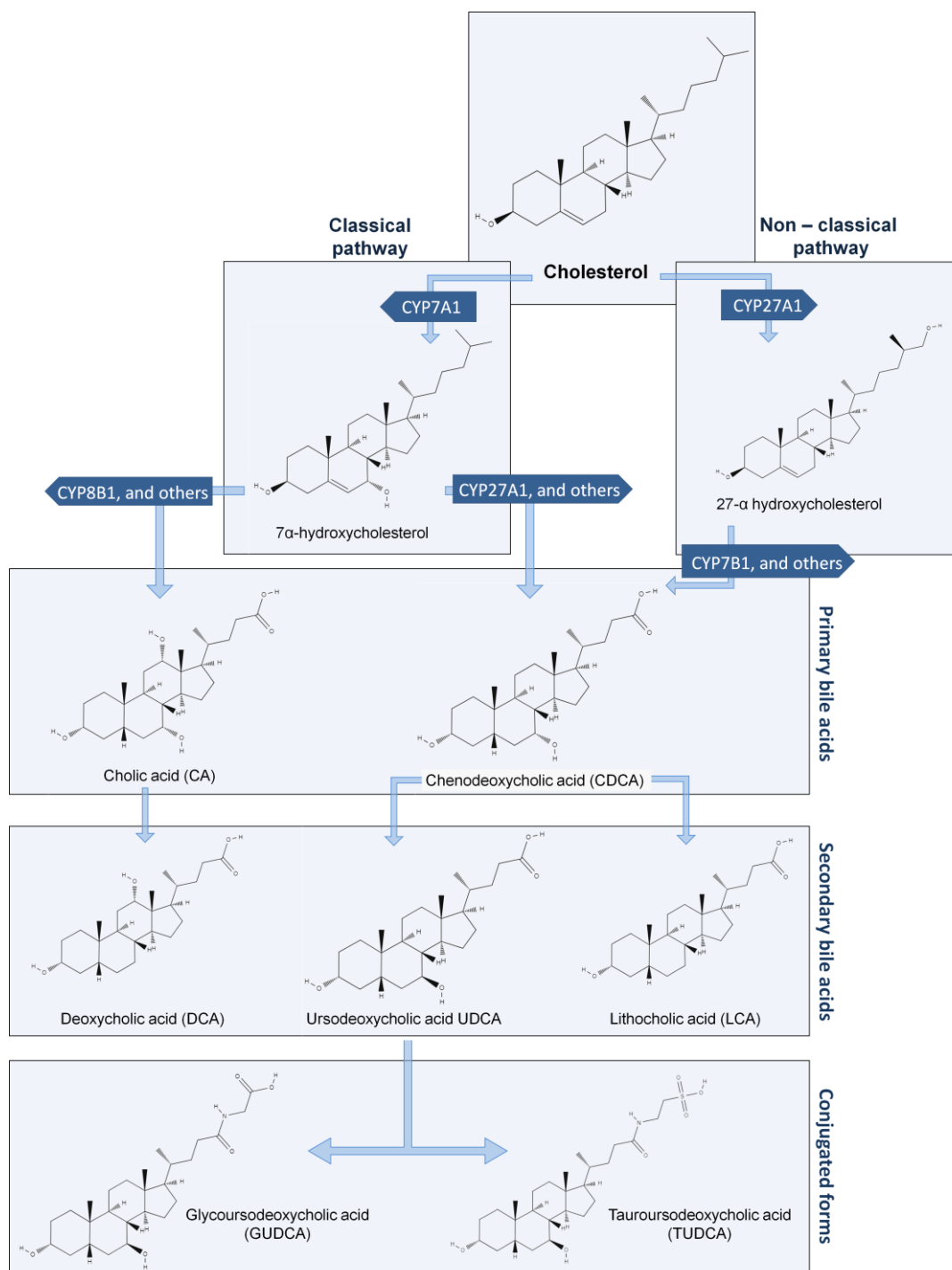


Figure 1.5 An overview of the bile acid pathway in humans.

The figure summarises bile acid synthesis pathway and shows the different forms of endogenous BAs.

Abbreviations: CYP27A1: sterol 27-hydroxylase, CYP7A1: cholesterol 7- α -monooxygenase, CYP8B1: sterol 12- α -hydroxylase, CYP7B1: oxysterol and steroid 7- α -hydroxylase.

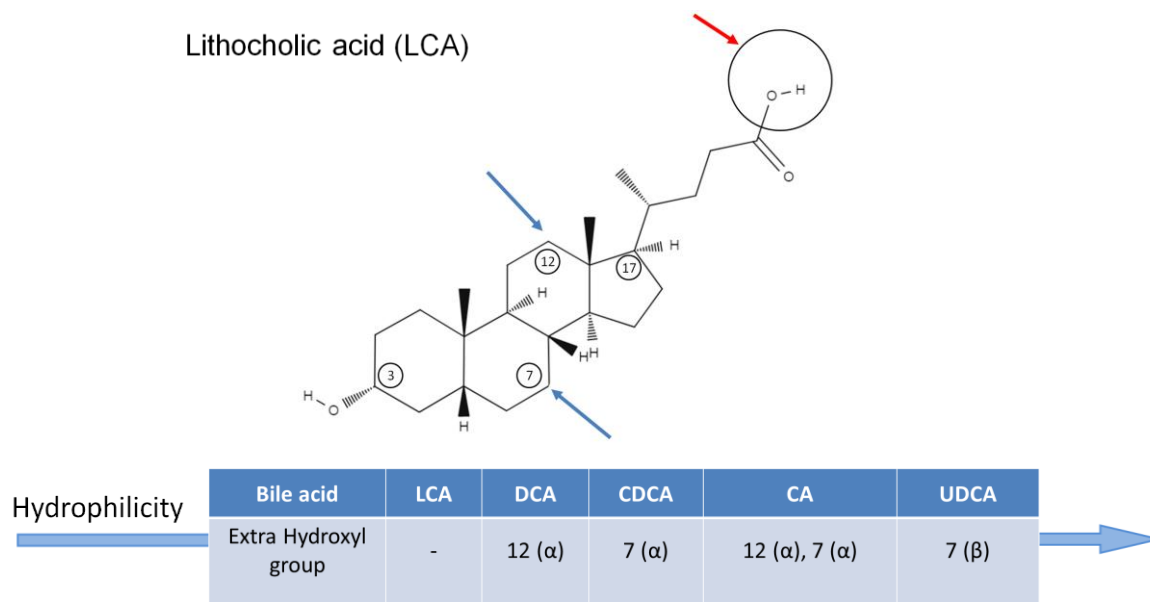


Figure 1.6 A comparison between bile acids in term of hydrophilicity.

The figure shows the chemical structure of LCA and illustrates how the addition of hydroxyl groups can change LCA into a different bile acid. Generally, the greater the number of hydroxyl groups, the greater the hydrophilicity. The only exception is for UDCA. Blue arrows indicate the site for hydroxylation. The red arrow indicates the site for conjugation with taurine/glycine, which will further increase the hydrophilicity.

Abbreviations: LCA: lithocholic acid, DCA: deoxycholic acid, CDCA: chenodeoxycholic acid, CA: cholic acid, UDCA: Ursodeoxycholic acid

1.7 Aims and objectives

In the light of the accumulative evidence of mitochondrial dysfunction in PD, the identified compounds in the screen undertaken in our group might be of significant promise as novel treatments. Although considerable work has been done to unveil the mechanism of action of UDCA in liver disease, little is known about the precise mechanisms in relation to PD. The main aim of this project is to assess and to investigate the rescue effect of UDCA in the context of PD.

Objectives:

- 1) To determine if the UDCA-mediated rescue effect is due to an increase in mitochondrial biogenesis;
- 2) To determine if treatment with UDCA activates the Nrf2 pathway and alleviates oxidative stress;
- 3) To assess the rescue effect of UDCA in human neuronal-like cell line, in which mitochondrial dysfunction was induced via the use of mitochondrial toxins;
- 4) To determine if UDCA exerts its rescue effect via AKT activation and, if so, identify AKT downstream targets.

Chapter 2. Materials and methods

2 Materials and methods

2.1 List of materials and reagents used in this project

Material	Catalogue	Company	Source
Tissue culture			
Multiwall plate for suspension culture, 24 well	662102	Greiner Bio One	Germany
CELL CULTURE MICROPLATE, 96 WELL, μ CLEAR [®] , BLACK	655090	Greiner Bio One	Germany
CELL CULTURE MICROPLATE, 96 WELL, μ CLEAR [®] , WHITE	655098	Greiner Bio One	Germany
Corning [®] 96 Well	3590	Corning	USA
CELL CULTURE MICROPLATE, 384 WELL, μ CLEAR [®] , BLACK	781091	Greiner Bio One	Germany
T75 Nunc [™] Cell Culture Treated EasYFlasks [™]	156499	Thermos Scientific	Denmark
T175 Nunc [™] Cell Culture Treated EasYFlasks [™]		Thermos Scientific	Denmark
Nunc [™] Cell Culture/Petri Dishes	150350	Thermo Fisher Scientific	Denmark
Cryovial	123263	Greiner Bio One	Germany
Countess [™] Cell Counting Chamber Slides	C10228	Thermo Fisher Scientific	USA
Haemocytometer	0640010	Marienfeld-superior	Germany
DMEM/F-12, GlutaMAX [™] supplement	10565018	Thermo Fisher Scientific	UK
Neurobasal [®] Medium	21103-049	Thermo Fisher Scientific	UK
MEM, no glutamine, no phenol red	51200046	Thermo Fisher Scientific	UK
MEM Eagle with Earle's BSS, with L-glutamine (EMEM)	BE12-611F	Lonza	Belgium
Dulbecco's Modified Eagle Medium (DMEM)	D5796	Sigma-Aldrich	USA
Glucose-free Dulbecco's Modified Eagle Medium (DMEM)	11966 - 025	Life Technologies	USA
Foetal Bovine Serum (LSP)	S-001-BR	Life Science Production	Brazil
Foetal Bovine Serum (sigma)	12105C	Sigma-Aldrich	USA
Foetal Bovine Serum (labtech)		labtech	UK
Uridine	A15227	Alfa Aesar	UK
10x trypsin	BE02-007E	Lonza	Belgium
Penicillin/Streptomycin (P/S)	DE17-603E	Lonza	Switzerland
MEM Eagle Vitamin Mixture (100X)	13-607C	Lonza	USA
Non-Essential Amino Acid Solution (NEAA) 100X	13-114E	Lonza	Belgium
Uridine	U-3003-5G	Sigma-Aldrich	USA
Sodium Pyruvate	S8636	Sigma-Aldrich	USA
D-(+)-Galactose	G5388	Sigma-Aldrich	China
2-Deoxy-D-glucose	D8375	Sigma-Aldrich	China
Retinoic acid	R2625	Sigma-Aldrich	China
N-2 Supplement (100X)	17502048	Thermo Fisher Scientific	USA
L-Glutamine (100X)	25030032	Thermo Fisher Scientific	USA

DMSO (TC)	D2650	Sigma-Aldrich	USA
Industrial methylated spirit	11442874	Fisher Scientific	UK
Drugs and toxins			
Ursocholic acid (UCA)	C7628-5G	Sigma-Aldrich	USA
Ursodeoxycholic acid (UDCA)	U5127-25G	Sigma-Aldrich	USA
Tauroursodeoxycholic acid	580549	Merck Millipore	Italy
Glycoursodeoxycholic acid	06863	Sigma-Aldrich	China
Resveratrol	R1776	LKT Laboratories	USA
Trolox	56510	Fluka	USA
BG12	242926	Sigma-Aldrich	USA
G 418 disulphate salt	A1720	Sigma-Aldrich	China
Triciribine hydrate	T3830	Sigma-Aldrich	USA
Recombinant Human IGF-I	291-G1	R&D Systems	USA
Rotenone	R8875	Sigma-Aldrich	USA
Carbonyl cyanide 4-(trifluoromethoxy)phenylhydrazone (CCCP)	C2920	Sigma-Aldrich	Israel
Antimycin A	A8674	Sigma-Aldrich	USA
Hydrogen peroxide solution	H1009	Sigma-Aldrich	Germany
Copper(II) sulphate pentahydrate	C7631	Sigma-Aldrich	USA
DMSO (anhydrous)	276855	Sigma-Aldrich	USA
Western blotting			
RIPA buffer	R0278	Sigma-Aldrich	USA
10x Protease Inhibitor Cocktail (PIC)	P8340	Sigma-Aldrich	USA
Phosphatase Inhibitor Cocktail 2	P5726	Sigma-Aldrich	USA
Coomassie protein reagent	1856209	ThermoScientific	USA
ProtoGel (30%)	EC-890	National Diagnostics	USA
TEMED	T3100	Melford	UK
Ammonium persulphate	A3678	Sigma-Aldrich	Japan
Sodium dodecyl sulphate	10090490	Fisher Scientific	UK
Isopropanol	P/7500/17	Fisher Scientific	UK
Methanol	M/4000/17	Fisher Scientific	UK
Immobilon®-P Polyvinylidene difluoride membranes (PVDF)	IPVH00010	Millipore	UK
Chromatography papers (filter papers)	3030-917	GE Healthcare	China
Precision Plus Protein™ Dual Color Standards	161-0374	Bio-Rad Laboratories	USA
Chemiluminescent reagents (EZ-ECL)	20-500-120	Biological Industries	Israel
Immunocytochemistry			
Triton™ X-100	T9284	Sigma-Aldrich	USA
Horse serum	H0146	Sigma-Aldrich	USA
Paraformaldehyde	P6148	Sigma-Aldrich	USA
RT-PCR			
Hard-Shell® 96-Well PCR Plates	HSP9635	Bio-Rad Laboratories	USA
Microseal® 'C' PCR Plate-Sealing Film	msc1001	Bio-Rad Laboratories	USA
Brilliant III Ultra-Fast SYBR	600882	Agilent Technologies	USA
DNase/RNase-Free Distilled Water	10977035	Thermo Fisher Scientific	UK
Cellular fractionation			
Sucrose	S0809	Melford	UK
D-Mannitol	A14030	Alfa Aesar	UK
HEPES Buffer, 1M Solution	BP2991	Thermo Fisher Scientific	USA

0.5M EDTA	1861275	Thermo Fisher Scientific	USA
DTT	R0861	Thermo Fisher Scientific	USA
Ultra-Clear Tube (5ml)	344057	Beckman	USA
Others			
DCF	C2938	Thermo Fisher Scientific	USA
Trypan Blue Solution, 0.4%	15250061	Thermo Fisher Scientific	USA
TWEEN 20	233360010	Acros Organics	USA
Phospho-AKT (Ser473) Blocking Peptide	1140	Cell Signalling Technology	USA
Minisart® NML Syringe Filter, 0.45µm	16555	sartorius	Germany
Bovine serum albumin (BSA)	EQBAH	Europa Bioproducts	UK
Sodium azide	S8032	Sigma-Aldrich	Germany
TRIS	B2005	Melford	UK
Glycine	G0709	Melford	UK
Sodium chloride	11904061	Fisher Scientific	UK

2.2 Cell lines

The fibroblasts were either obtained from Coriell/Rudgers Cell repository (<https://www.coriell.org/>, <https://nindsgenetics.org/>), or from the Sheffield-based clinic. Fibroblast details are listed in Table 2.1. Coriell/Rudgers fibroblasts are covered by the research agreement and Material Transfer Agreement (MTA) between the repository and Dr Heather Mortiboys at the University of Sheffield. Sheffield-based fibroblasts are covered by the local ethics committee under Sheffield Teaching Hospitals (STH) ethics number 16350. The two types of Chinese hamster ovary (CHO) cells, ARE-TK-GFP and TK-GFP reporter constructs, were a kind gift from Dr Richard Mead from the Sheffield Institute for Translational Neuroscience; the SH-SY5Y cells were a kind gift from Dr Adrian Higginbottom from the Sheffield Institute for Translational Neuroscience.

Table 2.1 Information on patient and control fibroblasts

Sample ID	Case	Age	Gender	Mutation	Source
OB064	control	67	male	-	Sheffield based
ND37731	<i>parkin</i>	64	female	40bp deletion in exon3; unspecified deletion in exon 3 and 4	Coriell/Rudgers Institute
ND30171	<i>parkin</i>	46	male	ARG42PRO	Coriell/Rudgers Institute
ND31618	<i>parkin</i>	63	female	ARG42PRO	Coriell/Rudgers Institute
GM07924	control	63	male	-	Coriell/Rudgers Institute
GM23967	control	52	male	-	Coriell/Rudgers Institute
GM02189	control	63	male	-	Coriell/Rudgers Institute

2.3 Tissue culture

2.3.1 Growing cells

The handling of the cells was performed under sterile conditions inside a class II biohazard cabinet. For optimum growth rate, the cells were fed with 10ml of cultured medium, replenished every two days [Table 2.2]. The cells were kept at 37°C in 5% CO₂ in air (the default cell incubating setting in this project). Fibroblasts were grown in T75 flasks, whereas CHO cells and SH-SY5Y were grown in 10 cm petri dishes. The medium was replaced every two to three days and the cells were tested for mycoplasma infections initially upon defrost and, subsequently, every two weeks. The galactose medium was prepared using glucose-free Dulbecco's Modified Eagle Medium (DMEM) supplement with galactose (at final concentration of 5mM) plus the other additives listed in Table 2.2.

Table 2.2 Contents of the prepared cultured medium for different types of cells

Constituent	concentration	Fibroblast	CHO	SH-SY5Y
Dulbecco's Modified Eagle's Medium (DMEM)	1x		√	√
MEM Eagle with Earle's BSS, with L-glutamine (EMEM)	1x	√		
Foetal Bovine Serum (sigma)	10% (v/v)		√	
Foetal Bovine Serum (labtech)	10% (v/v)	√		
Foetal Bovine Serum (LSP)	10% (v/v)			√
Penicillin/Streptomycin (P/S)	1% (v/v)	√	√	√
Sodium Pyruvate	1% (v/v)	√		
Uridine (50mg/ml solution)	0.1% (v/v)	√		
Non-Essential Amino Acid Solution (NEAA) 100X	1% (v/v)	√		
MEM Eagle Vitamin Mixture (100X)	1% (v/v)	√		

2.3.2 Collecting and passaging the cells

Cells were passaged when they had reached approximately 80–90% confluence, which was estimated through inspecting different areas of the flask/dish under a brightfield optic microscope at 10x objective. To passage the cells, the 10ml medium in the flask/dish was removed and they were washed with 5ml of phosphate buffered saline (PBS). Then the cells were trypsinised with 5ml of 1x trypsin, for approximately five to six minutes inside the incubator. A light tap on the side of the flask/dish ensured that most of the cells were detached from the floor, which was confirmed under the microscope. Subsequently, the removed medium was transferred back to the flask/dish to deactivate the trypsin. The mix in the flask/dish was then transferred into a 15ml falcon tube and centrifuged at 400rcf (brake 9, acceleration 9) for four minutes in a benchtop centrifuge (MSE – Harrier 15/80). The supernatant was aspirated and discarded and the cell pellet was re-suspended in an appropriate amount of corresponding culture medium. Fibroblasts were split into three new T75 flasks pre-loaded with 9ml of culture medium. CHO and SH-SY5Y cells were split into four new dishes pre-loaded with 9ml of culture medium. Unused cells and contaminated plasticware were disinfected and discarded according to the department protocol for biosafety.

2.3.3 Cryopreservation

A stock of live cells was made by storing early passages in liquid nitrogen. The harvested centrifuged cell pellet was re-suspended in 1ml of freezing-down medium (contents: culture medium, PBS and dimethyl sulfoxide (DMSO), in a volume ratio of 8:1:1, respectively). The re-suspended cells were split into two cryovials and cooled gradually to -80°C using alcohol-free cell freezing containers. Then, the cryovials were immersed in liquid nitrogen for long-term storage.

2.3.4 Pelleting cells

Cells to be used for DNA, RNA or protein extractions were pelleted and stored at -80 °C until needed. The cells were harvested and centrifuged as described before. The supernatant was then discarded. Then, the cell pellet was re-suspended in 1ml PBS to dilute any remnants of culture medium. The PBS-cell mix was transferred into a 1.5 Eppendorf, centrifuged at 400 rcf and the cell pellet was stored at -80°C after removing the supernatant.

2.3.5 Counting cells

A haemocytometer was used to estimate the concentration of cells suspended in the culture medium. 10 μ l of the suspension was pipetted onto one side of the haemocytometer. The chamber was examined by an optic microscope under 10x objective. The cells were counted in the four corner squares and the average was multiplied by 10⁴ to express the density as cells/ml. The chamber and the coverslip were then cleaned with 70% alcohol before and after every use. The required amount of medium was added to the cell suspension to reach the desired concentration using the formula: total cell count = cell concentration (cells/ml) x total volume of the suspension (ml). The cells were plated in a specific volume and density according to the design of the experiment.

2.3.6 Drugs and toxins

Drugs and toxins were prepared from their solid powders and were dissolved in anhydrous DMSO, except for CCCP, which was prepared in ethanol. Stock concentrations were prepared according to the following formula: concentration in mol/L [Molar or M] = (mass of solute in grams/ volume of solution in litres) x (1/ molecular weight in g/mol). The prepared drugs and toxins were either stored in oxygen and a moisture-free MultiPod storage system, or were aliquoted and stored at -80°C in order to avoid the thaw freeze cycle. The final concentrations of the drugs, as well as the type of containing medium were determined according to the design of the experiment. The dilution of stock concentration was performed according to the following formula: concentration of the stock solution x volume to be removed from stock solution = final concentration of the diluted solution x final volume of the diluted solution. Vehicle backfill was applied when the experiments required different concentrations and volumes of the tested drug to ensure that all conditions contained equal volumes of the vehicle. The application of the drugs was performed either manually or by the use of the ECHO 550 liquid handler (Labcyte).

2.3.7 Differentiation of SH-SY5Y cells

SH-SY5Y cells were plated in a 96-well plate or a 24-well plate, according to the design of the experiment, in regular SH-SY5Y culture medium [Table 2.2]. The cells were allowed to grow to reach 60% - 70% confluence before starting the differentiation protocol. At the first day of differentiation (day 0), the culture medium in the wells was completely replaced by an equal

volumes of the differentiation medium. Subsequently, only half of the volume of the differentiation medium in each well was replaced every two days. At day 14, drugs/toxins were added according to the design of the experiment. The differentiation medium constitutes of 50% volume Neurobasal® Media, 50% volume DMEM/F-12, GlutaMAX™ supplement, retinoic acid (RA) (10 µM), N-2 supplement (1X) and L-glutamine (1X). RA stock was aliquoted and kept in dark at -20°C, and was added to the prepared differentiation medium at the time of medium replacement.

2.4 Western blotting

2.4.1 Cell lysis

The stored frozen cell pellet from a T75 flask or a 10 cm dish was defrosted on ice and was lysed in a mixture of 44.5µl of RIPA buffer, 5µl of 10x Protease Inhibitor Cocktail and 0.5µl of Phosphatase Inhibitor Cocktail2. The cells were vortexed for 30 seconds to homogenise the suspension, kept on ice for 30 minutes and then centrifuged at 13,000 rpm for 30 minutes at 4°C. The protein-rich supernatant was then transferred into a new 1.5ml Eppendorf tube and the pellet of cellular debris was discarded. Protein extracts were kept on ice at all times.

2.4.2 BSA assay

To prepare the standard curve, 5µl of increasing concentrations of Bovine serum albumin (BSA) were pipetted into wells pre-loaded with 250µl of Coomassie protein reagent [Figure 2.1]. 5µl of diluted samples (1:10 in H₂O) were also added to other wells pre-loaded with 250µl of Coomassie. All conditions were prepared in triplicate using a clear 96 well plate (Corning® 96 Well). Protein absorbance was measured immediately using a Pherastar plate reader at a wavelength of 620nm (BMG Labtech). Microsoft Excel was used to calculate the protein concentration according to the linear regression analysis of the standards [Figure 2.1]. Once the concentration of the sample was calculated, the sample was diluted in H₂O to reach 2 µg/µl, and was then mixed with an equal volume of Laemmli buffer 2x (4% Sodium dodecyl sulphate (SDS), 20% glycerol, 10% 2-mercaptoethanol, 0.004% bromophenol blue and 0.125 M Tris HCl; PH6.8) to yield a final concentration of 1 µg/µl. Aliquots of the Protein-Laemmli mix were frozen at -80°C until needed.

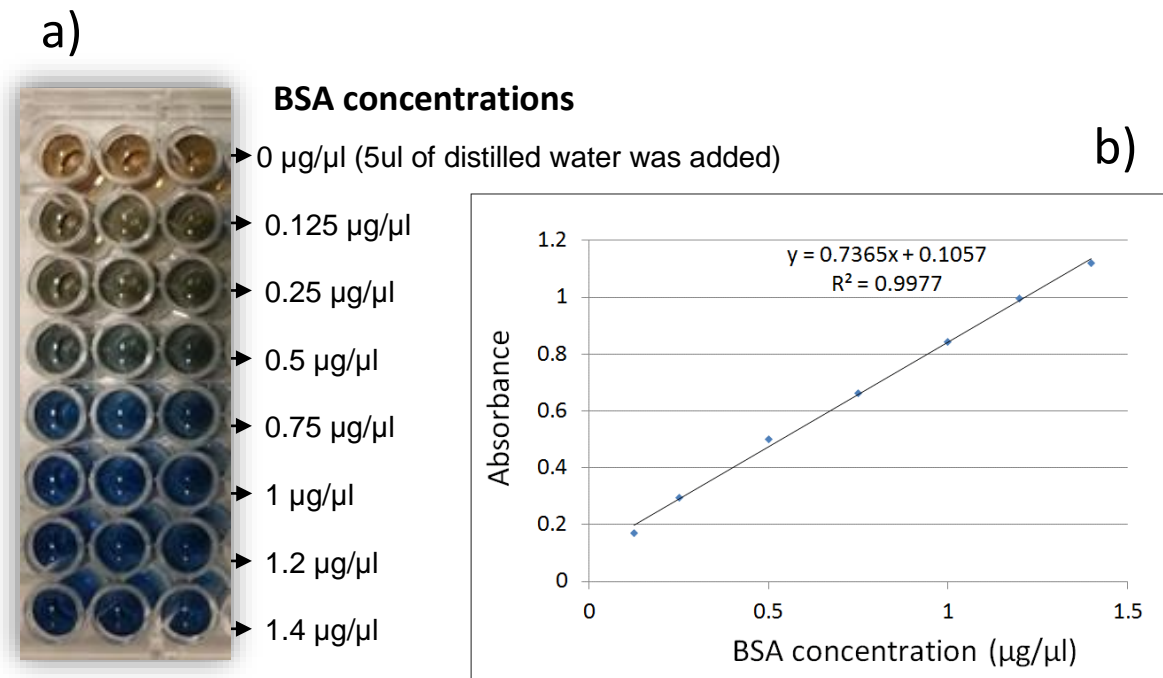


Figure 2.1 BSA assay for quantification of protein concentration.

(a) An image of a plate loaded with increasing concentrations of BSA to serve as standards. (b) The absorbance readings were plotted at the y axis against the concentrations of the standards. The obtained linear equation was then used to calculate the concentration of the protein sample.

2.4.3 Gel electrophoresis and transfer

SDS-PAGE was performed using the Mini-Protean Tetra Cell apparatus (Bio-Rad). The resolving gel solution (12%) was swiftly pipetted in between the 1.0 mm or 1.5 mm glass plates, leaving enough space for the stacking gel. A layer of isopropanol was added to eliminate any bubbles that might have formed while filling the casting cassette, and to prevent evaporation during the polymerisation process. The resolving gel was left to polymerise for 15 minutes, then the isopropanol layer was removed. The stacking gel was then swiftly pipetted into the remaining space and a suitable comb was inserted. The stacking gel was then left to polymerise for 15 minutes. The residual stacking and resolving gel solutions in the tubes were used as indicators to confirm gel polymerisation. The components of stacking and resolving gel are listed in Table 2.3. The gel-containing glass plates were then transferred into a gel holder assembly to form a closed inner compartment. The assembly was placed inside a tank and filled with running buffer (tank buffer) [Table 2.4]. Then the comb was carefully removed and the lanes were cleaned of any gel fragments by forceful repetitive pipetting to the side of the lanes. 5µl of Precision Plus

Protein™ ladder was loaded into the first lane. The protein samples were boiled at 95°C for two minutes before loading them into the gel (20 µg/lane). In order to run the sample through the stacking gel, a required voltage of 50V was applied for approximately 30 minutes. Then, the voltage was increased to 120V until sufficient separation of the ladder bands was seen, depending on the proteins to be separated.

Following electrophoresis, the gel was extracted and the stacking gel segment was removed. The gel was equilibrated in a tray filled with the transferring buffer [Table 2.4] and 10% (V/V) methanol. A proper size polyvinylidene fluoride (PVDF) membrane was activated in 100% methanol for 15 seconds (to facilitate the protein transfer) before being soaked in the transferring buffer. The transfer assembly was arranged in the transfer buffer-containing tray in the following order: sponge, filter paper, PVDF membrane, gel, filter paper, sponge. The transfer assembly was placed in a tank filled with transfer buffer. The tank was connected to a power pack with the right polarity orientation and the transfer was performed under a running current of 250 mA for 60 minutes. An ice pack was placed inside the tank to avoid overheating. Alternately, the transfer could be performed overnight under a running current of 40 mA at 4°C. Afterwards, the PVDF membrane was stained with Ponceau to confirm the transfer of the proteins. The Ponceau was washed with Tris-buffered saline with Tween 20 (TBST) [Table 2.4]. The membrane was subjected to 5% of Non-Fat Dry Milk (in TBST) at room temperature for 1 hour to block non-specific binding sites. Then the membrane was probed with the primary antibody.

Table 2.3 Components of stacking and resolving gel

	Components	Volume (μ l)
Stacking gel	30% acrylamide	600
	Tris in H ₂ O, 1.5M, pH6.8	888
	H ₂ O	2000
	TEMED	10
	10% APS	56
(12%) Resolving gel	30% acrylamide	4000
	Tris in H ₂ O, 1.5M, pH8.8	2500
	H ₂ O	3300
	10% SDS	100
	TEMED	4
	10% APS	100

Table 2.4 Buffers used in Western blotting (all made in H₂O)

Constituent	Tank buffer	Transfer buffer	TBST (pH 7.5)
TRIS	25mM	25mM	20mM
glycine	190mM	192mM	
SDS	3.5mM		
NaCl			150mM
tween20			0.1% (v/v)
methanol		20% (v/v)	

2.4.4 Probing and imaging

Primary and matched Horseradish peroxidase (HRP)-conjugated secondary antibodies were prepared in 5% of Non-Fat Dry Milk (in TBST) and were applied as shown in Table 2.5. Following the application of each antibody, the membrane was subjected to 3 x five-minute washes with TBST. For imaging purposes, equal volumes of chemiluminescent reagents A and B were mixed and kept in the dark for five minutes. Then, the mixture was evenly distributed over the membrane and kept in the dark for one minute. The G-Box chemi system (Syngene) was used to visualize the blot using the intellichemi mode. The size of the target proteins was estimated according to

the positions of the ladder bands. Following the imaging, the membrane was stored in TBST at 4°C. If the membrane was planned to be probed with a different antibody, a mild stripping was performed by soaking the membrane in the stripping solution (10µl 0.1% Sodium azide (in PBS) + 10ml 5% of Non-Fat Dry Milk (in TBST)) for at least six hours at 4°C. All equipment used in western blotting (WB), including the glass plates, were washed and cleaned before and after every use.

Table 2.5 Antibodies used in western blotting

Antibody type	Target	Catalogue number	Company	Dilutions	Application	Host
Primary	Total OXPPOS Human Antibody Cocktail	ab110411	Abcam	1:500	Overnight at 4°C	Mouse
Primary	Tyrosine Hydroxylase	ab112	Abcam	1:1000	Overnight at 4°C	Rabbit
Primary	Tom20	sc-11415	Santa Cruz	1:1000	Overnight at 4°C	Rabbit
Primary	Tom20	612278	Biosciences	1:1000	Overnight at 4°C	Mouse
Primary	NDUFA2	ab129752	Abcam	1:1000	Overnight at 4°C	Rabbit
Primary	Tim23	611223	Biosciences	1:1000	Overnight at 4°C	Mouse
Primary	Hexokinase	sc-374091	Santa Cruz	1:1000	Overnight at 4°C	Mouse
Primary	AKT	9272	Cell signalling	1:1000	Overnight at 4°C	Rabbit
Primary	pAKT	4060	Cell signalling	1:500	Overnight at 4°C	Rabbit
Primary	pAKT	MA1-20325	Thermofisher	1:500	Overnight at 4°C	Mouse
Primary	CREB	9104	Cell signalling	1:1000	Overnight at 4°C	Mouse

Primary	Phospho-CREB (Ser133)	9198	Cell signalling	1:1000	Overnight at 4°C	Rabbit
Primary	FoxO1	14952	Cell signalling	1:250	Overnight at 4°C	Mouse
Primary	Phospho-FoxO1 (Ser256)	9461	Cell signalling	1:1000	Overnight at 4°C	Rabbit
Primary	mTOR	4517	Cell signalling	1:1000	Overnight at 4°C	Mouse
Primary	Phospho-mTOR (Ser2448)	5536	Cell signalling	1:1000	Overnight at 4°C	Rabbit
Primary	β-actin	ab8227	Abcam	1:5000	Overnight at 4°C	Rabbit
Primary	GAPDH	CB1001	Millipore	1:5000	Overnight at 4°C	Mouse
Primary	GAPDH	2118	Cell signalling	1:5000	Overnight at 4°C	Rabbit
Primary	α-tubulin	62204	Thermofisher	1:5000	Overnight at 4°C	Mouse
Secondary	HRP Conjugate Anti-mouse	170-6516	Bio-Rad	1:5000	1 hour at room temperature	Goat
Secondary	HRP Conjugate Anti-rabbit	170-6515	Bio-Rad	1:5000	1 hour at room temperature	Goat

2.4.5 Quantitative analysis

Image analysis was performed using Geni Tool software (Syngene). The data obtained by the densitometric analysis were further processed by Microsoft Excel to normalise the values against the housekeeping gene and the untreated control.

2.5 Immunocytochemistry

2.5.1 Plating

Cells were plated either in a black 96-well plate or in a black 384-well plate. The cells were seeded at various densities according to the design of the experiment.

2.5.2 Fixation

Following drug/toxin treatment, the plated cells were washed once with PBS to remove any trace of medium, incubated with 4% paraformaldehyde (PFA) (in PBS) at room temperature for 30 minutes and then washed again with PBS. For SH-SY5Y, an alternative fixation method was used to reduce the detachment of the cells during the washing steps. In this method, half of the volume of the medium in the well was replaced with 4% PFA and the plate was kept in the incubator for 15 minutes. Then, the medium-PFA mixture was removed and the cells were covered with 4% PFA for 15 minutes at room temperature. The fixed cells were either stored at 4°C in PBS for a few days or in 0.1% sodium azide solution (in PBS) for up to four weeks.

2.5.3 Antibody staining

To prepare the fixed cells for immunostaining, they were first incubated in 0.1% of Triton X-100 (in TBST) at room temperature for ten minutes. Then, the Triton X-100 was removed and was followed by 3 x five-minute washes with TBST. The cells were blocked with 5% horse serum (in TBST) at room temperature for 60 minutes. Following the application of the primary antibody [Table 2.6], the cells were washed with TBST (3 x five minutes). Then, an appropriate fluorochrome-conjugated secondary antibody was applied for one hour [Table 2.6], and the cells were washed with TBST (3 x five minutes).

Table 2.6 Antibodies used in immunocytochemistry

Antibody type	Target	Catalogue number / company	Dilution	Application	Host	Alexa-flour
Primary	MAP2	M4403 / Sigma-Aldrich	1:1000	Overnight at 4°C	Mouse	-
Primary	FOXA2	ab108422 / abcam	1:500	Overnight at 4°C	Rabbit	-
Primary	Beta III Tubulin Antibody (TuJ1)	AB9354 / Millipore	1:1000	Overnight at 4°C	Chicken	-
Primary	Cleaved Caspase-3	9661 / Cell signalling	1:1000	Overnight at 4°C	Rabbit	-
Primary	AKT	9272 / Cell signalling	1:1000	Overnight at 4°C	Rabbit	-
Primary	pAKT	4060 / Cell signalling	1:250	Overnight at 4°C	Rabbit	-
Primary	CREB	9104 / Cell signalling	1:1000	Overnight at 4°C	Mouse	-
Primary	Phospho-CREB (Ser133)	9198 / Cell signalling	1:1000	Overnight at 4°C	Rabbit	-
Primary	FoxO1	14952 / Cell signalling	1:500	Overnight at 4°C	Mouse	-
Primary	Phospho-FoxO1 (Ser256)	9461 / Cell signalling	1:1000	Overnight at 4°C	Rabbit	-
Primary	mTOR	4517 / Cell signalling	1:1000	Overnight at 4°C	Mouse	-
Primary	Phospho-mTOR (Ser2448)	5536 / Cell signalling	1:1000	Overnight at 4°C	Rabbit	-
Primary	Tom20	612278 / Biosciences	1:1000	Overnight at 4°C	Mouse	-
Primary	Tom20	sc-11415 / Santa Cruz	1:1000	Overnight at 4°C	Rabbit	-
Secondary	Anti – mouse	A21202 / Life Technologies	1:1000	1 hour at room temperature	Donkey	488
Secondary	Anti – mouse	A11001 / Life Technologies	1:1000	1 hour at room temperature	Goat	488
Secondary	Anti – rabbit	A21428 / Life Technologies	1:1000	1 hour at room temperature	Goat	555
Secondary	Anti – chicken	A11039 / Life Technologies	1:1000	1 hour at room temperature	Goat	488

2.5.4 Nuclear staining and imaging

The cells were stained with Hoechst (10 μ M final concentration) for ten minutes at room temperature. Then, the cells were washed once with TBST and were kept in the dark at 4°C. The images were captured by the Opera Phenix confocal microscope (PerkinElmer) using 40x Objective Magnification and three channels with different excitation/emission wavelengths (Alexa 488: ex488/em522, Alexa 568: ex561/em599 and DAPI: ex405/em456). 20 fields per well were imaged. For each field, at least eight image planes were captured (to produce an image stack), and the maximum projection images were used in the analysis. Image analysis was performed using Harmony high-content analysis software. For the CHO-AKT experiments [Heading 6.2.2], the imaging was performed using confocal microscopy (Leica) (63x Objective Magnification, Leica/Alexa 555 and Leica/DAPI channels, 20 fields per well. For each field, 15 image planes were captured (to produce an image stack) and the maximum projection of the images was used in the analysis). The images were then analysed using ImageJ software. The IN Cell Analyser 2000 (GE Healthcare) was used to count the cell number in the DCF experiments (2x Objective Magnification, DAPI: ex350/em455) [Heading 4.3]. The In Cell Developer Toolbox 1.9 software was used to analyse the images and to calculate the total number of nuclei per well.

2.6 Quantitative real-time PCR

2.6.1 DNA extraction

DNA extraction was performed using a DNA extraction kit from Qiagen (DNeasy Blood & Tissue Kit # 69504, UK). The kit contains a buffer system that is optimised to allow direct cell lysis, which is followed by selective binding of DNA (nuclear and mitochondrial) to the DNeasy membrane. The DNeasy procedure efficiently recovers DNA fragments as small as 100 bp.

DNA extraction was performed according to the manufacturer's manual. The frozen cell pellet was equilibrated to room temperature before it was re-suspended in 200 μ l PBS, 200 μ l buffer AL (provided with the kit) and 20 μ l of proteinase k (provided with the kit). These volumes are adequate to lyse a maximum of 1x10⁷ cells. The cell suspension was mixed thoroughly through vortexing and the cells were lysed for 10 minutes at 56°C. Then, the lysate was mixed with 200 μ l of 100% ethanol through vortexing. The mix was transferred into a DNeasy Mini spin column,

placed in a 2ml collection tube (provided with the kit) and centrifuged at 6,000 x g for one minute. Ethanol and salts are used in the DNA extraction to precipitate the DNA and to prevent it from dissolving in the water. The collection tube, which contained the flowthrough of different cell components, was discarded. The spin column, which had the DNA trapped within the DNeasy membrane, was placed into a new 2ml collection tube. Then, it was subjected to two washing steps to remove the remaining contaminants and enzyme inhibitors. First, 500µl of buffer AW1 (provided with the kit) was added and the Mini spin column was centrifuged at 6,000 x g for one minute. Then, the Mini spin column was loaded with 500µl of buffer AW2 (provided with the kit) and centrifuged at 20,000 x g for 3 minutes. To elute the DNA, the spin column was placed in a 1.5ml Eppendorf, loaded with 200µl of buffer AE (provided with the kit), incubated for one minute at room temperature and centrifuged at 6,000 x g for a further minute. The extracted DNA was then stored at -20°C.

2.6.2 RNA extraction

RNA extraction was performed using a RNA extraction kit from Qiagen (RNeasy Mini Kit # 74104, UK). As with the DNA extraction kit, the RNA extraction is also based on the selective binding properties of a silica-based membrane and the speed of the microspin. The lysis buffer contains a highly denaturing guanidine-thiocyanate, which immediately inactivates RNases to preserve the integrity of the RNA. The system allows the purification of RNA molecules that are longer than 200 nucleotides and up to 100 µg. With the exception of mRNA, most RNAs are less than 200 nucleotides. Therefore, this kit provides an enrichment for mRNA, which makes it suitable for gene expression studies.

RNA extraction was performed according to the manufacturer's manual. The frozen cell pellet was equilibrated to room temperature before it was re-suspended in 600µl of buffer RLT (provided with the kit). This volume is adequate to lyse a maximum of 1×10^7 cells. Following vortexing, an equal volume of 70% ethanol (in H₂O) was added and mixed well through repetitive pipetting. Then 700µl of the mix was transferred into an RNeasy Mini spin column, placed in a 2ml collection tube (provided with the kit), and centrifuged at 8,000 x g for 15 seconds. The flowthrough was discarded and the remainder of the lysate was loaded into the same RNeasy Mini spin column

and re-centrifuged to accumulate the RNA in the membrane. Afterwards, the Mini spin column was placed in a new 2ml collection tube and was subjected to a series of washing steps to remove contaminants from the RNA. First, the Mini spin column was loaded with 700µl of buffer RW1 (provided with the kit) and centrifuged at 8,000 x g for 15 seconds. Then, 500µl of buffer PRE (provided with the kit) was loaded and centrifugation was repeated. Afterwards, 500µl of PRE was loaded and centrifugation was performed at 8,000 x g for two minutes. The Mini spin column was centrifuged for one minute at full speed at the end of the washing steps in order to dry the membrane. In order to elute the RNA, 30µl of RNase-free water was loaded and the Mini spin column was centrifuged at 8,000 x g for one minute. The extracted RNA was kept on ice and stored at -80°C.

2.6.1 Quality control

Qualitative and quantitative analysis of the extracted DNA and RNA were performed using a spectrophotometer (#ND-1000, NanoDrop, Wilmington, DE). Prior to loading the sample, the machine was calibrated using the media in which the DNA/RNA was eluted (buffer AE, RNase-free water, respectively). The ratios of A260/A230 and A260/A280 were used for qualitative assessment. The purity of the DNA samples was accepted when the values of A260/A280 and A260/A230 were at least 1.8 and 2, respectively. For RNA, the accepted value of A260/A280 was at least 2. The measurement of absorbance at these wavelengths is based on the fact that all nucleotides have absorbance maxima at 260, while proteins have absorbance maxima at 280. Other contaminants also absorb at 230; therefore, A260/A230 ratio was used as a secondary measure of nucleic acid purity. In comparison to DNA, RNAs are expected to have a higher 260/280 ratio because they have a higher uracil/thymine ratio.

2.6.2 cDNA synthesis

The superscript iii kit (#11752050, Thermo Fisher Scientific, USA) was used to synthesise cDNA for the subsequent qPCR. The reaction mix of 20µl/tube was prepared as follows: 10µl of 2x RT reaction mix, 2µl of RT enzyme mix, 1 µg of RNA sample and an adequate volume of DEPC-treated water to reach a total of 20µl (all provided with the kit). The required volume of the RNA sample to reach 1 µg was calculated according to the concentration obtained by spectrophotometry. Reverse transcriptase negative control was prepared by adding DEPC-

treated water instead of the sample. The sample and the RT mix were kept on ice at all times. The reaction was performed in accordance with the manufacturer's manual using G-Storm GS2 Multi Block Thermal Cycler (G-Storm): 25°C for ten minutes, 50°C for 30 minutes, and 85°C for five minutes. To eliminate remnant RNA in the mix, 1µl of Halics RNase (provided with the kit) was added and the mix was incubated at 37°C for 20 minutes. The synthesised cDNA was stored at -20°C.

2.6.3 qPCR reaction

UCSC Genome Browser and primer-BLAST tool were used to find and to design the primers used in this project [Table 2.7]. Using a 5µM stock, various concentrations of the forward/reverse primer were tested in order to find the optimum combination. The final tested concentrations in the qPCR reaction were (expressed in nM): F 150/R 150, F 150/R 300, F 300/R 150, F 300/R 300, F 300/R 600, F 600/R 300, F 600/R 600. Relative DNA quantification was performed using the CFX96 Touch™ Real-Time PCR Detection System (Bio-Rad). The content of each well of the 96-well PCR plates was prepared via mixing the following: 10µl of SYBR mix, 1µl of F primer (5µM stock), 1µl of R primer (5µM stock), 7µl of DNase/RNase-Free Distilled Water and 1µl of the DNA/cDNA sample. The qPCR plate was kept on ice during the loading and was sealed with plate-sealing film before it was loaded into the qPCR machine. The PCR programme was: 95°C for ten minutes; 95°C for 30 seconds; 62°C for one minute; plate read. The cycle was repeated 40 times. At the end, a melt curve was performed by monitoring loss of fluorescence signal after ten-second incubation steps, rising from 65 °C to 95 °C in 0.5 °C increments.

Five times of ten-fold serial dilution of an undiluted control sample was used to generate a standard curve for each primer to assess the efficiency. The loading of the samples, qPCR negative controls and/or reverse transcriptase negative control were done in triplicates. Since the amount of the loaded sample should double with every cycle, the C_t value of the prepared serial dilution is expected to be 3.3 cycles apart. The negative controls should have no signals below 35 cycles to exclude contamination. The cycle threshold was set to be within the straight line stretch in the log phase. A cycle threshold of 2,000 was set as standard for all qPCR reactions. When the standard dilutions were plotted, the efficiency was calculated

according to the slope of the linear regression. The efficiency indicates accurate dilution and pipetting but it is also affected if the primer design is not optimal. The accepted efficiency range was 90–110%. Following the qPCR, melt curve analysis was performed to assess the reaction specificity. The presence of a single peak or a single shoulder in the melting peak or the melting curve graphs indicates high specificity, which implies that the reaction leads to the amplification of only a specific sequence in the mix. The melting temperature, where most of the signal loss occurs, should match the expected melting point of the used primers.

The drug-induced expression of the gene of interest was assessed relatively by calculating the fold change in treated samples in comparison to the untreated ones using GAPDH as a loading control. The relative quantification of mtDNA was based on the fact that cells have multiple copies of mtDNA and only two copies of nuclear DNA. The mtDNA copy number was calculated according to the following equation: $2^{-(\Delta \text{CT of ND1 and B2M})}$.

Table 2.7 Primers used in q-PCR

Gene	Species	Sequence	Fragment size (bp)
<i>HMOX1</i>	Chinese hamster	F-ATATCGAGCATAGCCGGGAG	116
		R-CAAGGCCTCAGACAAGTCCT	
<i>NQO1</i>	Chinese hamster	F-TCCTGTGGCCAATTCAGAGTG	135
		R-CCAGTCGTTTCTTCCACCCT	
<i>GCLC</i>	Chinese hamster	F-TCAGCTGGCCACTATCTGCCCAA	106
		R-TGCAGAAATCACTCCCCAGCGACA	
<i>FTH1</i>	Chinese hamster	F-TGCAGAACCAACGAGGTGGCCGA	83
		R-TGCGTTCAGCCCCTCTCCCAGT	
<i>GAPDH</i>	Chinese hamster	F-ACTCCCTCAAGATTGTCAGCA	104
		R-GGTCATGAGTCCTTCCACAA	
<i>ND1</i>	Human	F-ACGCCATAAACTCTTCACCAAAG	111
		R-GGGTTCATAGTAGAAGAGCGATGG	
<i>B2M</i>	Human	F-CACTGAAAAAGATGAGTATGCC	231
		R-AACATTCCCTGACAATCCC	
<i>HMOX1</i>	Human	F- CAACGCCTGCCTCCTCTC	127
		R- GGCCTCTGACAAATCCTGGG	
<i>NQO1</i>	Human	F- AGAAAGGATGGGAGGTGGTG	105
		R- GAAAGTTCGCAGGGTCCTTC	
<i>GCLC</i>	Human	F- CCTGTCTGGGGAGAAAGTTC	118
		R- TCCTGGTGTCCCTTCAATCA	
<i>FTH1</i>	Human	F- GCCTCCTACGTTTACCTGTC	112
		R- CAGCATGTTCCCTCTCCTCA	
<i>GSTA1</i>	Human	F- AGTGGTTAACATGGCCCAGA	108
		R- GCAAGGCTCAGCTGATTACC	
<i>GAPDH</i>	Human	F-CAACTTTGGTATCGTGGAAGGAC	66
		R-ACAGTCTTCTGGATGGCAGTG	

2.7 ARE reporter assay

The CHO-ARE and the CHO-TK cell lines were used to assess ARE expression under various treatment conditions. The TK-EGFP reporter construct consists of a 123bp thymidine kinase promoter inserted in the multiple cloning site of the EGFP plasmid. The ARE-TK-EGFP contains four repeats of a 41bp GST ARE motif (TAGCTTGGAATGACATTGCTAATCGTGACAAAGCAACTTT) 3' to the TK promoter (Mead et al., 2013). Since the construct contains the G418 resistant gene, the cells were kept under selective pressure by growing them in a G418-containing medium (0.5 mg/ml). Following drug treatment, the expression of the EGFP was measured using the Pherastar plate reader (485 nm excitation, 520 nm emission detection) at 647 gain.

2.8 Oxidative stress assay

6-carboxy-2',7'-dichlorodihydrofluorescein (DCF) is a chemically reduced acetylated form of fluorescein that is commonly used as a sensor of ROS. When applied, DCF is trapped inside the cells due to its negative charges. Upon exposure to ROS, DCF is converted into a green fluorescence molecule.

The cells were cultured in a black 96-well plate and were treated according to the experiment design. On the day of the assay, the medium was removed and the cells were washed once with PBS. Then the cells were covered with phenol red free medium containing 20mM DCF and kept in the incubator for one hour. Afterwards, the fluorescence was measured by the Pherastar plate reader (485 nm excitation, 520 nm emission detection) at a fixed gain of 413. A series of ten readings (one minute apart) were performed to calculate the kinetic slope, which was used as an indicator of oxidative stress levels.

2.9 Cytotoxicity measurement

2.9.1 LDH assay

Cell death is associated with a deterioration in membrane integrity and concomitant leakage of various intracellular enzymes. Among them, lactate dehydrogenase enzyme (LDH) is the most stable one with a relatively long half-life (9 hours). The CytoTox 96® Non-Radioactive Cytotoxicity

Assay (G1781, Promega, Madison, USA) used in the project allows relative quantification of LDH. The assay measures the released LDH by supplying lactate, NAD⁺ and tetrazolium salt as substrates [Figure 2.2]. LDH drives the conversion of the tetrazolium salt into a red molecule in a dose-dependent manner. Therefore, the measurement of the colour should reflect the amount of the released LDH.

The cells were plated in a 96-well plate at a specific density according to the experiment design in a total volume of 200 µl/well. Matching wells for each condition were used to obtain the total LDH release. The total LDH release was used to calculate the percentage cytotoxicity of that condition. A CytoTox 96® Non-Radioactive Cytotoxicity Assay was performed according to the manufacturer's manuals. On the day of the assay, 20µl from each well assigned for total LDH release was replaced with an equal volume of 10x lysis buffer (provided with the kit). The cells were kept in the incubator for 45 minutes. Cell lysis was confirmed under optic microscopy. Then 50µl from each well was transferred to a transparent 96-well plate and mixed with an equal amount of the cytotox reagent. The plate was kept in the dark for 30 minutes at room temperature. Afterwards, 50µl of stopping solution was added to each well to stop the reaction, allowing a one-hour window to read the plate. The Pherastar plate reader was used to measure the absorbance at a wavelength of 490nm. In each experiment, cell-free wells were used to determine the medium background level, which was subtracted from the readings of all other wells. In addition, other cell-free wells were treated with 1µl of pure LDH (supplied with the kit) to ensure that the assay reagent was active and to obtain the maximum reading. All conditions were made in triplicates. The preparation and the storage of different the substrates and reagents was performed in accordance with the manufacturer's manuals.

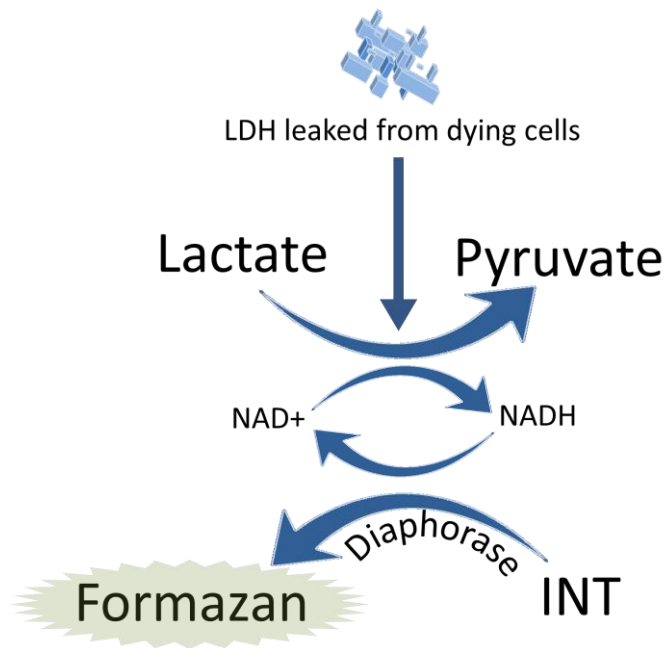


Figure 2.2 The principle of the CytoTox Cytotoxicity Assay.

The provided substrate mix contains lactate, NAD⁺ and iodonitrotriazolium violet (INT). The latter is converted into a red-colour molecule (Formazan) in the presence of LDH.

2.9.1 Trypan blue assay

An alternative approach to assessing cytotoxicity was performed by the use of trypan blue staining. The cells were cultured and treated according to the experiment design in a 24-well plate. To assess the cytotoxicity, the cells were detached from the well floor via repetitive pipetting of the medium. Then the total content of the well was aspirated and transferred into a 1.5ml tube and was subjected to four minutes of centrifugation at 400rcf (brake 9, acceleration 9). The supernatant was removed and the cells were re-suspended in 40µl of culture medium. Equal volumes of the cell suspension and trypan blue stain were mixed thoroughly. Then 10µl of the mix was loaded into one side of the Countess™ Cell Counting Chamber Slide and the cytotoxicity was assessed by the use of the Countess® Automated Cell Counter (Invitrogen). Trypan blue is unable to infiltrate an intact cellular membrane and, therefore, can only stain dead cells that lack membrane integrity. The automated cell counter differentiates between live and dead cells according to their staining pattern. The cytotoxicity was calculated as 100 minus the percentage of the live cells to the total cell count.

2.10 ATP assay

Relative quantification of total cellular ATP levels was achieved via the use of the ATPlite assay (6016941, PerkinElmer, Waltham, MA, USA). The ATPlite assay is an ATP monitoring system based on firefly (*Photinus pyralis*) luciferase. The assay provides substrates, which in the presence of ATP can emit light in a dose-dependent manner according to the reaction scheme in Figure 2.3.

The cells were plated in a white 96-well plate at a specific density according to the experiment design in a total volume of 200µl/well. All conditions were made in triplicates. The ATPlite assay was performed according to the manufacturer manuals. First, the medium was removed and the cells were washed once with PBS. Then, 50µl of mammalian cell lysis solution (provided with the kit) was added and the plate was subjected to 700rpm on an orbital shaker for five minutes to facilitate the lysis. This step was followed by the addition of 50µl of the ATP substrate solution, and the plate was shaken for another five minutes to ensure that the lysate and the substrate were homogeneously mixed. Subsequently, 100µl of PBS was added and the plate was kept in the dark at room temperature for ten minutes. The luminescence was measured by the Pherastar plate reader at 3,600 gain using the LUM plus mode. The preparation and storage of different substrates and reagents were performed in accordance with the manufacturer's manual. Afterwards, the readings were normalised against the DNA content in each well using CyQUANT NF Cell Proliferation Assays (#C35006, Thermo Fisher Scientific, USA) The 1x dye solution was prepared by adding the CyQUANT® NF dye to 5x HBSS buffer (provided with the kit) to distilled water in a ratio of 1:100:400. 50µl of the 1x dye solution was added and the plate was kept in the incubator for 45 minutes. The fluorescence was measured by the Pherastar plate reader (485 nm excitation, 520 nm emission detection) at a gain value of 100, which was fixed in all experiments.

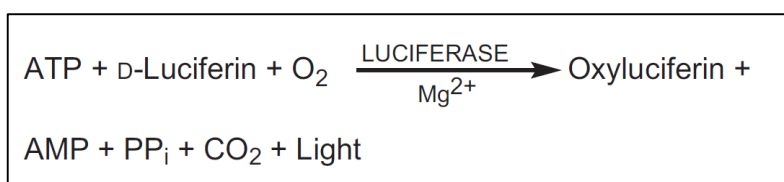


Figure 2.3 The principle of the ATP Detection Assay System.

The production of light is prompted by the reaction of ATP with added luciferase and d-luciferin.

2.11 Cellular fractionation

2.11.1 Mitochondrial isolation

The isolation of an enriched mitochondrial fraction was performed using a protocol that was adopted from (De Vos et al., 2011). Treated cells in a T175 flask were harvested via trypsinisation, as described previously. Consequently, the cells were washed twice in PBS before they were re-suspended in 250µl of mitochondrial isolation buffer (IB): mannitol (220mM), sucrose (70mM), 4-(2-hydroxyethyl)-1-piperazineethanesulfonic acid (HEPES) (10mM), ethylenediaminetetraacetic acid (EDTA) (1m), Dithiothreitol (DTT) (1mM), BSA (0.1%), 10x Protease Inhibitor Cocktail (5%), Phosphatase Inhibitor Cocktail2 (1%) in H₂O). Then the cells were homogenised using a IKA® dual-speed mixer (Merck). The lysate was centrifuged twice for five minutes at 600 x g to remove nuclei and unlysed cells. Afterwards, the supernatant was subjected to a centrifugation at 10000 x g for ten minutes to separate the mitochondrial fraction (the pellet) from the cytoplasmic fraction (the supernatant).

2.11.2 Mitochondria purification

Next, the mitochondrial extract was purified via centrifugation through two different concentrations of sucrose [Figure 2.4]. The mitochondrial pellet was re-suspended in 1ml of IB and carefully transferred into a 5ml tube that was pre-loaded with the sucrose gradient. The tube was pre-loaded with 1.5ml of 1.6M sucrose (in H₂O), followed by 2.5ml of 1.2M sucrose (in H₂O). HEPES, BSA and EDTA were added to the sucrose preparation at equal concentrations to the IB. Afterwards, the tube was subjected to high-speed centrifugation at 95,000 x g for one hour using the L-80 Ultracentrifuge (Beckman) (SW 55Ti rotor). During that process, the mitochondrial fraction progressed through the 1.2M sucrose and accumulated at the level of the 1.5M sucrose [Figure 2.4]. Following the centrifugation, the mitochondrial fraction (250–300µl) was recovered from the 1.6M/1.2M interface and was mixed with 600µl of IB. In order to pellet the mitochondria, the mix was subjected to centrifugation at 10000 x g for ten minutes. The samples and reagents were kept at 4°C at all steps of the fractionation. The mitochondrial pellet was lysed and prepared for WB as described before.

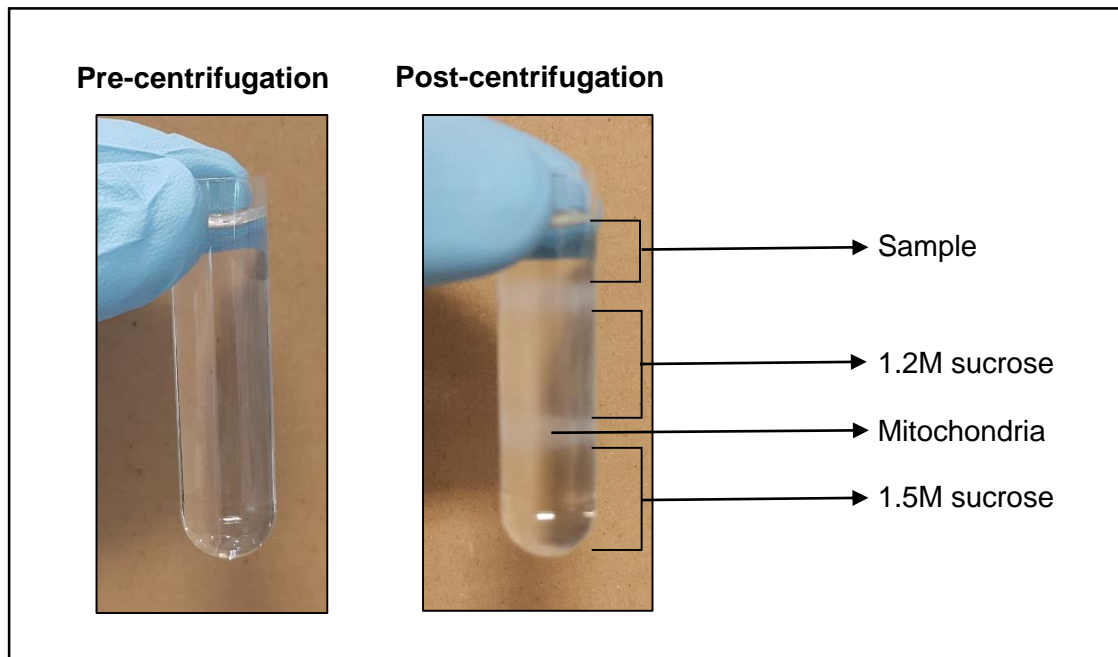


Figure 2.4 Purification of mitochondria by sucrose step density gradient centrifugation.

The image shows the 5ml centrifugation tube loaded with the sample and the sucrose gradient before and after the centrifugation step. The mitochondria accumulate at the 1.6M/1.2M interface and appear as a thin white layer.

2.12 Statistical analysis

All data analyses and statistical tests were performed using Graphpad prism V7.0 (Graphpad).

All experiments were performed in triplicates, unless otherwise stated, and all error bars represent the standard deviation of the mean (SD). The data were analysed using an unpaired t-test, one-way ANOVA or two-way ANOVA. Significance values were denoted following the GP formatting in Graphpad prism V7.0 : Not statistically significant (ns) = $p > 0.05$, * = $p < 0.05$, ** = $p < 0.01$, *** = $p < 0.001$, **** = $p < 0.0001$.

Chapter 3. Investigating the effect of UDCA on mitochondrial biogenesis in patient fibroblasts

3 Investigating the effect of UDCA on mitochondrial biogenesis in patient fibroblasts

3.1 Introduction

3.1.1 Parkinson's disease and mitochondrial biogenesis

Several studies have suggested a defect in mitochondrial biogenesis in PD, in particular in the context of Parkin deficiency. In SH-SY5Y cells, the transcription and replication of mitochondrial DNA is enhanced by Parkin overexpression and attenuated by (siRNA-mediated) Parkin repression (Kuroda et al., 2006). The mechanism of action involved was subject to debate until the discovery of Parkin interacting substrate (PARIS) (Shin et al., 2011). Parkin binds and ubiquitinates PARIS and, consequently, can regulate PARIS level through ubiquitin-mediated proteasomal degradation. In line with this, PARIS is expressed at a high level in *parkin* knockout mice, as well as in patients with *parkin* mutations (Stevens et al., 2015, Dawson and Dawson, 2014).

PARIS is a potent selective repressor of PGC-1 α (a transcriptional coactivator that coordinates the activity of diverse transcription factors involved in mitochondrial biogenesis). The expression of PGC1- α is sufficient by itself to facilitate the process of mitochondrial biogenesis (Scarpulla et al., 2012). Therefore, the Parkin–PARIS–PGC1- α axis is considered to be an important pathway in the pathogenesis of PD in patients with *parkin* mutations.

3.1.2 Mechanism of mitochondrial biogenesis

The process of mitochondrial biogenesis requires both mitochondrial and nuclear proteins to be expressed in a multistep, coordinated manner. Therefore, mitochondria are considered “semi-autonomous” despite the fact that they have their own DNA. mtDNA encodes only eleven messenger RNAs, which are translated into 13 respiratory chain proteins, 22 tRNAs and two rRNAs (Stewart and Chinnery, 2015, Calvo and Mootha, 2010). While mitochondria contain around 1200 proteins, only 90 are required for the synthesis of respiratory chain complexes (Gustafsson et al., 2016). Therefore, mtDNA-encoded proteins represent only a fraction of these complexes. However, their absence is sufficient to induce OXPHOS dysfunction (Gustafsson et al., 2016).

mtDNA is a double-stranded, circular molecule that consists of approximately 16.500 bp and is usually packed into nucleoids inside the mitochondrial lumen (Kukat and Larsson, 2013). Prior to mitochondrial biogenesis, mtDNA must be replicated. Numerous nDNA-encoded proteins are translocated to the mitochondrion for this purpose. One of these is DNA polymerase subunit gamma-1 (POLG), which contributes to the catalytic subunit of the mitochondrial DNA polymerase and possesses a proofreading ability. Mitochondrial DNA polymerase- γ is the only replicative polymerase in mitochondria. Other important proteins in mtDNA replication are the Twinkle helicase, which unwinds the double-stranded mtDNA, and the mitochondrial single-stranded DNA-binding protein (mtSSB), which maintains the integrity of the DNA strand at the replication fork, as mitochondrial DNA polymerase- γ is unable to bind double-stranded DNA (Fernández-Millán et al., 2015) (Akhmedov and Marín-García, 2015).

The transcription of mtDNA requires the RNA polymerase (POLRMT) and various transcription factors, such as mitochondrial transcription factor A (Tfam), mitochondrial transcription factor B2 (TFB2M), and mitochondrial transcription termination factor 1 (Scarpulla et al., 2012). Nuclear respiratory factor-1 and nuclear respiratory factor-2 regulate the transcription of nuclear genes that encode for a range of mitochondrial proteins, including cytochrome c and translocase of outer mitochondrial membrane 34 (Tom34) (Ploumi et al., 2017). They can also regulate mtDNA transcription through their ability to control the transcription of Tfam (Palikaras and Tavernarakis, 2014). Another important factor is Nrf2, which is mainly concerned with antioxidant response but has been found to regulate nuclear respiratory factor-1 *in vivo* and *in vitro* (Ploumi et al., 2017).

To develop the OXPHOS system, both nDNA- and mtDNA-encoded proteins must be translated, imported, inserted into the inner mitochondrial membrane and congregated into the five complexes (Ploumi et al., 2017). Mitochondrial mRNAs are translated in the cytosol and then cross the outer and inner mitochondrial membranes via mitochondrial translocases to be integrated with other proteins (Ploumi et al., 2017).

3.1.3 Objectives

Our group previously described increased activity in each of the individual respiratory chain enzymes after UCA treatment (Mortiboys et al., 2013). The aim of this chapter is to determine whether this is due to a positive effect of UCA/UDCA on mitochondrial biogenesis. The effects of each compound on the expression of mitochondrial proteins will be quantified in healthy and *parkin*-mutant fibroblasts, using WB. In addition, relative qPCR for mtDNA copy number will be used as a complementary method.

3.2 Experimental design

The experiments in this chapter aimed to investigate the mechanism of the rescue effect observed in previous work by our group (Mortiboys et al., 2013). Therefore, the drug treatment protocol was adopted from that study.

Fibroblasts were grown in regular glucose-containing medium until two days before the assay. Subsequently, they were switched to galactose-containing medium, and treated with the drugs. Growing fibroblasts in galactose medium instead of regular glucose medium should increase their dependence on mitochondrial OXPHOS. Hence, any mitochondrial defect in patient fibroblasts should be more pronounced. The effect of any mitochondrial rescuing compound should also be increased.

The effective doses in the Mortiboys paper (2013), of 100 nM for both UCA and UDCA in 24-hour treatment, were used in all experiments reported in this chapter. Skin fibroblasts from three *parkin* patients and three age-matched controls were used, grouped into pairs: pair1 (GM07924 and ND37731), pair2 (GM23967 and ND30171) and pair3 (GM02189 and ND30618). Information about these fibroblasts can be found in the methods chapter [Table 2.1].

3.3 Quantifying the expression of mitochondrial respiratory complexes via western blotting in patient fibroblasts

An increase in mitochondrial biogenesis should lead to an increase in the expression of the principal proteins involved in energy production. Therefore, we decided to use antibodies against proteins in each of the mitochondrial respiratory chain complexes [Figure 3.1]. WB and data analysis were performed as described in the methods section. In each round of these experiments, samples under different conditions for a given patient and its age-matched control were loaded onto a single WB gel and probed with the antibody mixture. This approach minimises variability and allows direct comparison between different treatment conditions in the patient and the control.

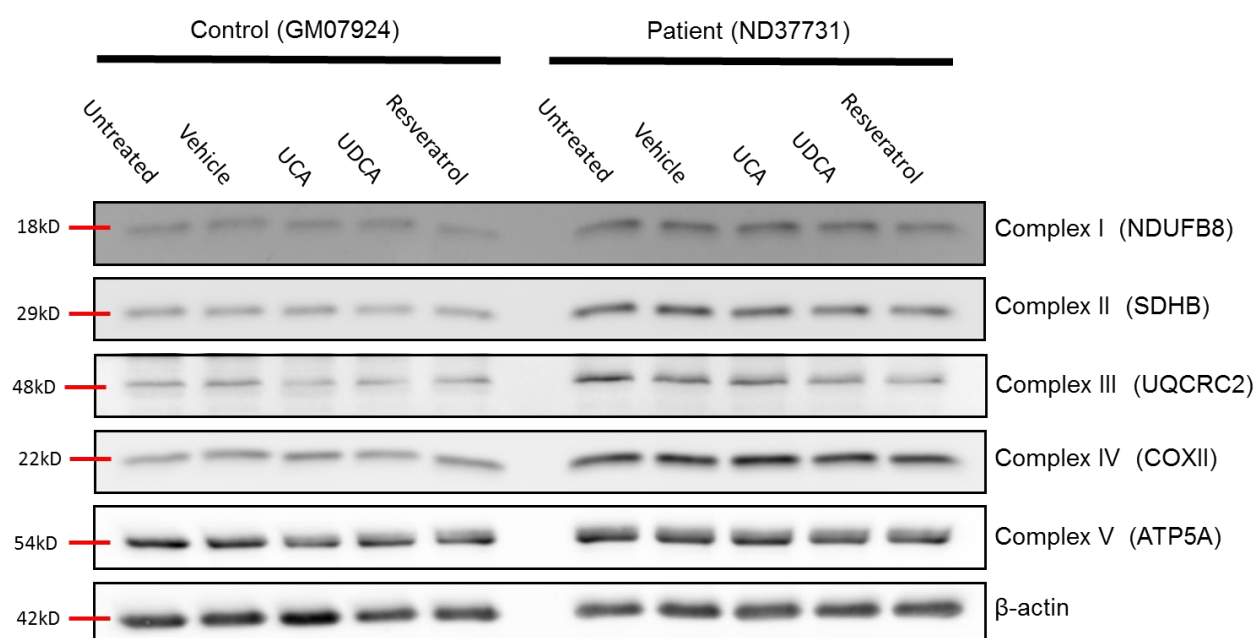


Figure 3.1 Total OXPHOS Human Antibody Cocktail proved to be efficient in detecting its target proteins in each mitochondrial respiratory complex.

The figure shows WB images of fibroblast extracts probed with the Total OXPHOS Human WB Antibody [Table 2.5], which binds to a protein from each respiratory chain complex. The figure shows that the antibody successfully binds to all target proteins at the predicted locations. Both control and patient fibroblasts were treated with 100 nM UCA or 100 nM UDCA for 24 hours, or with 25 μ M resveratrol for 48 hours, in galactose medium.

3.4 Positive control testing

There are many compounds reported to enhance mitochondrial biogenesis, such as nitric oxide, valproic acid, epigallocatechin-3-gallate and resveratrol. The latter was chosen as a positive control in this study because it upregulates mitochondrial biogenesis in various types of cells including human liver cancer cells (HepG2), Coronary artery endothelial cells (CAEC), human umbilical vein endothelial cells (HUVEC), human neuroblastoma cells SH-SY5Y, mouse myoblast cells (C2C12) and human skin fibroblasts of patients with inborn respiratory chain deficiency (de Oliveira et al., 2016, Costa et al., 2014).

More importantly, resveratrol has been proposed to increase mitochondrial biogenesis in fibroblasts obtained from PD patients with *parkin* mutations (Ferretta et al., 2014). In the study by Ferretta and colleagues, WB quantification of PGC-1 α showed increased levels in all patients and controls (2+2) after treatment with resveratrol. RT-qPCR of PGC-1 α downstream genes, such as Tfam, cytochrome c, cytochrome c oxidase I and superoxide dismutase 2 (SOD2), also revealed increased expression. Resveratrol is considered a candidate treatment for PD as it showed a neuroprotective effect *in vivo* and *in vitro* (Peng et al., 2016, Lofrumento et al., 2014). Resveratrol is an important component of red wine, but It is also present in a wide range of plants, such as grape, peanut, cocoa, tomato, blueberry and cranberry (de Oliveira et al., 2016).

In the literature, resveratrol has been applied to human skin fibroblasts in a wide range of doses [Table 3.1]. In this chapter, initial testing of resveratrol employed two doses (25 μ M and 50 μ M) and two treatment times (48 hours and 72 hours). The data show an increase in three complexes with the highest dose and the longest treatment time [Figure 3.2]. Therefore, we decided to repeat the experiment with the application of higher concentrations (50 μ M, 75 μ M and 100 μ M) [Figure 3.3]. However, no increase in the expression of mitochondrial respiratory complexes was seen. In addition, the small increase that was previously observed with 50 μ M was not reproducible [Figure 3.3]. These results indicate that resveratrol treatment is variable in its effects. Nevertheless, we chose to retain the resveratrol condition in our drug treatment experiments.

Table 3.1 Resveratrol doses in human fibroblasts.

Assessment	Dose	Cell line	Technique
Respiration rates	25 μ M for 48 hours	Primary fibroblasts from <i>parkin</i> patients	Oxygen electrode
Mitochondrial respiratory enzyme activities	25 μ M for 48 hours	Primary fibroblasts from <i>parkin</i> patients	Activity assay
Citrate synthase activity	25 μ M for 48 hours	Primary fibroblasts from <i>parkin</i> patients	Activity assay
mtDNA content	25 μ M for 24 hours	Primary fibroblasts from <i>parkin</i> patients	qPCR
PGC-1 α	25 μ M for 24 hours	Primary fibroblasts from <i>parkin</i> patients	WB
Respiratory chain complexes	75 μ M 48 hours	CI- and CIV-deficient human fibroblasts	WB
Citrate synthase activity	75 μ M 48 hours	CI- and CIV-deficient human fibroblasts	Activity assay
Mitochondrial respiratory enzyme activities	75 μ M 72 hours	CI- and CIV-deficient human fibroblasts	Activity assay
Mitochondrial content	75 μ M 48 hours	CI- and CIV-deficient human fibroblasts	Mitotracker green staining
Autophagy - LC3	(12.5–100 μ M) for 8 hours	Human dermal fibroblasts	WB
Mitochondrial enzyme activities	100 μ M for 48 hours	CII- and CIV-deficient human fibroblasts	Activity assay

Resveratrol application to human fibroblasts showing the dosages used and the techniques performed. References: (Ferretta et al., 2014, Costa et al., 2014, Choi et al., 2013, De Paepe et al., 2014).

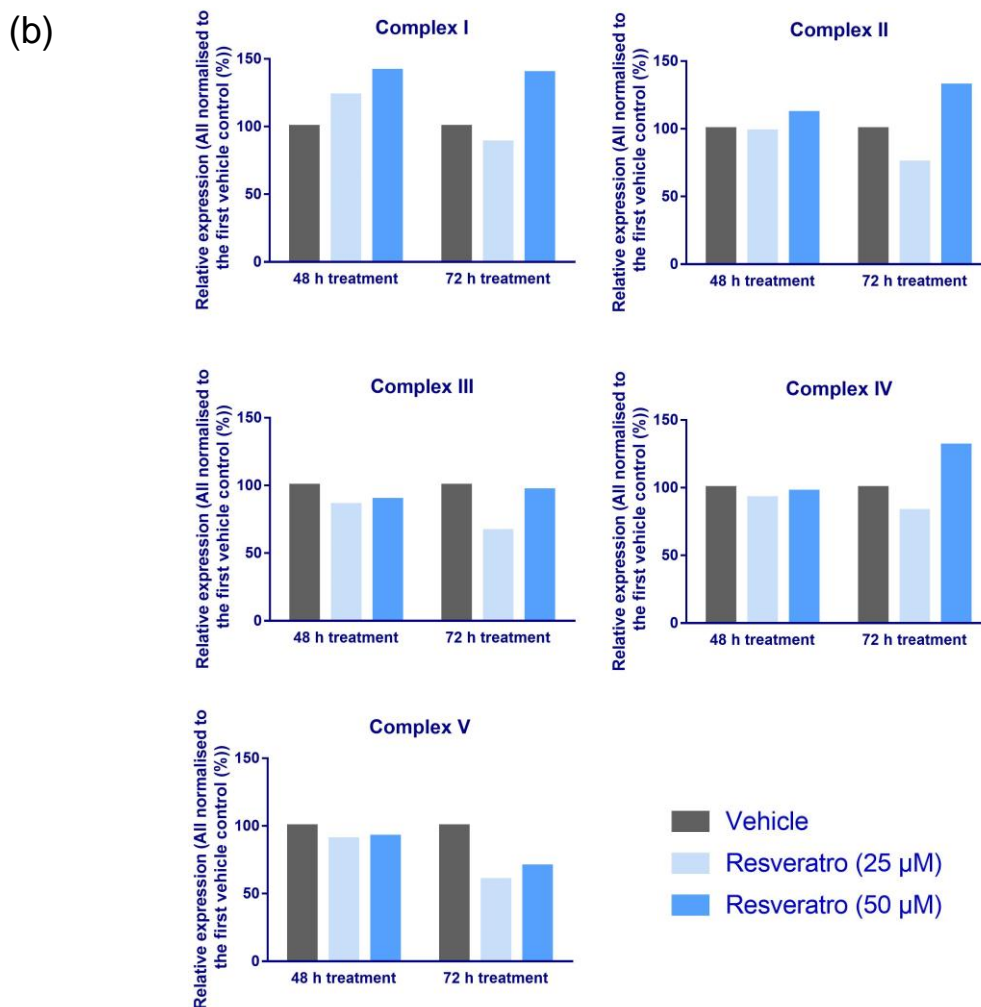
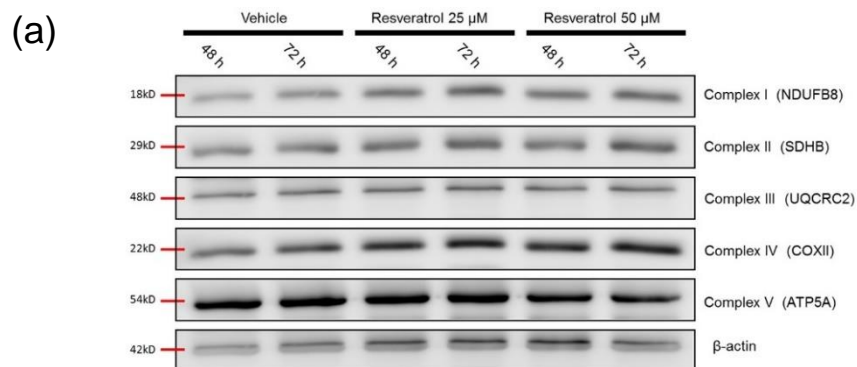


Figure 3.2 Resveratrol increased the expression of proteins from three mitochondrial respiratory complexes in a pilot test.

(a) A pilot WB test using extracts of control fibroblasts (OB064). The cells were treated with 25 μ M or 50 μ M for either 48 or 72 hours, in galactose medium. WB membranes were probed with the Total OXPHOS Human WB Antibody [Table 2.5], which binds to a protein from each respiratory chain complex. (b) Quantification of WB images, showing increased expression of complex I-, complex II- and complex IV-targeted proteins upon treatment with 50 μ M resveratrol for 72 h. The graph bars represent data from a single pilot experiment.

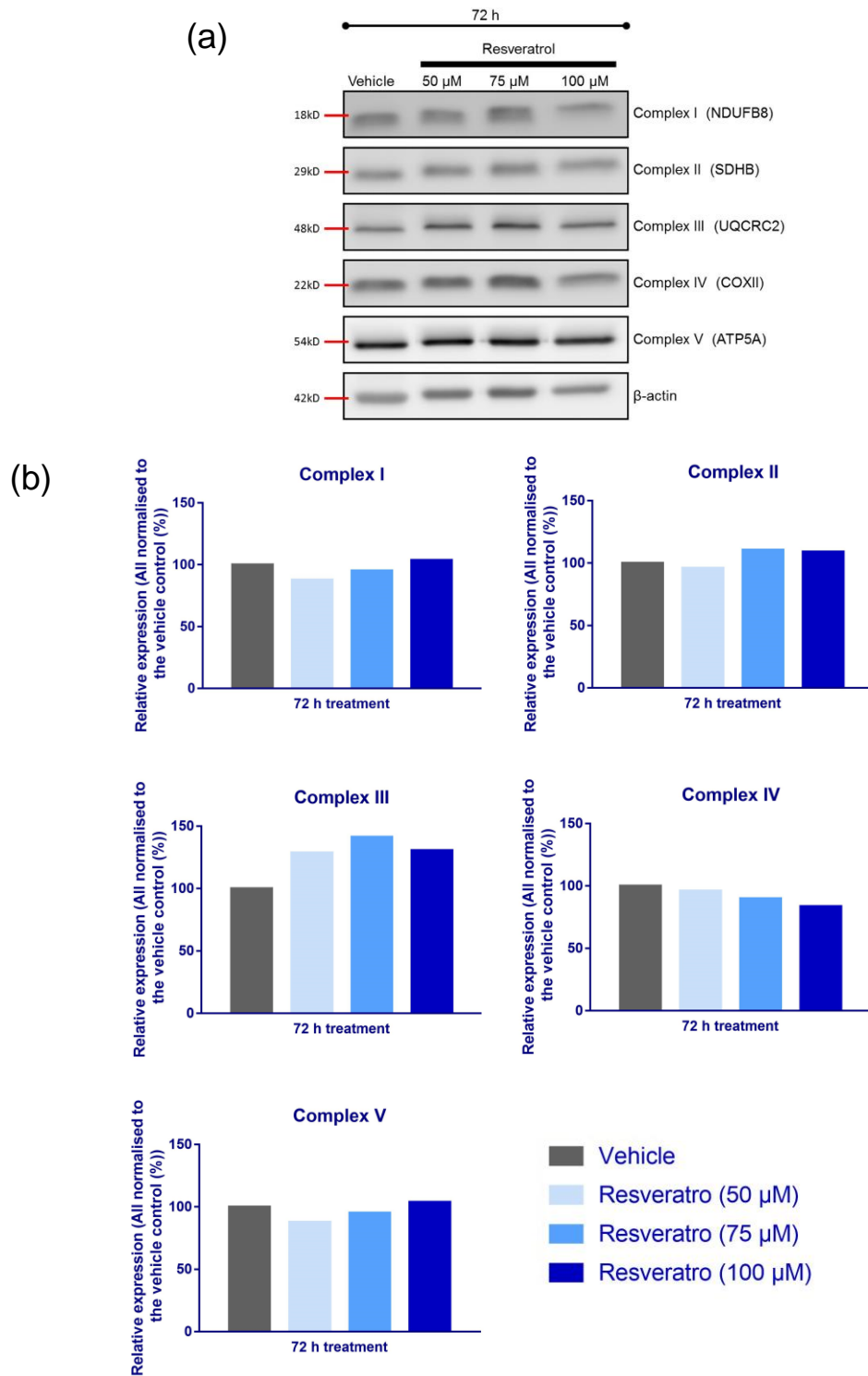


Figure 3.3 The positive effect of resveratrol on the expression of mitochondrial proteins was not reproducible despite the trial of higher doses.

(a) A WB test using extracts of control fibroblasts (OB064) treated with high resveratrol doses (50 μ M, 75 μ M and 100 μ M for 72 hours, in galactose medium). WB membranes were probed with the Total OXPHOS Human WB Antibody [Table 2.5], which binds to a protein from each respiratory chain complex. (b) Quantification of WB images, showing no change in the expression of the proteins except for a small increase in complex III with 50 μ M and 75 μ M resveratrol. The graph bars represent data from a single pilot experiment.

3.5 Assessing the effect of drug treatment on the expression of mitochondrial respiratory complexes in patient fibroblasts

Comparing the expression of the mitochondrial respiratory complexes in fibroblasts between the patients and the controls suggests a general increase in those of patients (not statistically significant) [Figure 3.4]. The only exception observed was in the expression of complex V protein, in which no difference was seen between the patient and the control in all three pairs. Treatment with either UCA, UDCA or resveratrol had no significant effect in all patient-control pairs.

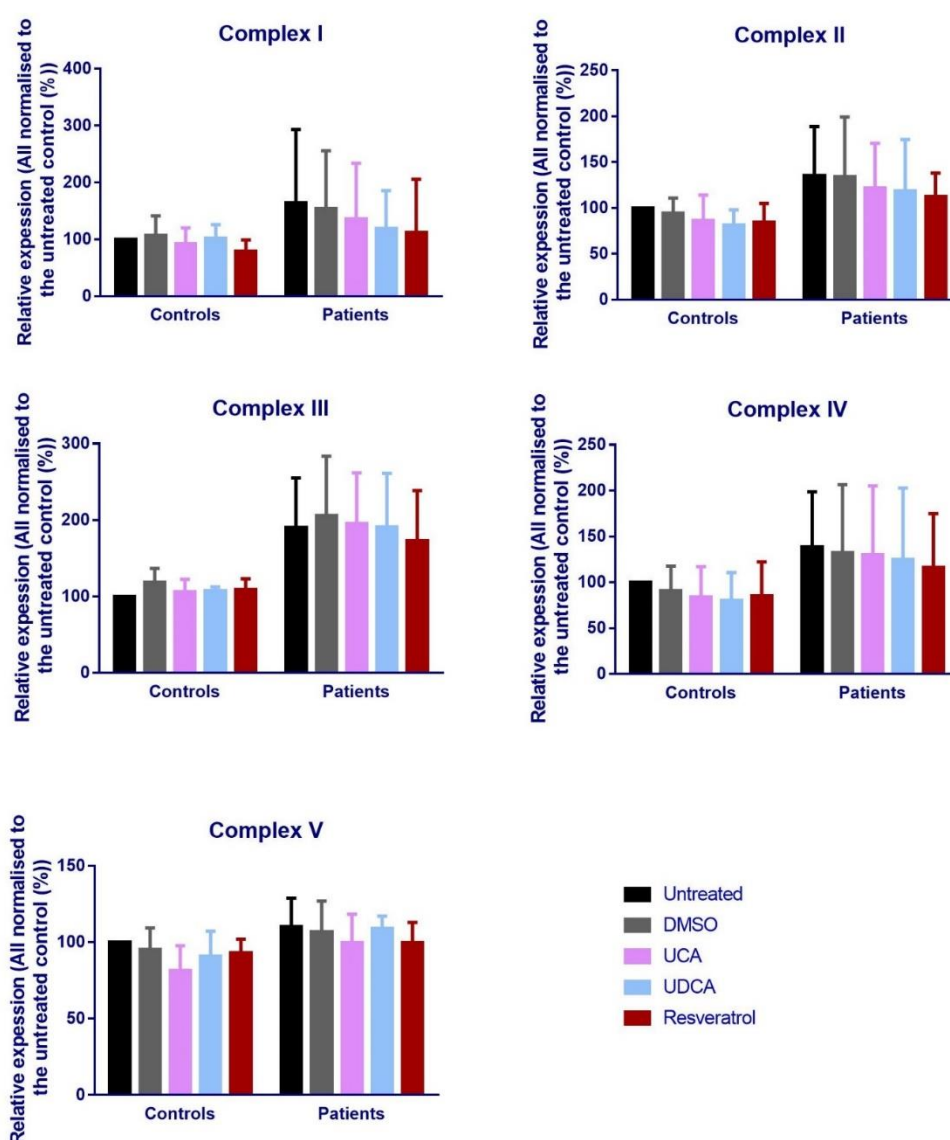


Figure 3.4 Neither UCA nor UDCA treatment altered the expression of mitochondrial respiratory proteins in control and patient fibroblasts.

These graphs quantify WB images that were obtained from three pairs of patients and age-matched controls. For each pair, means were obtained from three independent experiments. The data for each pair were normalised against β -actin and against the untreated control prior to combination. The cells were treated with 100 nM UCA or 100 nM UDCA for 24 hours, or 25 μ M resveratrol for 48 hours, in galactose medium. The graphs show that UCA and UDCA treatment did not increase the expression of the targeted mitochondrial components in the patients or controls. The error bars represent SD. Two-way ANOVA test.

3.6 Quantifying mtDNA via qPCR

Quantitative analysis of mtDNA copy number by qPCR is an established method for studying mitochondrial mass and biogenesis. The principle of the experiment is that each human cell has only two copies of any nuclear gene and multiple copies of mitochondrial genes, depending on the number of mitochondria within the cell. The readings at the end of qPCR cycles can be used to calculate the average mtDNA copy number per cell in a given sample. Further details on this approach can be found in the method chapter [2.6.3].

In this set of experiments, the primers used were previously tested and employed in human cells by our group and others (Cree et al., 2008, Samuels et al., 2017). Beta-2-microglobulin (*B2M*) was targeted as the nuclear reference gene and NADH dehydrogenase subunit 1 (*ND1*) was targeted to deduce the mtDNA copy number. Upon testing, the standard curve and the melt peaks, which were obtained from a serial tenfold dilution of the untreated sample, demonstrated high efficiency and specificity [Figure 3.5].

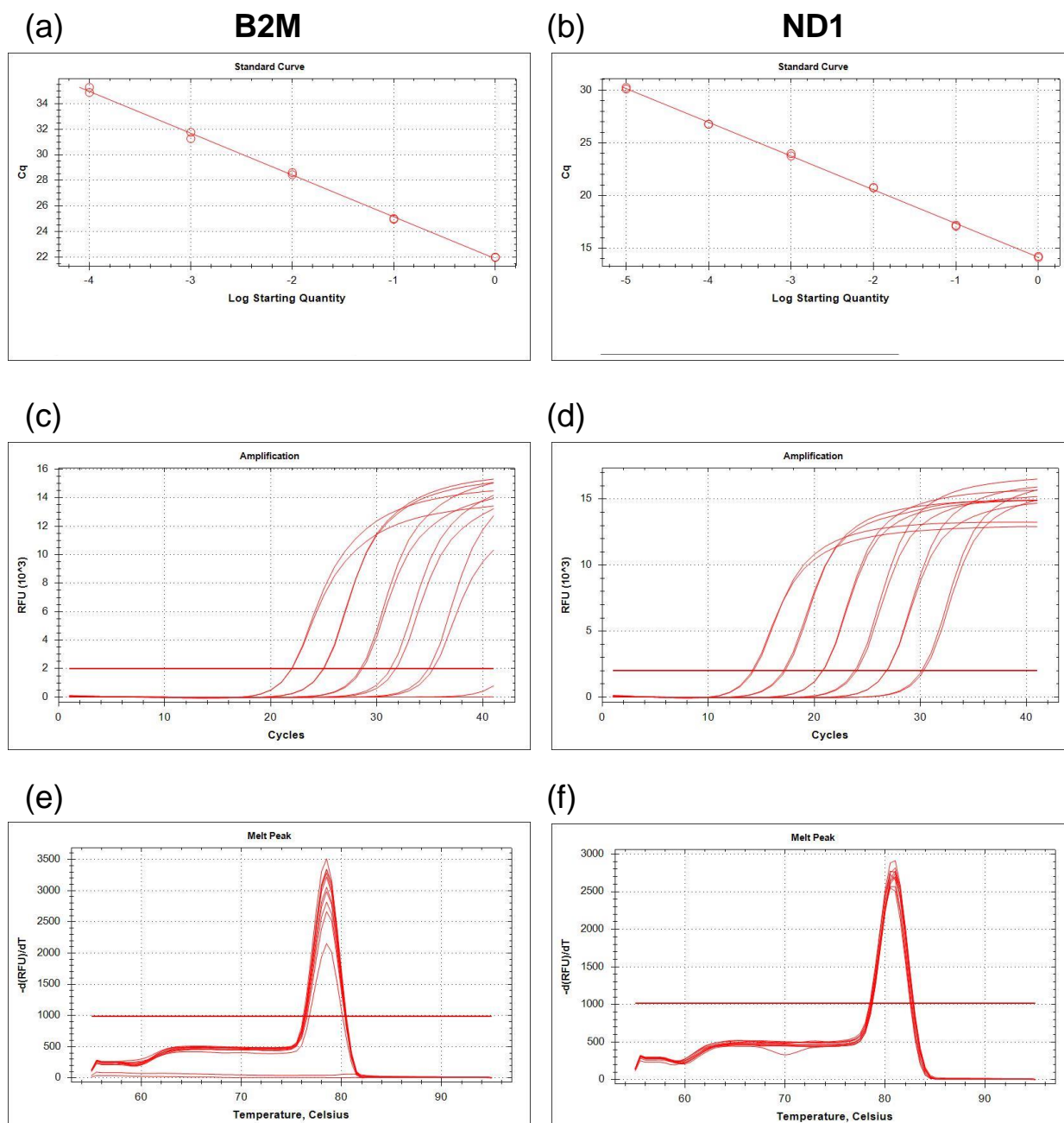


Figure 3.5 *B2M* and *ND1* primers have high efficiency and specificity in qPCR reactions.

Efficiency and specificity were assessed using tenfold serial dilution of untreated samples. The standard curves (a and b) were obtained following the generation of the amplification curves (c and d), and reveal an efficiency of 102% for *B2M* and 105.2% for *ND1*. Melt peak graphs (e and f) show single peaks with all dilutions of the sample indicating high specificity.

3.7 Assessing the effect of drug treatment on mtDNA copy number in patient fibroblasts

During cell culture, a fraction of the treated cells that were allocated for WB was separated and subjected to DNA extraction and subsequent qPCR. Quantitative analysis of mtDNA copy number by qPCR did not show a difference between patients and controls in any of the three pairs [Figure 3.6]. In addition, Drug treatments had no effect on mtDNA copy number.

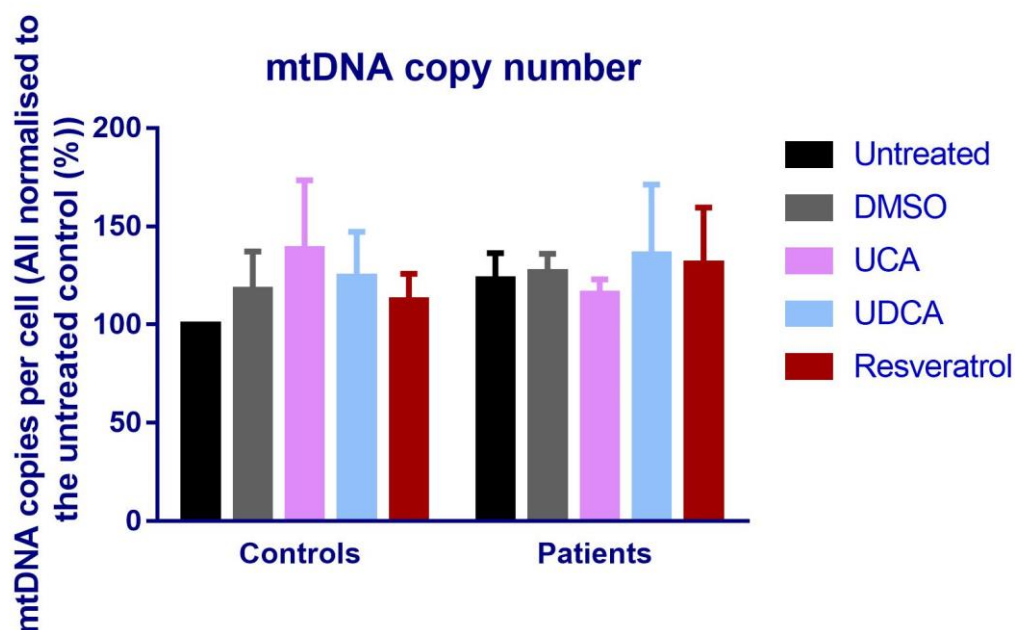


Figure 3.6 Neither UCA nor UDCA treatment altered mtDNA copy number in control and patient fibroblasts.

Data analysis of qPCR results for three pairs of patients and age-matched controls. For each pair, means were obtained from three independent experiments. The data for each pair were normalised against β -actin and against the untreated control prior to combination. The cells were treated with 100 nM UCA or 100 nM UDCA for 24 hours, or 25 μ M resveratrol for 48 hours, in galactose medium. The graph shows that UCA and UDCA treatment did not increase mtDNA copy number in the patients or the controls. The error bars represent SD. Two-way ANOVA test was performed.

3.8 Discussion

A wide range of methods and techniques have been used to study mitochondrial biogenesis. The most common is direct visualisation of mitochondria via microscopic examination. The 3D nature of mitochondria should be taken into account when using microscopy; otherwise, the results could be misleading. This issue was avoided in our study through the use of WB to quantify the expression of mitochondrial proteins. This is an indirect method which was used to confirm whether or not mitochondrial biogenesis had increased.

More direct approaches involve targeting the key proteins and transcripts that are usually upregulated in mitochondrial biogenesis, such as POLG, and PGC-1 α . However, the regulation of these factors is tight and their expression is frequently transient. Moreover, their expression levels in fibroblasts in particular are generally low (Scarpulla et al., 2012, Garcia-Giménez et al., 2011). Mitochondrial DNA quantification through Southern blotting or qPCR, as performed in this chapter, should also help to confirm increased mitochondrial biogenesis. However, this should not be considered as definitive readout because the mtDNA copy number varies within each mitochondrion, ranging between two and ten.

The expression of the mitochondrial respiratory complexes in *parkin* fibroblasts has been assessed previously. Pacelli and colleagues found that the expression of complex I, complex II, complex IV, complex V and mitochondrial outer membrane protein, porin, is lower in patients in comparison to controls (Pacelli et al., 2011). Conversely, the expression of PGC-1 α was higher in patients. The authors postulated a compensatory mechanism behind this unexpected elevation. However, there was no increase in the expression of PGC-1 α downstream targets (Pacelli et al., 2011).

The results in this chapter do not show a decrease in the expression of mitochondrial respiratory complexes. Instead, there was a non-significant trend toward increased expression. The fibroblasts in Pacelli's study were grown in regular glucose medium, while in this project the fibroblasts were grown in galactose medium. It is possible that an induced increased dependency on mitochondrial respiratory complexes led to a decrease in the removal of mitochondrial proteins. The effect was more prominent in patient cells, since they have lower ATP levels (Mortiboys et

al., 2013). Additionally, these are *parkin*-mutant cells and therefore it is expected that they have primary mitophagy impairment, though this has not been studied in patient fibroblasts. The data does not support that the increased expression of mitochondrial respiratory complexes in the patients is due to increased mitochondrial biogenesis, since both patients and controls showed comparable mtDNA copy numbers.

The effects of UCA and UDCA on the expression of mitochondrial respiratory complexes and mtDNA content have never been assessed before. Our results do not show significant changes in either controls or in patients. Therefore, these findings suggest that UCA/UDCA treatment does not enhance mitochondrial biogenesis. However, it is important to point out that only two methods were used to investigate mitochondrial biogenesis and that there were no positive results after treatment with the positive control. Additionally, the applied doses, treatment protocol, and type of culture medium might not be optimal to induce mitochondrial biogenesis, even though they were associated with increased mitochondrial function (Mortiboys et al., 2013). Therefore, more work is needed in the future to verify the findings in this chapter. Experiments should additionally include alternative models, as fibroblasts might not be the best choice for studying mitochondrial biogenesis. Since fibroblasts are metabolically and energetically less active than neurons, it is possible that they are inherently unable to respond efficiently to enhancers of mitochondrial biogenesis.

Chapter 4. Investigating the beneficial effect of UCA and UDCA on oxidative stress, ATP and cytotoxicity in the ARE reporter cell line

4 Investigating the beneficial effect of UCA and UDCA on oxidative stress, ATP and cytotoxicity in ARE reporter cell line

4.1 Introduction

4.1.1 Nrf2 pathway

According to the 'oxidative stress hypothesis' (proposed by Fahn and validated by subsequent experimental data), oxidative stress is one of the main drivers for neuronal degeneration in PD (Fahn and Cohen, 1992, Blesa et al., 2015). The mechanism through which this occurs is explained in detail in the introduction chapter [Heading 1.3]. Accordingly, drugs that ameliorate oxidative stress can be novel treatments for PD. The most important antioxidant pathway in cellular biology, the Nrf2 pathway, will be briefly discussed in this section.

4.1.2 Nrf2 structure

The Nrf2 pathway is regulated by a highly conserved transcription factor called nuclear factor (erythroid-derived 2)-like 2, also known as NFE2L2 or Nrf2 (Buendia et al., 2016). Other members of the Nrf family include Nrf1 and Nrf3. Nrf1 and Nrf2 are ubiquitously expressed, while the expression of Nrf3 is limited to certain tissues such as the placenta, B-cells and monocytes. In contrast to Nrf2 and Nrf3, Nrf1 is essential for development and knockout (K/O) embryos die at early stages. However, the function of Nrf1 is still unknown (Tebay et al., 2015). Human Nrf2 consists of 605 amino acids and is composed of seven different distinct domains called the Nrf2-ECH homology (Neh) domains (Canning et al., 2015) [Figure 4.1]. The Neh1 domain has the Cnc-basic leucine zipper (Cnc-bZIP) region that is unique to Cap 'n' Collar (Cnc) proteins, and possesses a DNA-binding ability, which is an important characteristic of transcription factors (Itoh et al., 1999). The Neh2 domain plays a role in regulating the activity of Nrf2 and will be addressed in the next section. The Neh3 domain regulates the function of domain 1 and thus controls the transcriptional activity of Nrf2 (Nioi et al., 2005). Neh4 and Neh5 enhance the transcriptional activity via their binding to the coactivator CREB-binding protein (CBP) (Kato et al., 2001). Inversely, Neh6 has the ability to downregulate Nrf2 activity through a mechanism that will be addressed later. Neh7 is the most recent and least described domain. However, it has been

suggested that it might control transcriptional activity through binding to different regulatory proteins (Wang et al., 2013, Tebay et al., 2015) [Figure 4.1].

4.1.3 Regulation of Nrf2 activity

It is believed that the net balance between Nrf2 synthesis and degradation is one of the main determinants of its activity. Although most of the work investigating Nrf2 regulation focuses on degradation, some interesting findings about Nrf2 regulation have been obtained from studying Nrf2 at its transcriptional level. The Nrf2 gene has a xenobiotic response element sequence. This sequence promotes the transcription of the genes when exposed to potentially harmful xenobiotics through the action of the aryl hydrocarbon receptor. Interestingly, the activation of the Nrf2 consequently downregulates aryl hydrocarbon receptor. These findings indicate that regulatory feedback loops play a role in Nrf2 control (Tebay et al., 2015).

The degradation of Nrf2 is regulated via its binding to the Kelch-like ECH-associated protein 1 (Keap1) (Buendia et al., 2016). More specifically, the Neh2 domain of Nrf2 has two sites (ETGE and DLG) where two molecules of Keap1 can bind. Keap1 has the ability to ubiquitinate the lysine residues in the Neh domain with the aid of a specific protein adaptor, Ligase Cullin-3. The ubiquitination mediates proteasomal degradation (Suzuki and Yamamoto, 2015). Therefore, Keap1 acts as a down-regulator of Nrf2. Importantly, Keap1 activity is tightly linked to the level of xenobiotic and oxidative stress. This association is attributed to the high number of cysteine residues within Keap1 that can be modified by different stressors. The cysteine code hypothesis suggests that each group of Nrf2 activators has a preferable specific cysteine residue. The modification of these residues breaks the bond between Keap1 and the DLG motif in Nrf2, but not ETGE (Huang et al., 2015). This allows structural changes in the Keap1-Nrf2 complex (hinge and latch), which consequently prevent Nrf2 ubiquitination [Figure 4.1].

The regulation of Nrf2 activity is complex and extends beyond the discussed Keap1-ubiquitin interactions. For example, there is evidence that Nrf2 itself can regulate the transcription of Keap1 and Cullin-3 (Kaspar and Jaiswal, 2010). More importantly, several different protein kinases increase the levels of Nrf2 via a mechanism that is not clear, but involves the direct phosphorylation of Nrf2 residues. These kinases include PKC α , casein kinase II, PI3K, c-Jun N-

terminal kinase (JNK), ERK and MAPKs (Sun et al., 2009, Numazawa et al., 2003, Pi et al., 2007, Nakaso et al., 2003, Keum et al., 2006). In contrast, phosphorylation of Nrf2 residues by certain kinases, such as glycogen synthase kinase 3 beta (GSK3 β), facilitates Nrf2 degradation. GSK3 β phosphorylates the DSGIS motif in Neh6. Then, The degradation follows via direct recognition of the phosphorylated residue by E3 ligase (Chowdhry et al., 2013, Buendia et al., 2016).

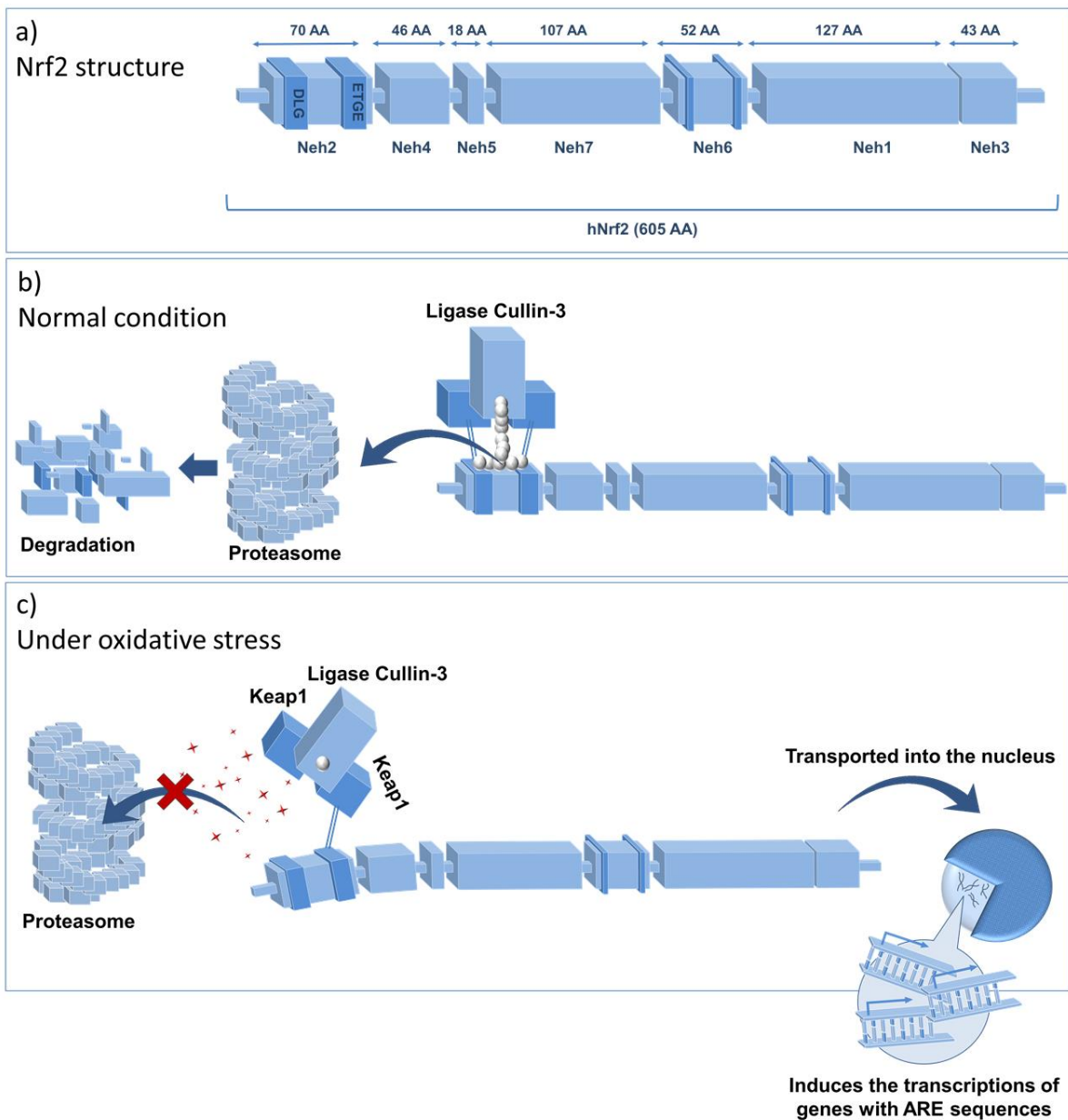


Figure 4.1 Overview of the structure and the regulation of Nrf2.

(a) The identified domains within the Nrf2 protein. (b) The proteasomal-mediated degradation of Nrf2 in the basal condition is facilitated by the ubiquitination by Keap1 and Cullin-3. (c) In the case of oxidative stress, the Keap1-DLG bond breaks and the ubiquitination stops. The increased amount of Nrf2 in the nucleus stimulates the transcription of ARE in the targeted genes.

Abbreviations: Neh: Nrf2-ECH homology, Nrf2: Nuclear factor erythroid 2-like 2, Keap1: Kelch-like ECH-associated protein 1, ARE: antioxidant response element.

4.1.4 Nrf2 genes and the mechanism of action

In the nucleus, Nrf2 binds to Maf proteins to form dimers. Subsequently, the dimers recognise the cis-acting elements (commonly known as the antioxidant response elements (ARE)) within the promoters of Nrf2 downstream genes and facilitate their transcription (Suzuki and Yamamoto, 2015, Tebay et al., 2015). Besides defending the cells against oxidative stress, the Nrf2-targeted genes, also called Nrf2 regulon, have other protective functions that include homeostasis, efflux and drug metabolism [Table 4.1] (Tufekci et al., 2011).

Table 4.1 Examples of Nrf2 target genes

Group	Gene	Function
Glutathione homeostasis	GSH (γ-glutamyl-cysteinyl-glycine)	Maintains redox Homeostasis during oxidative stress
	GST (Glutathione-S-transferase)	Cellular detoxification
	Gcl (Glutamate cysteine ligase)	Catalyses glutathione synthesis
	Gcl (Glutamate cysteine ligase)	
	GS (Glutathione Synthetase)	
	GPx (Glutathione Peroxidase)	Catalyses reduction of H₂O₂
GR (Glutathione Reductase)	Catalyses reduction of oxidised GSSH to GSH	
Drug metabolism	NQO-1 (NAD(P)H quinone oxidoreductase-1)	Catalyses two-electron reduction of quinones
	Ugt (UDP-glucuronosyltransferases)	Catalyses endogenous and exogenous substances with glucuronic acid
	mEH (Microsomal epoxide hydrolase)	Inactivates epoxides converting to vicinal dihydrodiol
Stress response proteins/iron metabolism	Ferritin	Iron-binding protein having role in iron oxidative stress
	HO-1 (Haem oxygenase-1)	Catalyses oxidative cleavage of Fe-protoporphyrin-IX

The main response to the Nrf2 activation is the expression of the antioxidant genes. However, the table demonstrates that the Nrf2 is involved in various other functions as well. Source: (Tufekci et al., 2011)

Oxidative stress occurs when the production of ROS exceeds their physiological levels. The utilisation of glucose to produce energy via OXPHOS is one of the major sources of physiological cellular ROS. The insufficient oxidation and the electron leak that occurs during aerobic respiration leads to the formation of several ROS, such as superoxide anions ($O_2^{\cdot-}$), hydrogen peroxide (H_2O_2), and hydroxyl radical (HO^{\cdot}). ROS are neutralised by several basally expressed proteins. For example, GSH, which is the most abundant synthesised antioxidant in the central nervous system (CNS) (present in millimolar concentration), serves as an electron donor in a reaction that oxidises the free thiol groups into disulphide bonds: $H_2O_2 + 2 GSH = GS-SG + 2H_2O$ (Gandhi and Abramov, 2012). Another example is superoxide dismutase, which catalyses the reduction of superoxide anions into hydrogen peroxides, which is consequently converted into oxygen and water molecules (Bauer, 2014). In addition to the direct antioxidant mechanism, there is an indirect mechanism that involves the induction of gene expression and is considered as a secondary line of defense. The induced genes are not only involved in the synthesis of new antioxidant molecules but also in the reactivation of certain antioxidants that possess redox-active properties. For example, the restoration of the reduced GSH is achieved via the action of glutathione reductase (Jozefczak et al., 2012). Other members of the indirect antioxidants family include NAD(P)H:quinone oxidoreductase-1(NQO1) and glutathione S-transferase (GST) (Tebay et al., 2015). Of note, all of the aforementioned antioxidant-related proteins are expressed upon Nrf2 activation, which demonstrates why Nrf2 is considered to be one of the most important antioxidant pathways in cells (Tebay et al., 2015).

4.1.5 Objectives

In this chapter, the ability of UDCA to activate the Nrf2 pathway will be assessed via the use of reporter cell lines that were specifically developed for this purpose. As mentioned in the method chapter [Heading 2.7], the ARE-CHO reporter cell line was designed to express green fluorescent protein (GFP) only when the transcription of the ARE sequence is stimulated. The TK-CHO cell line lacks the ARE sequence in the construct, and therefore it was used to demonstrate that the expression of GFP is strictly linked to the activation of the ARE sequence and not to any other part of the inserted construct. To validate the effect of UCA/UDCA on the Nrf2 pathway, qPCR for

Nrf2 downstream genes was performed. Moreover, the ability of UDCA to reduce oxidative stress was investigated in CuSO₄-stressed cells.

UDCA rescued mitochondrial function in genetic models of PD (Mortiboys et al., 2013). To determine whether this beneficial effect is not just limited to patient tissue or genetically induced models, the effect of UDCA on ATP level and viability was investigated in CHO cells with mitochondrial dysfunction, which was induced via the application of commonly used toxins.

4.2 Investigating the effect of UCA and UDCA on the Nrf2 pathway in CHO cells

4.2.1 Assessing the effects of UCA/UDCA on ARE expression in CHO cells

Testing positive controls and the CHO-ARE reporter

Dimethyl fumarate (BG12) – the methyl ester of fumaric acid – has a robust, Nrf2-mediated antioxidant effect (Lastres-Becker et al., 2016). A pilot test showed that treating ARE-CHO reporter cells with BG12 significantly increased the expression of GFP [Figure 4.2].

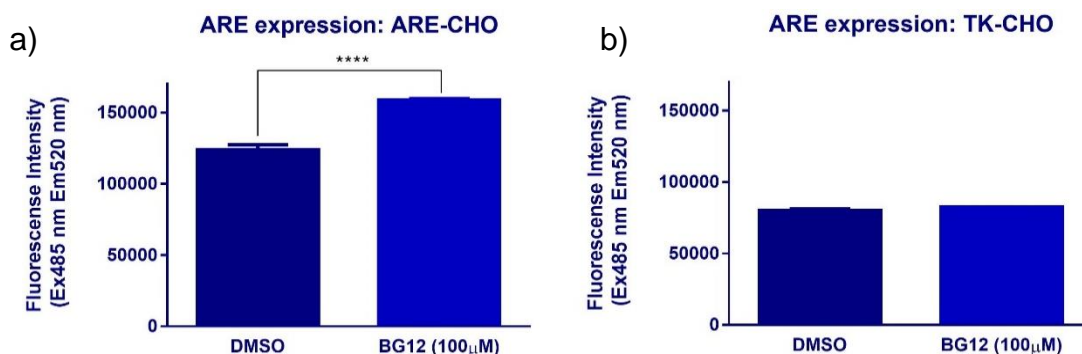


Figure 4.2 BG12 significantly increased ARE expression in CHO reporter cells.

(a) GFP readings of ARE reporter cell lines (ARE-CHO) treated with BG12, and showing a significant increase in ARE expression. By contrast, no increase was observed in the CHO reporter that lacks the ARE sequence in construct (TK-CHO) (b). The cells were treated with 100 μM BG12 for 24 hours in a serum-free medium. The error bars represent the SD of a technical triplicate. **** p < 0.0001, unpaired t-test.

Subsequently, increasing concentrations of BG12 (0.1 μM –100 μM) as well as another known Nrf2 activator, RTA 408 (a synthetic oleanane triterpenoid compound), were tested. Both BG12 and RTA408 showed a dose-dependent response that follows the classical drug response curve [Figure 4.3]. RTA408 was more potent than BG12 but had a higher toxicity, which was apparent when the cells were examined under the optic microscope. The cells were not able to tolerate more than 1 μM , and as a result, there was a massive decrease in ARE expression readings at this concentration and above [Figure 4.3]. Therefore, it was decided to use BG12 only as a positive control in drug treatment experiments.

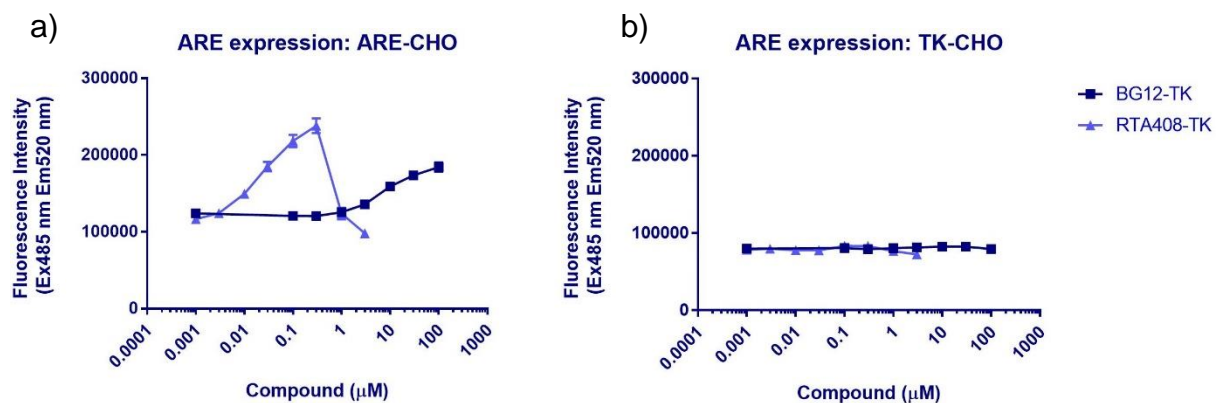


Figure 4.3 BG12 and RTA408 induced a dose dependant increase in ARE expression in CHO reporter cells.

(a) GFP readings of ARE reporter cell lines (ARE-CHO) treated with two positive controls, BG12 and RTA408. RTA408 was more potent but the signal dropped significantly at 1 μM due to cytotoxicity, which was apparent when the cells were examined via optic microscope. (b) As expected, BG12 and RTA408 did not increase the GFP readings in the (TK-CHO) cell line which lack the ARE sequence in the construct [Heading 2.7]. The lowest starting concentrations on the graphs represent the vehicle-treated condition. The cells were treated for 24 hours in a serum-free medium. The error bars represent the SD of a technical triplicate.

Determining the effect of UCA/UDCA on ARE expression in CHO cells

UCA and UDCA treatment was tested at various concentrations (1 μM –300 μM) and time points (2 hours, 16 hours, 24 hours and 48 hours) to assess possible Nrf2 activation by these compounds. The results suggest a small but dose-dependent increase in the GFP readings with UCA and UDCA [Figure 4.4]. The increase in the readings appeared at two hours of treatment and was stable between 16 and 24 hours of treatment. As expected, all the readings of the TK-CHO line of the corresponding conditions remained unchanged, regardless of the increasing concentrations or treatment time [Figure 4.4].

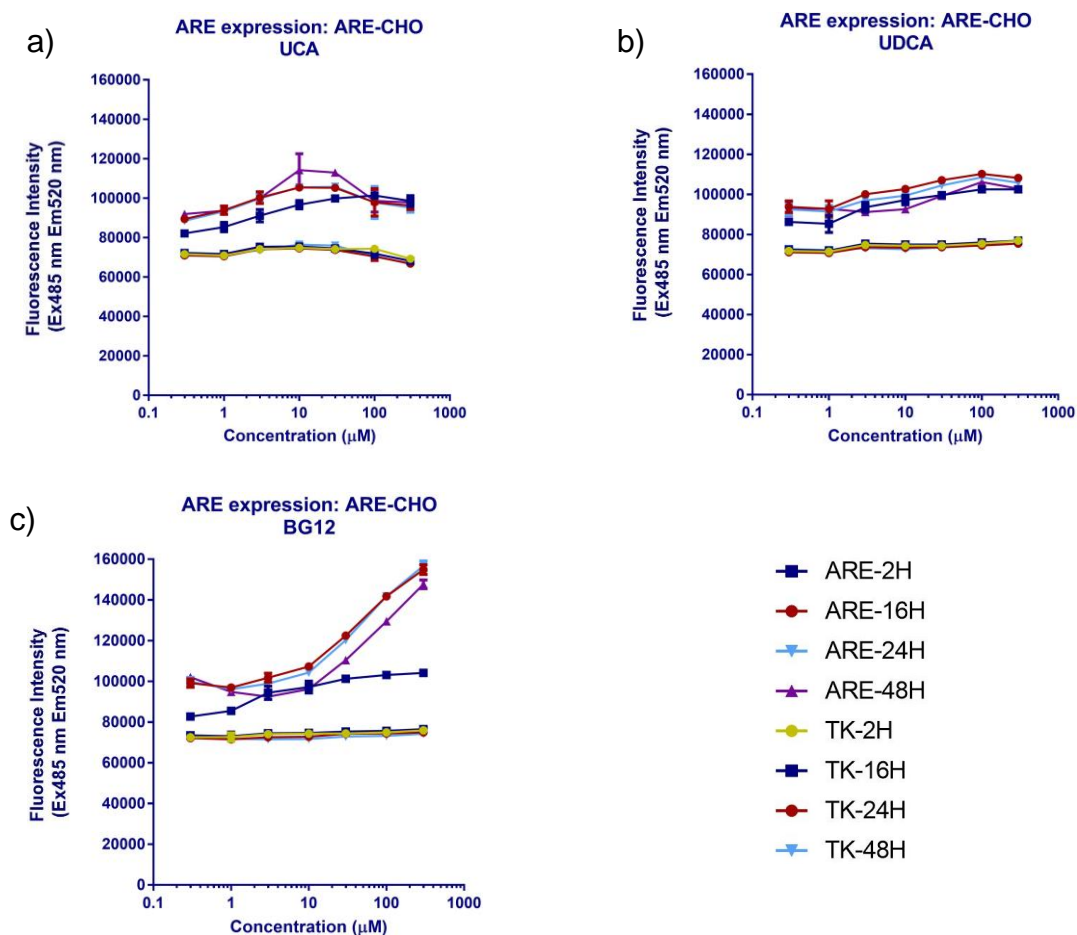


Figure 4.4 UCA and UDCA induced a dose dependant increase in ARE expression at different time points.

GFP readings of CHO reporter cell lines treated with UCA (a), DUCA (b), and BG12 (c). The upper group of lines in each figure represent data obtained from the ARE reporter cell line (ARE-CHO) and the lower groups of lines represent data obtained from the TK-CHO cell line (ARE-deficient reporter). The cells were treated for 2,16, 24 and 48 hours in a serum-free medium. The graphs show a small dose-dependent increase in ARE expression with UCA and UDCA treatment, and a remarkable dose-dependent increase with BG12 treatment. As expected, GFP readings remained unchanged in all treatment conditions. The lowest starting concentrations on the graphs represent the vehicle-treated condition. Drug treatment was performed in a serum-free medium. The error bars represent the SD of a technical triplicate.

To confirm the effect of the drugs on ARE expression, three independent experiments were performed using a wider concentration range (0.1 μM – 1000 μM) of UCA and UDCA for 24 hours [Figure 4.5]. Two conjugated forms of UDCA; TUDCA and GUDCA, were added as well for comparison since most of the UDCA in human is conjugated. The results showed that all the tested UDCA derived compounds exerted a positive effect on ARE expression [Figure 4.5 a]. Although the effect was small in comparison to the positive control, it was statistically significant and positively correlated with the treatment doses.

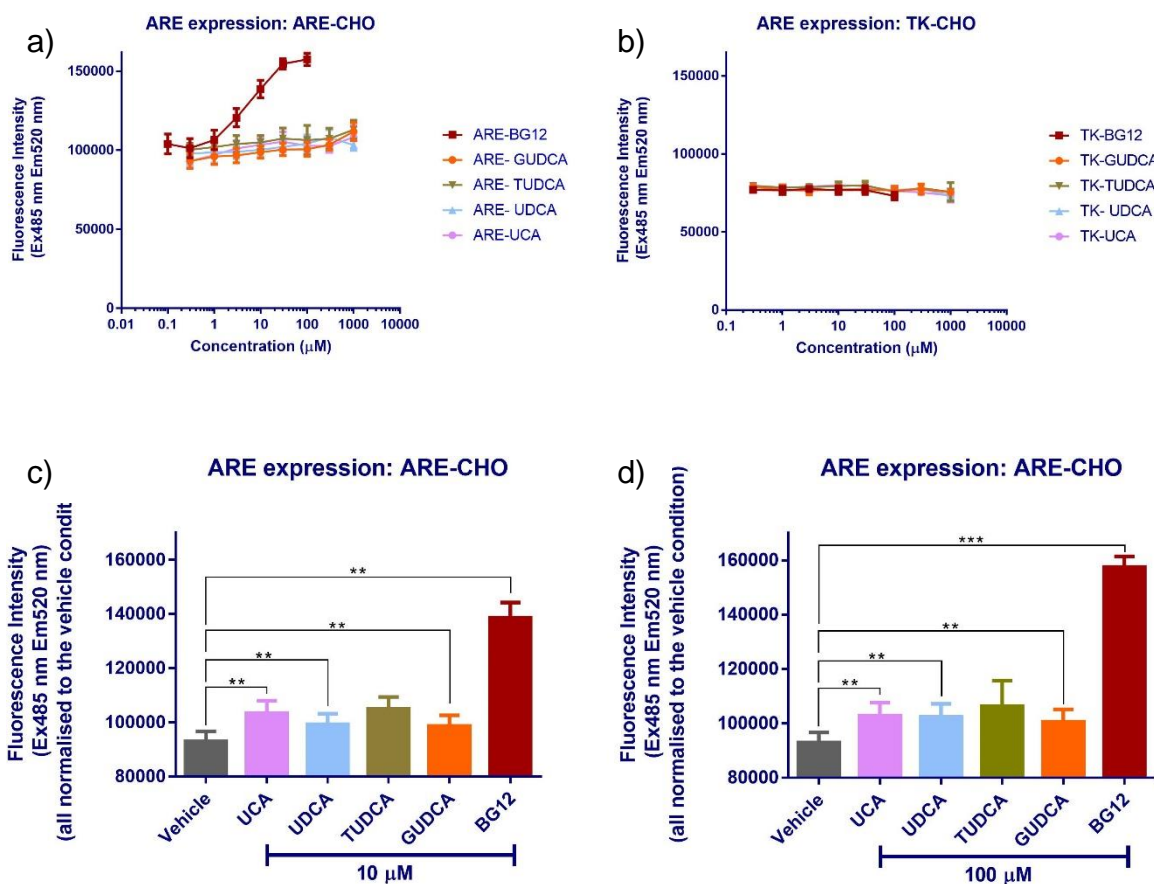


Figure 4.5 24 hours of treatment with increasing concentrations of UCA, UDCA, TUDCA and GUDCA induced a small increase in ARE expression.

(a) GFP readings of ARE reporter cell line (ARE-CHO) treated with increasing concentrations of BG12, GUDCA, TUDCA, UDCA and UCA. The graph demonstrates a comparable dose-dependent increase in ARE expression in all treatment conditions except for BG12 which had a pronounced effect on ARE expression. (b) Equally treated TK-CHO cell lines (ARE-deficient reporter) showed no increase in GFP readings as expected. (c) and (d) Data from the 10 μM and 100 μM conditions in column graphs to elucidate the effect of drugs on ARE expression. The lowest starting concentrations in (a) and (b) represent the vehicle-treated conditions. The cells were treated with 100 μM BG12 for 24 hours in a serum-free medium. The results were obtained from three independent experiments. The error bars represent the SD. ** $p < 0.01$, *** $p < 0.001$, one-way ANOVA test.

4.2.2 Assessing the effect of the UCA/UDCA on the expression of Nrf2 genes in CHO cells

Initial testing of the primers

To verify/confirm the results obtained from the ARE-CHO reporter experiments, the expression of the Nrf2 downstream genes was assessed via RT-qPCR using RNA extracts of the treated cells. Primers for four Nrf2 genes were designed (*NQO1*, *FTH1*, *GCLC* and *HMOX1*), and different concentrations of the forward and the reverse primers were tested as described in the method chapter [Heading 2.6.3] in order to find the optimum combination. All tested concentrations produced similar amplification curves and melt peaks except for *HMOX1* [a and b in Figure 4.6 – Figure 4.10]. To assess the specificity and the efficiency of the reaction, the standard curve and the melt peak were obtained from a serial of ten-fold dilution of the samples. The results revealed a high efficiency and specificity for all primers with the exception of *HMOX1* [d and e in Figure 4.6 – Figure 4.10]. Standard curves of *FTH1* revealed an efficiency of 80%, which is lower than accepted minimum in this project (90%). However, the *FTH1* primers were used in drug treatment experiments because the positive control, BG12, significantly increased the expression of this gene in initial testing [f in Figure 4.8]. Pilot tests also showed that BG12 significantly increased the expression of *NQO1*, and to a lesser extent *GCLC* [f in Figure 4.7 and Figure 4.9]. However, the expression of *HMOX1* was not increased [f in Figure 4.10]. Since *HMOX1* primers showed low specificity and efficiency, it was decided to omit *HMOX1* from the subsequent experiments.

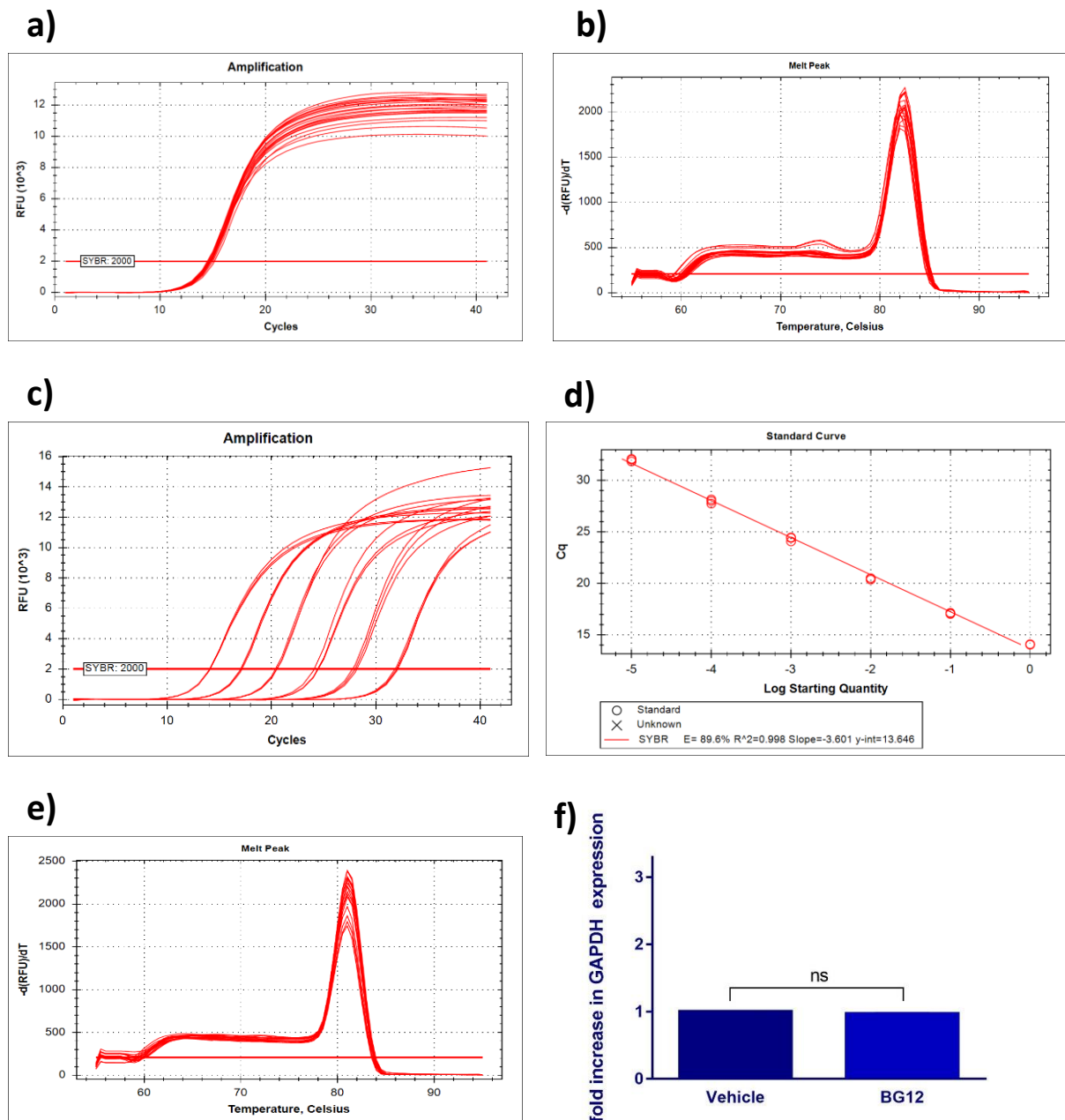


Figure 4.6 *GAPDH* primers have high efficiency and specificity in qPCR reactions.

(a) and (b) Testing combinations of different concentrations of the forward and the reverse primers [Heading 2.6.3]. All combinations showed comparable amplification curves and melt peaks. (c), (d) and (e) Assessing the reacting efficiency and specificity using a ten-fold serial dilution of the sample. The standard curves revealed an efficiency of 89.6 %. The melt peak graph showed single peaks with all dilutions of the sample indicating high specificity. (f) Analysed qPCR results of BG12 treated samples. As expected, the treatment did not increase the expression of *GAPDH*. The error bars represent the SD of a technical triplicate. ns $p > 0.05$, unpaired t-test.

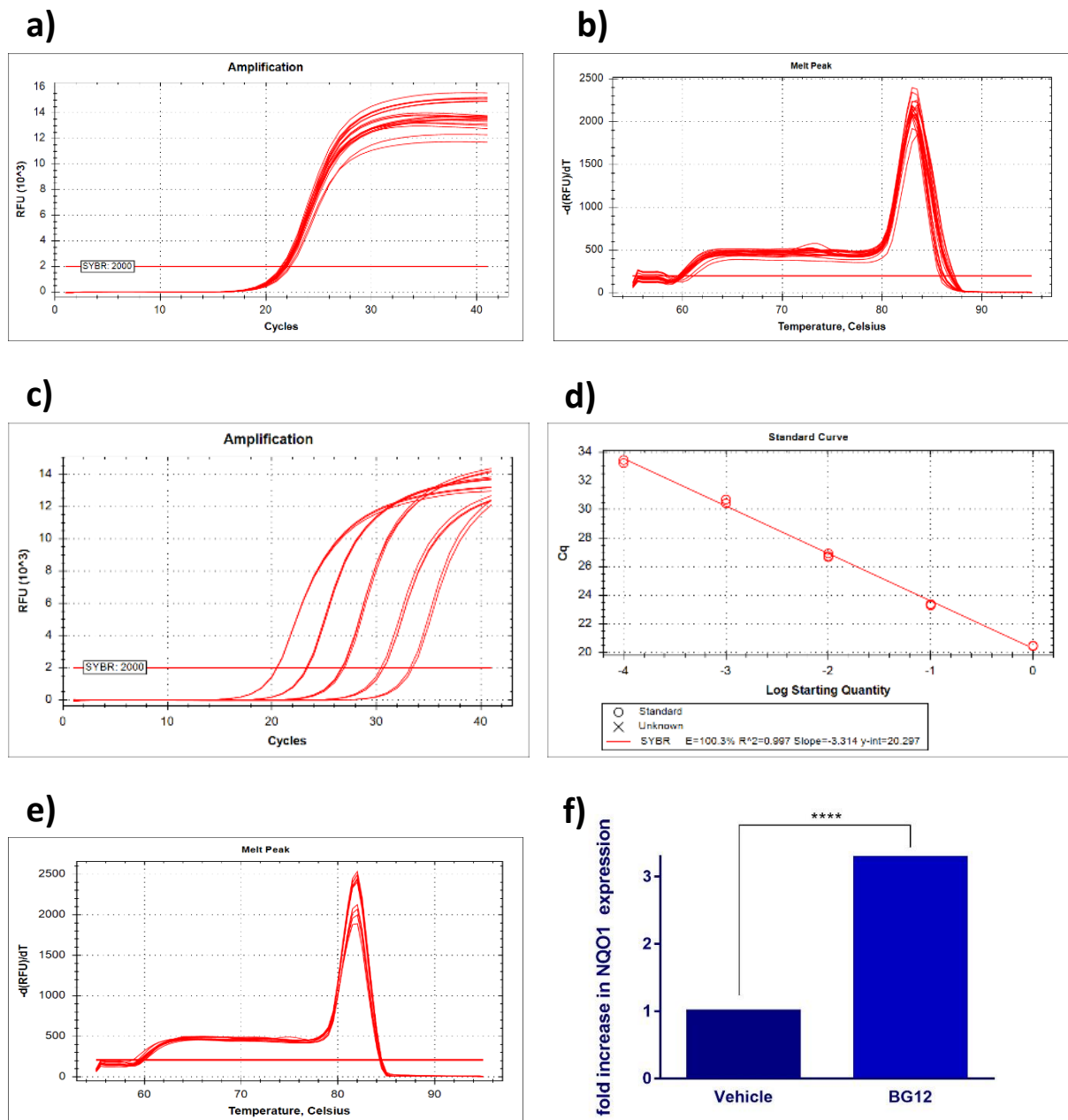


Figure 4.7 *NQO1* primers have high efficiency and specificity in qPCR reactions.

(a) and (b) Testing combinations of different concentrations of the forward and the reverse primers [Heading 2.6.3]. All combinations showed comparable amplification curves and melt peaks. (c), (d) and (e) Assessing the reacting efficiency and specificity using a ten-fold serial dilution of the sample. The standard curves revealed an efficiency of 100.3%. The melt peak graph showed single peaks with all dilutions of the sample indicating high specificity. (f) Analysed qPCR results of BG12 treated samples. BG12 significantly increased the expression of *NQO1*. The error bars represent the SD of a technical triplicate. **** $p < 0.0001$, unpaired t-test.

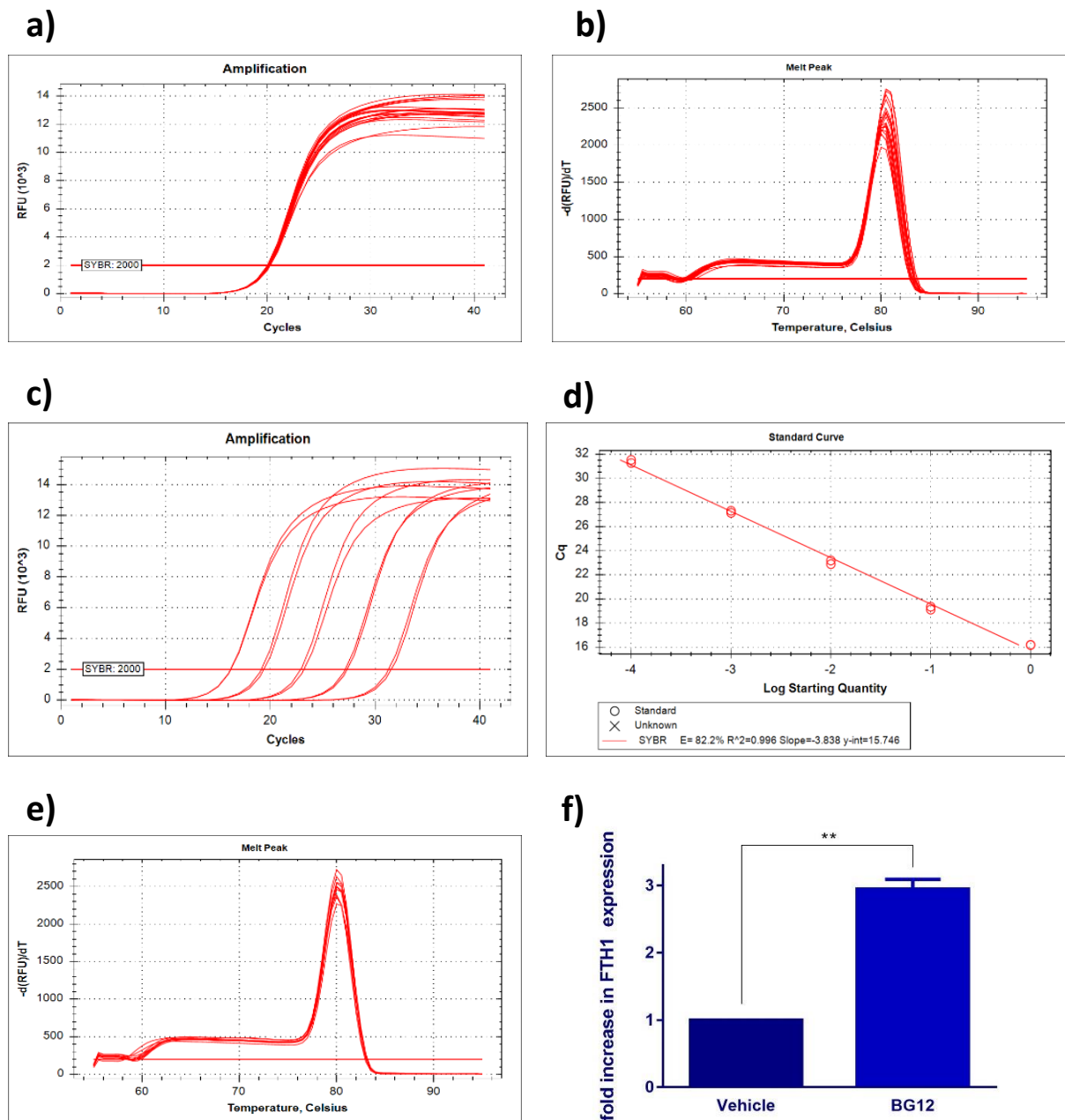


Figure 4.8 *FTH1* primers have sub-optimal efficiency and high specificity in qPCR reactions.

(a) and (b) Testing combinations of different concentrations of the forward and the reverse primers [Heading 2.6.3]. All combinations showed comparable amplification curves and melt peaks. (c), (d) and (e) Assessing the reacting efficiency and specificity using a ten-fold serial dilution of the sample. The standard curves revealed an efficiency of 82.2%. The melt peak graph showed single peaks with all dilutions of the samples indicating high specificity. (f) Analysed qPCR results of BG12 treated sample. BG12 significantly increased the expression of *FTH1*. The error bars represent the SD of a technical triplicate. ** $p < 0.01$, unpaired t-test.

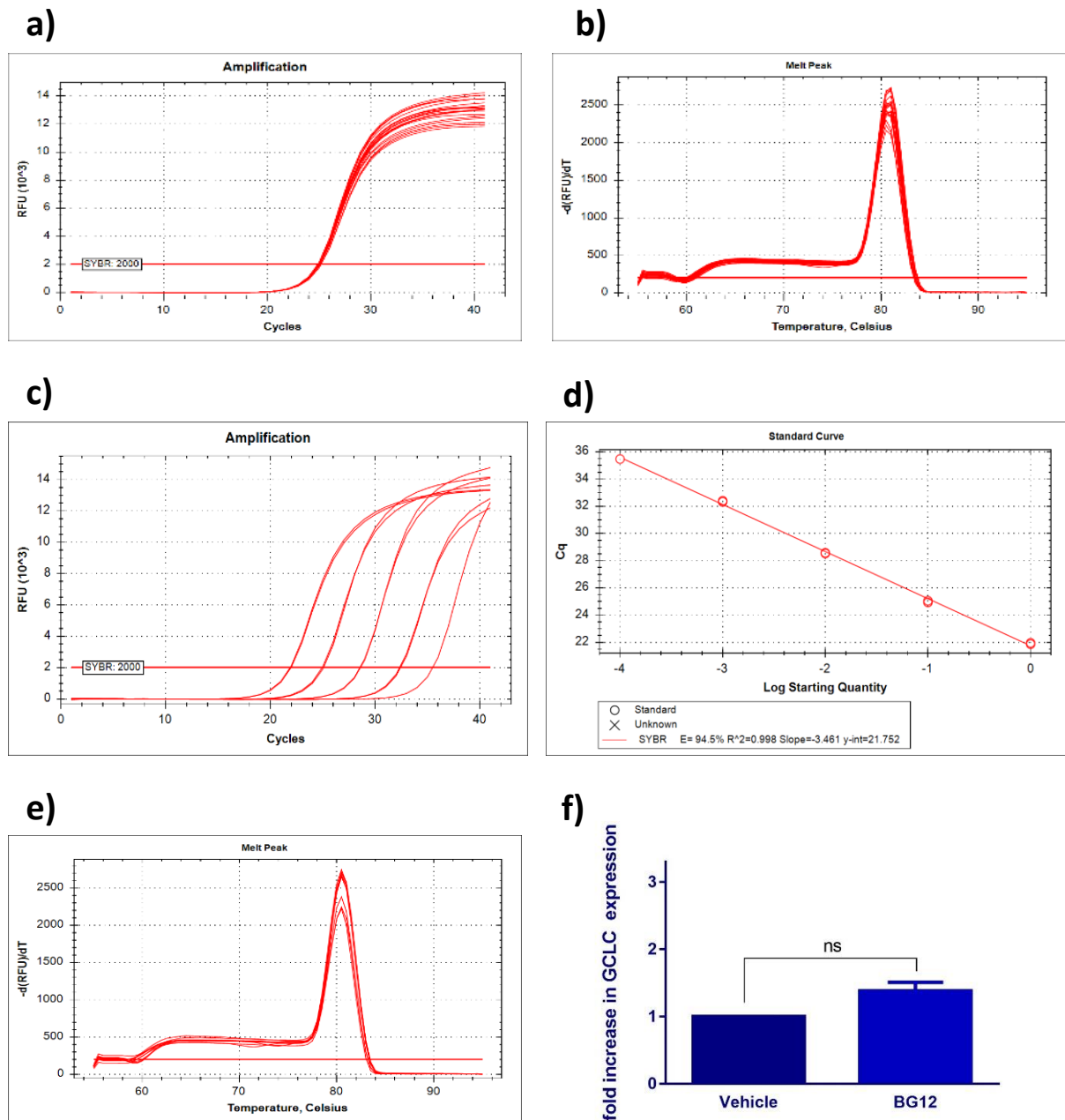


Figure 4.9 GCLC primers have high efficiency and specificity in qPCR reactions.

(a) and (b) Testing combinations of different concentrations of the forward and the reverse primers [Heading 2.6.3]. All combinations showed comparable amplification curves and melt peaks. (c), (d) and (e) Assessing the reacting efficiency and specificity using a ten-fold serial dilution of the sample. The standard curves revealed an efficiency of 94.5 %. The melt peak graph showed single peaks with all dilutions of the sample indicating high specificity. (f) Analysed qPCR results of BG12 treated samples. BG12 treatment resulted in a small non-significant increase in *GCLC* expression. The error bars represent the SD of a technical triplicate. ns $p > 0.05$, unpaired t-test.

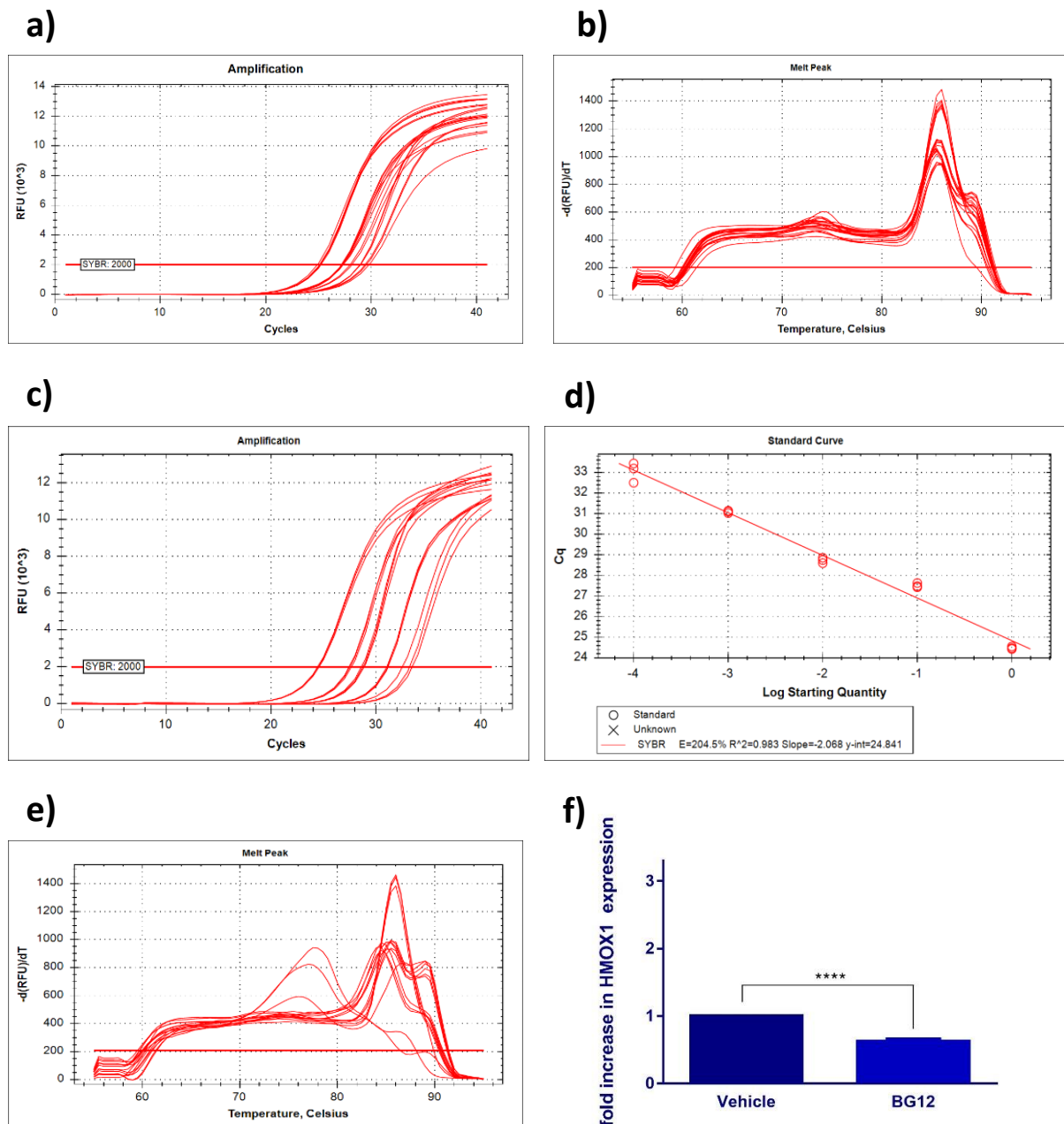


Figure 4.10 *HMOX1* primers have low efficiency and specificity in qPCR reactions.

(a) and (b) Testing combinations of different concentrations of the forward and the reverse primers [Heading 2.6.3]. The results showed variable amplification curves and double peaks in the melt peak graphs. (c), (d) and (e) Assessing the reacting efficiency and specificity using a ten-fold serial dilution of the sample. The standard curves revealed an efficiency of 204.5 %. The melt peak graph showed multiple peaks with all dilutions of the sample indicating that the reaction is not specific. (f) Analysed qPCR results of BG12 treated samples. Unexpectedly, BG12 treatment resulted in a decrease in *HMOX1* expression. The error bars represent the SD of a technical triplicate. **** $p < 0.0001$, unpaired t-test.

Assessing the effect of UCA and UDCA on the expression of Nrf2 downstream genes in CHO cells

Based on the previously obtained result using the ARE reporter cell line [Figure 4.5], it was decided to treat the cells with 10 μ M of the drugs for 24 hours. The results showed that the response to drug treatment was not comparable in these three genes. Upon treatment with UCA, there was a significant increase in the expression of *GCLC* and *FTH1*, and a decrease in the expression of *NQO1*. UDCA, on the other hand, only increased the expression of *NQO1*. BG12 treatment significantly increased the expression of *NQO1* and induced a small non-significant increase in *FTH1* [Figure 4.11].

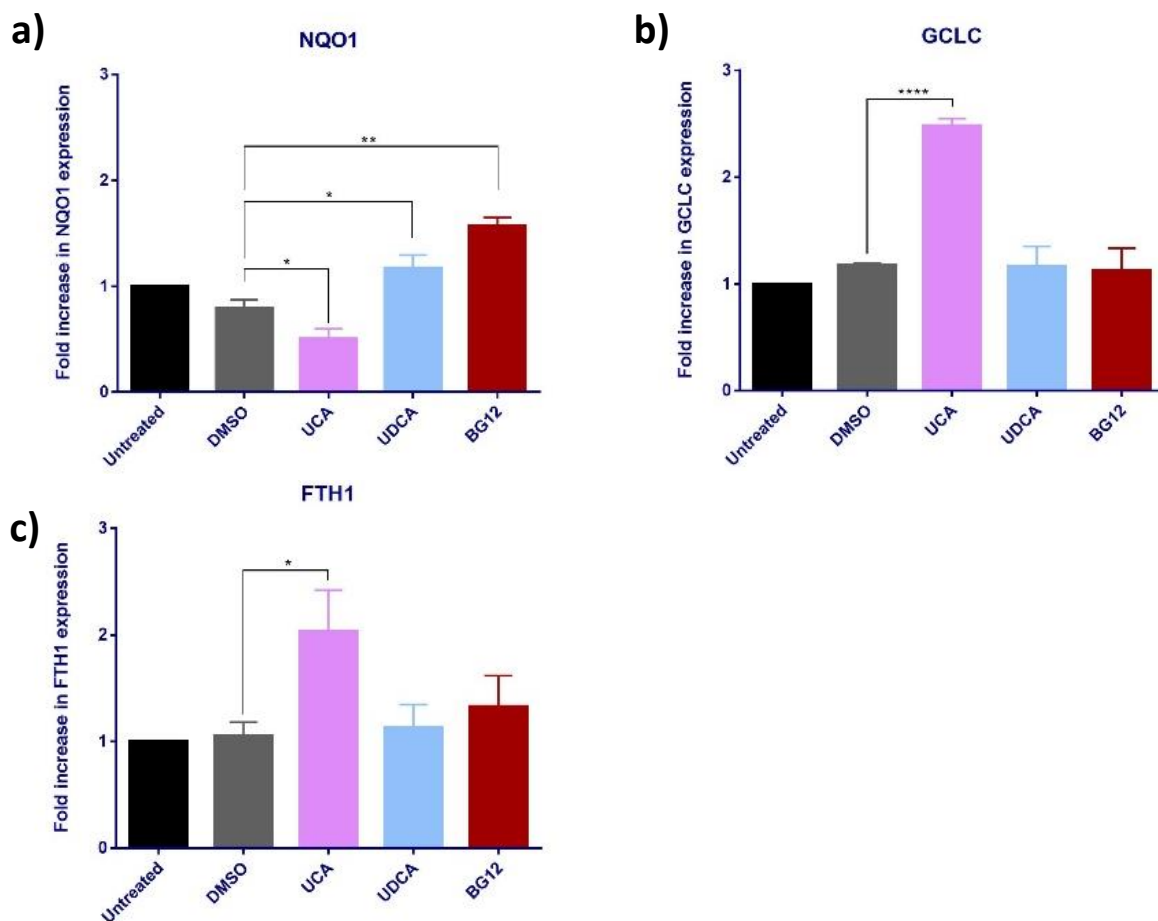


Figure 4.11 UCA and UDCA exert variable effect on the expression of Nrf2 downstream genes.

Assessing the effect of the drugs on the Nrf2 downstream genes in CHO cells was performed by qPCR. Data analysis revealed that UDCA significantly increased the expression of *NQO1* (a) but did not increase the expression of *GCLC* (b) and *FTH1* (c). The cells were treated with 10 μ M of the drugs for 24 hours in a serum-free medium. The graphs represent data of three independent experiments. The error bars represent SD. * $p < 0.05$, ** $p < 0.01$, **** $p < 0.0001$, one-way ANOVA test.

4.3 Assessing the ability of UCA and UDCA to ameliorate oxidative stress in CHO cells

4.3.1 Optimising DCF concentrations and assessing the effect of different stressors

The effect of the drugs on ROS levels in stressed cells was assessed through the use of DCF reagent, which transforms into a fluorescent molecule upon exposure to hydroxyl radicals. Different stressors were tested as ROS inducers in this pilot experiment, but the increase in fluorescence was only seen with CuSO_4 (40% - 50% increase) [Figure 4.12 a, b, c,]. The stressors were added one hour before the application of the DCF. Notably, upon stressing the cells with CuSO_4 , the signals of stressed and unstressed conditions were simultaneously positively correlated with the concentrations of the DCF [Figure 4.12 b]. 20 μM of DCF was selected as the default for all experiments in this chapter. Negative control conditions in Figure 4.12 d indicate that the DCF produced signals only when it was within the cells and that there were no other sources of green fluorescence in the culture.

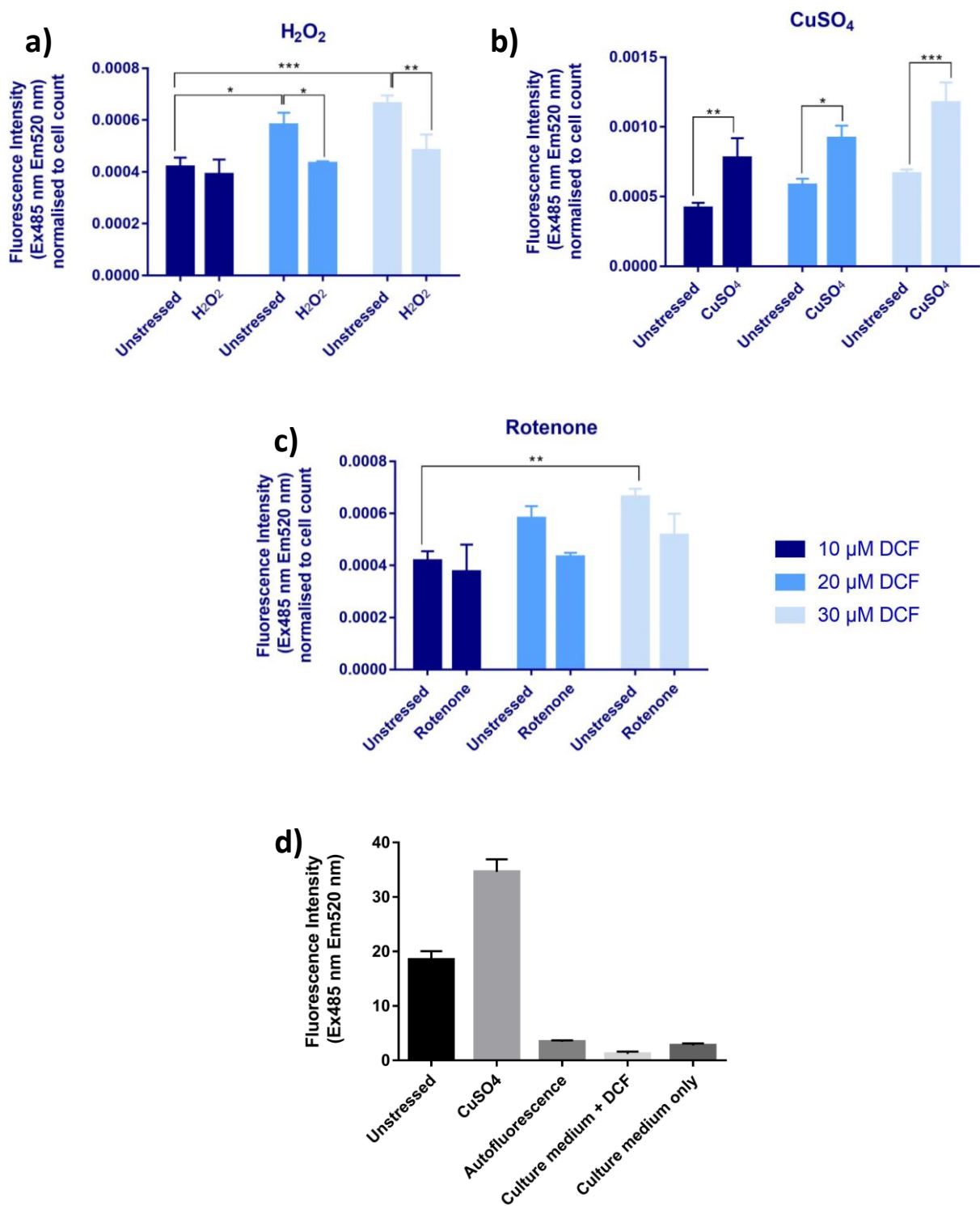


Figure 4.12 DCF readings are significantly increased in CuSO₄ stressed CHO cells.

The CHO cells were serum starved for 24 hours and the stressor was added one hour prior to the application of the DCF. (a), (b) and (c) Evaluating the effect of rotenone (20 nM), H₂O₂ (400 μM) and CuSO₄ (400 μM) on oxidative stress levels using different DCF concentrations (10 μM, 20 μM and 30 μM). Only CuSO₄ treatment induced a significant increase in green fluorescent readings (indicating DCF conversion due to ROS exposure), which was apparent in all tested DCF concentrations. (d) A comparison between the readings of unstressed and stressed cells to the background conditions. Auto fluorescence represents the reading of untreated cells unexposed to DCF. Culture medium + DCF represent cell-free wells with 20 μM DCF. The culture medium condition contains the medium only, without cells and DCF. The error bars represent the SD of a technical triplicate. * p < 0.05, ** p < 0.01, *** p < 0.001, two-way ANOVA test.

4.3.2 Assessing the effect of UCA/UDCA on CuSO₄ stressed CHO cells

The effect of the drugs on the ROS level was assessed in unstressed and CuSO₄-stressed cells. The results showed that treatment with UCA, UDCA and BG12 induced 20% increase in DCF readings in unstressed cells [Figure 4.13]. The application of CuSO₄ increased the signals by 30% in comparison to the unstressed conditions. However, both UDCA and BG12 treatment failed to ameliorate the increase in DCF readings in stressed cells. Notably, UCA treatment induced a significant increase in DCF readings.

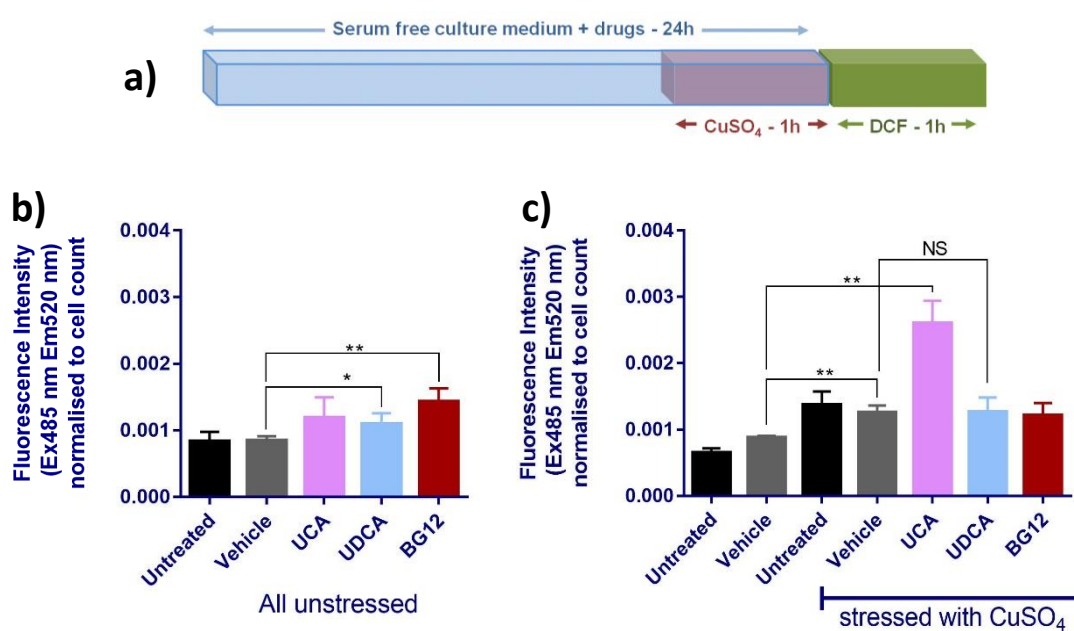


Figure 4.13 Initial experiments showed that UCA and UDCA do not decrease DCF readings in CuSO₄-stressed cells.

(a) A diagrammatic representation of the experiment design. The CHO cells were treated and serum starved for 24 hours, and the stressor was added 1 hour prior to the application of the DCF. (b) and (c) Green fluorescent readings of ROS-exposed DCF in unstressed (a) and stressed (b) cells. UDCA treatment failed to reduce DCF readings in the stressed cells. In contrast, UCA significantly increased DCF signals in the stressed cells. The cells were treated with 10 μ M of each drug in serum-free medium according to the experiment design. Cells were stressed with 400 μ M CuSO₄. The graphs represent data of three independent experiments. The error bars represent SD. * p < 0.05, ** p < 0.01, one-way ANOVA test.

4.3.3 Evaluating the effect of CuSO₄ using a second stressing method (protocol B)

The aim of this experiment was to assess the ability of UCA and UDCA to decrease oxidative stress using an alternative stressing method. In this protocol, the stressor and the drug were applied for one hour. Then the stressor was removed and the drug was kept for a certain time before the application of the DCF [Figure 4.14 a]. Prior to performing the drug treatment experiments, many different concentrations of CuSO₄ were tested with various recovery times [Figure 4.14 b]. The results generally showed that there is no statistically significant difference between unstressed and stressed cells except for the 24 hours' conditions with 200 μM CuSO₄ (27%) and 300 μM CuSO₄ (30%) [Figure 4.14 b].

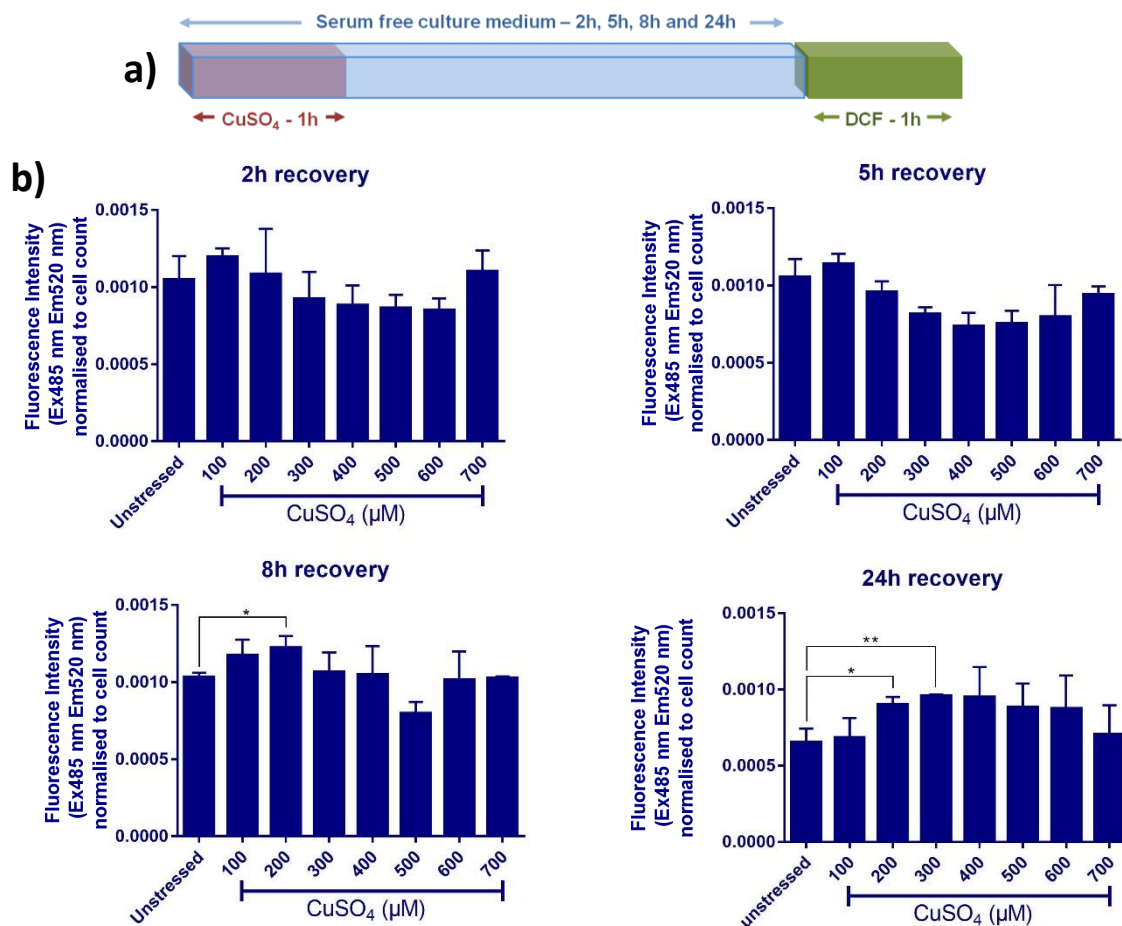


Figure 4.14 Testing a second stressing method (protocol B) demonstrated an increase in DCF reading with 24h recovery time.

(a) A diagrammatic representation of the experiment design. The CHO cells were serum starved for 24 hours. CuSO₄ was applied for one hour and cells were allowed to recover for a certain time (2, 5, 8 or 24 hours) before the application of the DCF. (b) Evaluating the effect different recovery times on oxidative stress levels in cell treated with increasing concentrations of CuSO₄. The results showed an increase in DCF readings when CuSO₄ (200 μM and 300 μM) was removed 24 hours prior the application of the DCF. The error bars represent the SD of a technical triplicate. * p < 0.05, ** p < 0.01, one-way ANOVA test.

4.3.4 Assessing the effect of UCA/UDCA on CuSO₄-stressed CHO cells (protocol B)

In accordance with the results in the previous section, it was decided to test the drugs with two concentrations of CuSO₄: 200 μM and 300 μM. However, the small increase that was observed in the previous test was not present when the experiment was repeated [Figure 4.15 c, d]. Nevertheless, the UCA and UDCA did not decrease DCF readings in all conditions [Figure 4.15]. Since the BG12 did not show a positive effect in the previous experiments, it was decided to add Trolox as an alternative positive control. Trolox is an analogue of vitamin E that has been used in biological and biochemical applications to reduce oxidative stress. Multiple concentrations of Trolox were tested but there was no decrease in DCF levels in stressed and unstressed cells [Figure 4.15].

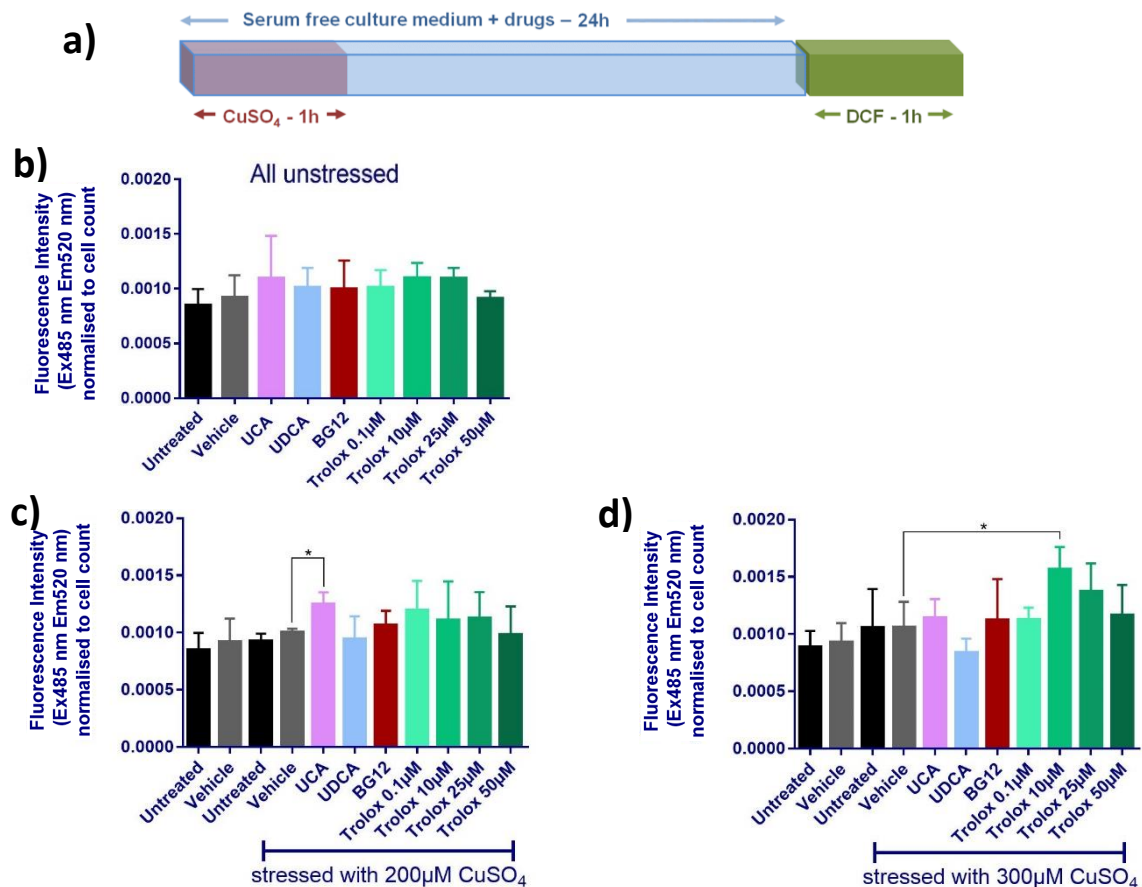


Figure 4.15 UCA and UDCA had no positive effect in CuSO₄-stressed cells (protocol B).

A diagrammatic representation of the experiment design. The CHO cells were serum starved for 24 hours. CuSO₄ was applied for one hour and cells were allowed to recover for 24 hours before the application of the DCF. (b), (c) and (d) Green fluorescent readings of ROS-exposed DCF in unstressed and stressed cells. The cells were treated with Trolox as an additional antioxidant positive control. All treatments failed to reduce DCF readings in the stressed cells. The cells were treated with 10 μM of each drug in serum-free medium according to the experiment design. The graphs represent data of three independent experiments. The error bars represent SD. * p < 0.05, one-way ANOVA test.

4.3.5 Evaluating the effect of CuSO₄ using a third stressing method (protocol C)

Since CuSO₄ failed to demonstrate consistent results in the previous experiments, it was decided to test a third stressing method. In this protocol, the stressor and the drug were applied simultaneously for 24 hours before the application of the DCF [Figure 4.16 a]. Testing different concentrations of CuSO₄ revealed a clear dose-dependent increase in DCF signals [Figure 4.16 b]. Examining the cells under light microscopy showed that high doses, 500 μ M and – to some extent – 400 μ M, had a negative effect on cell morphology and viability, which was not noticed in the previous experiments. Therefore, it was decided to use 200 μ M and 300 μ M CuSO₄ in the drug treatment experiment.

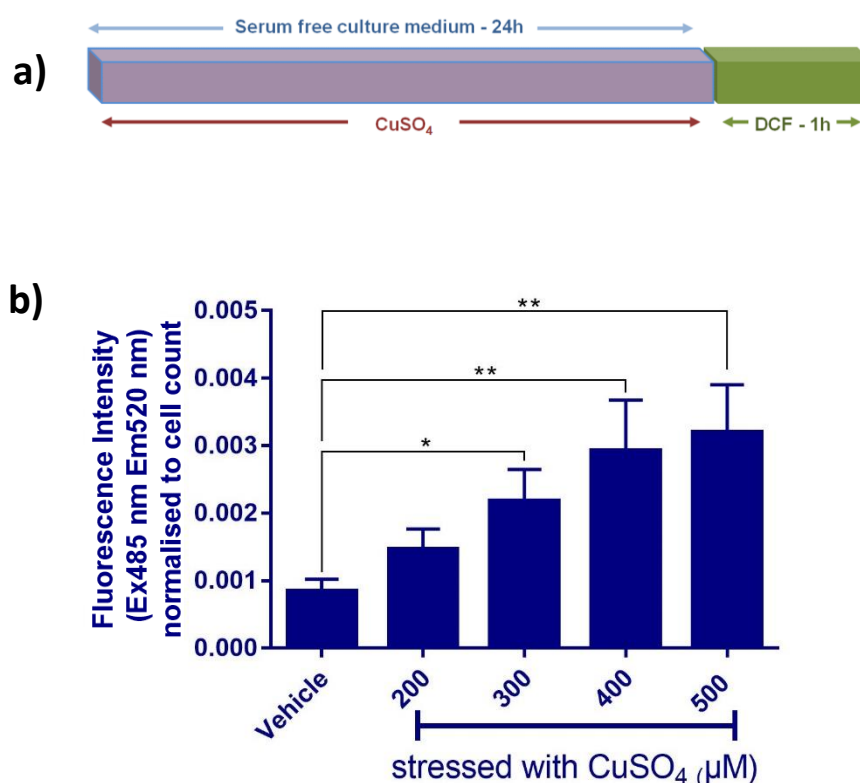


Figure 4.16 Testing a third stressing method (protocol C) demonstrated clear dose-dependent increase in DCF reading.

(a) A diagrammatic representation of the experiment design. The CHO cells were serum starved and treated with CuSO₄ for 24 hours before the application of the DCF. (b) Evaluating the effect of increasing CuSO₄ doses on converted DCF signals (green fluorescent readings) revealed a clear dose-dependent response. The graphs represent data of three independent experiments. The error bars represent SD. * p < 0.05, ** p < 0.01, one-way ANOVA test.

4.3.6 Assessing the effect of UCA/UDCA on CuSO₄-stressed CHO cells (protocol C)

As shown in the previous experiment, the third stressing method proved to be reliable in increasing the DCF readings. The application of 200 μM CuSO₄ increased DCF readings by 55%, while the application of 300 μM CuSO₄ increased DCF readings by 65% [Figure 4.17 c, d]. However, UCA and UDCA treatment failed to reduce DCF readings. Similar findings were also seen with BG12 and Trolox [Figure 4.17].

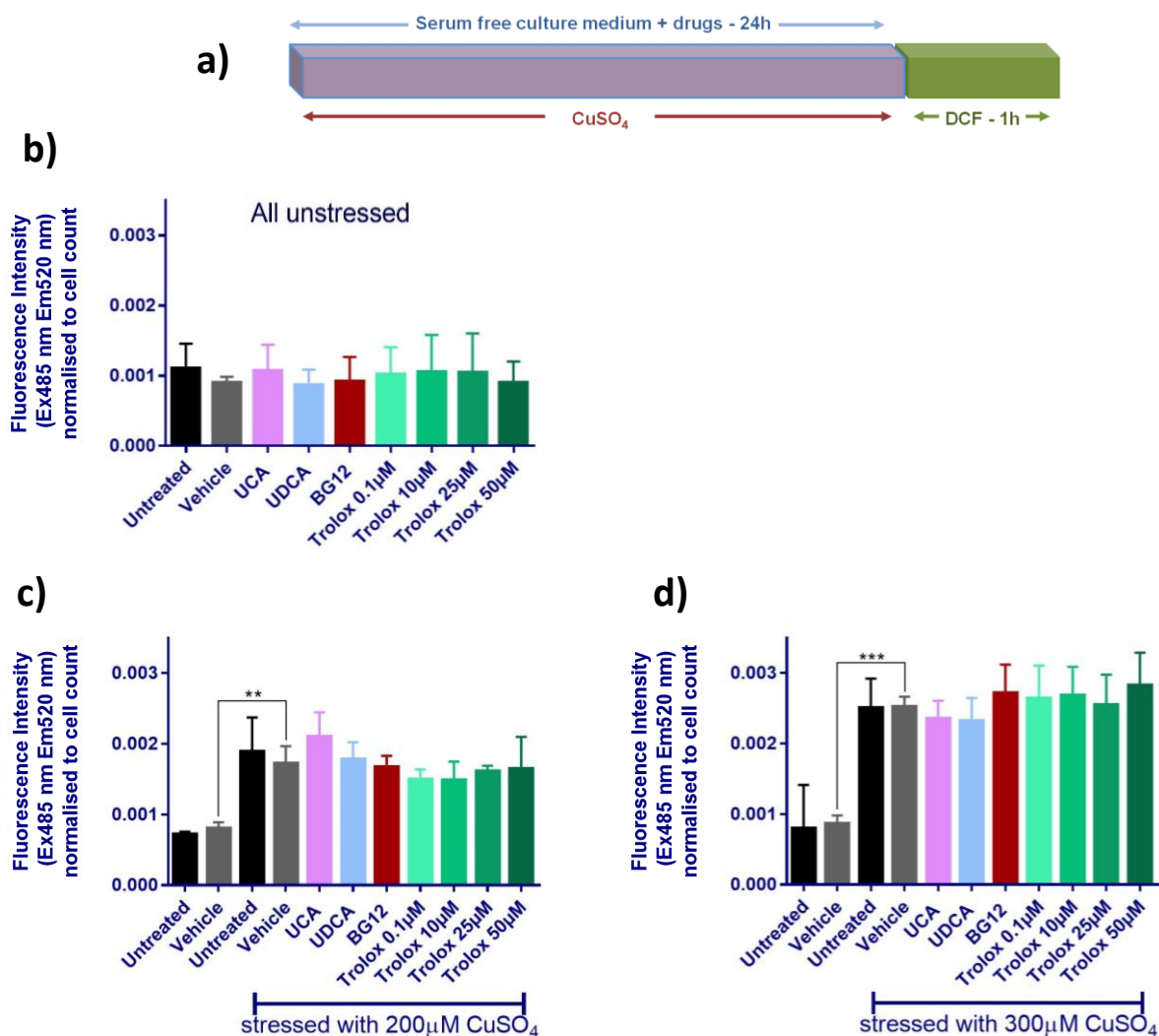


Figure 4.17 UCA and UDCA had no positive effect in CuSO₄-stressed cells (protocol C).

A diagrammatic representation of the experiment design. The CHO cells were serum starved and treated with CuSO₄ and the drugs for 24 hours before the application of the DCF. (b) (c) and (d) Green fluorescent readings of ROS-exposed DCF in unstressed cells (b) and in cells stressed with either 200 μM CuSO₄ (c) or 300 μM CuSO₄ (d). The cells were treated with Trolox as an additional antioxidant positive control. Although CuSO₄ significantly increased DCF signals, all treatment conditions did not reduce DCF readings in the stressed cells. The cells were treated with 10 μM of each drug in serum-free medium according to the experiment design. The graphs represent data of three independent experiments. The error bars represent SD. ** $p < 0.01$, one-way ANOVA test.

4.4 Investigating the ability of UCA/UDCA to rescue mitochondrial function in stressed CHO cells

4.4.1 Optimisation experiments for rotenone treatment

Optimisation of culture medium

The initial rotenone-dosing experiment showed that rotenone (up to 10 μM) had no effect on cytotoxicity [Figure 4.18 a]. Assessing ATP reduction after rotenone treatment showed 45% decrease in ATP level with 0.1 μM rotenone. However, this percentage did not change with the application of higher rotenone doses (up to 10 μM) [Figure 4.18 a]. Similar findings regarding ATP levels were observed when the experiment was repeated using a different mitochondrial inhibitor, antimycinA [Figure 4.18 b].

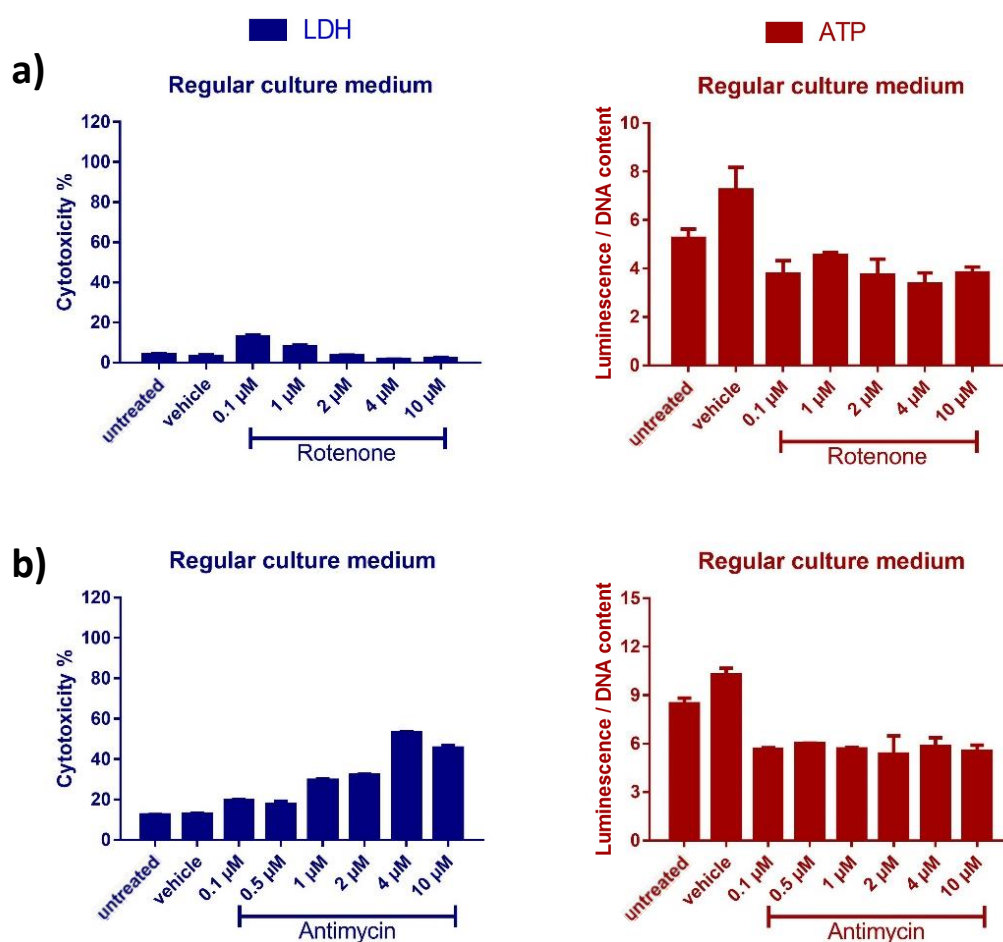


Figure 4.18 Rotenone and antimycinA did not show a dose-dependant effect on LDH and ATP readings in regular culture medium.

Cytotoxicity and ATP levels were measured using LDH and ATP assays as described in the method chapter [2.9.1, 2.10]. The CHO cells were stressed with increasing concentrations of either rotenone (a) or antimycinA (b) for 48 hours in regular culture medium. The results did not show a dose-dependent decrease in ATP with both toxins. The error bars represent the SD of a technical triplicate.

It might be possible that higher concentrations of the toxins are needed to produce a greater drop in ATP levels. However, a more plausible explanation is that the cells were able to compensate for the rotenone/antimycinA-induced ATP reduction. Since rotenone and antimycinA interfere with OXPHOS by inhibiting complex I and complex III of the mitochondrial respiratory chain, the cells probably relied on glycolysis to produce energy. When the glucose in the medium was replaced by galactose to force the cells to depend on oxidative phosphorylation, there was a dramatic increase in the sensitivity towards the rotenone [Figure 4.19 a]. The lowest tested rotenone concentration (0.1 μM) was sufficient to induce marked cytotoxicity. To verify the results, the experiment was repeated using a regular culture medium supplemented with 2-Deoxy-D-Glucose, a glucose analogue that inhibits glycolysis via its actions on hexokinase. As expected, the results were comparable to what was observed with the galactose medium [Figure 4.19 b].

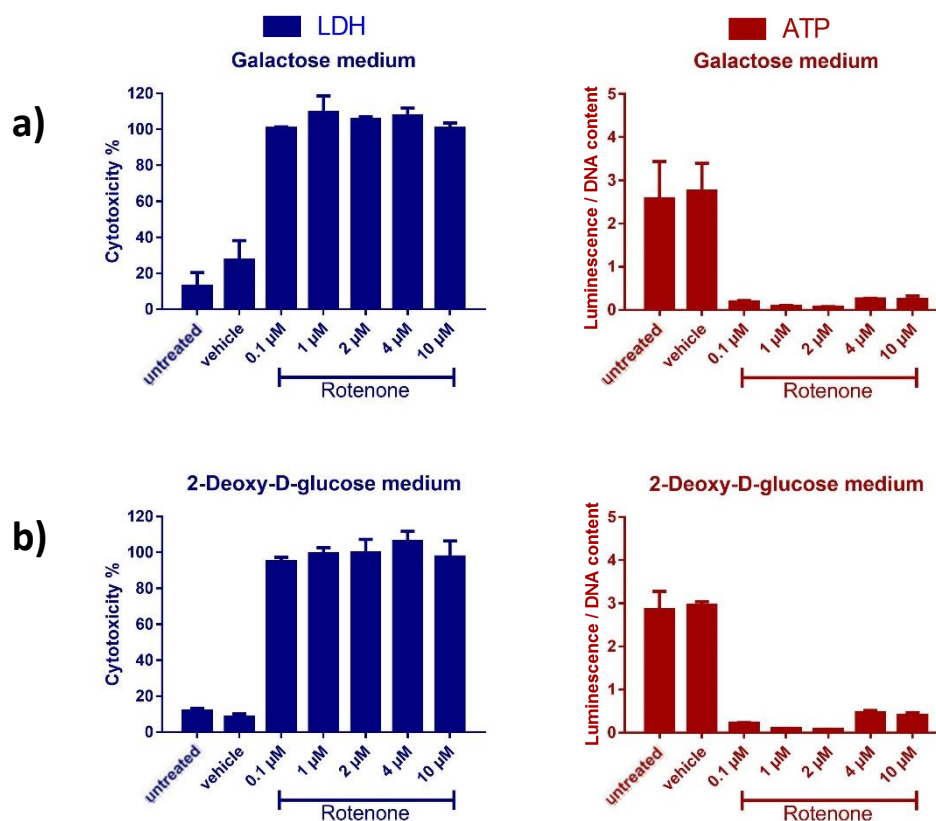


Figure 4.19 The sensitivity toward rotenone was significantly increased in galactose and 2-Deoxy-D-Glucose medium.

Cytotoxicity and ATP levels were measured using LDH and ATP assays as described in the method chapter [Heading 2.9.1, 2.10]. The CHO cells were stressed for 48 hours with increasing concentrations of rotenone in either galactose medium (a) or 2-Deoxy-D-Glucose medium (b). The results showed a remarkable increase in the sensitivity towards the rotenone as the lowest tested concentration (0.1 μM) was toxic to the cells. The error bars represent the SD of a technical triplicate.

Optimisation rotenone dose and treatment time

The CHO cells became highly sensitive to rotenone when they were cultured in galactose medium. Lower concentrations of rotenone needed to be tested since the lowest concentration (0.1 μM) in the previous experiment was lethal to the cells. In this experiment a range of low rotenone concentrations at the scale of nanomolar (20 nM -120 nM) were tested at different time points (24 hours and 48 hours). The results showed that treatment with 20 nM of rotenone did not induce LDH leakage in the 24 hour condition but was associated with a massive reduction in ATP levels [Figure 4.20].

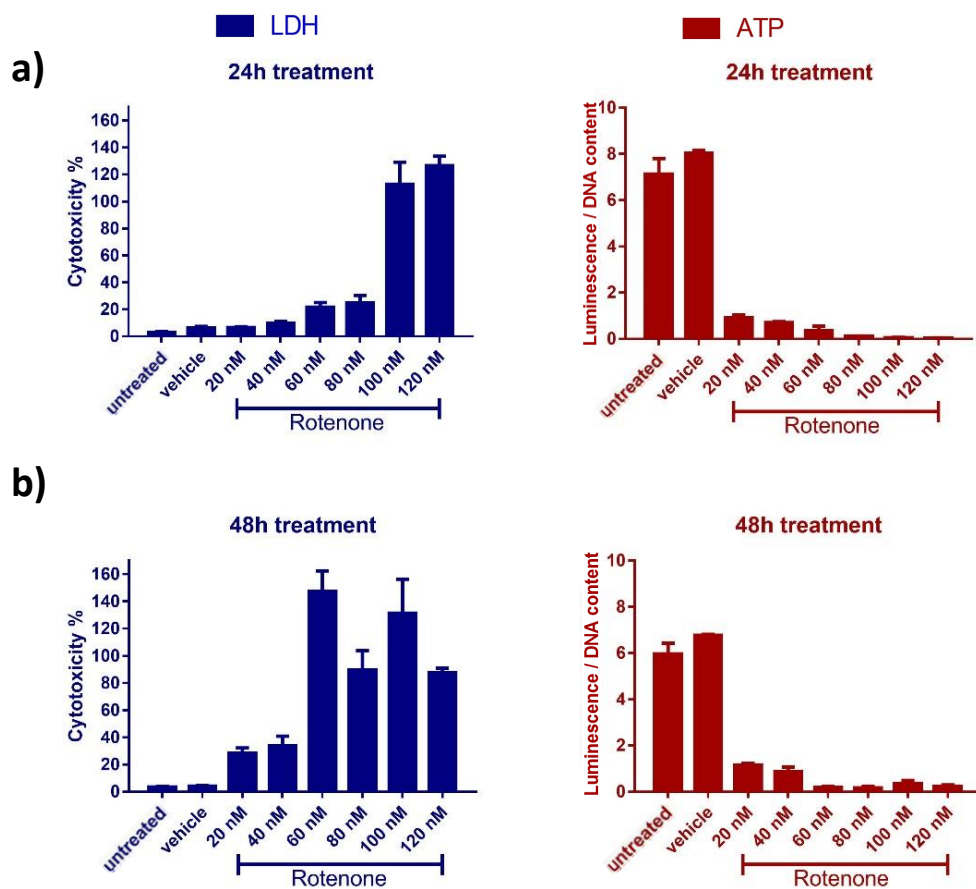


Figure 4.20 Low rotenone doses had massive effects on LDH and ATP readings when the cells were culture in galactose medium.

Cytotoxicity and ATP levels were measured using LDH and ATP assays as described in the method chapter [Heading 2.9.1, 2.10]. The CHO cells were stressed for either 24 hours (a) or 48 hours (b) with increasing concentrations of rotenone in galactose medium. The results showed that the lowest tested concentration (20nM) was associated with massive decrease in ATP levels. The error bars represent the SD of a technical triplicate.

Accordingly, the experiment was repeated with the addition of lower rotenone concentrations (15 nM, 10 nM and 5 nM). Treatment with 10 nM and 20 nM rotenone induced approximately a 75% and 85% reduction in ATP levels when applied for 24 hours, and a 70% and 85% reduction when applied for 48 hours [Figure 4.21]. For drug treatment experiments, it was decided to stress the cells with 20 nM of rotenone for 24 hours and 10 nM rotenone for 48 hours.

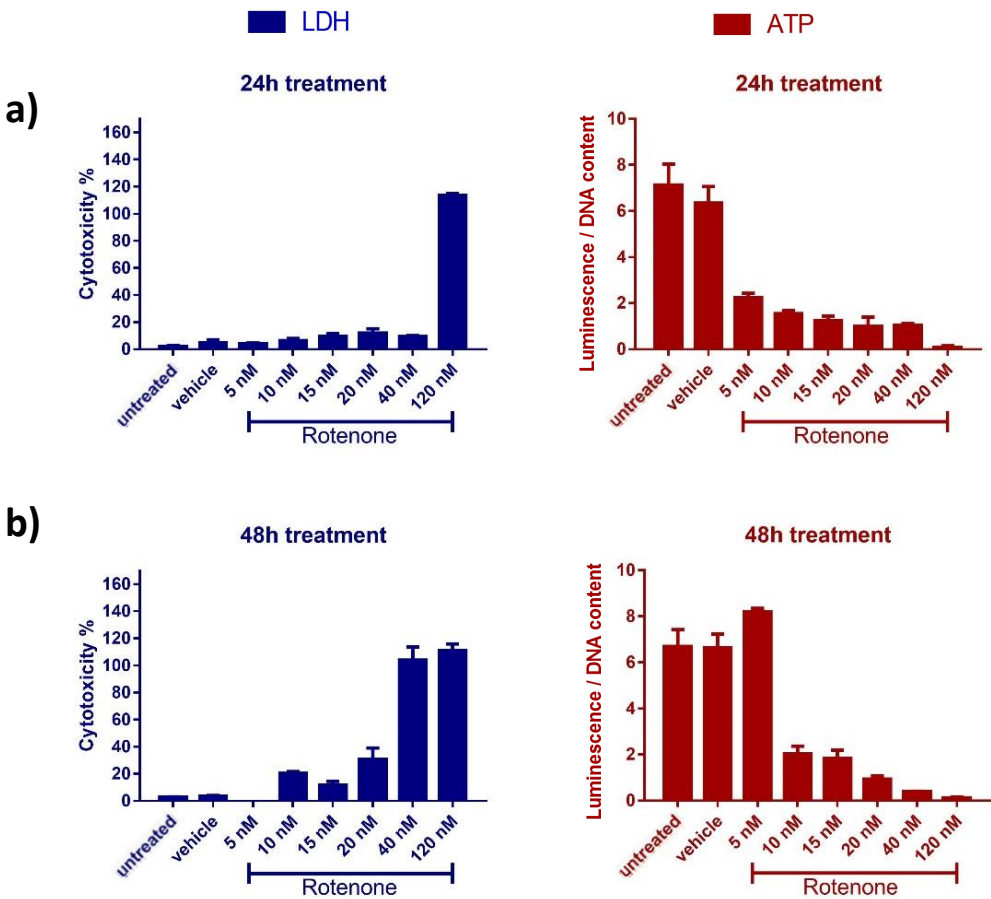


Figure 4.21 Assessing the effect of extra low rotenone doses on LDH and ATP readings at different time points in galactose medium.

Cytotoxicity and ATP levels were measured using LDH and ATP assays as described in the method chapter [Heading 2.9.1, 2.10]. The CHO cells were stressed for either 24 hours (a) or 48 hours (b) with increasing concentrations of rotenone in galactose medium. The results revealed a 70–85 % reduction in ATP with 10 nM and 20 nM rotenone treatment. The error bars represent the SD of a technical triplicate.

4.4.2 Assessing the effect of UCA/UDCA on rotenone-stressed CHO cells

The stressing conditions were determined according to the results of the previous optimisation experiments. In the first drug treatment experiment, both rotenone and UCA/UDCA were applied simultaneously for 24 hours [Figure 4.22]. As expected, there was no significant change in LDH readings when the cells were stressed with rotenone but there was a significant decrease in ATP levels. UCA and UDCA treatment had no positive effect despite the trial of various doses (1 μ M, 10 μ M and 100 μ M) [Figure 4.22].

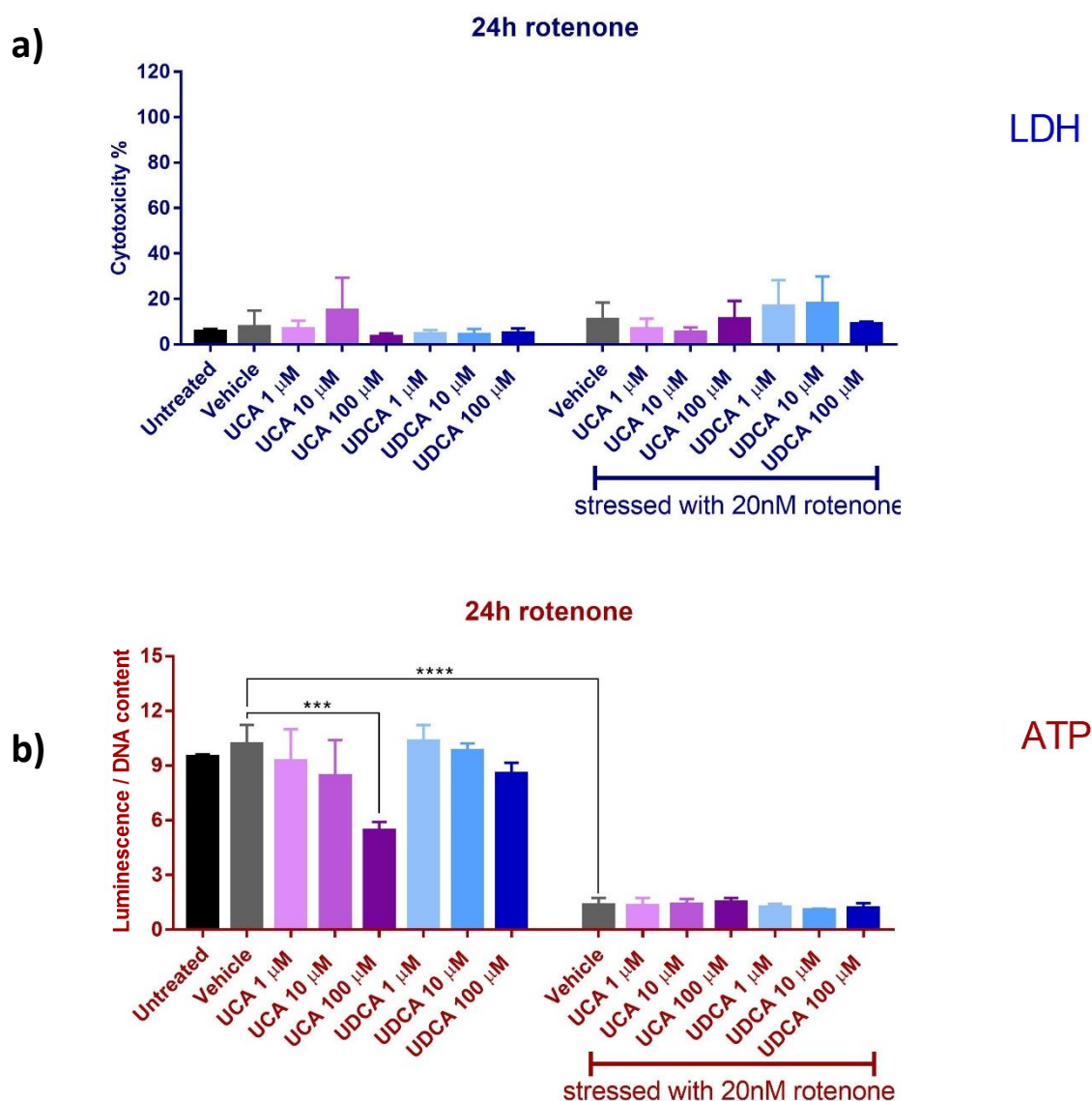


Figure 4.22 Multiple concentrations of UCA and UDCA did not induce a positive effect in unstressed and rotenone-stressed CHO cells (24h rotenone).

Cytotoxicity and ATP levels were measured using LDH and ATP assays as described in the method chapter [Heading 2.9.1, 2.10]. The rotenone and the drugs were applied simultaneously for 24 hours. The results showed that none of the tested UDCA and UCA doses increased ATP levels in rotenone-stressed cells. The error bars represent the SD of three independent experiments. *** $p < 0.001$, **** $p < 0.0001$, two-way ANOVA test.

Subsequently, an alternative treatment method was tested. In this method, the CHO cells were stressed for 24 hours before the addition of UCA/UDCA, which were kept for 24 hours [Figure 4.23]. Again, UCA and UDCA failed to increase ATP levels in the stressed cells.

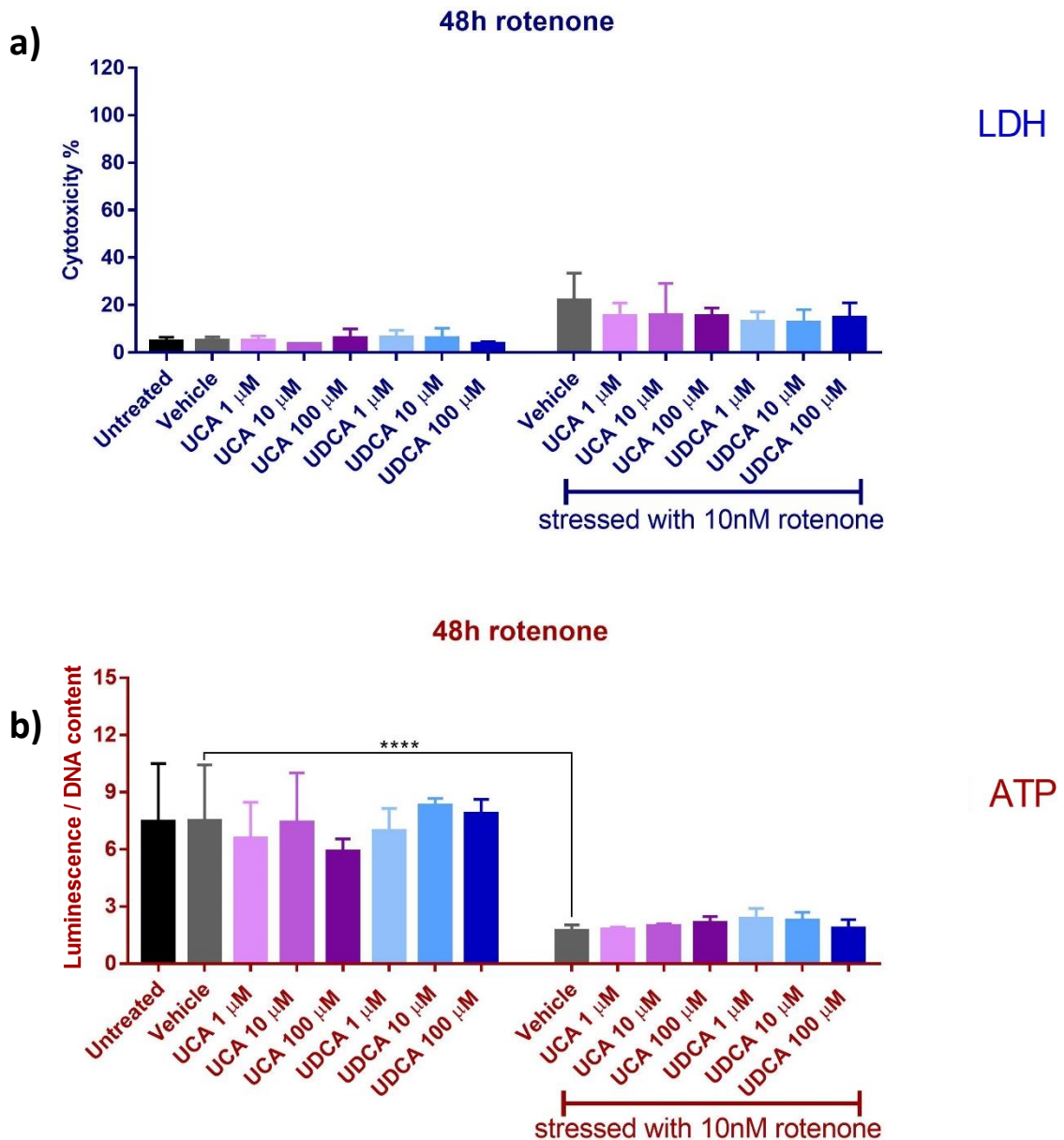


Figure 4.23 Multiple concentrations of UCA and UDCA did not induce a positive effect in unstressed and rotenone-stressed CHO cells (48h rotenone).

Cytotoxicity and ATP levels were measured using LDH and ATP assays as described in the method chapter [Heading 2.9.1, 2.10]. The rotenone was applied for 24 hours. Then the CHO cells were treated with the drugs for 24 hours. The results showed that none of the tested UDCA and UCA doses increased ATP levels in rotenone-stressed cells. The error bars represent the SD of three independent experiments. **** p < 0.0001, two-way ANOVA test.

Finally, the rescue effect of UCA and UDCA was assessed by a third treatment method. In this method, the CHO cells were pre-treated with the drugs for 24 hours and the rotenone was added afterwards for a further 24 hours [Figure 4.24]. UCA and UDCA treatment had no positive effect with this treatment method as well. Taken together, these results suggest that neither UCA nor UDCA can restore ATP levels in rotenone-stressed CHO cells.

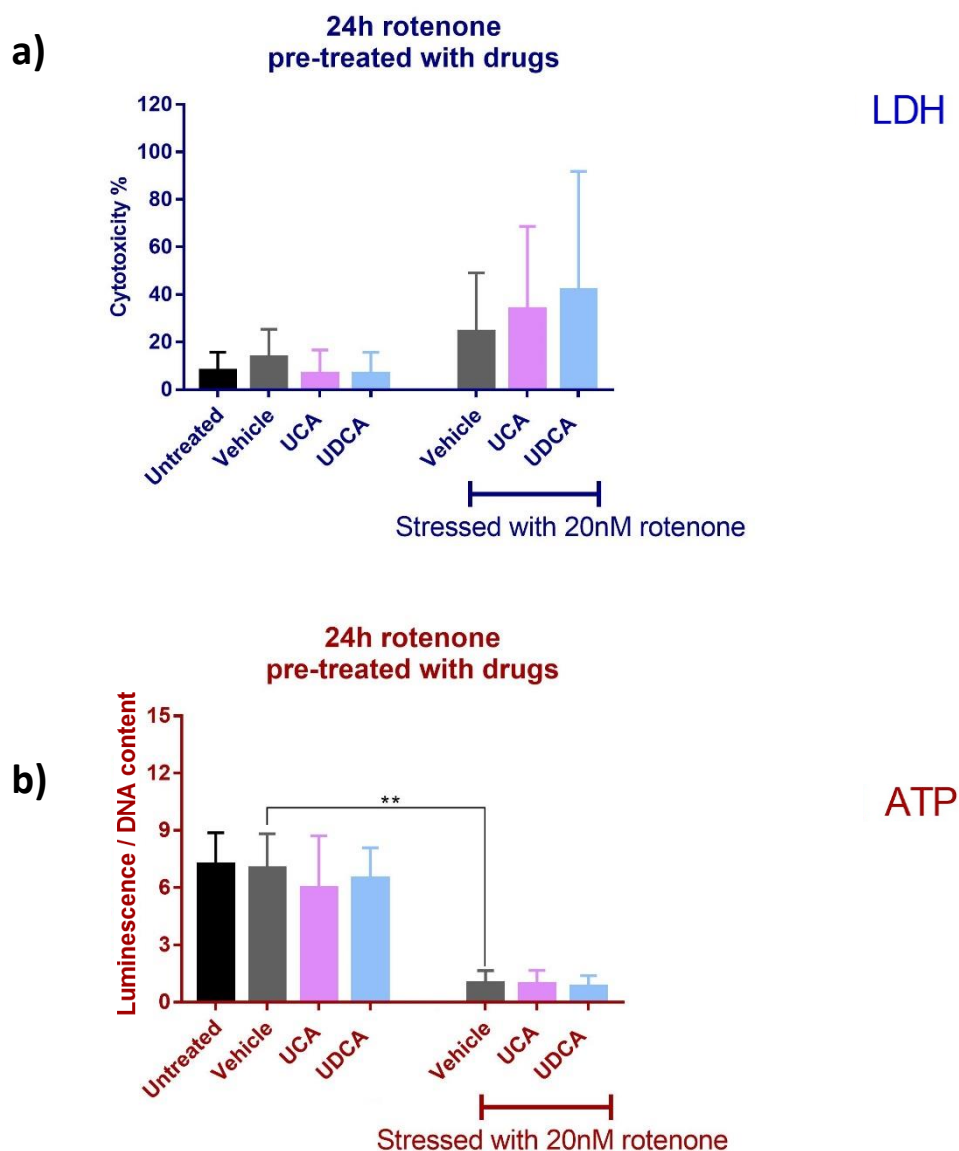


Figure 4.24 pre-treatment with UCA and UDCA did not induce a positive effect in unstressed and rotenone-stressed CHO cells.

Cytotoxicity and ATP levels were measured using LDH and ATP assays as described in the method chapter [Heading 2.9.1, 2.10]. The CHO cells were pre-treated with 10 μ M UCA and 10 μ M UDCA for 24 hours. Then the rotenone was added and kept for 24 hours. The results showed that neither UDCA nor UCA were able to increase ATP levels in rotenone-stressed cells. The error bars represent the SD of three independent experiments. ** $p < 0.01$, two-way ANOVA test.

4.4.3 Optimisation experiments for CCCP treatment

Optimising culture medium and CCCP concentration

Since the UCA/UDCA failed to rescue mitochondrial function in rotenone-stressed CHO cells it was decided to repeat the experiments using an alternative toxin, CCCP (mitochondrial uncoupler), which is a known inducer of mitochondrial dysfunction. Initial testing of CCCP in regular culture medium showed similar findings to what was previously observed with rotenone [Figure 4.18]; the cells were able to resist the CCCP-induced ATP depletion via glycolysis when cultured in glucose-containing medium [Figure 4.25].

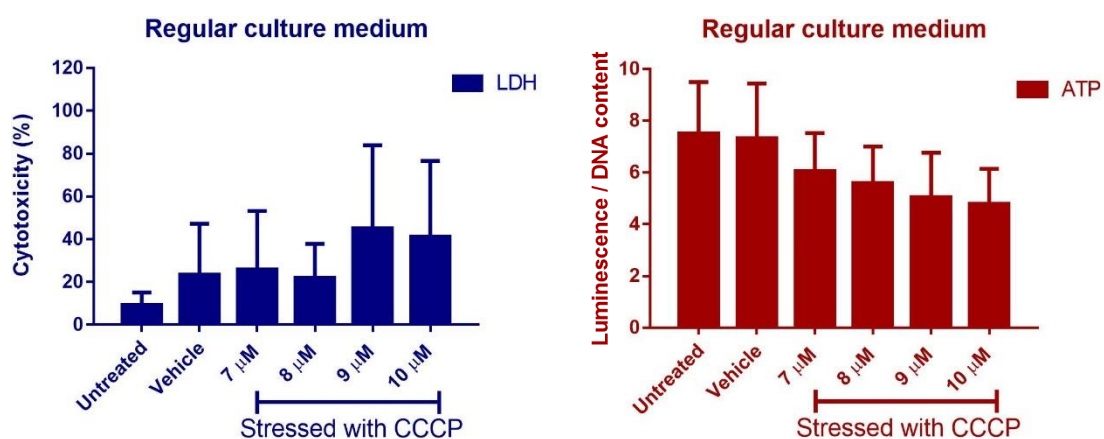


Figure 4.25 CCCP did not show a dose-dependant effect on LDH and ATP readings in regular culture medium.

Cytotoxicity and ATP levels were measured using LDH and ATP assays as described in the method chapter [Heading 2.9.1, 2.10]. The CHO cells were stressed with increasing concentrations of CCCP for 48 hours in regular culture medium. The results did not show a significant dose dependant decrease in ATP levels. The error bars represent the SD of a technical triplicate.

Consequently, galactose medium was also used in CCCP experiments. A wide range of doses were tested. As expected, the sensitivity of the cells to CCCP was dramatically increased when galactose medium was used [Figure 4.26]. There was a clear dose-dependent increase in LDH readings and a clear decrease in ATP levels with increasing doses of CCCP [Figure 4.26]. In accordance with these results, concentrations of 3 μM and 4 μM were selected for the drug treatment experiments.

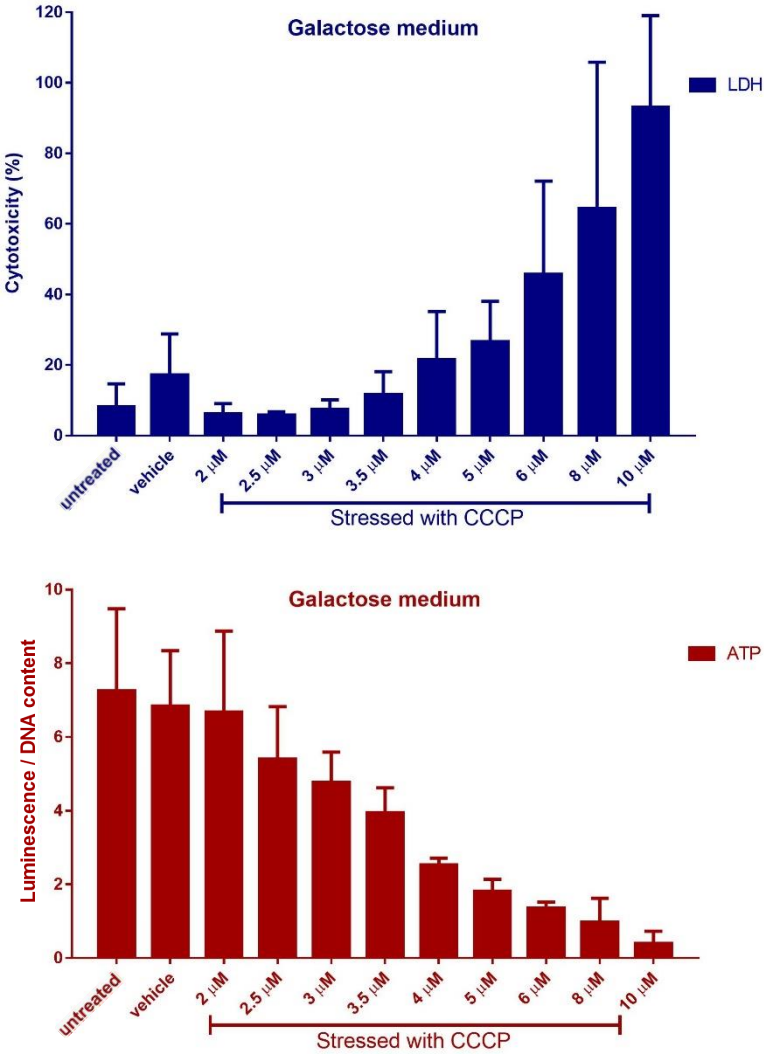


Figure 4.26 Wide range of CCCP concentrations induced a clear dose-dependant effect on LDH and ATP readings in galactose medium.

Cytotoxicity and ATP levels were measured using LDH and ATP assays as described in the method chapter [Heading 2.9.1, 2.10]. The CHO cells were stressed with increasing concentrations of CCCP for 48 hours in galactose medium. The results showed a clear dose-dependent decrease in ATP levels. The error bars represent the SD of three independent experiments.

4.4.4 Assessing the effect of UCA/UDCA on CCCP-stressed CHO cells

The aim of this experiment was to assess the ability of UCA/UDCA to rescue mitochondrial function when CCCP is used as an alternative stressor to rotenone. However, the drugs did not show positive results either in cells stressed with 3 μM or in cells stressed with 4 μM of CCCP [Figure 4.27].

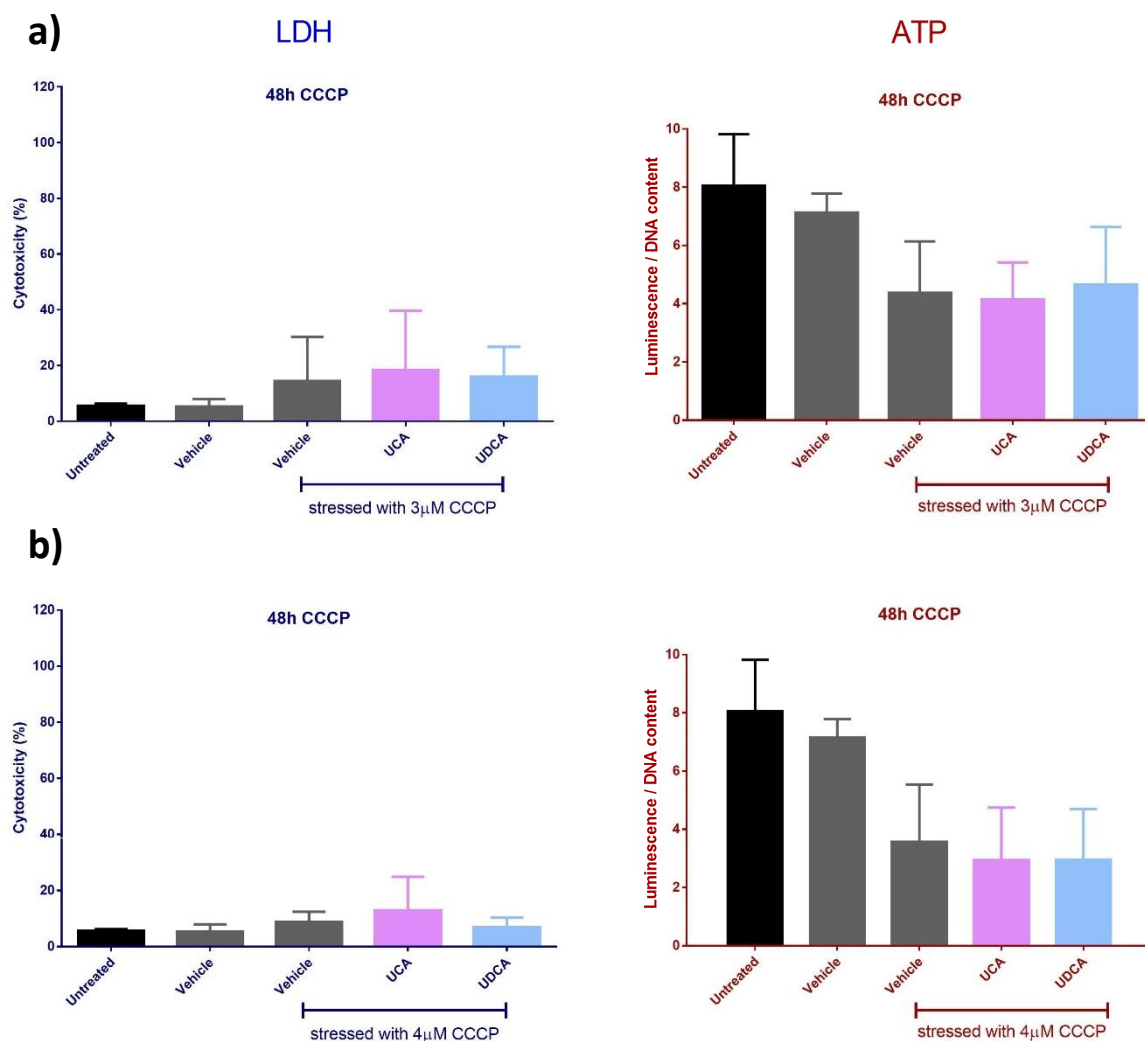


Figure 4.27 UCA and UDCA did not induce a positive effect in unstressed and CCCP-stressed CHO cells (48h CCCP).

Cytotoxicity and ATP levels were measured using LDH and ATP assays as described in the method chapter [Heading 2.9.1, 2.10]. Two concentrations of CCCP: 3 μM (a) and 4 μM (b) were applied for 24 hours. Then the CHO cells were treated with 10 μM UCA and 10 μM UDCA for 24 hours. The drugs failed to rescue mitochondrial function in both conditions. The error bars represent the SD of three independent experiments.

The previously applied pre-treatment protocol was also used with CCCP but the drugs failed to restore the ATP levels [Figure 4.28]. Taken together, the data suggest that UCA and UDCA are unable to rescue mitochondrial function in toxin-stressed CHO cells.

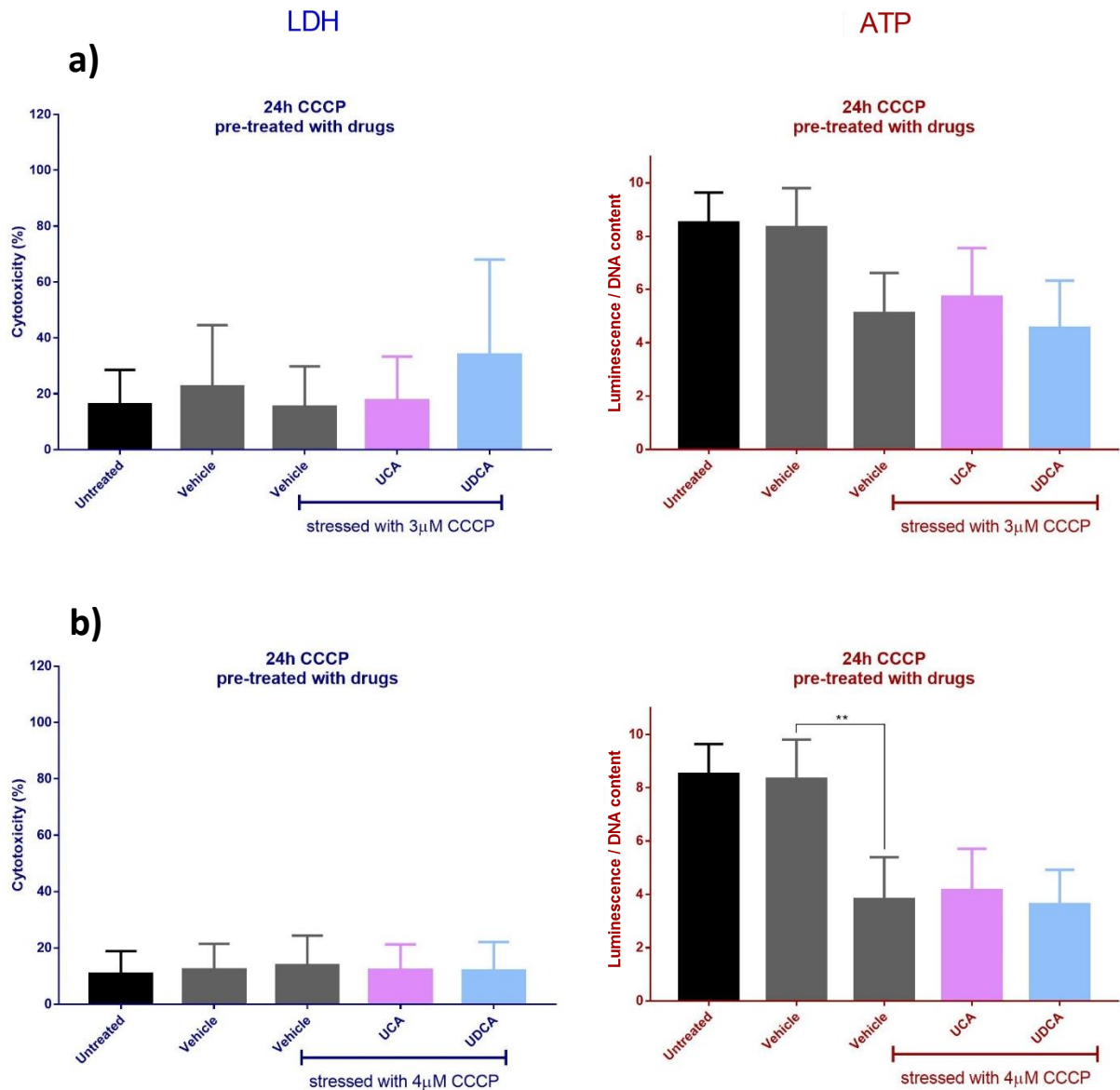


Figure 4.28 Pre-treatment with UCA and UDCA did not induce a positive effect in unstressed and CCCP-stressed CHO cells.

Cytotoxicity and ATP levels were measured using LDH and ATP assays as described in the method chapter [Heading 2.9.1, 2.10]. The CHO cells were pre-treated with 10 μM UCA and 10 μM UDCA for 24 hours. Then 3 μM (a) and 4 μM (b) CCCP was added and kept for 24 hours. The results showed that neither UDCA nor UCA were able to increase ATP levels in CCCP-stressed cells. The error bars represent the SD of three independent experiments. ** $p < 0.01$, two-way ANOVA test.

4.5 Discussion

The beneficial effect of Nrf2 activation has been reported in multiple models of PD. For example, Nrf2 activation alleviated DA neuronal death in a α -synuclein *Drosophila* model of PD (Barone et al., 2011, Todorovic et al., 2016). In addition, the treatment with BG12 alleviated 6-OHDA-induced toxicity in SH-SY5Y cells and mice models (Jing et al., 2015). The Nrf2-mediated response included reduced cytotoxicity, oxidative stress levels, DA neuron loss and locomotor dysfunction. This is in agreement with a previously conducted study which demonstrated that tert-butylhydroquinone – an alternative Nrf2 activator – had a significant protection against 6-OHDA-induced damage *in vitro* mouse model (rat DA neuron cell line) (Jakel et al., 2007).

There is also increasing evidence of the involvement of the Nrf2 in mitochondrial function and biology. Complex I activity as well as mitochondrial membrane potential were reduced in Nrf2-KO neurons, and were increased when the Nrf2 was upregulated (Holmström et al., 2013). Enhanced production of mitochondrial substrates such as pyruvate seems to be the main mechanism by which Nrf2 influences mitochondrial function (Holmström et al., 2013). Studies also suggested that Nrf2 enhances OXPHOS efficiency and alters mitochondrial bioenergetics (Dinkova-Kostova and Abramov, 2015). In wild type neurons, the application of OXPHOS inhibitor, oligomycin, significantly reduced ATP levels. However, this effect was not reproducible in Nrf2-KO cells where the ATP production was only blocked upon the application of glycolysis inhibitor (iodoacetic acid) (Holmström et al., 2013). This suggests that Nrf2 pressures the cells to rely on OXPHOS instead of glycolysis.

The use of CHO-ARE reporter cell line [Heading 2.7] allowed us to determine the increase in ARE expression effectively via measuring the GFP fluorescence. The selected positive control, BG12, demonstrated the classical drug curve response and proved to be an efficient ARE inducer [Figure 4.3]. The cytoprotective effect of BG12 via Nrf2 activation is well characterised and BG12 itself is a candidate treatment for PD (Lastres-Becker et al., 2016). Although the results showed that UCA and UDCA exerted a positive effect on ARE expression, the increase was minor compared to BG12. This suggests that the mechanism of action of UCA and UDCA may not mainly depend on ARE activation. UDCA has been reported to activate Nrf2 in unstressed and ferric nitrate-stressed

hepatic cells (Okada et al., 2008, Arisawa et al., 2009). The activation was associated with an increase in the expression of Nrf2 genes such as GSH and GCLC, and a decrease in the production of ROS. This effect was abolished when the activation of Nrf2 was inhibited (Arisawa et al., 2009). However, the inhibition of the Nrf2 was achieved via blocking the AKT pathway which raises the possibility of an alternative AKT-related pathway responsible for this antioxidant response. Nonetheless, UDCA treatment in other types of cells such as smooth muscle cells has been found to ameliorate oxidative stress in a Nrf2-dependent manner, which was demonstrated via the use of Nrf2-siRNA (Liu et al., 2016).

Since most of the secreted UDCA in bile is conjugated (predominantly with taurine), it was decided to compare the effect of conjugated forms of UDCA with the unconjugated ones. However, the results were similar with regard to ARE expression [Figure 4.5]. Therefore, it was decided to use UDCA only in the subsequent experiments. To confirm the UCA/UDCA-mediated activation of the Nrf2 pathway, we quantified the copy number of the Nrf2 regulated transcripts of three genes, which are either directly or indirectly involved in the antioxidant mechanism: *NQO1*, *GCLC* and *FTH1*. *NQO1* is one of the most extensively investigated phase 2 enzymes. *NQO1* mediates the reduction of quinones via the use of NADH/NADPH as cofactors (Yang et al., 2015). *GCLC* acts as an antioxidant via facilitating the formation of the glutathione precursor, γ -glutamyl cysteine (Park et al., 2017). *FTH1* is involved in the synthesis of ferritin, which controls free iron levels and iron redox reaction via sequestering iron into protein complexes (Kerins and Ooi, 2017). The results showed that UCA significantly increased the expression of *FTH1* and *GCLC*. However, UCA treatment reduced the expression of *NQO1*, which is the only gene that showed a consistent response to the positive control. On the other hand, no significant change was seen with UDCA other than a small increase in *NQO1* expression.

The expression of Nrf2 downstream genes depends on a complex signaling network and might be influenced by cell type, metabolic state and even by the structure of the activator compound. Therefore, it is not expected that a given Nrf2 activator should upregulate all of the Nrf2 genes. This might explain why treatment with the positive control was not associated with an increase in all of the investigated genes. Taken all together, it is difficult to conclude that UCA and UDCA are

potent Nrf2 activators, at least in CHO cells. Nonetheless, it was decided to assess the ability of the UCA and UDCA to ameliorate oxidative stress, not only because both increased ARE expression but also because they might lessen oxidative stress by a mechanism independent of Nrf2.

Three oxidative stress inducers were tested in this chapter: H₂O₂, rotenone and CuSO₄. H₂O₂ itself is a member of the ROS family [Figure 4.29]. It is endogenously generated from superoxide anions, which are produced as a result of a one-electron reduction of molecular oxygen. Usually, superoxide anions are immediately converted by SOD1 and SOD2 into H₂O₂. Rotenone inhibits complex I, and therefore results in an increase in the electron leak and the production of superoxide and H₂O₂. Importantly, only free radicals (not H₂O₂ by itself) are capable of oxidising H₂DCF into DCF (Karlsson et al., 2010). Hydroxyl radicals can indistinguishably damage lipids, proteins and DNA (Schieber and Chandel, 2014). Typically, hydroxyl radicals are generated from H₂O₂ in the presence of ferrous ions during Fenton-type reactions [Figure 4.29 b], or – to a lesser extent – through unspecific enzymatic oxidation by cytochrome C (Karlsson et al., 2010). Despite the availability of H₂O₂, heavy metals like Fe or Cu are crucial for the Fenton-type reactions. Our results showed that there was no increase in DCF readings when the cells were stressed with H₂O₂ and rotenone, but there was a significant increase when the cells were stressed with CuSO₄ [Figure 4.12].

The hydroxyl radicals are extremely reactive. However, they have a short lifespan (9–10 seconds) (Jomova et al., 2012). This might explain why there was no increase in DCF readings when the CuSO₄ was removed two hours and five hours before the application of the DCF (protocol B) [Figure 4.14]. In addition, the cells might be able to eliminate the hydroxyl radicals via the antioxidant mechanisms during the CuSO₄-free period. Only a small increase in DCF signals was seen when CuSO₄ was removed eight hours and 24 hours before the application of the DCF [Figure 4.14]. However, this increase was not reproducible in drug treatment experiments [Figure 4.15]. In contrast, the DCF readings were significantly increased in the experiments where the CuSO₄ was present in the medium until the application of DCF (protocol C) [Figure 4.16]. In the literature, only a few studies have investigated ROS production in CHO cells via the DCF.

However, in these studies, the stressor was removed only at the time of the application of the DCF (Orhan et al., 2006, Kang et al., 2006).

Although BG12 had a significant positive effect on the ARE activation, it failed to reduce DCF signals in CuSO₄-stressed CHO cells. BG12 has not been reported to alleviate copper-induced oxidative stress. However, it has been reported to ameliorate oxidative stress induced by various toxins such as MPTP, 6-OHDA, H₂O₂ (Campolo et al., 2017, Linker et al., 2011, Wang et al., 2015, Jing et al., 2015). Consequently, it was decided to test Trolox as an alternative antioxidant control. Trolox has a well-known radical scavenging activity and has been used as a reference for the antioxidant capacity of other compounds (Wang et al., 2016, Lee et al., 2016). Despite the different tested concentrations and stressing protocols, there was no decrease in DCF readings [Figure 4.15] [Figure 4.17]. Similarly, UCA and UDCA did not reduce DCF readings in all experiments. Since the BG12 and Trolox showed no effect, it is difficult to conclude that UCA and UDCA are ineffective against oxidative stress. The usage of DCF might obscure the effect of the positive controls, UCA and UDCA since it only detects one type of ROS. Therefore, assessing oxidative stress using an alternative reagent is recommended for future work.

In this chapter, the rescue effect of UCA and UDCA was assessed in cells stressed with two mitochondrial toxins, rotenone, which has been associated with increased risk of PD, and CCCP, which is a mitochondrial uncoupler commonly used in PD-related research. The results showed that the cells were able to compensate for the induced ATP reduction via glycolysis. Consequently, the cells were cultured in galactose medium to force them to rely on OXPHOS, which makes them metabolically closer to the neurons (Bolaños et al., 2010). The ability of UCA and UDCA to increase ATP levels in rotenone-stressed cells was investigated using different experimental designs and different treatment times and doses. However, no significant rise in ATP levels was seen [Figure 4.22] [Figure 4.23] [Figure 4.24]. Notably, the decrease in ATP readings with rotenone was rather abrupt and did not show a gradual decrease with increasing concentrations of rotenone [Figure 4.21]. Further experiments were performed to assess the effect of the drugs using CCCP as an alternative stressor. CCCP dosing experiments showed a clear dose-dependent decrease in ATP levels [Figure 4.26]. Accordingly, two CCCP doses that

induced two different degrees of ATP reduction were selected for drug treatment experiments. However, no increase in ATP levels was seen after the application of the drugs, regardless of the different tested protocols and CCCP concentrations [Figure 4.27] [Figure 4.28].

In this chapter, a LDH-based cytotoxicity assay was used to assess the degree of cytotoxicity induced by rotenone and CCCP, and to investigate whether the drugs are able to ameliorate this toxicity. In comparison to ATP readings, the effect of the stressors on LDH levels was generally smaller, especially when rotenone was used. Despite the occasionally observed variability, the drugs did not show a significant cytoprotective effect in all experiments. Collectively, our results showed that neither UCA nor UDCA were able to rescue mitochondrial function nor to decrease cytotoxicity in rotenone and CCCP-stressed CHO cells. It is appreciated that the used cell line and the introduced defects are different from those in the drug screening paper (Mortiboys et al., 2013) and, therefore, might contribute to these negative results. In an attempt to tackle these limitations, the ability of the drugs to rescue mitochondrial function will be assessed in a cell line of human origin in the next chapter.

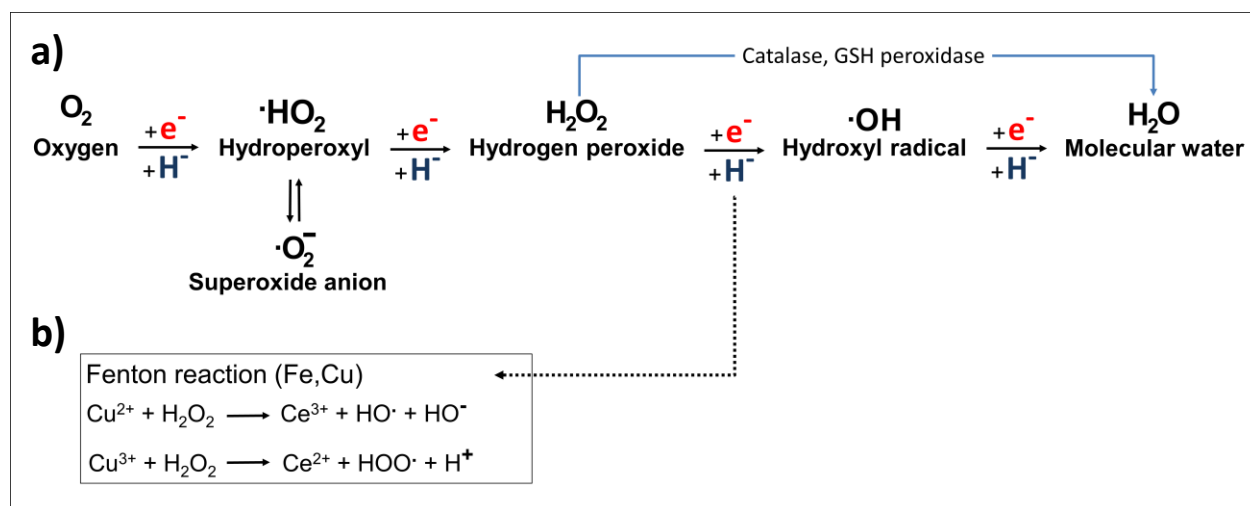


Figure 4.29 An overview of the reactive oxygen species.

(a) Shows common types of ROS and their production pathway. (b) The Fenton-type reaction and the formation of hydroxyl radicals.

Chapter 5. Investigating the beneficial effect of UDCA on ATP levels and cytotoxicity in SH-SY5Y cells

5 Investigating the beneficial effect of UDCA on ATP levels and cytotoxicity in SH-SY5Y cells

5.1 Introduction

5.1.1 SH-SY5Y Origin

The neuroblastoma-derived SH-SY5Y cell line is commonly used in the field of PD research. These cells were obtained after a series of sub-cloning of bone marrow biopsies of neuroblastoma patients. In this process, the most neuron-like cells were selected and isolated for further expansion. The cells were initially named SK-N-SH, then SH-SY and finally SH-SY5Y (Biedler et al., 1973, Biedler et al., 1978).

5.1.2 SH-SY5Y characteristics

The genetic characterisation of SH-SY5Y showed that most of the PD-related genes and pathways are unimpaired, which is important given the nature of the origin of these cells (Krishna et al., 2014). The initial characterisation of SH-SY5Y revealed modest levels of dopamine- β -hydroxylase and a small amount of choline acetyl-transferase, acetylcholinesterase, noradrenaline and TH (Biedler et al., 1978, Pählman et al., 1984, Ross and Biedler, 1985). The expression of these proteins indicates that SH-SY5Y has a catecholaminergic phenotype and therefore it is important to note that these cells are not exclusively dopaminergic. Xicoy and colleagues performed a systematic review of published papers that have used SH-SY5Y cells to study PD and found that almost half of the published papers stated that they used DA cells without providing or citing previous experimental evidence (Xicoy et al., 2017). The other half of the papers did not provide any information about the phenotype of SH-SY5Y, and only 5% of the papers investigated the dopaminergic characteristics of the used cells. In less than 1% of the papers, the noradrenergic and the cholinergic phenotypes were reported (Xicoy et al., 2017).

5.1.3 SH-SY5Y differentiation

SH-SY5Y can be differentiated into more neuron-like cells, which makes them more relevant for PD-related research. There are several published methods and protocols to differentiated SH-SY5Y cells. RA is the most commonly used substance to drive the differentiation. Studies have shown that terminally differentiated cells by RA express a higher level of DA markers and are more sensitive to toxins (Korecka et al., 2013, Lopes et al., 2010). However, these findings are

not consistent with other reports where no increase in DA markers have been observed (Cheung et al., 2009). Additionally, an increase in cholinergic markers has been reported (Hashemi et al., 2003). Since RA is used at different concentrations for different time periods, it is possible that this variation could affect the final phenotype of the cells. In addition, the type of culture medium might also play a role, as well as the percentage and the type of added supplements such as FBS. The variation might also arise from the difference in cell source and passage number. Therefore, it is not surprising to know that more than 80% of papers used only undifferentiated SH-SY5Y (Xicoy et al., 2017). It has been proposed that RA acts via the activation of nuclear retinoic acid receptors and retinoid X receptors. Consequently, RA upregulates the transcription of various differentiation-related genes that harbour retinoic acid response elements (RARE) in their promoters (Das et al., 2014). Additionally, the RA mechanism involves non-genomic pathways such as ROS-mediated signalling (Kunzler et al., 2017).

Alternatively, sequential treatment with RA and brain-derived neurotrophic factor (BDNF) has also been used to differentiate SH-SY5Y (Xicoy et al., 2017). This method should give a more homogenous population. However, the characterisation of the outcome is also controversial as it has shown a sympathetic / cholinergic phenotype in some reports and a DA phenotype in others (Goldie et al., 2014, Mastroeni et al., 2009). Other compounds that have been used in combination with RA include 12-O-tetradecanoylphorbol-13-acetate (TPA), dibutyryl cyclic adenosine monophosphate (dbcAMP) and tissue plasminogen activator (Xicoy et al., 2017). Furthermore, SH-SY5Y can be differentiated by the use of other compounds such as growth/differentiation factor 5 (GDF5), recombinant bone morphogenetic protein 2 (BMP2) and glial cell line-derived neurotrophic factor (GDNF) (Xicoy et al., 2017).

5.1.4 Objectives

In the previous chapter, UDCA failed to rescue toxin-stressed CHO cells regardless of different tested conditions. Although toxin-induced mitochondrial dysfunction might be relevant to PD in terms of modelling, CHO cells are not an appropriate cell line for investigating treatments for PD since they are non-human and are not neuronal in nature. Therefore, SH-SY5Y cells were selected to investigate the rescue effect of UDCA further. In this chapter, an RA-based protocol will be used to differentiate the SH-SY5Y into more neuron-like cells. The differentiation will be evaluated through studying cell proliferation, morphology and expression of neuronal-specific markers. The effect of UDCA on ATP and cytotoxicity will be determined in both undifferentiated and differentiated SH-SY5Y cells. Subsequently, the mechanism of action of UDCA will be investigated via assessing the activation of the Nrf2 pathway in UDCA-treated SH-SY5Y cells.

5.2 Assessing the ability of UCA/UDCA to rescue mitochondrial function in stressed undifferentiated SH-SY5Y cells

5.2.1 Optimisation of culture medium and rotenone concentration

Initial rotenone-dosing experiment showed an increase in cytotoxicity at 1 μM , which remained unchanged regardless of subsequent treatment with increasing rotenone doses (up to 10 μM) [Figure 5.1 a]. Similarly, assessing ATP reduction after rotenone treatment showed that the decrease in ATP levels was comparable regardless of the applied rotenone doses (1 μM –10 μM) [Figure 5.1 b]. This trend is comparable to what was previously observed in CHO cells. The sensitivity of SH-SY5Y cells to rotenone was significantly increased when they were cultured in galactose medium [Figure 5.1 c, d]. This indicates that SH-SY5Y cells also utilise glycolysis to produce energy. For the drug treatment experiments, it was decided to test multiple rotenone concentrations (15 nM - 40 nM), which induced a decrease in ATP levels that ranged between 20% and 80%.

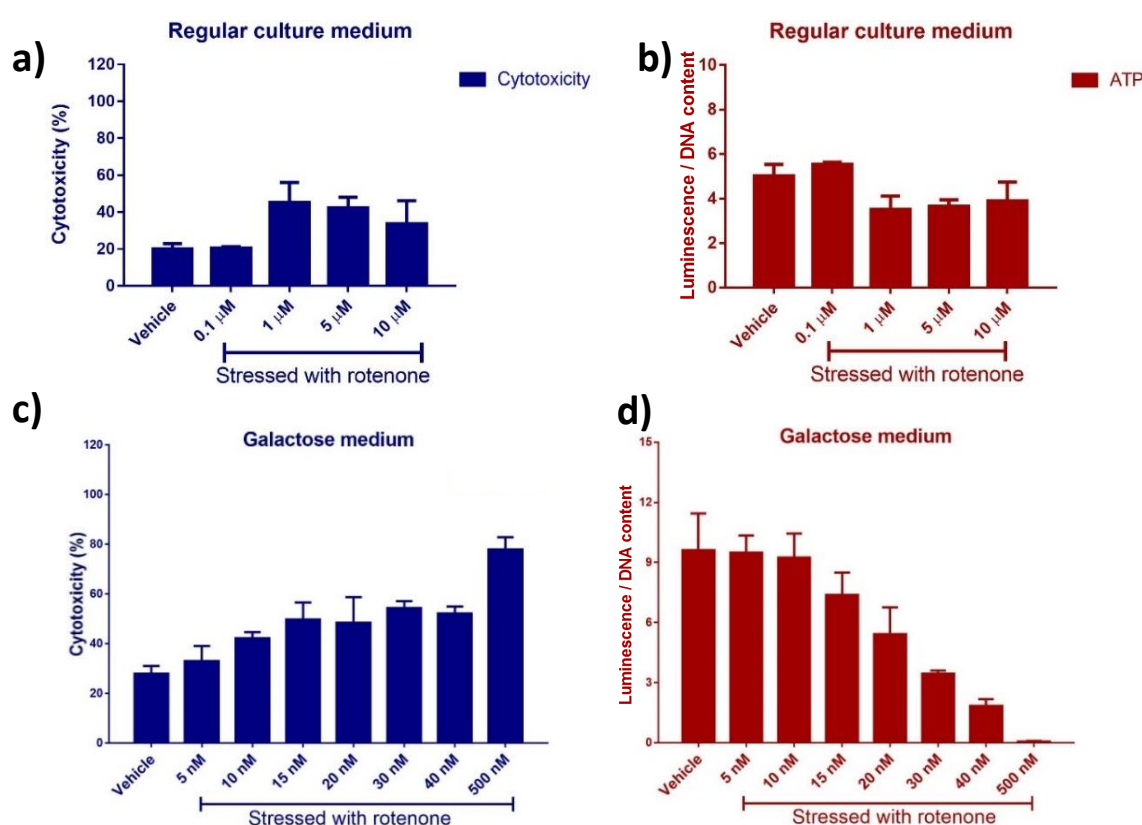


Figure 5.1 Rotenone induced a dose-dependant effect on cytotoxicity and ATP readings in galactose culture mediums.

Cytotoxicity and ATP levels were measured using trypan blue staining and ATP assay, as described in the method chapter [Heading 2.9.1, 2.10]. The SH-SY5Y cells were stressed for 24 hours in either regular culture medium (a, b) or galactose medium (c, d). Stressing the cells in galactose medium significantly increased their sensitivity to rotenone and induced a clear dose-dependent effect. The error bars represent the SD of three independent experiments.

5.2.2 Assessing the effect of UCA and UDCA in rotenone-stressed SH-SY5Y cells

The cells were pre-treated with 10 μM of each drug for 24 hours prior to the addition of rotenone. The changes in cytotoxicity and ATP readings in rotenone-stressed cells were comparable to what was previously observed in the rotenone-dosing experiments. UCA and UDCA treatment had no positive effect in all conditions [Figure 5.2].

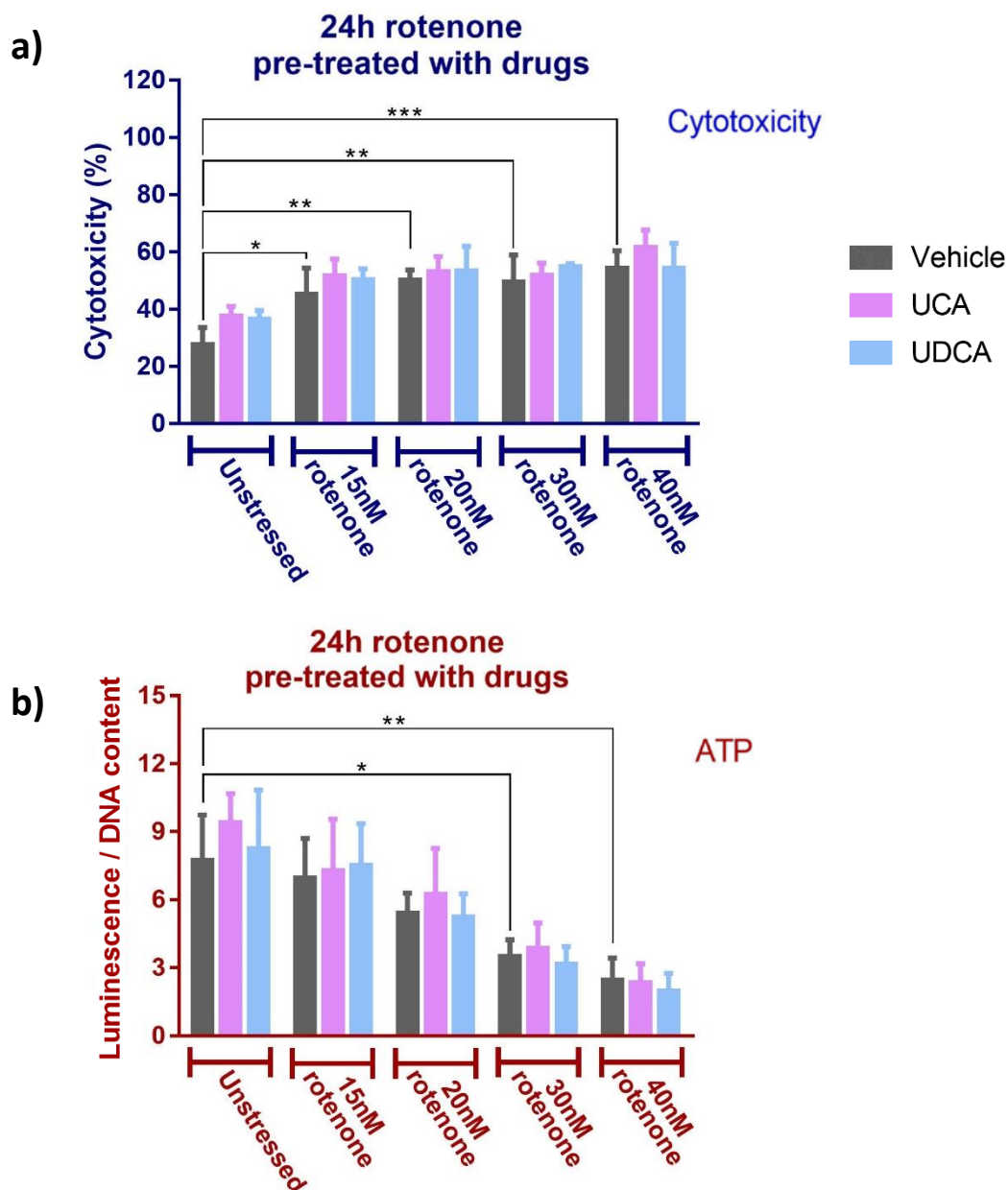


Figure 5.2 UCA and UDCA did not induce a positive effect in unstressed and rotenone-stressed SH-SY5Y.

Cytotoxicity and ATP levels were measured using trypan blue staining and ATP assay as described in the method chapter [Heading 2.9.1, 2.10]. The cells were pre-treated with 10 μM of the drug for 24 hours. Then the rotenone was added and kept for 24 hours. Rotenone significantly increased cytotoxicity (a) and decreased ATP levels (b) but no rescue effect was seen with UCA and UDCA treatment in all conditions. The error bars represent the SD of three independent experiments. The error bars represent SD. * $p < 0.05$, ** $p < 0.01$, *** $p < 0.001$, two-way ANOVA test.

5.2.3 Assessing the effect of UCA and UDCA in CCCP-stressed SH-SY5Y cells

In this set of experiments, the dosing and the treatment times of the CCCP and the drugs were adopted from a recently published paper (Fonseca et al., 2017), in which TUDCA exerted a positive effect on ATP and cytotoxicity in CCCP-stressed SH-SY5Y (Fonseca et al., 2017). Accordingly, the cells were stressed with two CCCP concentrations (25 μ M and 50 μ M), and were treated with 100 μ M UDCA and 100 μ M TUDCA in addition to the previously tested conditions (10 μ M UCA and 10 μ M UDCA) [Figure 5.3]. Both CCCP concentrations increased cytotoxicity (155% with 25 μ M CCCP, 227% with 50 μ M CCCP) and decreased ATP levels (50% with 25 μ M CCCP, 70% with 50 μ M CCCP). No positive effect was observed with 10 μ M UCA/UDCA and 100 μ M TUDCA. However, there was a notable insignificant positive effect with 100 μ M UDCA, which was apparent in ATP levels and cytotoxicity in the 50 μ M CCCP condition.

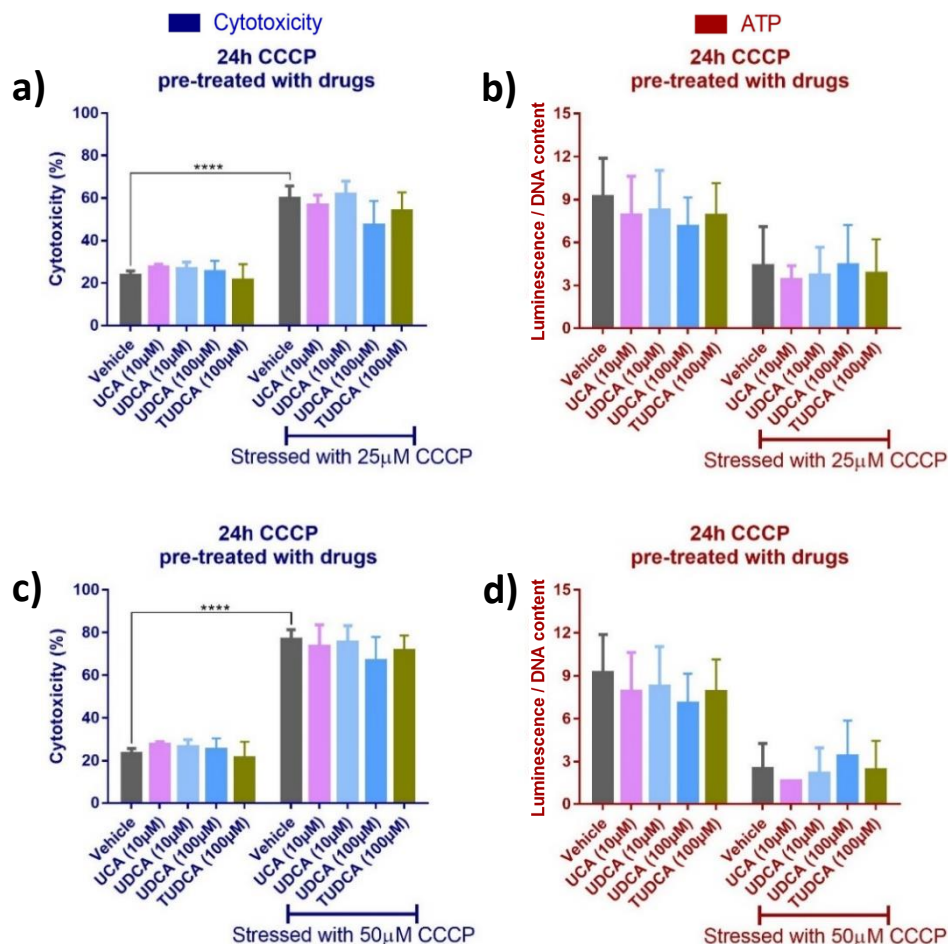


Figure 5.3 UDCA induced a small non-significant positive effect in CCCP-stressed SH-SY5Y.

Cytotoxicity and ATP levels were measured using trypan blue staining and ATP assays as described in the method chapter [Heading 2.9.1, 2.10]. The SH-SY5Y cells were pre-treated for 12 hours with the drugs and then were further incubated with either 25 μ M CCCP (a, b) or 50 μ M CCCP (c, d) for 24 hours. The results showed a small insignificant rescue effect with 100 μ M UDCA. The error bars represent the SD of three independent experiments. **** p < 0.0001, two-way ANOVA test.

Accordingly, higher doses of UDCA were tested [Figure 5.4 a, b]. The results showed significant positive changes in cytotoxicity (25% decrease) and ATP levels (65% increase) when the cells were treated with 300 μM UDCA [Figure 5.4 a, b]. Higher UDCA doses, 600 μM and 900 μM , increased the toxicity in unstressed cells. The rescue effect of treatment with 300 μM UDCA was also apparent when the cells were examined under the optic microscope [Figure 5.4 c].

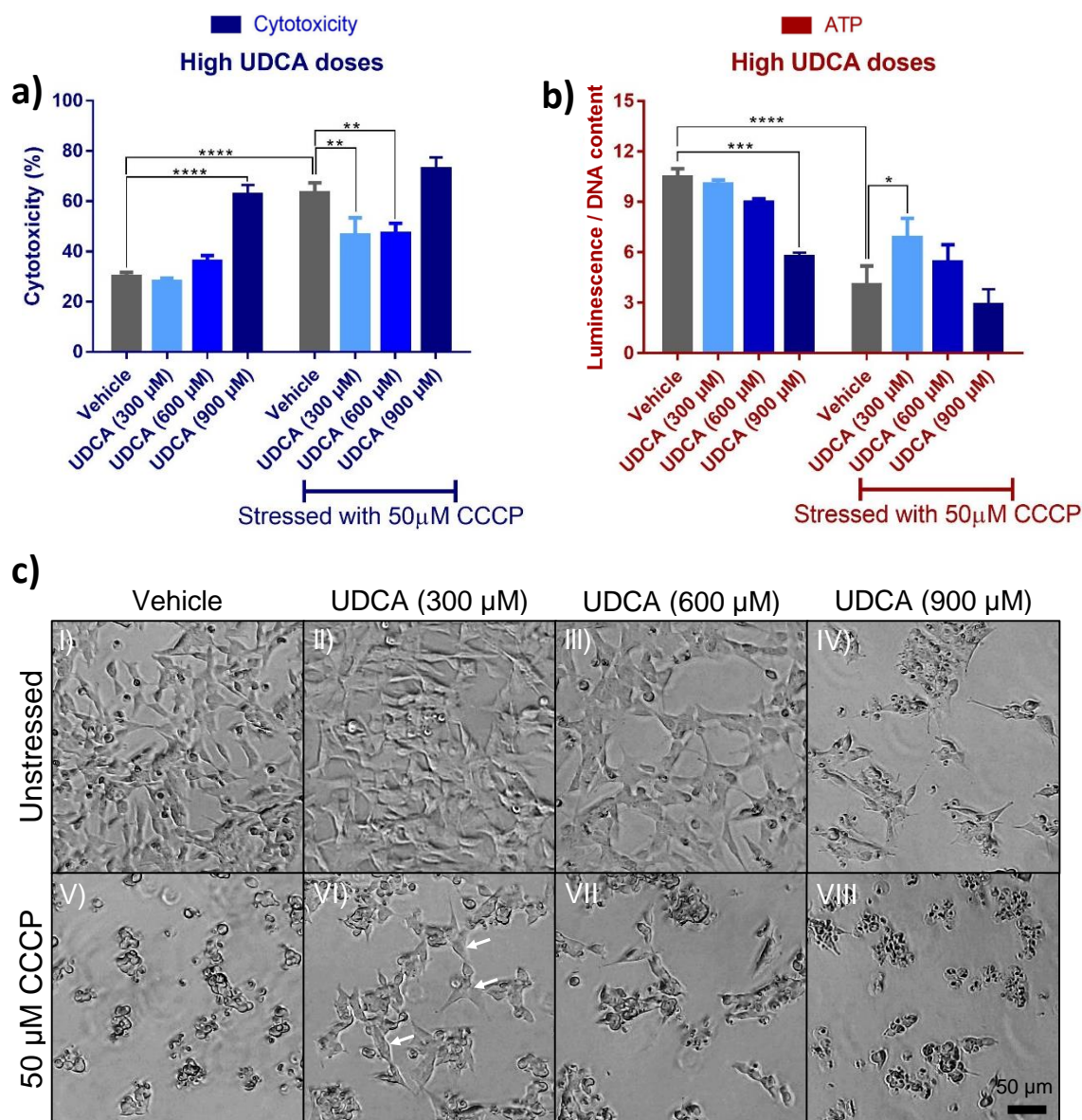


Figure 5.4 A UDCA dose of 300 μM induced a significant positive effect on ATP and LDH levels in CCCP-stressed SH-SY5Y.

(a), (b) Cytotoxicity and ATP levels were measured using trypan blue staining and ATP assays as described in the method chapter [Heading 2.9.1, 2.10]. The cells were pre-treated for 12 hours with UDCA before the addition of 50 μM CCCP, which was kept for 24 hours. The results showed a significant rescue effect with 300 μM UDCA (a, b). (c) Bright field microscopy images showing the surviving cells in the UDCA-treated condition (VI). The white arrows point to some of the healthy-looking cells which are not present in the CCCP-only condition (V). The error bars represent the SD of three independent experiments. ** $p < 0.01$, *** $p < 0.001$, **** $p < 0.0001$, two-way ANOVA test. Scale bar = 50 μm .

5.3 Assessing the ability of UDCA to rescue mitochondrial function in stressed differentiated SH-SY5Y cells

5.3.1 Characterisation of differentiated SH-SY5Y

Proliferation assay: The differentiation of SH-SY5Y cells alters their transcription profile to transform them into neuron-like cells. In this process, the cells do not only express higher levels of neuronal markers but also become non-proliferative. To assess cell growth, the cell count was determined regularly using an automated counter throughout the differentiation course. The cells were plated in a 24-well plate at equal densities and the differentiation protocol was commenced as described in the method section. Every two days, the contents of three wells were collected separately in order to conduct a cell count. An identical parallel culture plate was prepared to compare the cell count to undifferentiated cells grown in regular culture medium. As expected, the results showed that the increase in the total cell count with time was significantly lower in the differentiating cells [Figure 5.5]. Yet the presence of increasing total cell count with time in differentiated cells indicates a non-homogenously differentiated population, which is one of the limitations of the protocol used. Although the total number of growing undifferentiated cells was higher than the differentiated cells, the number of dead cells was comparable, indicating that there were a number of differentiating cells that died throughout the process, which was also noticed when the plate was examined under the optic microscope [Figure 5.6 a]. Of note, the number of viable undifferentiated cells dropped significantly towards the end of the second week due to the overgrowth of the cells and consequent competition for space and nutrition.

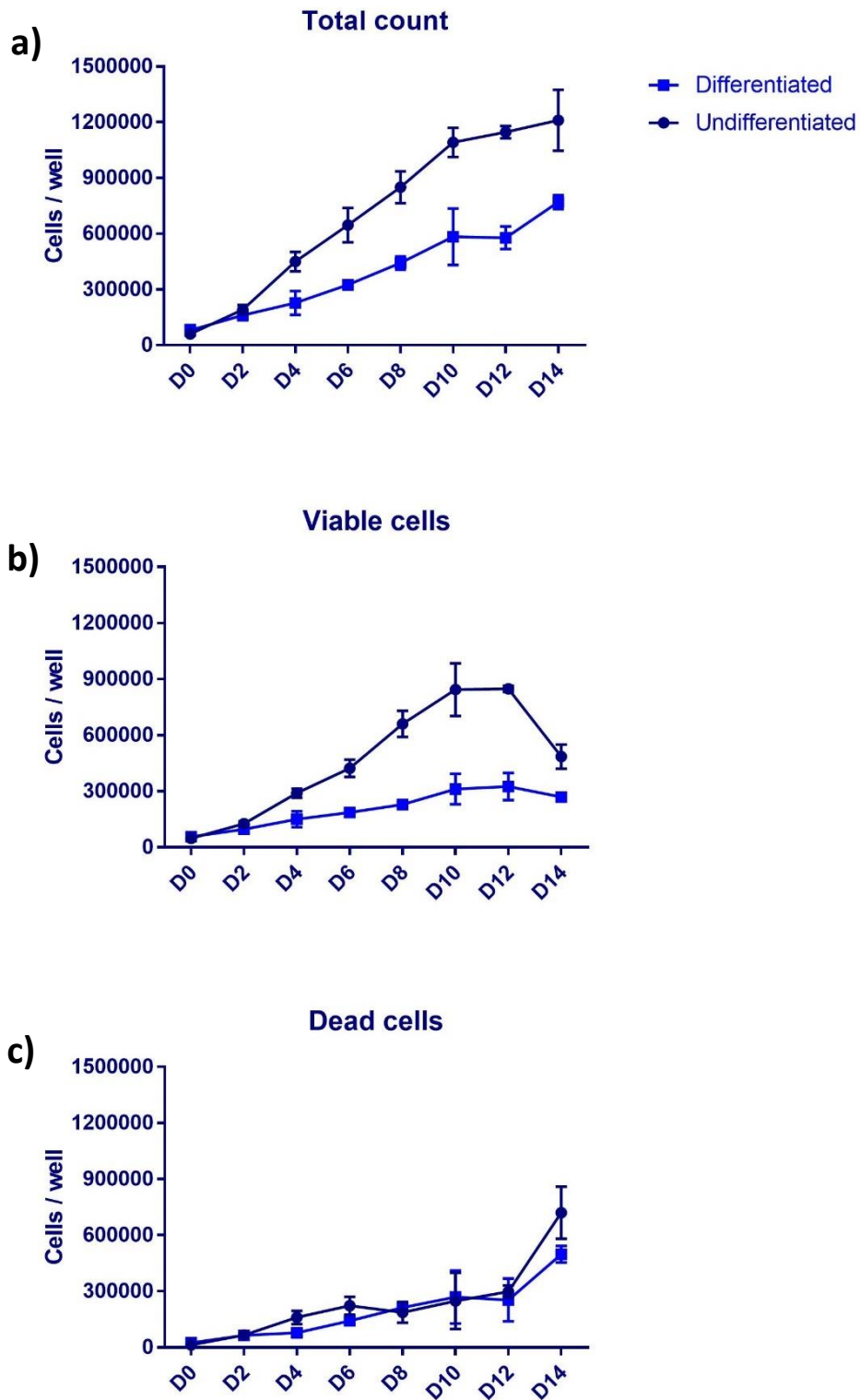


Figure 5.5 Differentiating SH-SY5Y cells have lower growth rate and higher cell death rate in comparison to the undifferentiated cells.

The readings were obtained by the use of an automated counter and trypan blue staining [Heading 2.9.1], which enables the determination of total cell count (a), viable cell count (b) and dead cell count (c). The graphs show that the proliferation of differentiating cells was reduced as the total cell count and the viable cell count were lower in comparison to the undifferentiated cells. The error bars represent the SD of three technical replicates.

Morphological analysis: Differentiated SH-SY5Y demonstrated a remarkable change in morphology in terms of neurite growth [Figure 5.6 a]. Immunocytochemistry (ICC) staining showed that these neurites expressed the Neuron-specific class III β -tubulin (Tuj1) [Figure 5.6 b]. The images were analysed using the 'Find Neurites' building block on the Harmony software (PerkinElmer). This analysis protocol can identify neurites growing from cell bodies and consequently measures various parameters such as maximum neurite length, total neurite length, number of extremities and number of roots. Since undifferentiated cells have no dendritic structure, only the total neurite length was used to assess neurite growth and was significantly increased in differentiated cells.

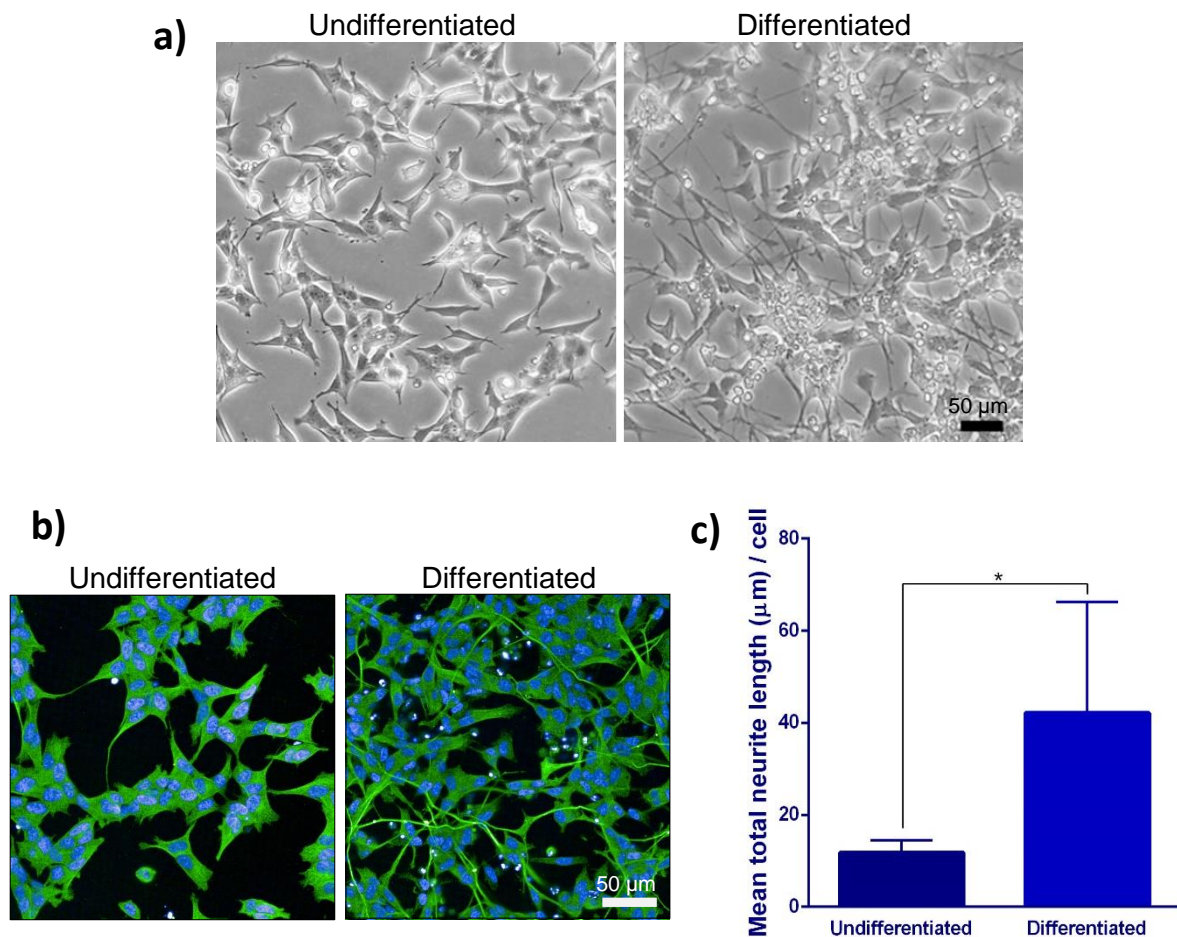


Figure 5.6 Differentiated SH-SY5Y cells exhibited remarkable change in their morphology.

(a) Optic microscopy images of SH-SY5Y cells pre/post differentiation. Differentiated SH-SY5Y cells showed a significant increase in neurite growth. (b) Confocal microscopy images of SH-SY5Y cells pre/post differentiation stained with Tuj1. The images showed that the neurites of the differentiated cells were positively stained with Tuj1. (c) Analysis of Tuj1 images showed a significant increase in neurite growth. ICC and imaging were performed as described in the method section. * $p < 0.05$, unpaired t-test. Scale bar = 50 μm .

Neuronal markers: The differentiated SH-SY5Y cells showed a significant increase in the expression of microtubule-associated protein 2 (MAP2), which is a protein that stabilises microtubules in the dendrites and post-mitotic cells (Poulain and Sobel, 2010) [Figure 5.7 a]. The DA phenotype of the differentiated cells was determined via staining with FOXA2, which is a member of the forkhead/winged helix transcription factor family that has a significant role in the development and maintenance of DA neurons (Stott et al., 2013) [Figure 5.8 a]. Notably, FOXA2 staining was not as intense in the nucleus as was expected. However, the increase in the expression of FOXA2 in differentiated cells was observed in both cytoplasmic and nuclear regions. In addition, WB revealed a significant increase in the expression of TH, a rate-limiting enzyme in dopamine synthesis, which further confirmed the DA phenotype of the differentiated cells [Figure 5.8 c].

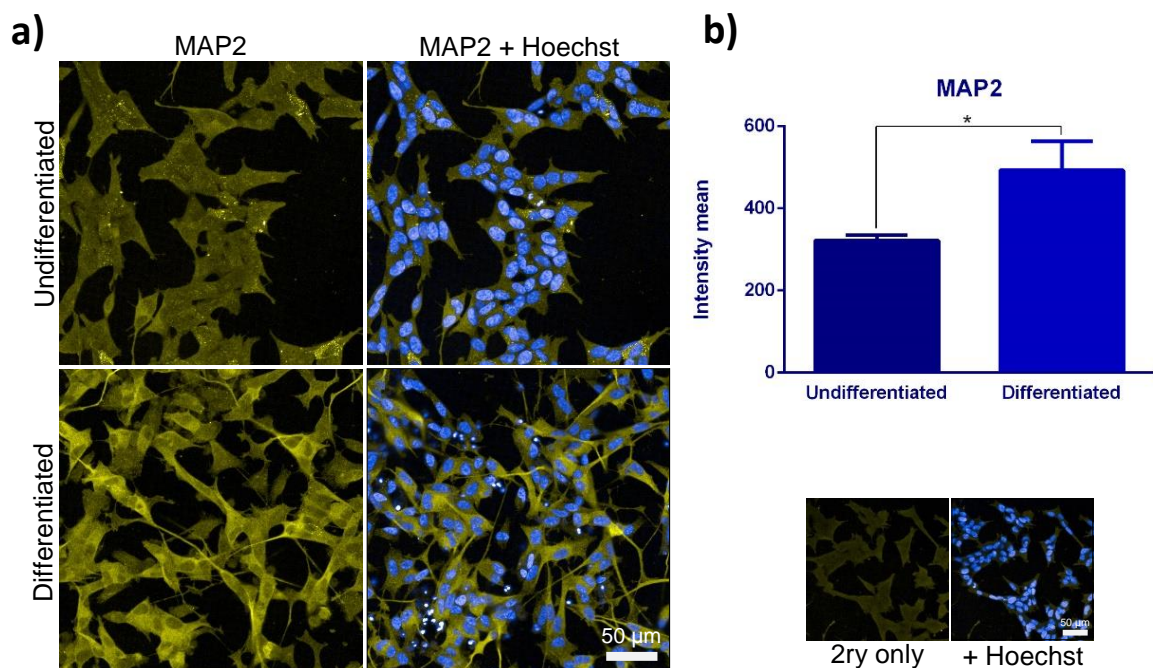


Figure 5.7 The expression of the neuronal marker MAP2 is significantly higher in differentiated SH-SY5Y cells.

ICC was performed as described in the method section and the images were captured using a confocal microscope. The cells were probed with MAP2 (a) antibody and the images were analysed using the Harmony software (b). The images show a significant increase in the expression of MAP2 in differentiated SH-SY5Y cells. The error bars represent the SD of three independent experiments. * $p < 0.05$, unpaired t-test. Scale bar = 50 μm.

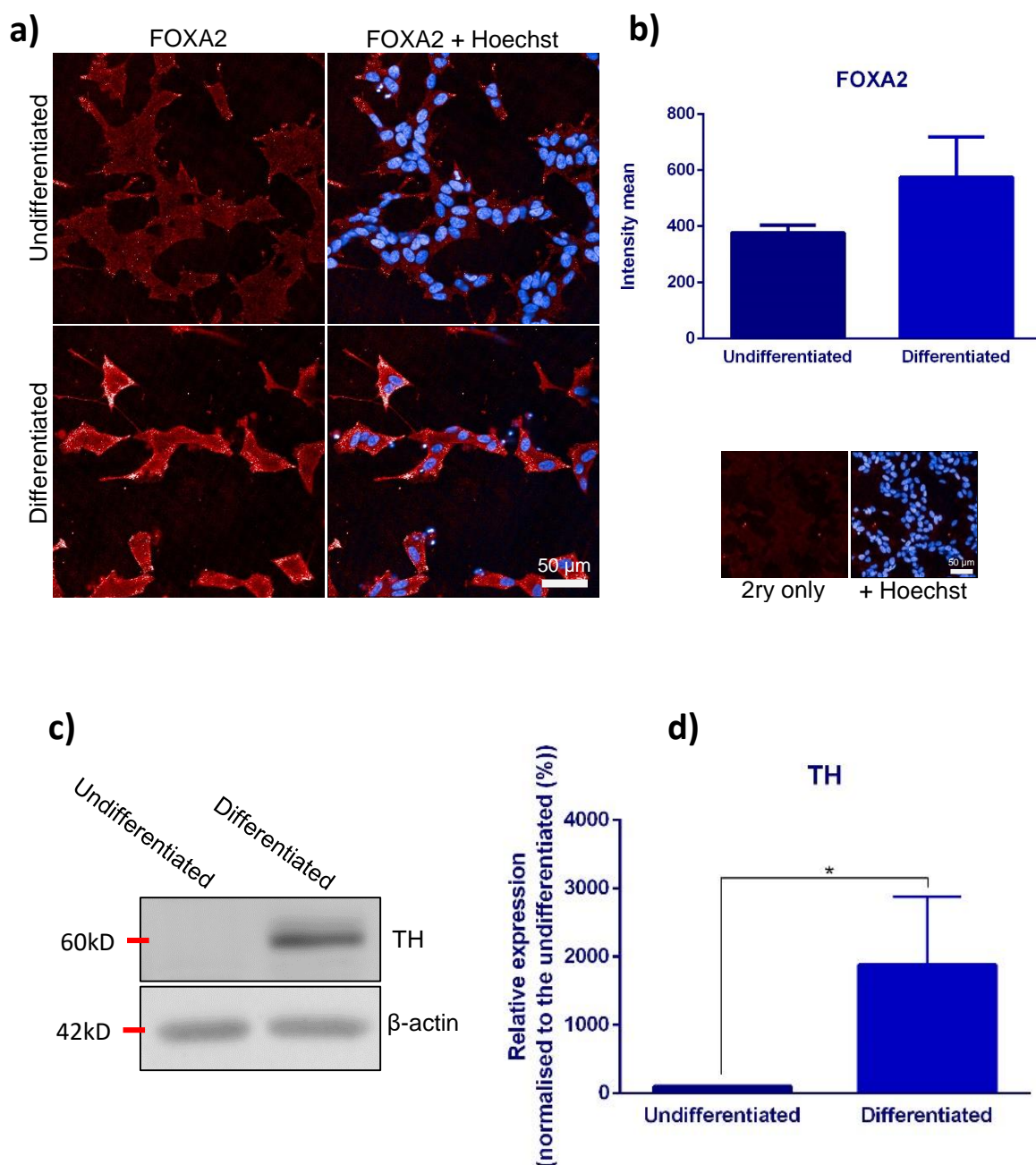


Figure 5.8 The expression of the dopaminergic markers is significantly higher in differentiated SH-SY5Y cells.

(a) ICC was performed as described in the method section and the images were captured using a confocal microscope. The cells were probed with FOXA2 antibody and the images were analysed using the Harmony software (b). Marker-specific positive cells were selected according to a pre-set intensity threshold. The images show a significant increase in the expression of both markers in differentiated SH-SY5Y cells. (c) WB images showing a marked increase in TH levels in differentiated cells. WB was performed using total cell lysates as described in the method section. (d) Densitometric analysis of WB images. The expression of TH was remarkably increased in the differentiated cells. The error bars represent the SD of three independent experiments. * $p < 0.05$, unpaired t-test. Scale bar = 50 μ m.

5.3.2 Optimising CCCP concentration

Differentiated SH-SY5Y cells are more vulnerable to toxins (Forster et al., 2016). Therefore, CCCP doses need to be optimised before the application of the UDCA. As expected, the previously used dose of CCCP (50 μ M) was highly toxic to the differentiated cells [Figure 5.9]. The results also showed high basal cytotoxicity in differentiated cells (more than 50%). This is probably attributed to the presence of dead cells that accumulated during the differentiation process, which were consequently included in the counting process, and in the ATP assay as well.

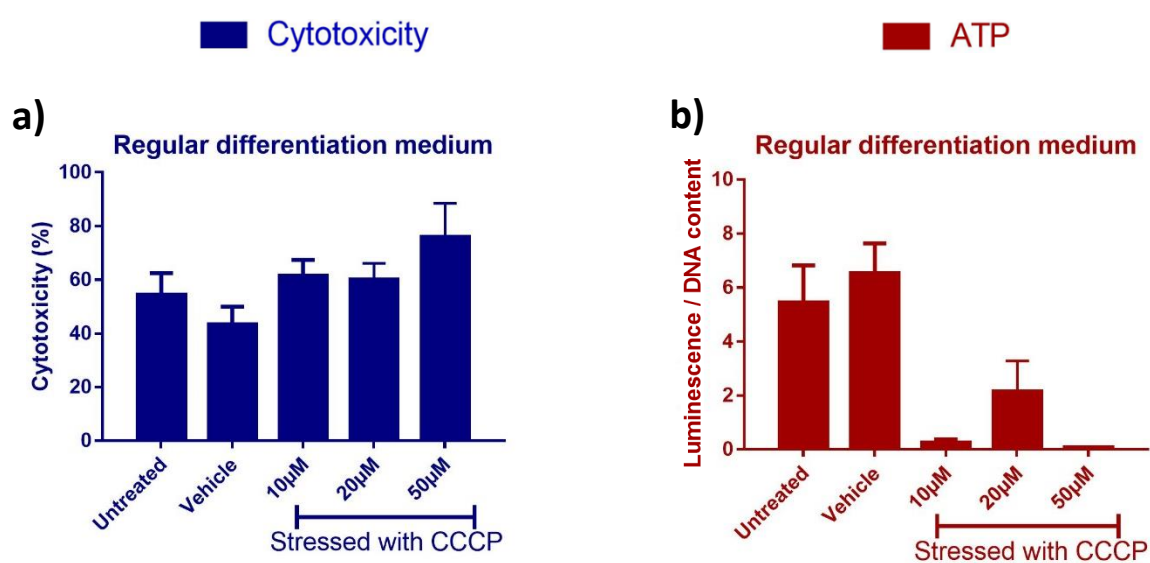
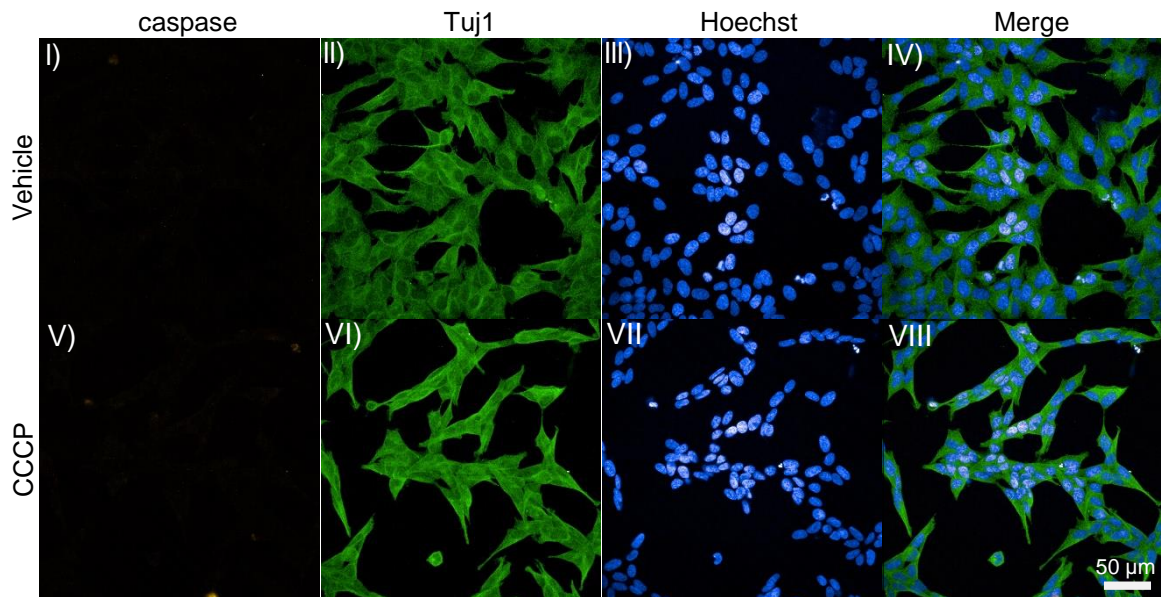


Figure 5.9 A pilot experiment to optimise CCCP concentration demonstrated high basal toxicity readings in unstressed differentiated SH-SY5Y.

Cytotoxicity and ATP levels were measured using trypan blue staining and ATP assays, as described in the method chapter [Heading 2.9.1, 2.10]. The cells were stressed with CCCP for 24 hours in regular culture medium. The graphs showed a significant increase in basal cytotoxicity levels (a) and marked reduction in ATP levels with the lowest tested CCCP concentration, 10 μ M (b). The error bars represent the SD of three technical replicates.

To minimise the effect of dead cells on the results in the following experiments, the wells were routinely washed with differentiation medium during the course of the differentiation. In addition, the cytotoxicity was assessed via ICC as an alternative method. The cells were probed with cleaved caspase-3 antibody and imaged using confocal microscopy [Figure 5.10]. The image analysis protocol was programmed to exclude dead cells based on the size and the intensity of the nuclei [Figure 5.11].

a) Undifferentiated SY-SY5Y



b) Differentiated SY-SY5Y

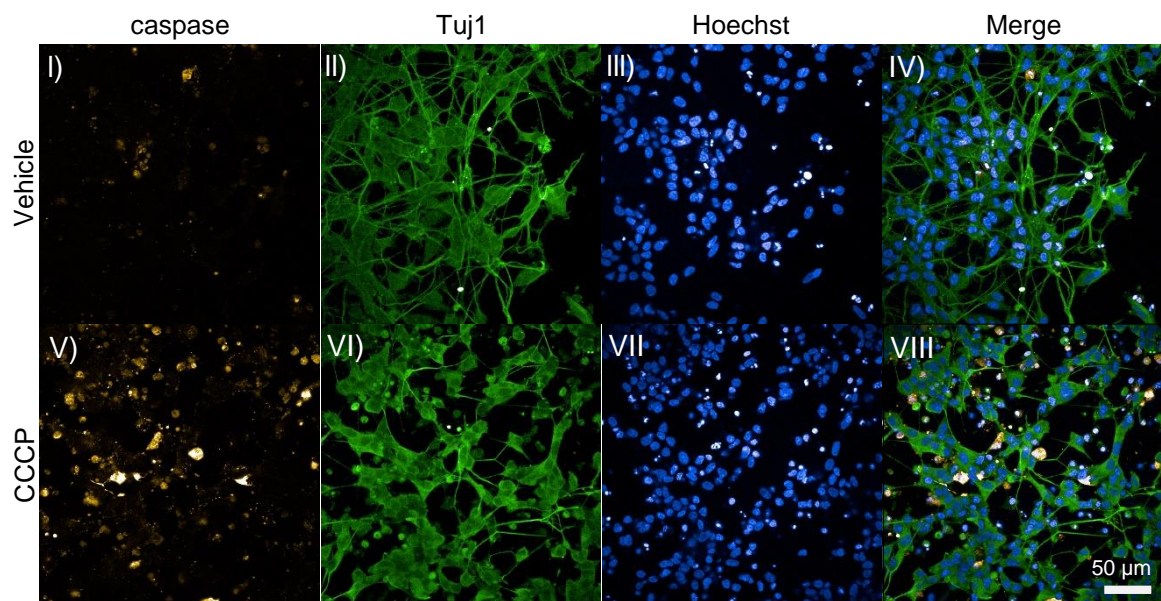


Figure 5.10 Cleaved caspase 3 staining is an efficient approach to assess cytotoxicity in differentiated SH-SY5Y.

ICC images of caspase stained cells as an alternative approach to assess CCCP cytotoxicity. The cells were stressed with 10 µM CCCP for 24 hours. ICC was performed as described in the method section, and images were captured using confocal microscopy. Images of the first column (I and V) show staining with cleaved caspae-3 (yellow). Images of the second column (II and VI) show staining with Tuj1 (green). Images of the third column (III and VII) show staining with Hoechst (blue). Images of the forth column (IV and VIII) show the merged image. The images show a significant increase in caspase staining in CCCP-stressed differentiated cells. Scale bar = 50µm.

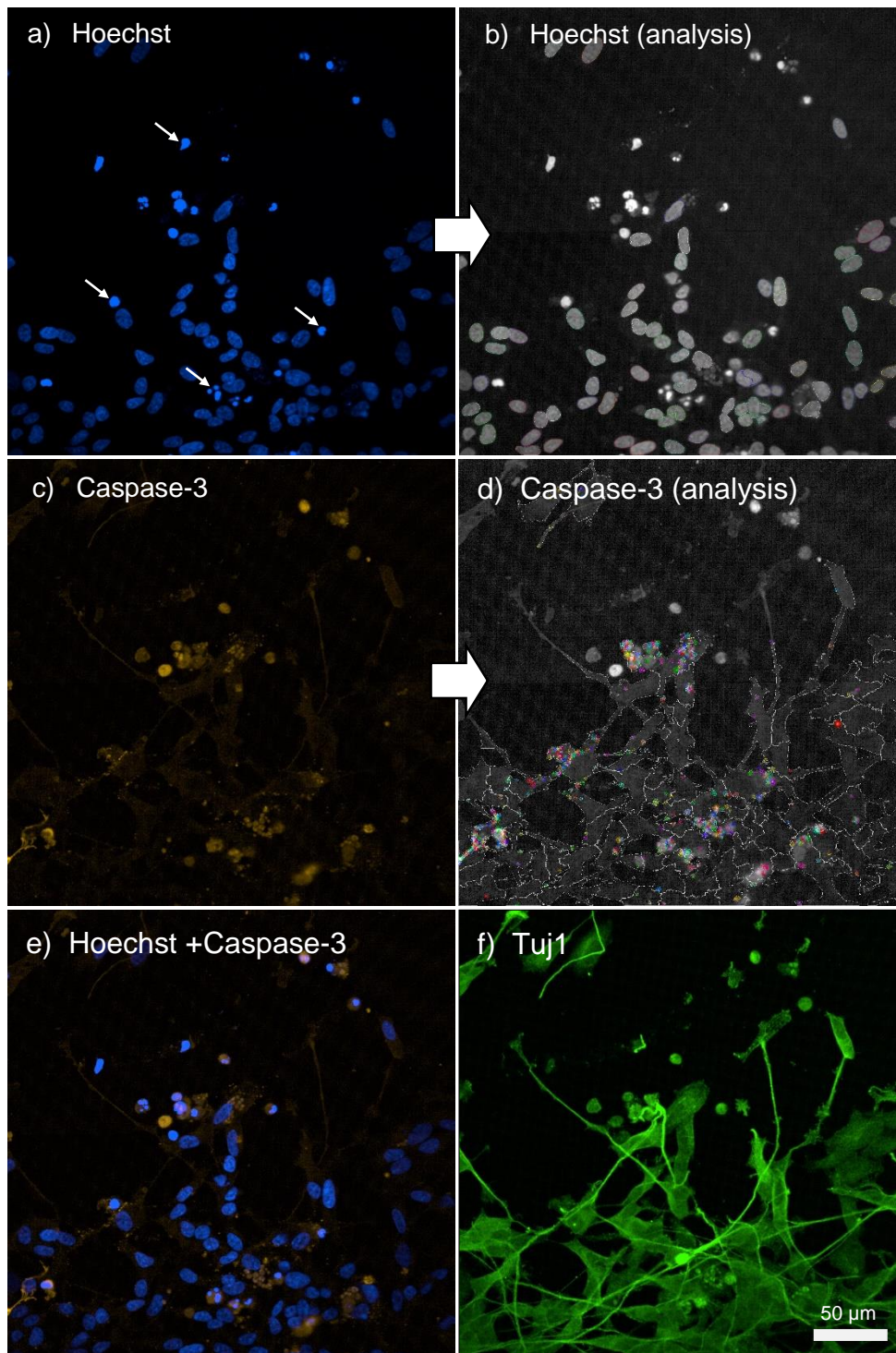


Figure 5.11 Image analysis software can detect and exclude dead cells co-stained with Hoechst and caspase-3.

An illustration of the protocol used to analyse caspase staining. Untreated differentiated SH-SY5Y cells were probed with cleaved caspase-3 antibody and were stained with Hoechst. The images were captured by confocal microscopy, as described in the method section, and then were analysed using the Harmony software. (a) Hoechst staining to visualise the nuclei. White arrows point to some of dead cells with condensed shrunken nuclei. (b) Shows the viable nuclei that were selected by the software for subsequent analysis (enclosed within coloured circles). (c) Cleaved caspase-3 staining of untreated differentiated cells. (d) Shows caspase spots identified by the analysis software (the coloured areas). Only caspase spots of viable cells were analysed by the software. (e) A merged image of Hoechst and caspase staining. (f) The cells were also probed with Tuj1 to determine the cytoplasmic regions. Scale bar = 50 μ m.

Consequently, image analysis of caspase staining was set to calculate different parameters [Figure 5.12] [Figure 5.13]. Those were labelled as follows: number of spots / cell count = the average number of caspase spots per cell, number of spots per area of cells = the average number of detected spots divided by the area of the cell region, total spot area / cell count = the average of the area of all spots detected per cell, spot area = the average area of individual spot, relative spot intensity = the fraction of stain aggregated in spots compared to total amount of stain in the cell, region intensity = the mean intensity of the spot search region where the particular spot is located.

Testing low CCCP doses revealed a dose-dependent increase in caspase spot numbers and the total caspase spot areas [Figure 5.12]. The tested CCCP doses also increased the readings of other parameters of caspase analysis [Figure 5.13], and collectively demonstrated a clear effect of CCCP treatment on the amount of cleaved caspase-3. With regard to ATP levels, the lowest tested CCCP concentration had no effect, while both 5 μ M and 10 μ M CCCP induced around a 40% decrease [Figure 5.14]. Notably, differentiated cells had higher basal ATP levels (almost double) in comparison to the undifferentiated cells. In accordance with the ATP and cytotoxicity results, it was decided to use 10 μ M CCCP in the drug treatment experiments.

Cytotoxicity

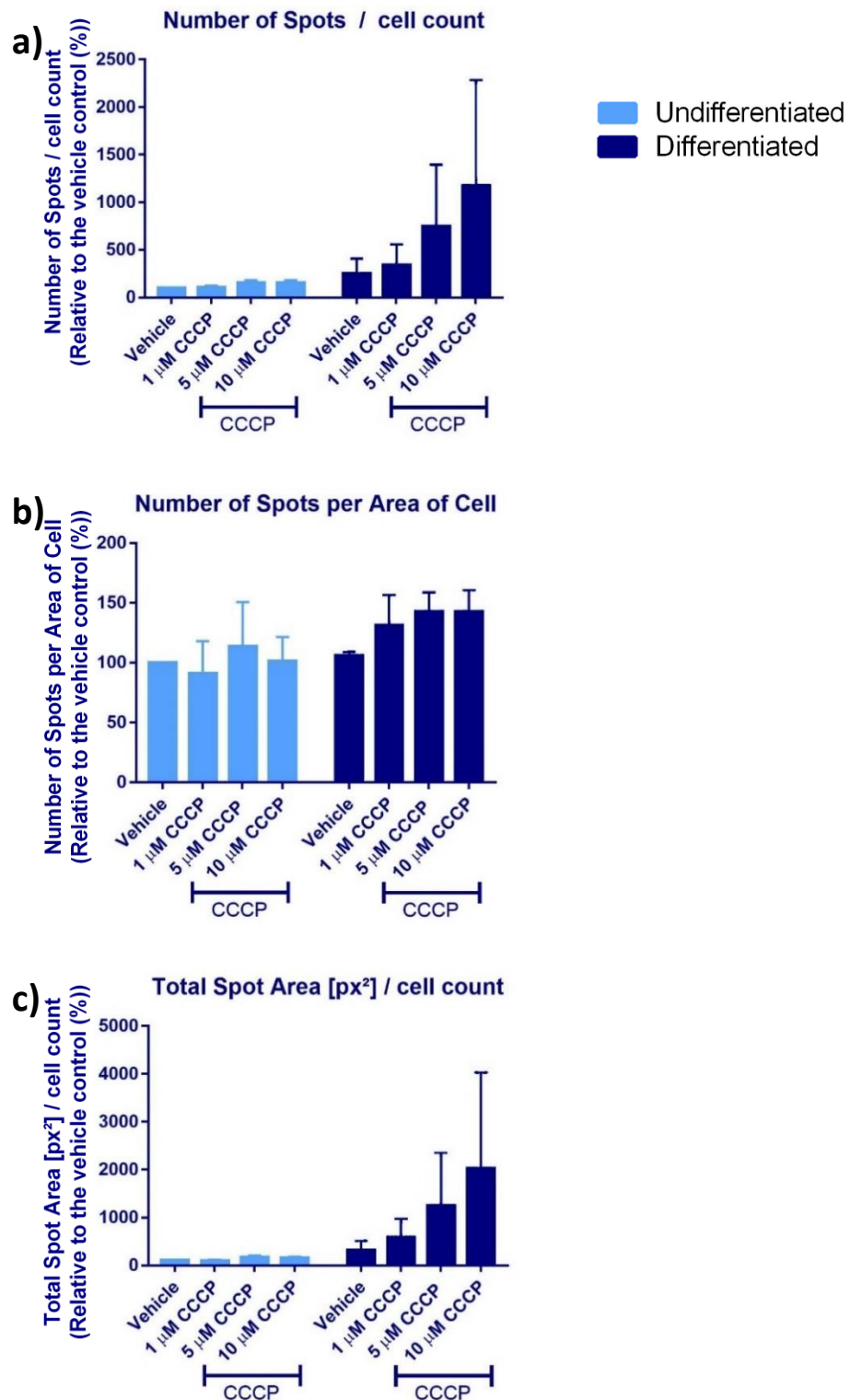


Figure 5.12 Multiple CCCP concentrations induced a dose-dependent effect on several parameters of caspase-3 spots analysis (1/2).

The results of image analysis of caspase staining of CCCP-stressed cells. Undifferentiated and differentiated SH-SY5Y cells were treated with 1 μ M, 5 μ M and 10 μ M of CCCP for 24 hours. ICC was performed as described in the method section, and images were captured using confocal microscopy. The cells were co-stained with Tuj1 to determine the cell boundaries, and with Hoechst to determine the cell counts. Analysis of caspase spots was performed by the Harmony software to determine the number of spots per cell (a), the number of spots per area (b) and the total spot area per cell (c). The results showed a dose dependant increase in the number of spots and total spot area in differentiated cells. All readings were normalised to the undifferentiated control. The error bars represent the SD of three independent experiments.

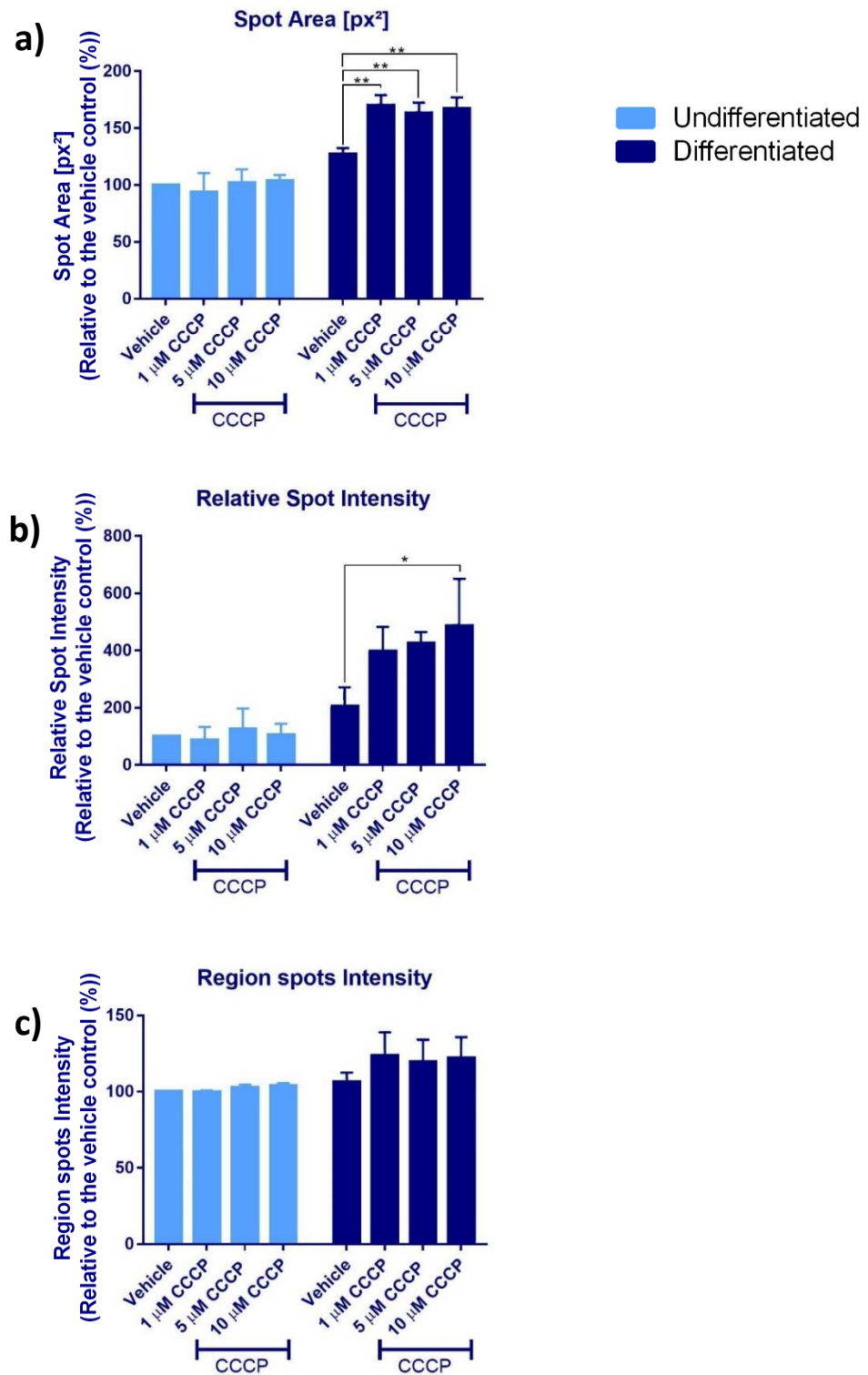


Figure 5.13 Multiple CCCP concentrations induced a dose-dependent effect on several parameters of caspase-3 spots analysis (2/2).

The results of image analysis of caspase staining of CCCP-stressed cells. The cells were treated with 1 μM, 5 μM and 10 μM of CCCP for 24 hours. ICC was performed as described in the method section, and images were captured using confocal microscopy. The cells were co-stained with Tuj1 to determine the cell boundaries, and with Hoechst to determine the cell counts. Analysis of caspase spots was performed by the Harmony software to determine the average spot area (a), relative spots intensity (b) and region spots intensity (c). The results showed a significant increase in spot area and relative spot intensity in CCCP-stressed differentiated cells. All readings were normalised to the undifferentiated control. The error bars represent the SD of three independent experiments. * p < 0.05, ** p < 0.01, two-way ANOVA test.

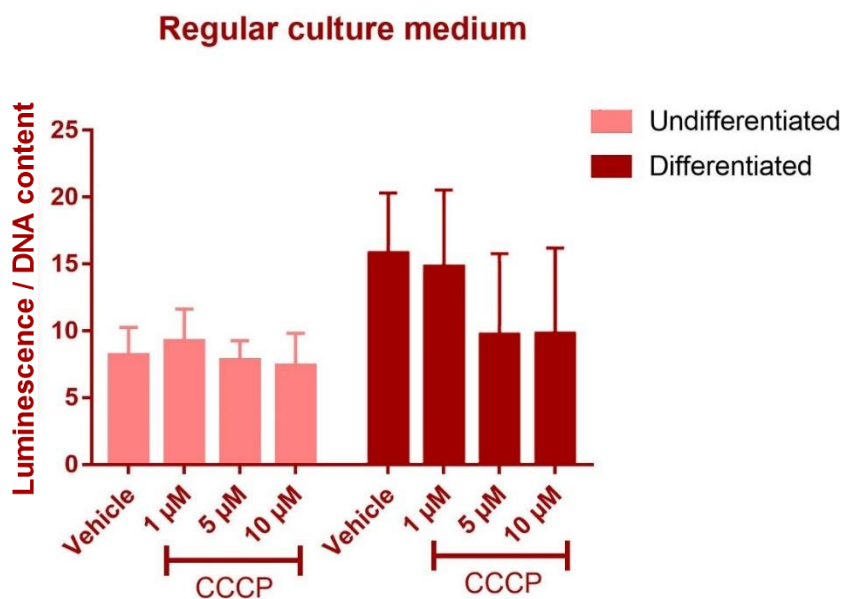


Figure 5.14 Assessing the effect of multiple CCCP doses on ATP readings demonstrated comparable responses with 5 μM and 10 μM .

ATP levels were measured using ATP assays as described in the method chapter [Heading 2.10]. The cells were stressed with CCCP for 24 hours. 5 μM and 10 μM CCCP induced approximately a 40% decrease in ATP level in differentiated SH-SY5Y cells. The error bars represent the SD of three independent experiments.

5.3.3 Assessing the effect of UDCA in CCCP-stressed differentiated SH-SY5Y

Differentiated SH-SY5Y cells have an altered transcription profile and a higher sensitivity to CCCP. Therefore, the effective UDCA dose in these cells might differ from that of the undifferentiated cells. Accordingly, three doses of UDCA were tested in this experiment (10 μM , 100 μM and 300 μM). The assay window of a 40% decrease in ATP levels was reproducible; however, none of the tested UDCA doses ameliorated the cytotoxicity of CCCP [Figure 5.15] [Figure 5.16]. Similarly, UDCA treatment failed to increase ATP levels [Figure 5.17]. The difference between the stressed and unstressed cells was statistically insignificant due to the variation between the replicates, which make it difficult to interpret the data. Although there was an increase of 35% with 10 μM UDCA in comparison to the untreated control, the variability between control conditions (CCCP-untreated and CCCP-Vehicle) and long error bars made it difficult to conclude that this increase was real. Overall, the results suggest that the previously observed UDCA-mediated rescue effect in undifferentiated SH-SY5Y was not reproducible in differentiated SH-SY5Y.

Cytotoxicity

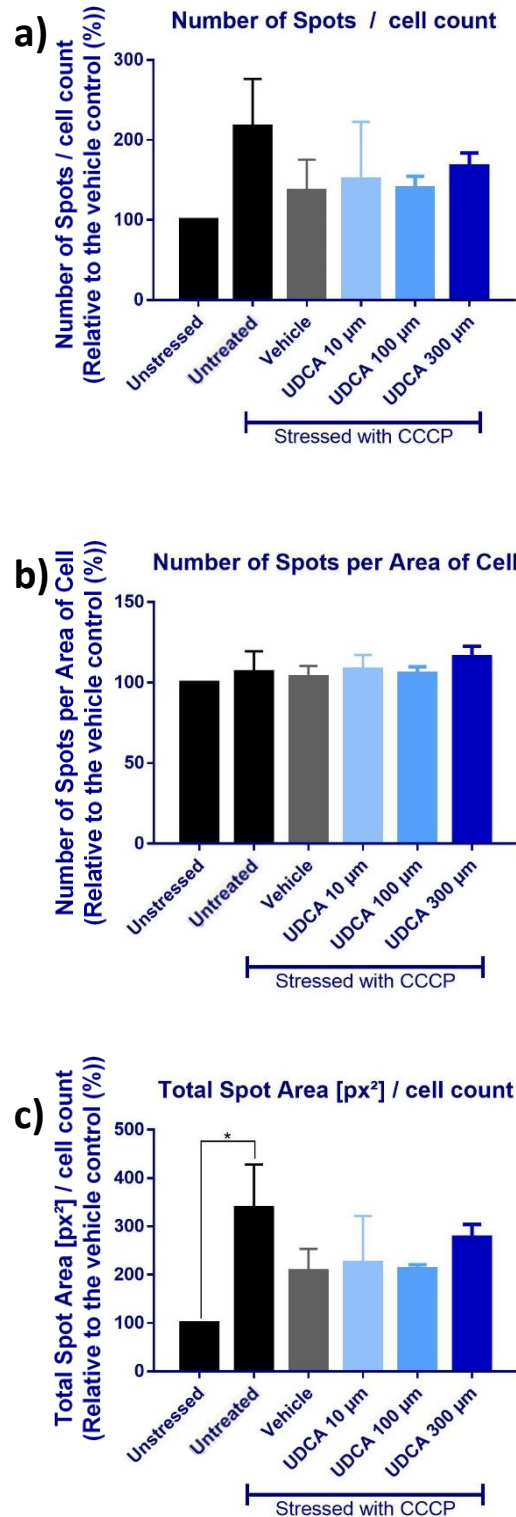


Figure 5.15 Multiple doses of UDCA did not induce a positive effect on cleaved caspase 3 staining in CCCP-stressed differentiated SH-SY5Y cells (1/2).

Image analysis of caspase staining of treated SH-SY5Y cells. The cells were pre-treated for 12 hours with UDCA. Then, they were further incubated with 10 μ M CCCP for 24 hours. The results show that UDCA treatments did not ameliorate cytotoxicity in stressed cells. The cells were co-stained with Tuj1 to determine the cell boundaries, and with Hoechst to determine the cell counts. Analysis of caspase spots was performed by the Harmony software to determine the number of spots per cell (a), the number of spots per area (b) and the total spot area per cell (c). All readings were normalised to the unstressed control. The error bars represent the SD of three independent experiments. * $p < 0.05$, one-way ANOVA test.

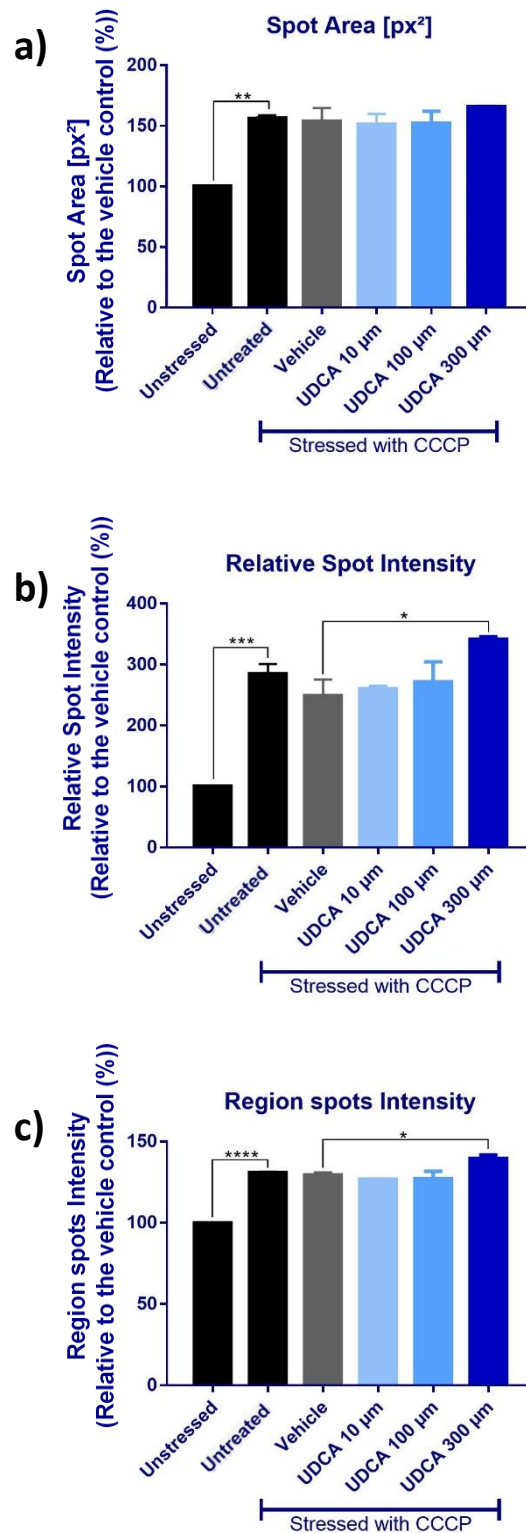


Figure 5.16 Multiple doses of UDCA did not induce a positive effect on cleaved caspase 3 staining in CCCP-stressed differentiated SH-SY5Y cells (2/2).

Image analysis of caspase staining of treated SH-SY5Y cells. The cells were pre-treated for 12 hours with UDCA. Then, they were further incubated with 10 µM CCCP for 24 hours. The results show that UDCA treatments did not ameliorate cytotoxicity in stressed cells. The cells were co-stained with Tuj1 to determine the cell boundaries, and with Hoechst to determine the cell counts. Analysis of caspase spots was performed by the Harmony software to determine the average spot area (a), relative spots intensity (b) and region spots intensity (c). All readings were normalised to the unstressed control. The error bars represent the SD of three independent experiments. * $p < 0.05$, ** $p < 0.01$, *** $p < 0.001$, **** $p < 0.0001$ one-way ANOVA test.

ATP

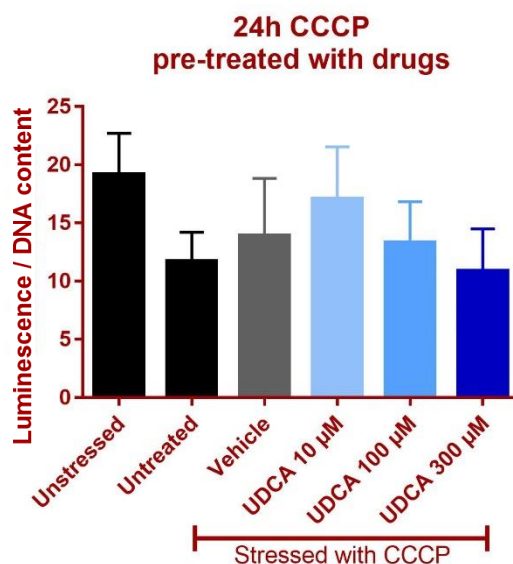


Figure 5.17 Multiple doses of UDCA did not induce a significant positive effect on ATP levels in CCCP-stressed differentiated SH-SY5Y cells.

ATP levels were measured using ATP assays as described in the method chapter [Heading 2.10]. The cells were pre-treated for 12 hours with UDCA. Then they were further incubated with 10 µM CCCP for 24 hours. The results show that UDCA treatments did not increase ATP readings in stressed cells. The error bars represent the SD of three independent experiments.

5.4 Evaluating the effect of UDCA on the expression of Nrf2 genes in stressed undifferentiated SH-SY5Y cells

5.4.1 Initial testing of the primers

Since UDCA increased ARE expression in unstressed CHO cell [Figure 4.5], it was decided to investigate if the rescue effect in CCCP-stressed SH-SY5Y cells was mediated via the Nrf2 pathway. To assess Nrf2 activation, we quantified the expression of Nrf2 target genes via RT-qPCR using RNA extracts of treated cells. Primers of six Nrf2 genes were designed and tested, as described in the method section. Upon testing different concentrations of the forward and the reverse primers, *HMOX1* and *NQO1* showed double peaks on the melt peak curves and therefore were excluded from the subsequent experiments [Figure 5.22]. The primers of the other genes (*GAPDH*, *GST2A*, *GCLC* and *FTH1*) produced similar amplification curves and melt peaks in all tested concentrations [(a) and (b) in Figure 5.18 to Figure 5.21]. Subsequently, standard curves and melt peaks were obtained from a serial of ten-fold dilution of the samples. The results reveal a high sensitivity and specificity for these four primers [(c), (d) and (e) in Figure 5.18 to Figure 5.21].

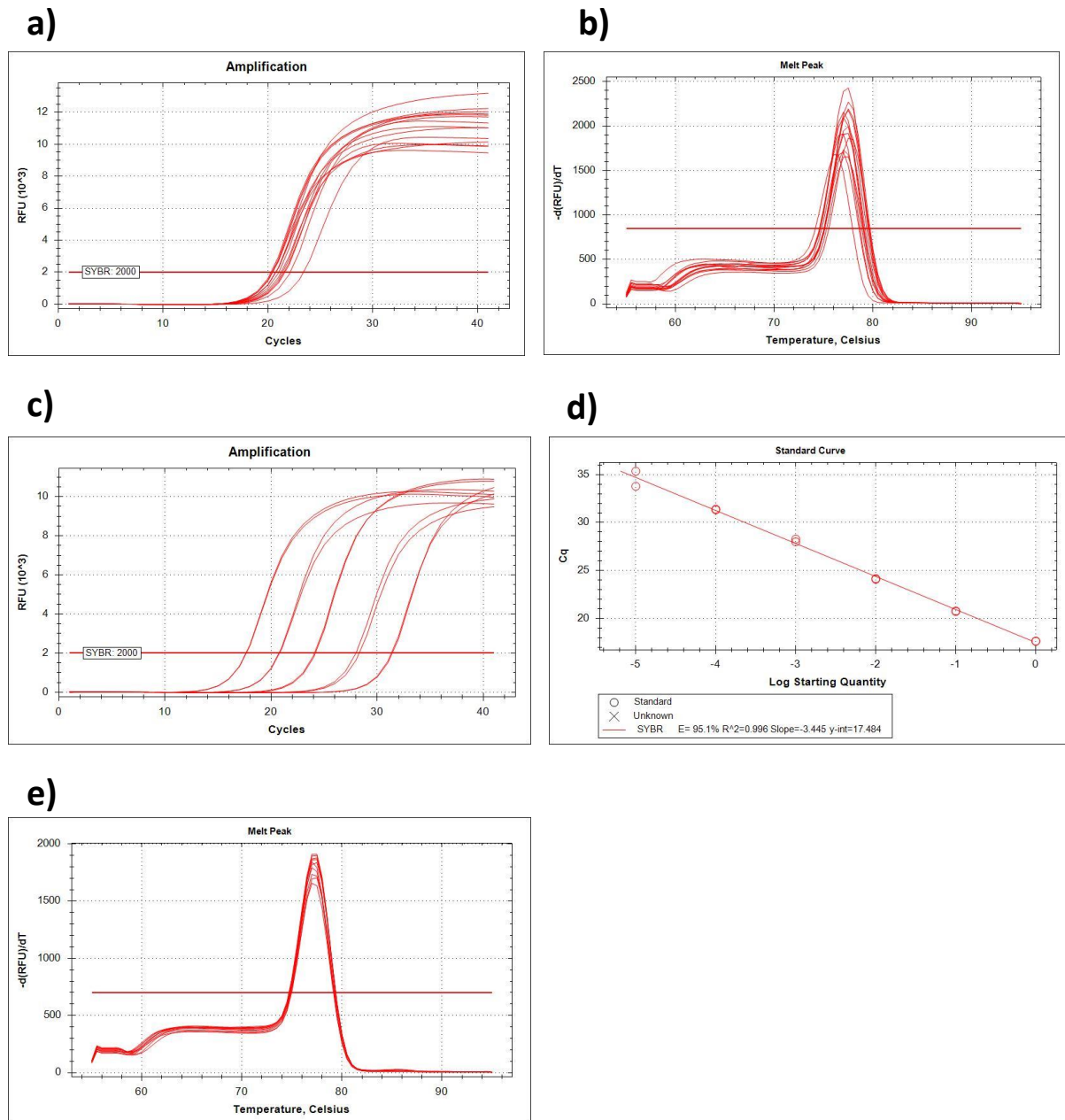


Figure 5.18 *GAPDH* primers have high efficiency and specificity in qPCR reactions.

(a) and (b) Testing combinations of different concentrations of the forward and the reverse primers [Heading 2.6.3]. All combinations showed comparable amplification curves and melt peaks. (c), (d) and (e) Assessing the reacting efficiency and specificity using a ten-fold serial dilution of the sample. The standard curves revealed an efficiency of 95.1 %. The melt peak graph showed single peaks with all dilutions of the sample indicating high specificity.

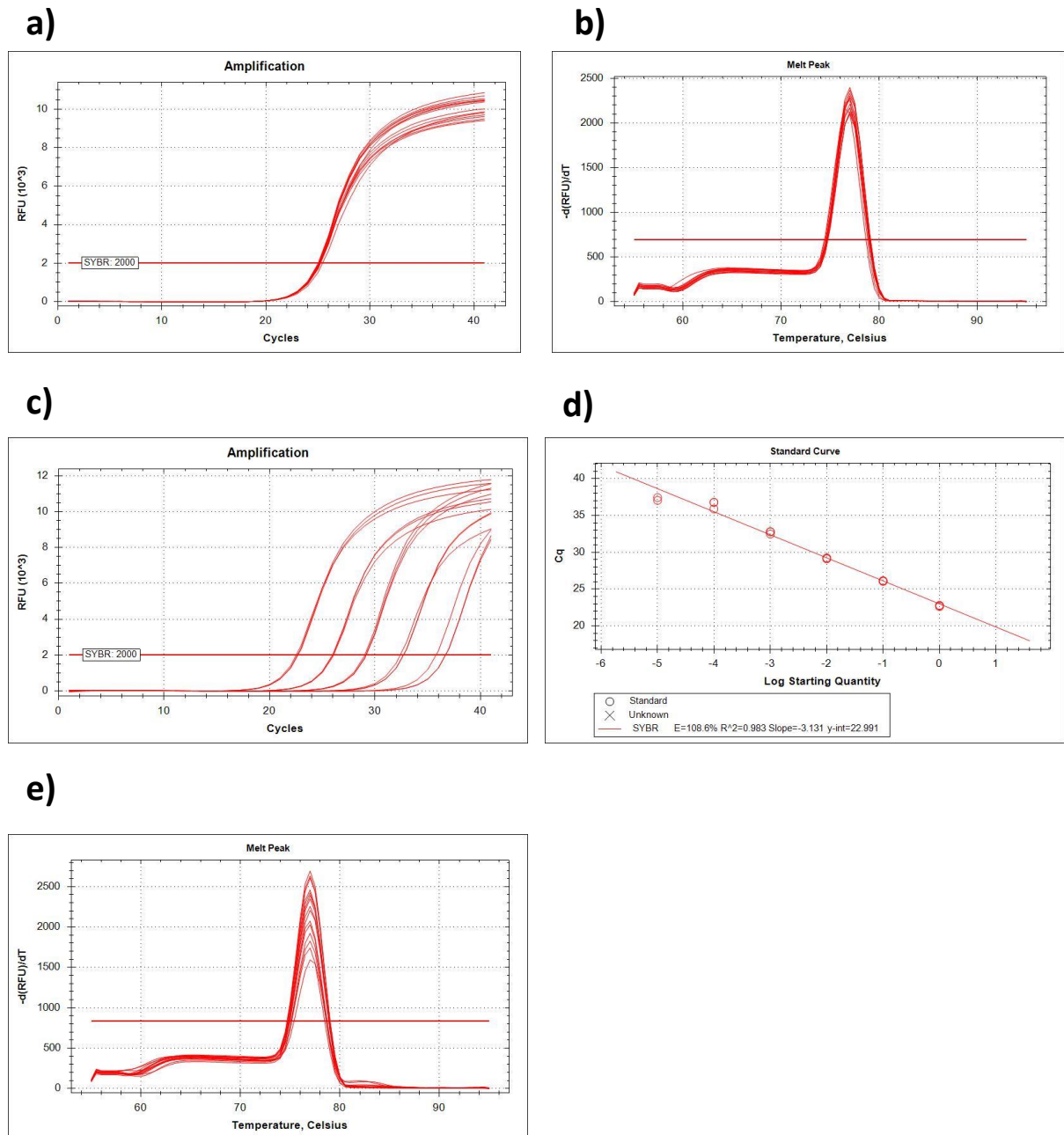


Figure 5.19 GST2A primers have high efficiency and specificity in qPCR reactions.

(a) and (b) Testing combinations of different concentrations of the forward and the reverse primers [Heading 2.6.3]. All combinations showed comparable amplification curves and melt peaks. (c), (d) and (e) Assessing the reacting efficiency and specificity using a ten-fold serial dilution of the sample. The standard curves revealed an efficiency of 108.6 %. The melt peak graph showed single peaks with all dilutions of the sample indicating high specificity.

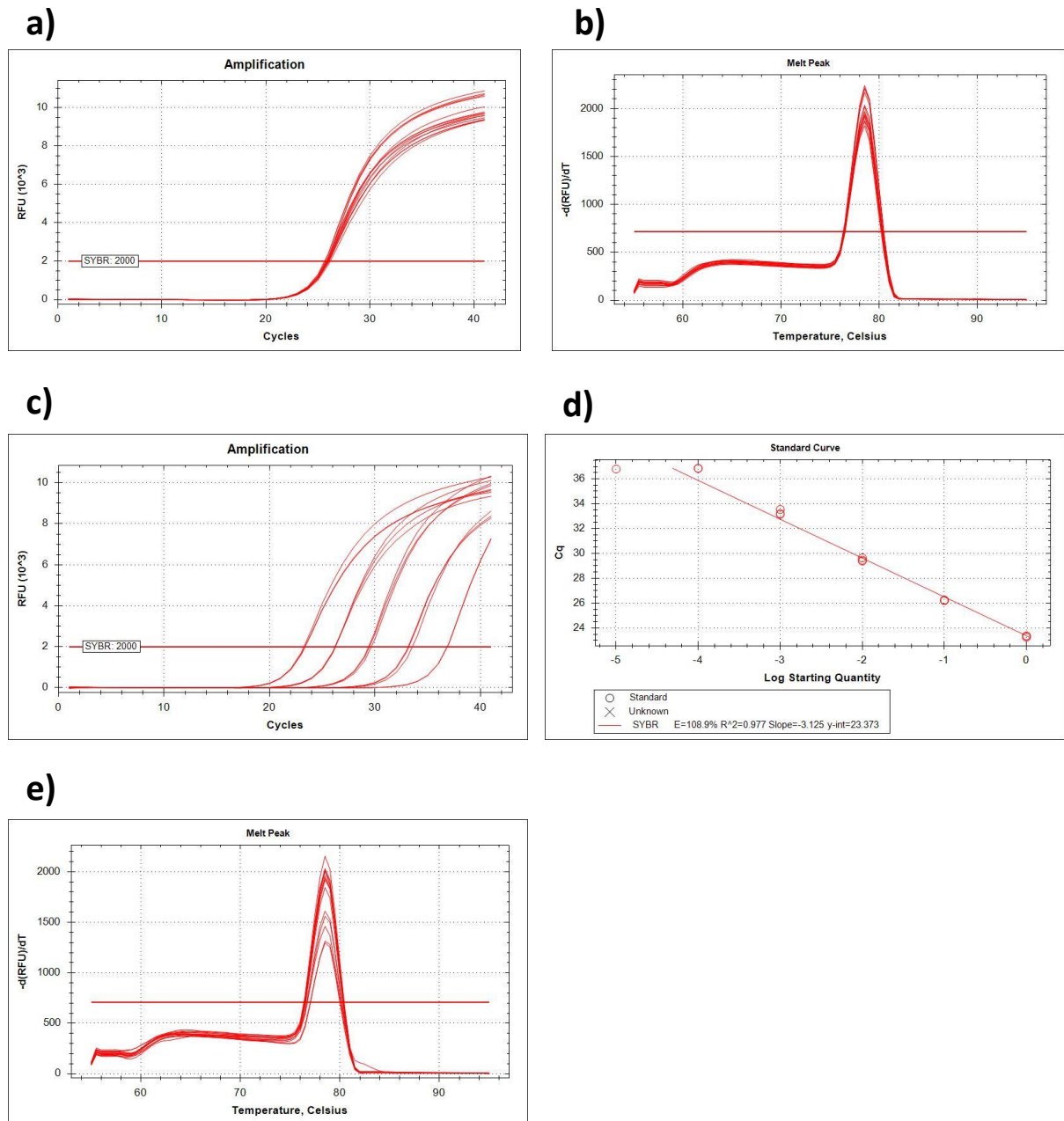


Figure 5.20 GCLC primers have high efficiency and specificity in qPCR reactions.

(a) and (b) Testing combinations of different concentrations of the forward and the reverse primers [Heading 2.6.3]. All combinations showed comparable amplification curves and melt peaks. (c), (d) and (e) Assessing the reacting efficiency and specificity using a ten-fold serial dilution of the sample. The standard curves revealed an efficiency of 108.9 %. The melt peak graph showed single peaks with all dilutions of the sample indicating high specificity.

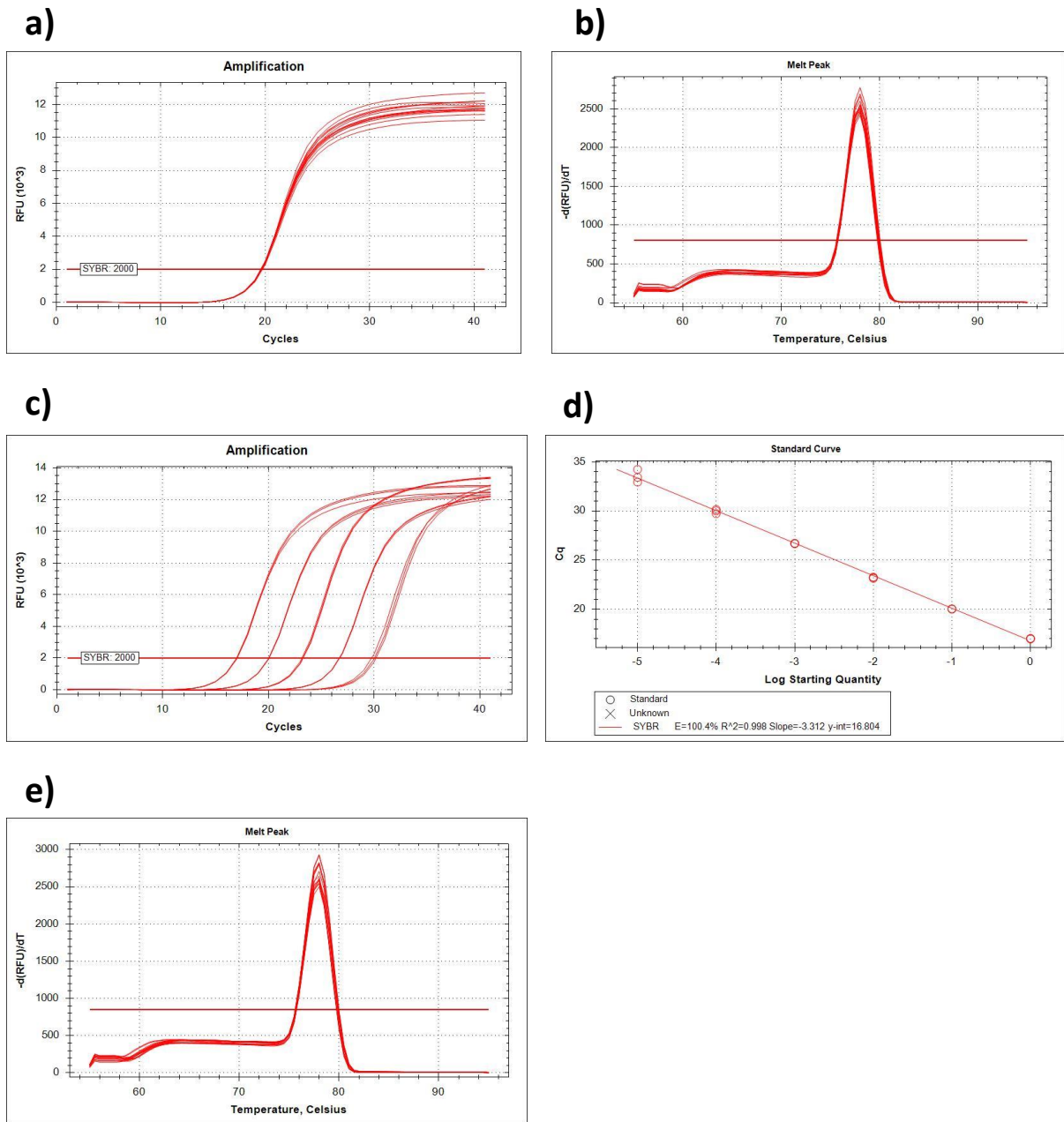
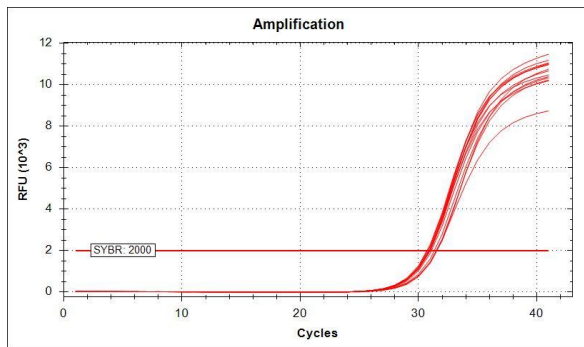


Figure 5.21 *FTH1* primers have high efficiency and specificity in qPCR reactions.

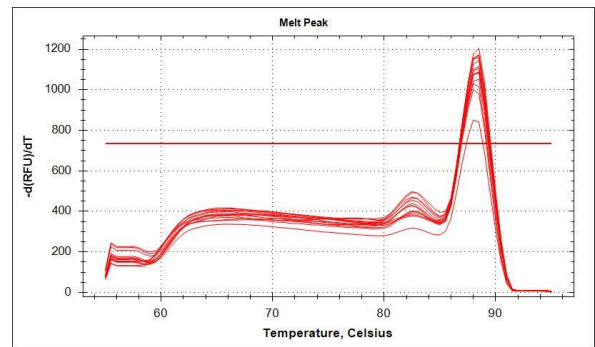
(a) and (b) Testing combinations of different concentrations of the forward and the reverse primers [Heading 2.6.3]. All combinations showed comparable amplification curves and melt peaks. (c), (d) and (e) Assessing the reacting efficiency and specificity using a ten-fold serial dilution of the sample. The standard curves revealed an efficiency of 100.4%. The melt peak graph showed single peaks with all dilutions of the sample indicating high specificity.

HMOX1

a)

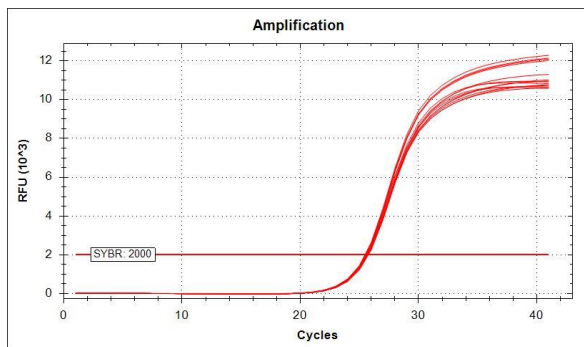


b)



NQO1

c)



d)

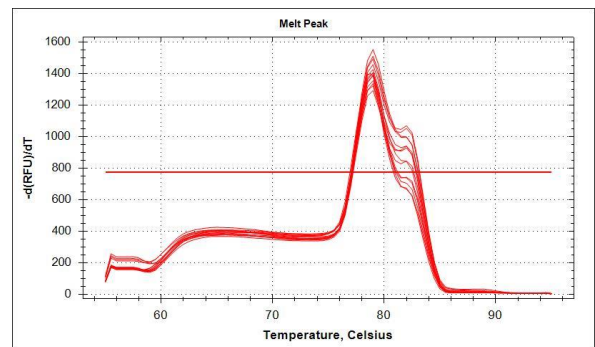


Figure 5.22 HMOX1 and NQO1 primers showed secondary peaks in melt peak graphs in qPCR reactions.

Testing combinations of different concentrations of the forward and the reverse primers [Heading 2.6.3]. Secondary peaks were observed with all combinations of HMOX primers (b) and NQO1 primers (d). Therefore, these primers were excluded from drug treatment experiments.

5.4.2 Assessing the effect of UDCA and BG12 on the expression of Nrf2 downstream genes in undifferentiated SH-SY5Y cells

The SH-SY5Y cells were treated with 300 μ M UDCA as this was the most effective dose in CCCP-stressed cells (undifferentiated SH-SY5Y) [Figure 5.4]. In addition, the cells were treated with different concentrations of the positive control, BG12 (2 μ M, 10 μ M and 30 μ M). Notably, CCCP significantly increased the expression of *GCLC* (140%) and *FTH1* (680%) but had no effect on *GST2A* [Figure 5.23]. The results showed that UDCA treatment did not increase the expression of Nrf2 genes in CCCP-stressed cells (undifferentiated SH-SY5Y). In contrast, there was a decrease in the expression of *GST2A* (20%), and a statistically significant decrease in the expression of *FTH1* (25%) [Figure 5.23]. Despite the treatment with different concentrations of BG12, none of them significantly increased the expression of the selected Nrf2 genes.

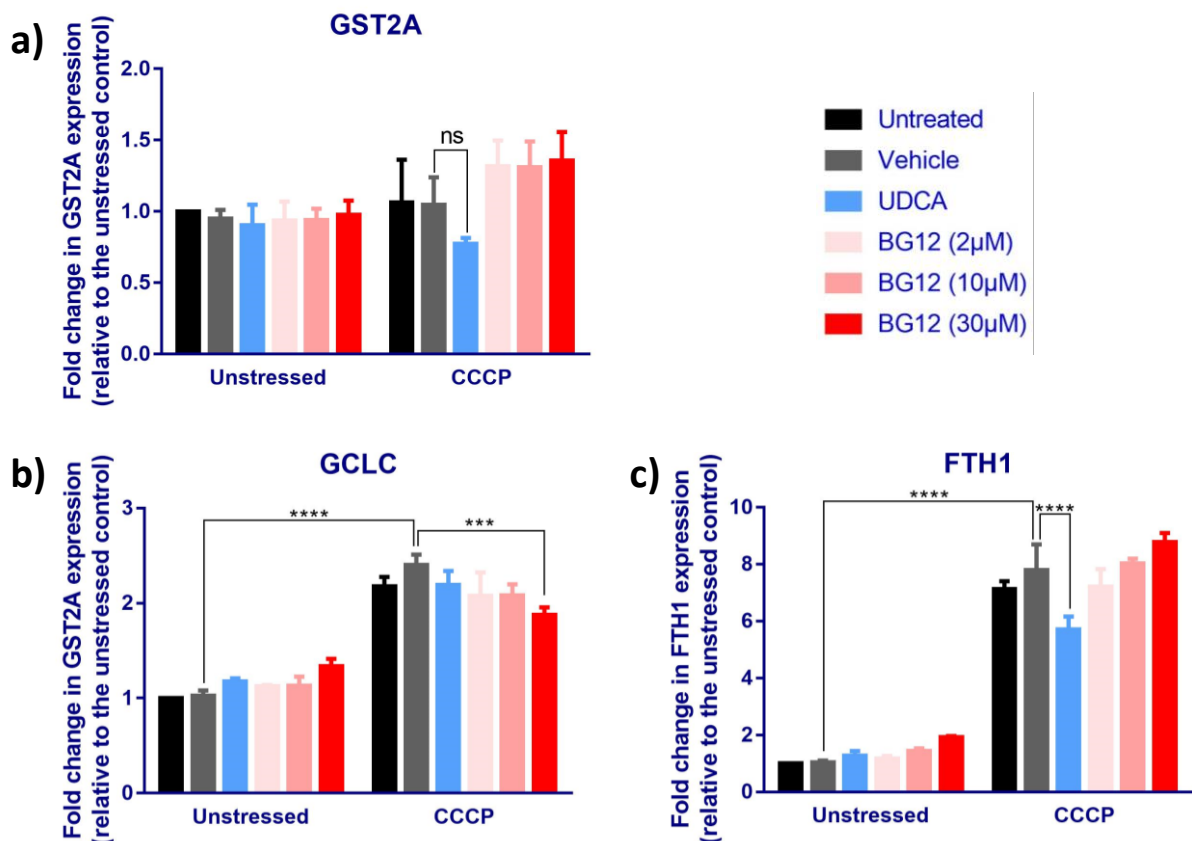


Figure 5.23 UDCA treatment induced variable effects on the expression of Nrf2 downstream genes in undifferentiated SH-SY5Y cells.

Determining the effect of UDCA on the Nrf2 downstream genes was performed by qPCR. The cells were pre-treated with 300 μ M UDCA for 12 hours before the addition of 50 μ M CCCP, which was kept for 24 hours. Data analysis revealed that UDCA reduced the expression of *GST2A* (a) and *FTH1* (c), but did not affect the expression of *GCLC* (b). The graphs represent data of three independent experiments. The error bars represent SD., *** $p < 0.001$, **** $p < 0.0001$, two-way ANOVA test.

5.5 Discussion

The objective of this chapter is to demonstrate the rescue effect of UDCA in a human cell line of neuronal nature. As performed with the CHO cells, toxin-induced (rotenone/CCCP) mitochondrial dysfunction was used to model PD pathology. The results of the initial rotenone testing in the regular culture medium using SH-SY5Y cells were comparable to what was previously observed in CHO cells, where CHO cells were able to compensate the inhibition of OXPHOS via upregulating glycolysis [Figure 4.18]. Since SH-SY5Y cells originate from tumors, they are expected to have increased glycolytic activity due to the Warburg effect (Aminzadeh et al., 2015). Culturing SH-SY5Y cells in galactose medium significantly increased their vulnerability to the rotenone. However, treatment with 10 μ M UCA and UDCA failed to rescue cells stressed with various doses of rotenone [Figure 5.2]. Prior to starting the CCCP experiments, Fonseca et al. (2017) published a paper that showed a significant TUDCA-mediated rescue effect in CCCP-stressed SH-SY5Y cells (Fonseca et al., 2017). Notably, higher doses of both CCCP and the drug were used in her paper (50 μ M CCCP, 100 μ M TUDCA), and the experiments were performed using glucose-containing medium. Accordingly, it was decided to adopt their treatment protocol in the CCCP experiment in this chapter. The previously used 10 μ M UCA and 10 μ M UDCA conditions were kept, and 100 μ M UDCA and 100 μ M TUDCA were added. The cells were also stressed with a lower CCCP dose, 25 μ M. While the TUDCA effect was not reproducible, UDCA treatment with doses up to 300 μ M significantly increased ATP levels and ameliorated cytotoxicity [Figure 5.4].

Possible explanation for the absence of the TUDCA-mediated positive effect on undifferentiated SH-SY5Y cells might be the difference in the culturing mediums. In this project, SH-SY5Y cells were cultured in DMEM medium supplemented with 10% FBS [Table 2.2], while in the paper the cells were grown in Ham's F12:EMEM (1:1) supplemented with 15% FBS in addition to 1% non-essential amino acids. Providing the cells with more supportive nutrition might enable the cells to respond positively to the TUDCA treatment. Treatment with higher UDCA doses (>300 μ M) was toxic to the unstressed cells [Figure 5.4]. Therefore, the 300 μ M UDCA was used as standard in

all subsequent experiments investigating the mechanism of action of UDCA in undifferentiated SH-SY5Y.

In this project, the RA-based differentiation protocol was adopted from published studies that demonstrated successful SH-SY5Y differentiation (Lopes et al., 2017, Popova et al., 2017). The differentiated cells in this project showed significant morphological changes that were associated with an increase in the expression of the neuronal marker, MAP2. The transformation into a terminal post-mitotic state (deduced from reduced cell growth) and the presence of Tuj1 in the neurites of differentiated cells further confirms successful differentiation. More than one third of the published papers declare that the differentiated SH-SY5Y cells in use have a DA phenotype without providing supportive evidence (Xicoy et al., 2017). In this chapter, the DA nature of the differentiated cells was determined by assessing the expression of two DA markers, FOXA2 and TH [Figure 5.8]. Although the expression of TH is commonly used to identify DA cells, it is important to point out that this is an indirect method. An example of the direct approach would be the detection of dopamine using the ELISA technique, which allows the quantification of synthesised dopamine within the cells and the released dopamine in the culture medium.

Throughout the course of the differentiation, a significant percentage of the cells failed to tolerate this process and died in the wells, which negatively affected the accuracy of the cytotoxicity assessment via trypan blue staining. Even with the repetitive washing procedure, some of these cells stuck to the well floor and were subsequently included in cell counting. Using an LDH assay would not improve the results, as accumulated dying cells would have contributed to the total LDH released in the medium. To overcome this limitation, ICC was used to assess cytotoxicity as it enables the exclusion of dead cells in image analysis. The cells were probed with cleaved caspase-3 antibody, which is mainly produced in the apoptotic cells via the action of initiator caspases, such as caspase 8 and caspase 9 on pro-caspase-3 (Maes et al., 2015, Kiraz et al., 2016). Unlike cleaved caspase-3 staining, trypan blue staining does not differentiate between apoptotic and necrotic cells. Therefore, cleaved caspase-3 staining, is superior since necrosis is not implicated in cell death in PD.

Differentiated SH-SY5Y cells are vulnerable to toxins that elevate oxidative stress, such as H₂O₂ and 6-OHDA (Lopes et al., 2017, Forster et al., 2016, Piras et al., 2017). Equally, caspase staining in this chapter showed that CCCP induced a dose-dependent effect on cytotoxicity in differentiated SH-SY5Y [Figure 5.12]. Notably, the basal cytotoxicity in differentiated cells was higher than in undifferentiated cells. This is consistent with previously published studies that showed increased cleaved caspase-3 levels in retinoic acid-differentiated SH-SY5Y (Mak et al., 2010). Research shows that RA-mediated elevation in ROS and oxidative stress is critical for SH-SY5Y differentiation (Kunzler et al., 2017). The basal ATP levels in differentiated cells were higher than in undifferentiated cells. This finding has been previously reported (Lopes et al., 2017). Since RA enhances the expression of glucokinase (an enzyme responsible for the conversion of glucose into glucose-6-phosphate) (Cabrera-Valladares et al., 2001), it is plausible that the increase in ATP is achieved via upregulation in glycolysis. However, experimental data suggest that differentiated SH-SY5Y cells have enhanced OXPHOS instead. The oxygen consumption rate was found to be significantly increased in RA-treated SH-SY5Y cells, and this increase was not affected by the inhibition of glycolysis, indicating increased dependency on OXPHOS (Xun et al., 2012). This increase is proposed to be mediated via elevated levels of metabolic substrates such as Acetyl-CoA or via the utilisation of a different pathway such as fatty acid catabolism (Xun et al., 2012). Since brain neurons are predominantly oxidative, these changes in bioenergetics in differentiated SH-SY5Y cells make them better models of mature neurons (Raefsky and Mattson, 2017).

According to the cytotoxicity and ATP results of CCCP-stressed differentiated SH-SY5Y cells, it was decided to use 10 µM CCCP in the drug treatment experiments. Three different concentrations of UDCA were tested. The results showed an occasional inconsistency between the untreated and vehicle conditions as well as variability between replicates, which made it difficult to interpret the data. This variability might have arisen from non-homogenous differentiation of the cells as well as differences between independent experiments. Nonetheless, the results suggest that none of the tested UDCA doses had a positive effect on cytotoxicity or ATP levels. One of the possible explanations for these negative results is that the used differentiation protocol

is inappropriate for studying the rescue effect of UDCA. In the used protocol, the cells were grown in a serum-free medium. This might have induced a significant stress load on the cells and rendered them unable to respond properly to drug treatment. In line with that notion, the differentiation of SH-SY5Y cells was associated with a significant degree of cell death [Figure 5.6 a]. Therefore, it is recommended that the protocol is optimised in future experiments, which was not accomplished in this project due to the time limit. Possible adjustments include the use of alternative differentiation medium and the addition of a small percentage of FBS (1–5%) to support the health of differentiating cells. The addition of BDNF to the medium helps to induce a homogenous cell culture (Shiple et al., 2016), which should help to reduce the variability in the results. It is also recommended to increase the number of technical replicates in each round of drug treatment, and to use alternative methods such as flow cytometry (to assess caspase activation) to improve the accuracy of the results.

Although the results were inconsistent in differentiated SH-SY5Y experiments, UDCA significantly increased ATP levels and viability in CCCP-stressed undifferentiated SH-SY5Y cells at a dose of 300 μ M [Heading 5.2.3]. Consequently, we investigated whether this beneficial effect was associated with activation of the Nrf2 pathway, since UDCA showed a dose-dependent increase in ARE expression in CHO cells [Figure 4.5]. Notably, the results showed that CCCP significantly increased the expression of 2/3 Nrf2 genes (GCLC and FTH1) [Figure 5.23]. This upregulation is expected since CCCP treatment damages the mitochondria and increases oxidative stress levels in the cells (Fonseca et al., 2017). In addition, CCCP directly reacts with Keap1 thiol groups, resulting in breaking the bond between Keap1 and Nrf2, and consequently increasing Nrf2 content in the nucleus (Kane et al., 2017). The mechanism of Nrf2 activation was previously discussed in Chapter 4 [Heading 4.1.3].

The results in this chapter show that UDCA treatment did not increase the expression of the selected Nrf2 genes in CCCP-stressed SH-SY5Y cells. In contrast, there was an unexpected decrease in the expression of GST2A and FTH1. This does not rule out the possibility of UDCA-mediated antioxidant effect as it could be achieved via other adaptive stress response pathways such as AP-1 and JNK.

It is also possible that UDCA triggered an alternative cytoprotective pathway that decreased oxidative stress levels and, as a result, the expression of the Nrf2 genes was not increased as much as in the untreated CCCP-stressed condition. According to the literature, the activation of the AKT pathway is one of the most plausible mechanisms of the UDCA-mediated cytoprotective effect. Therefore, the ability of UDCA to activate the AKT pathway will be investigated in the next chapter.

Chapter 6. Investigating the effect of UDCA on the AKT pathway

6 Investigating the effect of UDCA on the AKT pathway

6.1 Introduction to the AKT pathway

6.1.1 Background

Protein kinase B, more commonly known as AKT, is a serine/threonine kinase that plays a key role in multiple physiological processes, including cardiovascular homeostasis, glucose metabolism, synaptic signalling, apoptosis, and cellular growth and proliferation. Abnormal AKT signalling has been linked to various pathologies that include cancer, diabetes, cardiomyopathy and vascular diseases (Risso et al., 2015).

AKT dysregulation is implicated in PD. Immunostaining of post-mortem tissue demonstrates that AKT phosphorylation is considerably decreased in the DA neurons of PD patients (Greene et al., 2011). In addition, activation of the AKT pathway has been beneficial in various PD-related models (Zhang et al., 2013a, Castro-Caldas et al., 2012, Gong et al., 2012). The activation of AKT induced axonal growth and re-innervation is associated with partial improvement in motor functions in a 6-OHDA mouse model (Kim et al., 2011).

AKT was discovered in 1987 following the isolation of the transforming retrovirus from an AKR mouse T-cell lymphoma (Staal, 1987). Afterwards, it was possible to clone and sequence the viral oncogene v-AKT and to find the human homologue, which was given the name AKT (Toker and Marmiroli, 2014) (Testa and Tschlis, 2005).

6.1.2 Activation and regulation of the AKT pathway

The AKT protein consists of three highly conserved domains (hydrophobic, catalytic and pleckstrin homology (PH) domains), which are critical for its regulation and function [Figure 6.1] (Hanada et al., 2004, Song et al., 2005). The activation of AKT is dependent on the phosphoinositide 3 (PI3) kinase signalling pathway [Figure 6.1]. G protein-coupled receptors and membrane-associated receptor tyrosine kinases activate the PI3 kinase via phosphorylation. The activated PI3 kinase in turn phosphorylates the membrane lipid phosphatidylinositol 4,5-bisphosphate (PIP2) to produce phosphatidylinositol 3,4,5 trisphosphate (PIP3) (Hers et al., 2011). This process is controlled by phosphatase and tensin homologue (PTEN), which has the ability to dephosphorylate the 3-OH position of PIP3 (Song et al., 2005). PIP3 is crucial for AKT activation,

as it localises AKT to the cell membrane, along with pyruvate dehydrogenase kinase (PDK1), and mediates changes to the structure of AKT to expose its activating sequence [Figure 6.1].

The binding of AKT to the cell membrane is achieved via the interaction between the membrane lipids and the PH domain. The latter is an N-terminal domain that consists of 100 amino acids and is named after the protein that PKC targets in platelets, pleckstrin (Song et al., 2005).

The phosphorylation of a threonine residue within the catalytic domain by the action of PDK1 results in a 100-fold increase in the activity of AKT. However, this is only a partial activation of AKT. To reach its fully activated state, serine 473 in the hydrophobic domain must be phosphorylated as well. The primary kinase for this step is mechanistic target of rapamycin (mTOR) complex 2 (mTORC2) [Figure 6.1] (Hers et al., 2011, Toker and Marmiroli, 2014). Other possible Ser473 phosphorylators include MAPKAP kinase 2, an isoform of PDK1, integrin-linked kinase (ILK) and AKT itself (Hers et al., 2011). Once phosphorylated, AKT can interact with different substrates in either the cytoplasm or the nucleus.

The regulation of AKT function is a highly complex process. It requires the phosphorylation of other residues on AKT as well as different types of PTM, for instance acetylation, ubiquitination and glycosylation. It has been suggested that these PTMs modulate AKT's activity, specificity and movement inside cells. Cells also have the means to deactivate AKT. As mentioned previously, PTEN can interfere with PIP3 formation, which is an upstream activator of AKT. Src homology domain 2 (SH2)-containing inositol phosphatase (SHIP) also interferes with PIP3 formation, which could be labelled as an indirect mechanism to deactivate AKT by reducing its phosphorylation rate. However, there are proteins, such as protein phosphatase 2A (PP2A) and PH-domain leucine-rich repeat protein phosphatases (PHLPPs), which are capable of dephosphorylating AKT at its Thr308 and Ser473 residues directly (Risso et al., 2015).

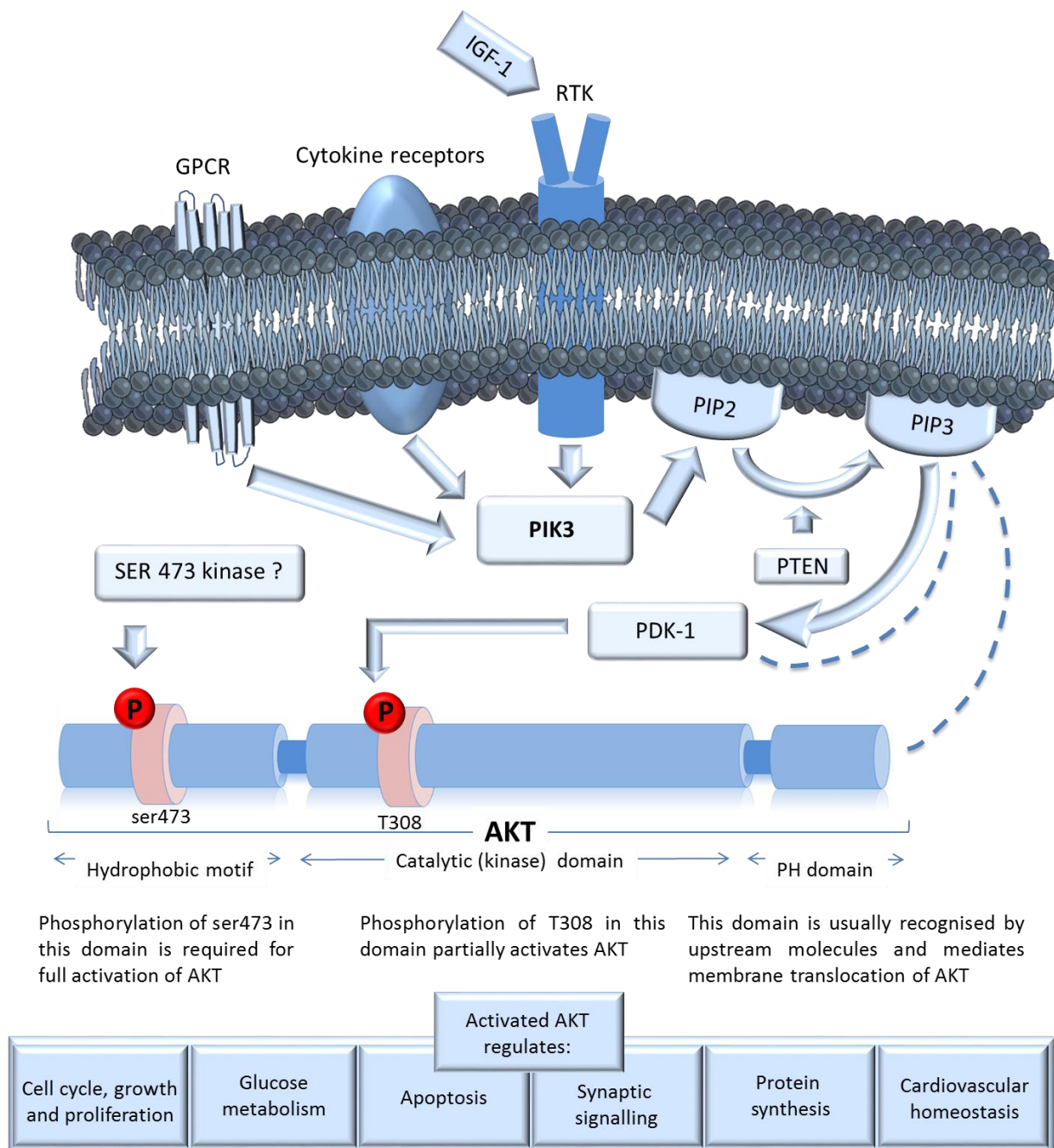


Figure 6.1 Overview of the structure and activation of AKT.

AKT activation depends mainly on the action of several kinases, such as RTK, PIK3 and PDK1. Two sites need to be phosphorylated in order to achieve the fully activated state. Once activated, AKT can interact with a vast number of substrates to control various biological functions.

Abbreviations: IGF-1: Insulin-like growth factor 1; RTK: receptor tyrosine kinase; GPCR: G protein-coupled receptor; PIP2: Phosphatidylinositol 4,5-bisphosphate or PtdIns(4,5); PIP3: Phosphatidylinositol (3,4,5)-triphosphate; PIK3: Phosphatidylinositol-4,5-bisphosphate 3-kinase; PTEN: Phosphatase and tensin homologue; PDK1: phosphoinositide-dependent kinase; PH: Pleckstrin homology.

6.1.3 AKT downstream

A number of AKT targets that are relevant to mitochondria and PD were investigated in this chapter. They are briefly overviewed below.

CREB

cAMP response element binding (CREB) is a transcription factor that is implicated in diverse brain functions. It consists of multiple domains that enable it to dimerise and bind to either DNA or other transcriptional complexes (Sakamoto et al., 2011). CREB is activated when the Ser133 residue in its kinase-inducible domain (KID) is phosphorylated (Wen et al., 2010). Activated CREB binds to the KID-interacting domain (KIX) or CREB-binding domain in the p300-CBP coactivator family, which enables the induction of CREB-mediated transcription (Wen et al., 2010).

Besides its role in the synthesis of proteins that regulate neuronal plasticity and memory formation (Barco and Marie, 2011) (Kandel, 2012), CREB is involved in neuronal development and survival. It has been previously reported that the cortical expression of dominant negative CREB (CREB S133A) results in significant neurodegeneration in adult mice (Ao et al., 2006). CREB protects neurons against ROS, as it enhances the expression of antioxidant genes such as HMOX1 (Lee et al., 2009). In a recent study, hydrocortisone significantly increased Parkin expression and protected cells against oxidative stress in a CREB-dependent manner. Remarkably, knocking out endogenous CREB abolished the hydrocortisone-mediated Parkin induction and consequent protection (Ham et al., 2017).

mTOR

mTOR is a serine/threonine protein kinase that regulates multiple cellular functions, for instance gene transcription and translation, metabolism, proliferation and survival (Saxton and Sabatini, 2017). mTOR is present in cells within two distinct complexes, mTORC1 and mTORC2. AKT has been reported to activate mTOR via direct phosphorylation at serine 2448, although it has been proposed that this phosphorylation is achieved indirectly via a positive feedback loop downstream of mTOR involving the ribosomal protein S6 kinase beta-1 (S6K1) (also known as p70S6 kinase) (Chiang and Abraham, 2005). AKT also activates mTORC1 via phosphorylating tuberous sclerosis complexes (TSC) 1 and 2 (Inoki et al., 2002). The resulting

inactivation of TSC1/2 leads to an increase in the concentration of Ras homolog enriched in the brain (RHEB), the main activator of mTORC1.

Neurotoxins that are commonly used in modelling PD such as MPTP and 6-OHDA were associated with reduced mTOR signaling in mice DA neurons (Malagelada et al., 2008, Rieker et al., 2011, Bockaert and Marin, 2015). By contrast, increased mTORC activity is protective in stressed DA neurons (Choi et al., 2010, Kim et al., 2012). In addition, it has been reported that the activation of mTOR signalling in toxin-treated DA neurons can promote the regeneration of axons (Kim et al., 2012, Kim et al., 2011).

FOXO1

FOXO1 belongs to the forkhead box O (FOXO) family of transcription factors that functions in various intracellular processes, including apoptosis, oxidative stress, cell cycle and metabolism (Golson and Kaestner, 2016). The activation of AKT results in its translocation into the nucleus, where it phosphorylates FOXO1 at three conserved residues (Thr24, Ser256 and Ser319) (Xiangshan et al., 2004). This phosphorylation drives the binding of FOXO1 to the 14-3-3 regulatory protein and consequently inhibits FOXO1, as it becomes localised in the cytoplasmic region of the cell (Eijkelenboom and Burgering, 2013). When cells are stressed, the activation of JNK overrides the effect of AKT and dissociates FOXO1 from the 14-3-3 regulatory protein (Eijkelenboom and Burgering, 2013). Nonetheless, the regulation of FOXO is complex as various other signalling pathways and PTM are involved.

Although the activation of AKT is cytoprotective, the consequent inhibition of FOXO1 seems to be disadvantageous to cells. FOXOs are considered an important determinant in human ageing and longevity (Martins et al., 2016). It has been suggested that FOXOs regulate ageing and age-related disorders by increasing the antioxidant capacity of cells, depending on posttranslational modifications (Storz and signaling, 2011). In line with this, FOXO1 levels are positively correlated with ageing in the human brain (Hwang et al., 2018). The protective role of this upregulation has been demonstrated in *FOXO1* knockout mice, which display accelerated age-associated axonal tract degeneration (Hwang et al., 2018).

Hexokinase

Hexokinase is a constitutively active kinase that facilitates the first reaction of glucose metabolism (Irwin and Tan, 2014). Hexokinase phosphorylates glucose into glucose-6-phosphate (G6P), which serves as a glycolysis precursor (Irwin and Tan, 2014). Hexokinase II maintains close contact with mitochondria through binding to the mitochondrial outer membrane protein VDAC (Pastorino and Hoek, 2008), which couples glycolysis to oxidative phosphorylation. Mitochondrion-bound hexokinase has preferential access to the generated ATP, which is used to phosphorylate glucose molecules (Roberts and Miyamoto, 2015). An increased amount of G6P in turn inhibits hexokinase-mitochondrion binding (Roberts and Miyamoto, 2015). In addition, such binding can be prevented via the phosphorylation of VDAC by GSK3 β (Sutherland, 2011). When AKT is activated, it inhibits GSK3 β via phosphorylation and thus indirectly increases mitochondrial hexokinase II binding (Manning and Toker, 2017). It has also been reported that AKT directly phosphorylates hexokinase II at Thr473 and facilitates mitochondrion-hexokinase binding (Roberts et al., 2013).

6.1.4 Objectives

The first objective of this chapter is to determine if UDCA treatment can lead to increase AKT phosphorylation in CHO cells. The second objective is to assess if UDCA treatment can lead to increase AKT phosphorylation in CCCP-stressed SH-SY5Y cells, in which UDCA exerted a cytoprotective effect. The third objective is to investigate the role of AKT activation in the UDCA-mediated effect, which will be determined via the use of an AKT inhibitor. To determine if the mitochondrial rescue effect of UDCA is mediated via direct interaction between the mitochondria and either the AKT or its downstream protein, the hexokinase, the translocation of AKT and hexokinase into mitochondria will be examined through cellular fractionation. Finally, the effect of UDCA treatment on phosphorylated and total CREB, mTOR and FOXO1 will be assessed via WB and ICC.

6.2 Determining the ability of UCA and UDCA to activate AKT in CHO cells

6.2.1 Testing AKT antibodies and IGF as a positive control in CHO cells

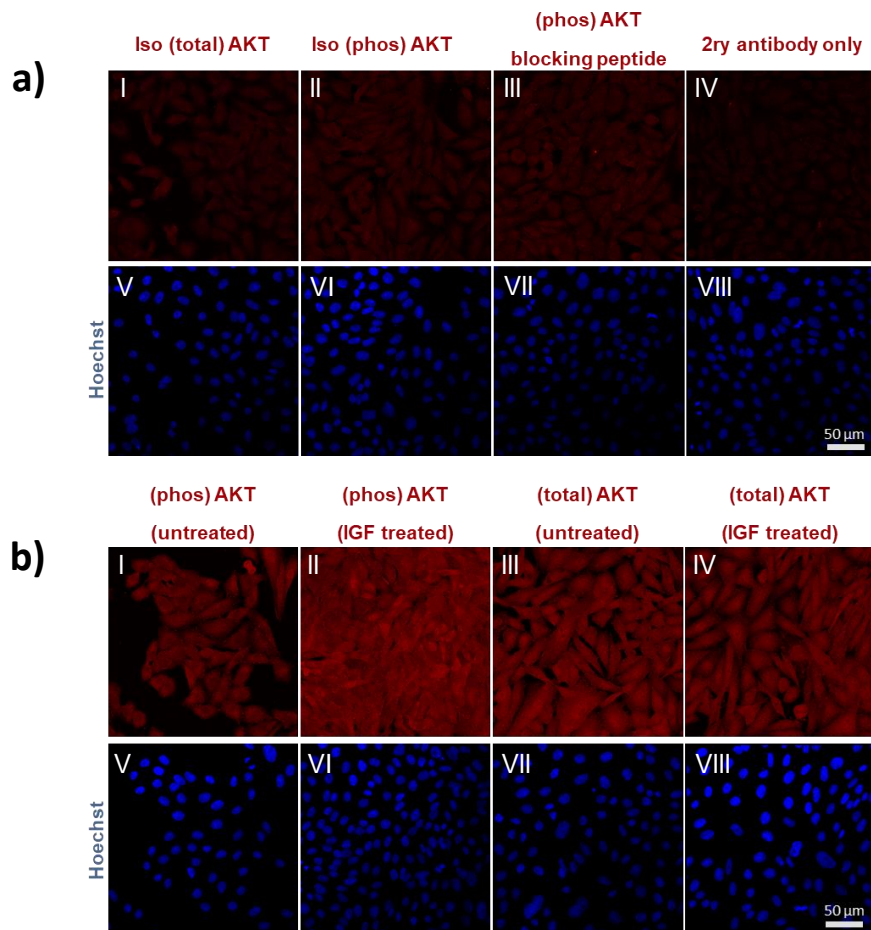
The level of AKT activation within cells is positively correlated with the ratio of (phos) AKT to (total) AKT. To assess AKT phosphorylation, we performed ICC and probed the CHO cells with (phos) AKT, as described in the methods chapter [Heading 2.5]. Parallel wells matching each treatment condition were prepared and probed with (total) AKT antibody. In addition, the ratio between (phos) AKT intensity and (total) AKT intensity was used as an indicator of AKT activation.

Prior to starting UCA and UDCA treatment experiments, the specificity of the AKT antibodies was assessed through the application of various controls, including isotype control and (phos) AKT blocking peptide [Figure 6.2]. The isotype control is an antibody of the same class and host as the primary antibody that lacks specificity to the target. Therefore, it reveals the non-specific interactions of the immunoglobulin with the sample. The utilised (phos) AKT and (total) AKT antibodies were both rabbit IgG and applied at different concentrations. The results show that the corresponding concentrations of the isotype produced minor signals in ICC [Figure 6.2 a].

The (phos) AKT blocking peptide was also used to confirm that the (phos) AKT antibody is highly specific. The (phos) AKT blocking peptide resembles the epitope recognised by the primary (phos) AKT antibody. Pre-incubation of the (phos) AKT blocking peptide with the (phos) AKT antibody should block the targeting site of the (phos) AKT antibody. Consequently, no signals should be detected when ICC is performed unless the (phos) AKT antibody has an element that binds non-specifically.

The results show that the use of (phos) AKT blocking peptide significantly decreased the detected signals [Figure 6.2 a (III)] in comparison to (phos) AKT probing of untreated cells [Figure 6.2 b (I)], indicating high specificity of the (phos) AKT antibody. Non-specific binding of the secondary antibody was also tested and found to be insignificant [Figure 6.2 a (IV)].

As expected, treating the cells with IGF significantly increased the intensity of (phos) AKT but not of (total) AKT, which implies increased AKT activation [Figure 6.2 b]. Taken together, these results demonstrate that the AKT antibodies employed are reliable in assessing AKT activation.



(phos) AKT and (total) AKT immunocytochemistry controls

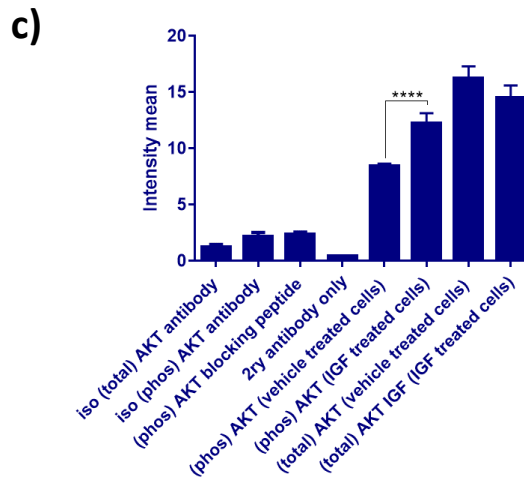


Figure 6.2 pilot test of AKT antibodies and IGF as a positive control in CHO cells.

(a) Representative images of the conditions used to assess the specificity of the AKT antibodies. Cells in (I) and (II) were probed with the isoantibodies, cells in (III) were probed with the (phos) AKT antibody mixed with (phos) AKT blocking peptide, and cells in (IV) were probed only with the secondary antibody. All images show signals with low intensities, indicating high specificity of the AKT antibodies. (V–VIII) show nuclei under the corresponding conditions. (b) Assessment of IGF as a positive control revealed a significant increase in (phos) AKT intensity (II) in comparison to the untreated condition (I). As expected, the intensity of (total) AKT remained unchanged (III and IV). (V–VIII) show nuclei under the corresponding conditions. (c) Analysis of ICC images. The images were captured by confocal microscopy, as described in the method section. The error bars represent the SD of the data, obtained from five random fields per cover slip. Scale bar = 50μm.

6.2.2 Assessing the effect of UCA and UDCA on AKT activation in CHO cells

CHO cells were treated following the treatment protocol that was previously used in the ARE experiments [Heading 4.2.1]. Although UCA and UDCA treatment increased the expression of ARE [Figure 4.5], it seems that this increase is not associated with activation of AKT. Analysis of images obtained via confocal microscopy revealed a significant increase in the (phos) AKT / (total) AKT ratio when the cells were treated with IGF (25%) but no increase was observed with UCA and UDCA treatment [Figure 6.3].

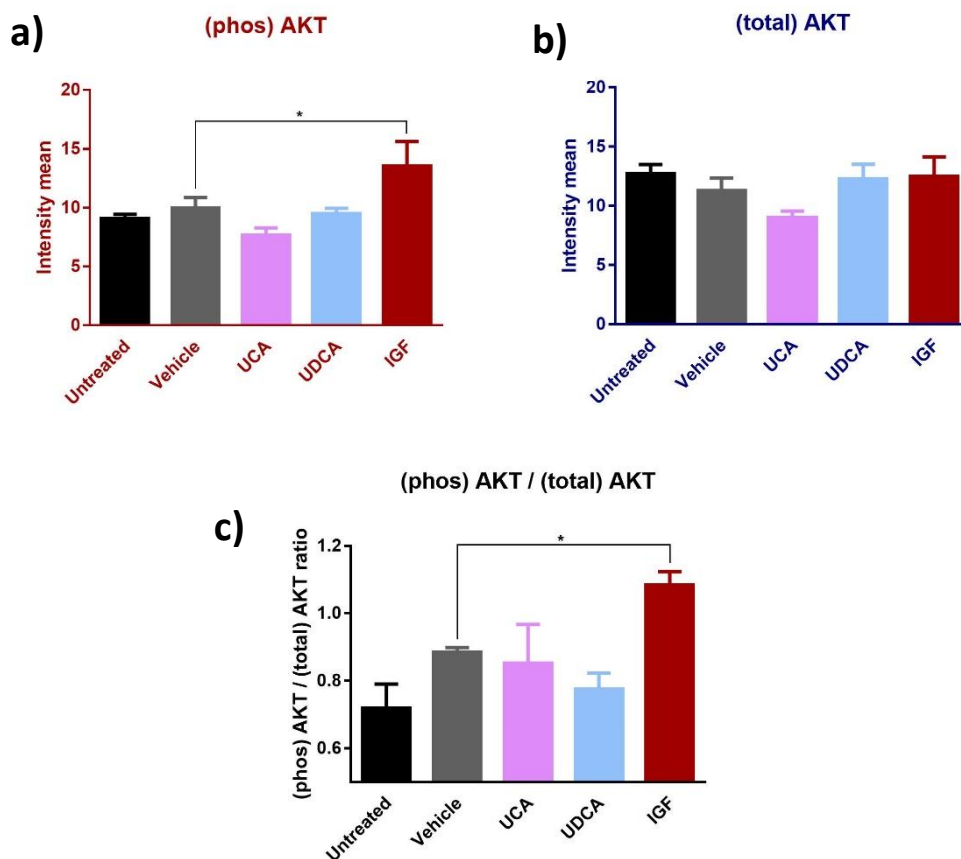


Figure 6.3 UCA and UDCA treatments did not induce significant effects on AKT phosphorylation in unstressed CHO cells.

Analysis of (phos) AKT (a) and (total) AKT (b) images obtained via confocal microscopy. (c) AKT activation levels were calculated as the ratio between (phos) AKT and (total) AKT. The cells were treated with 10 μ M UCA and 10 μ M UDCA for 24 hours in serum-free culture medium. IGF (100nM) was applied for 10 minutes before the fixation process. IGF significantly activated AKT but no effect was seen with UCA and UDCA treatment. ICC and imaging were performed as described in the methods section. The error bars represent the SD of three independent experiments. In each experiment, at least 20 fields per condition were captured and the average of the intensity readings was used as a readout. * $p < 0.05$, one-way ANOVA test.

6.3 Determining the ability of UDCA to activate AKT in SH-SY5Y cells

6.3.1 Optimisation experiments

In the previous chapter, the positive effect of UDCA on ATP and cytotoxicity was only observed at a high UDCA concentration (300 μ M). Therefore, we decided to investigate the ability of UDCA to activate AKT using the exact treatment protocol of that experiment.

However, while the ATP/cytotoxicity experiments were performed in regular culture medium, the AKT experiments in this chapter were performed in serum-free medium. Serum contains various types of growth factors and cytokines that might induce negative feedback mechanisms and render cells unable to respond to an exogenous activator. In addition, serum starvation synchronises cells to arrest at the G0 phase, which decreases variability in AKT activation level, which varies according to cell cycle stage (Liu et al., 2014).

Accordingly, we chose to assess the effect of increasing concentrations of serum on AKT activation in unstimulated and IGF-stimulated cells prior to the drug treatment experiments. Unexpectedly, the results show that the addition of serum had no significant effect on basal levels of (total) AKT and (phos) AKT [Figure 6.4]. Additionally, IGF-stimulated cells revealed that the level of AKT activation was not significantly dependent of the concentration of the serum in the culture medium. Taken together, these results confirm that AKT activation can be assessed in serum-containing media.

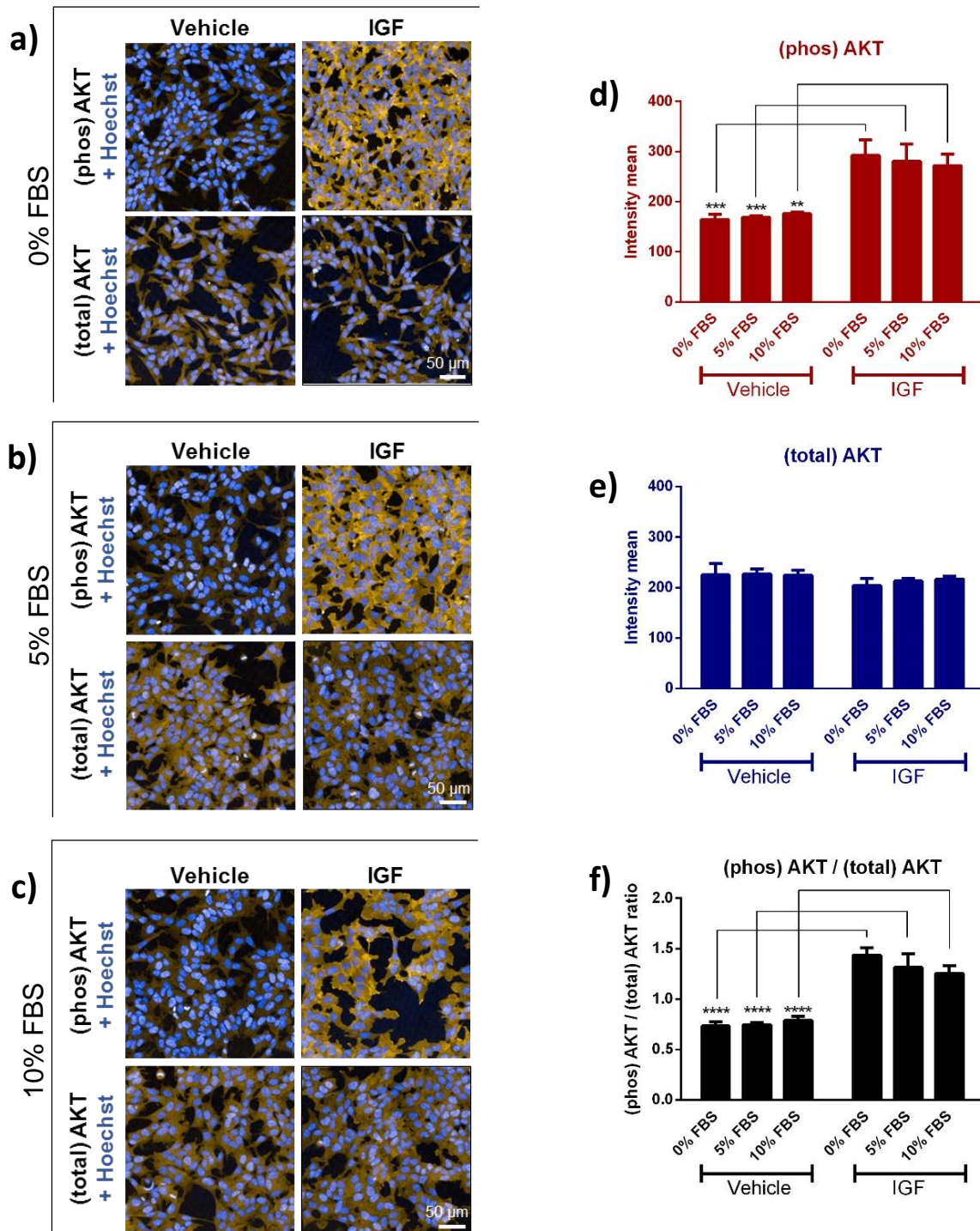


Figure 6.4 The addition of serum to the culture medium has no effect on IGF-mediated AKT activation.

(a, b and c) Representative images obtained via confocal microscopy showing the effect of IGF treatment on AKT phosphorylation in SH-SY5Y cells grown in culture medium with 0% FBS (a), 5% FBS (b) and 10% FBS (c). The SH-SY5Y cells were also treated with IGF (100 nM) for 10 minutes prior to the fixation process. ICC and imaging were performed as described in the methods section. The cells were probed either with (phos) AKT or (total) AKT (both in yellow) and co-stained with Hoechst (in blue). Analysis of (phos) AKT (d) and (total) AKT (e) images shows that the addition of serum to the culture medium did not affect the basal AKT phosphorylation level nor alter the response to IGF treatment. (f) AKT activation levels ((phos) AKT / (total) AKT). The error bars represent the SD of three technical replicates. In each replicate, at least 25 fields per condition were captured and the average of the intensity measures was used as a readout. ** $p < 0.01$, *** $p < 0.001$, **** $p < 0.0001$, two-way ANOVA test. Scale bar = 50 μm .

CCCP-stressed cells were easily detached from the well floor during the washing steps in ICC, which made ICC an unsuitable technique for this experiment. We therefore decided to use WB to assess AKT activation as an alternative. The AKT antibodies used in ICC were also reliable in WB [Figure 6.5]. Assessing the levels of AKT activation in CCCP-stressed cells revealed significantly higher basal readings in comparison to the unstressed cells (700%). This probably attributed to the stimulation of the survival pathway in stressed cells, which is mainly dependent on the activation of the AKT pathway. The IGF-induced activation of AKT was observed in unstressed (380%) and – to a much lesser extent (60%) with more variability – in CCCP-stressed cells [Figure 6.5].

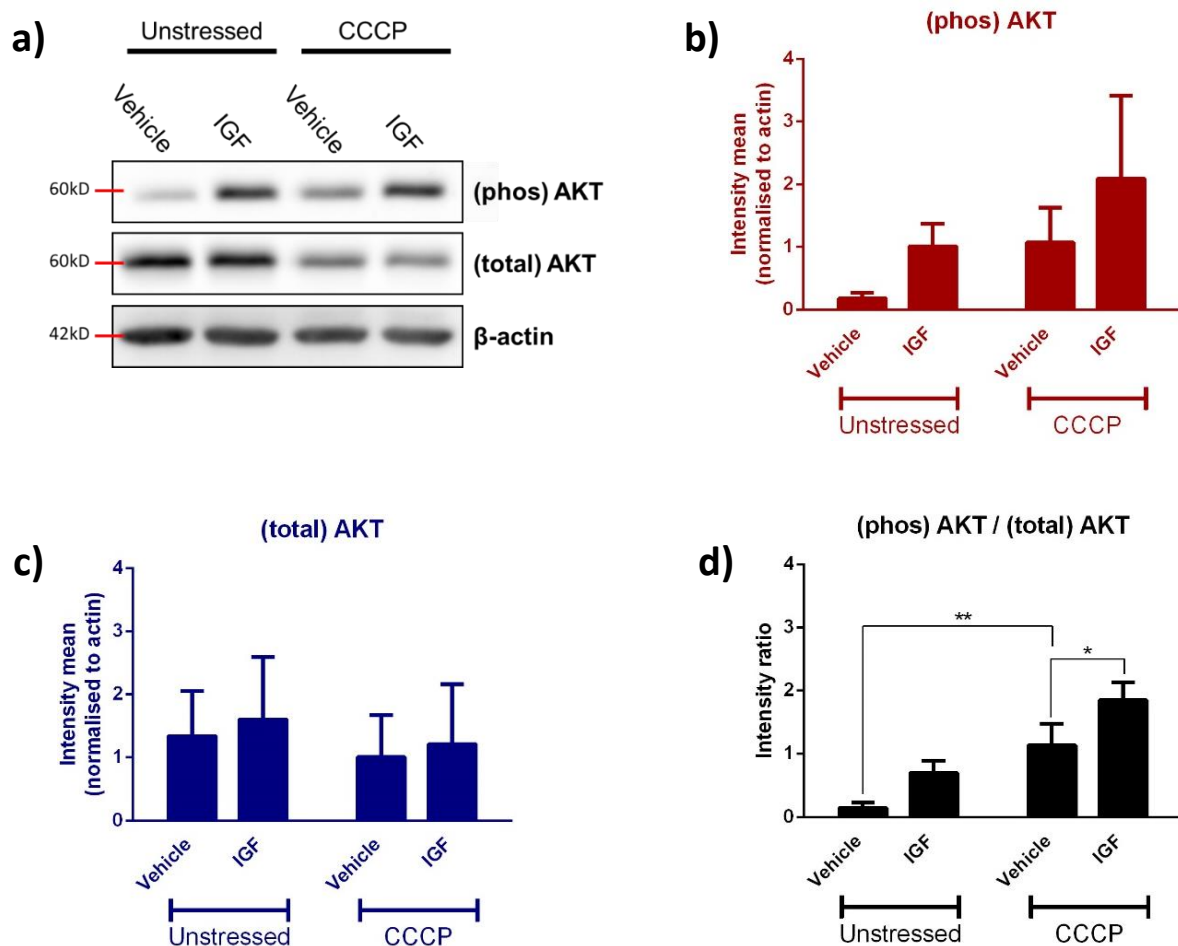


Figure 6.5 The AKT antibodies are usable in western blotting experiments.

(a) WB images showing increased levels of (phos) AKT after treatment with IGF in both unstressed and stressed cells. (b), (c) Densitometric analysis of (phos) AKT and (total) AKT WB images. (d) AKT activation levels calculated as the ratio between (phos) AKT and (total) AKT. The cells were treated with IGF (100 nM) for 10 minutes. WB and imaging were performed as described in the methods section. The cells were probed with (phos) AKT antibody (mouse), and then the membrane was stripped and re-probed with (total) AKT (rabbit). The error bars represent the SD of three independent experiments. * p < 0.05, ** p < 0.01, two-way ANOVA test.

6.3.2 Drug treatment experiments

The SH-SY5Y cells were stressed and treated following the protocol used in the previous chapter [Figure 5.4]. In addition to the condition found to improve ATP and cytotoxicity (300 μ M UDCA for 24 hours with 12 hours of pre-treatment), a lower concentration of UDCA (10 μ M) was added in order to check whether AKT activation was present in conditions that were not associated with a cytoprotective effect [Figure 6.6]. This could indicate that AKT activation is not the driver of the observed rescue effect. UDCA was also applied for shorter periods to detect transient AKT activation (if present). While AKT activation was not significantly increased under these new conditions, the results showed a significant increase in AKT activation (85%) when the stressed cells were treated with 300 μ M UDCA for 24 hours [Figure 6.7].

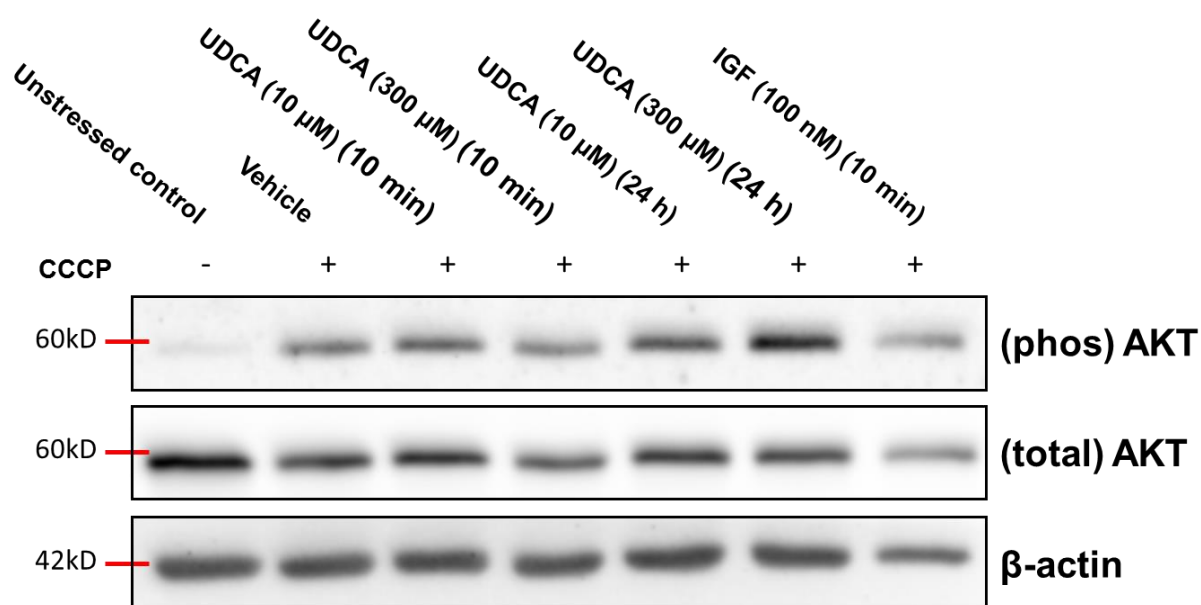


Figure 6.6 300 μ M UDCA significantly increased AKT phosphorylation in CCCP-stressed SH-SY5Y cells (western blot images).

WB images show an increased level of (phos) AKT after treatment with 300 μ M UDCA for 24 hours. The cells were pre-treated with UDCA for 12 hours before the addition of 50 μ M CCCP, which was kept for 24 hours. For the 10-minute treatment conditions, the cells were pre-treated with the vehicle for 12 hours before the addition of 50 μ M CCCP, which was applied for 24 hours, and the drug was applied 10 minutes prior to collecting the cells for WB. WB and imaging were performed as described in the methods section. The cells were probed with (phos) AKT antibody (mouse), and then the membrane was stripped and re-probed with (total) AKT (rabbit).

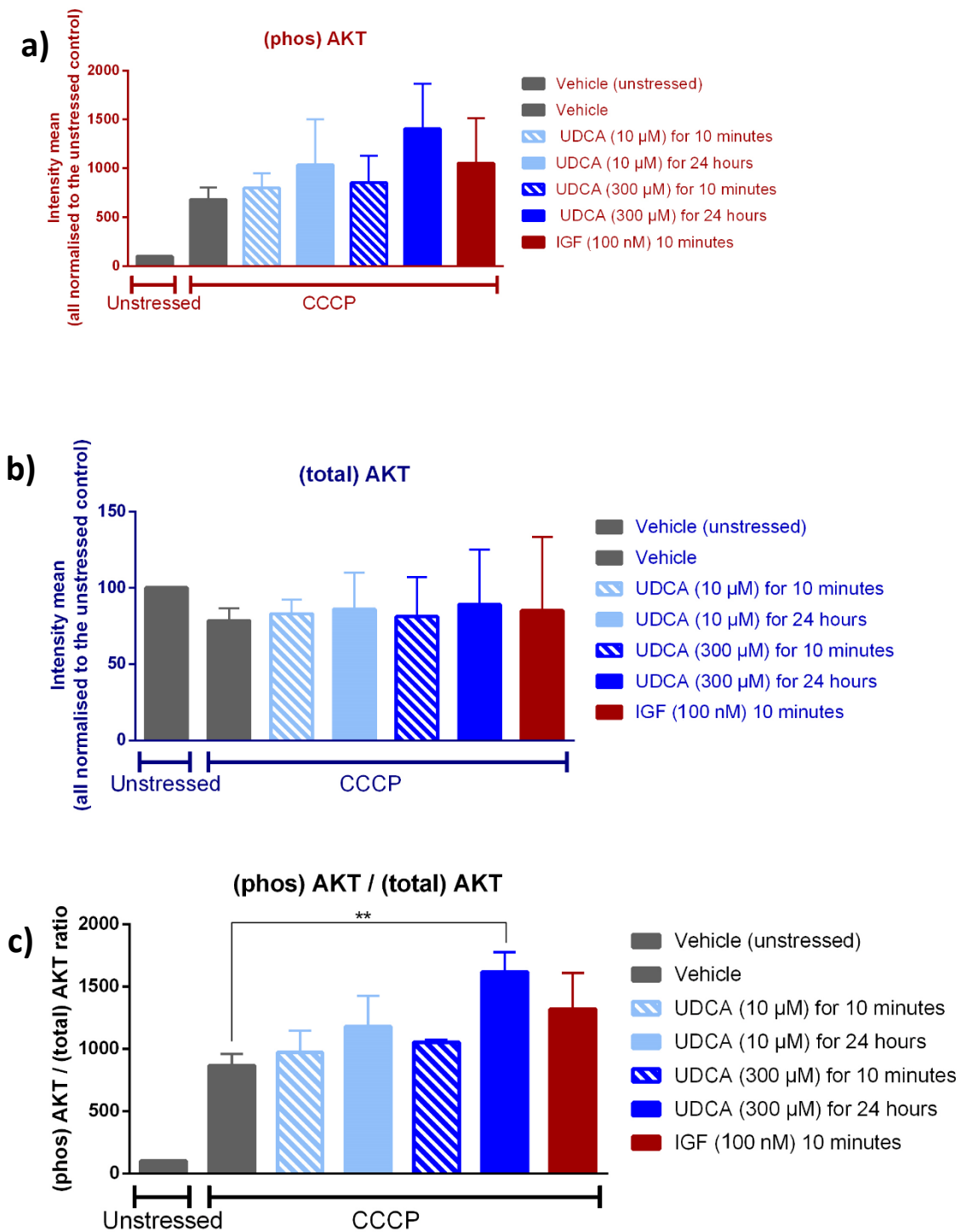


Figure 6.7 300 μ M UDCA significantly increased AKT phosphorylation in CCCP-stressed SH-SY5Y cells (data analysis).

(a), (b) Densitometric analysis of (phos) AKT and (total) AKT WB images. (c) AKT activation levels calculated as the ratio between (phos) AKT and (total) AKT. The cells were pre-treated with UDCA for 12 hours before the addition of 50 μ M CCCP, which was kept for 24 hours. For the 10-minute treatment conditions, the cells were pre-treated with the vehicle for 12 hours before the addition of 50 μ M CCCP, which was kept for 24 hours, and the drug was applied 10 minutes prior to collecting the cells for WB. The graphs show significant activation of AKT in CCCP-stressed cells treated with 300 μ M UDCA (24 hours). WB and imaging were performed as described in the methods section. The error bars represent the SD of three independent experiments. ** $p < 0.01$, one-way ANOVA test.

6.4 Investigating the role of AKT activation in the UDCA-mediated rescue effect in SH-SY5Y cells

The rescue effect of UDCA in CCCP-stressed SH-SY5Y cells was associated with significant AKT activation. To examine whether the rescue effect is dependent on the activation of AKT, we decided to repeat the experiment in cells in which AKT was pharmacologically inhibited via the use of triciribine, a selective inhibitor of AKT phosphorylation. Upon testing, triciribine was able to inhibit IGF-induced AKT phosphorylation in unstressed and CCCP-stressed cells [Figure 6.8].

As expected, triciribine significantly reduced AKT activation in CCCP-stressed cells that were treated with UDCA [Figure 6.8]. Consequently, ATP and cytotoxicity assays were performed with the application of triciribine. On examination with an optic microscope, it appeared that the rescue effect of UDCA was not eliminated upon the addition of triciribine [Figure 6.9 a]. Equally, cytotoxicity assessment showed that the reduction in cytotoxicity induced by UDCA was not altered when the triciribine was applied [Figure 6.9 b]. On the other hand, triciribine significantly reduced ATP levels in UDCA-treated cells to match those of untreated controls [Figure 6.9 c]. The application of triciribine to untreated cells resulted in a decrease in ATP levels but did not affect their viability.

These findings demonstrate that the rescue effect of UDCA is not entirely dependent on the AKT pathway. They also support a direct relation between AKT and mitochondria. Accordingly, in the next section, the translocation of AKT into mitochondria in UDCA-treated cells will be investigated.

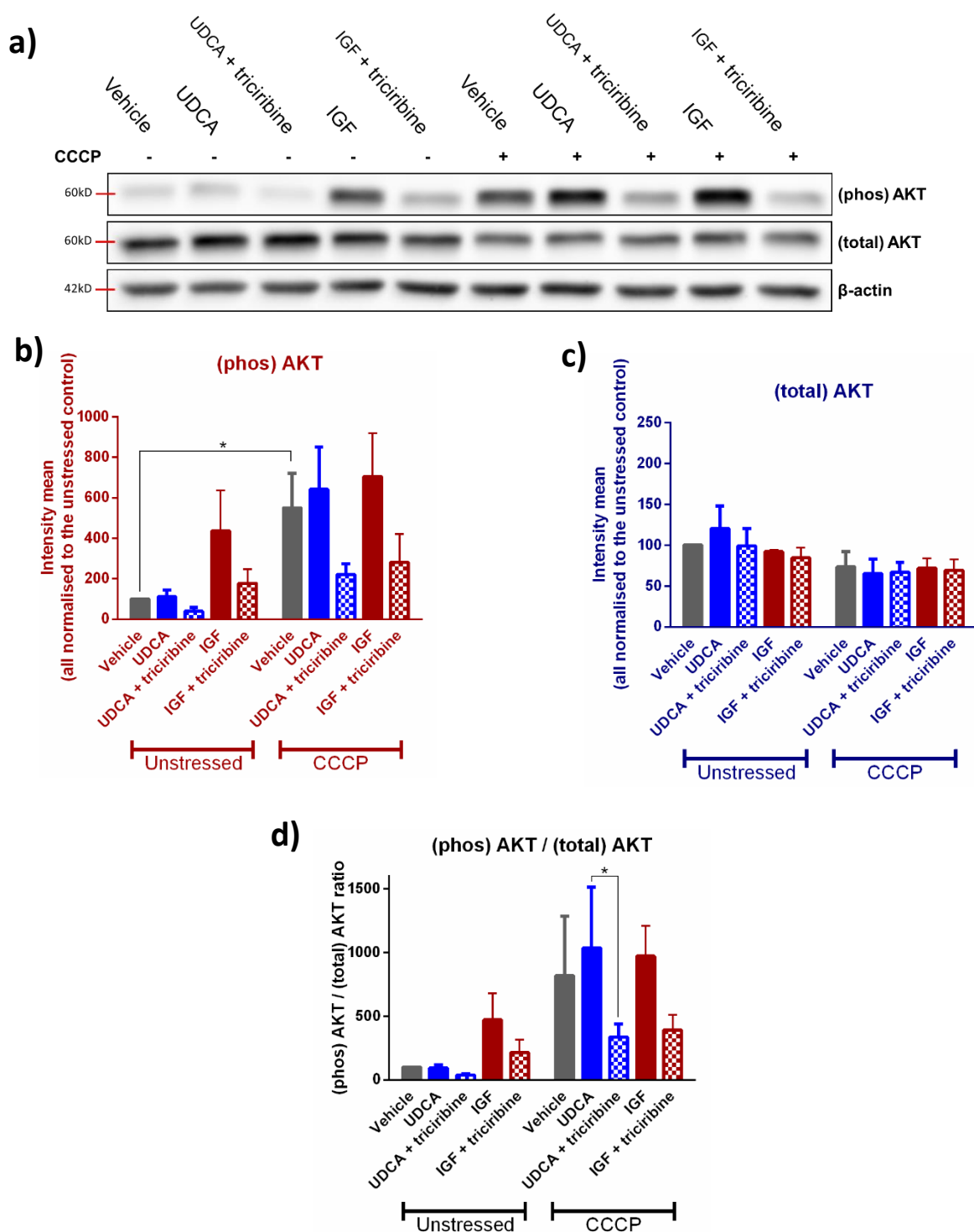


Figure 6.8 Triciribine treatment inhibited AKT phosphorylation in UDCA/IGF treated cells.

(a) WB images demonstrating the effect of triciribine on AKT phosphorylation in SH-SY5Y cells treated with UDCA and IGF. The cells were pre-treated with 300 μ M UDCA and 0.5 μ M triciribine for 12 hours before the addition of 50 μ M CCCP, which was applied for 24 hours. IGF (100nM) was applied for 10 minutes prior to the collection of the cells. WB and imaging were performed as described in the methods section. The cells were probed with (phos) AKT antibody (mouse) and then the membrane was stripped and re-probed with (total) AKT (rabbit). The images show that triciribine significantly inhibited AKT phosphorylation in IGF- and UDCA-treated cells (under CCCP conditions). (b), (c) Densometric analysis of (phos) AKT and (total) AKT WB images. (d) AKT activation levels calculated as the ratio between (phos) AKT and (total) AKT. The error bars represent the SD of three independent experiments. * $p < 0.05$, two-way ANOVA test.

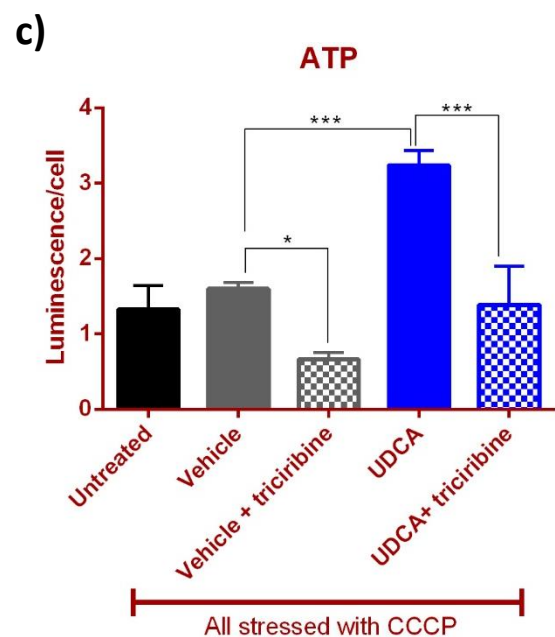
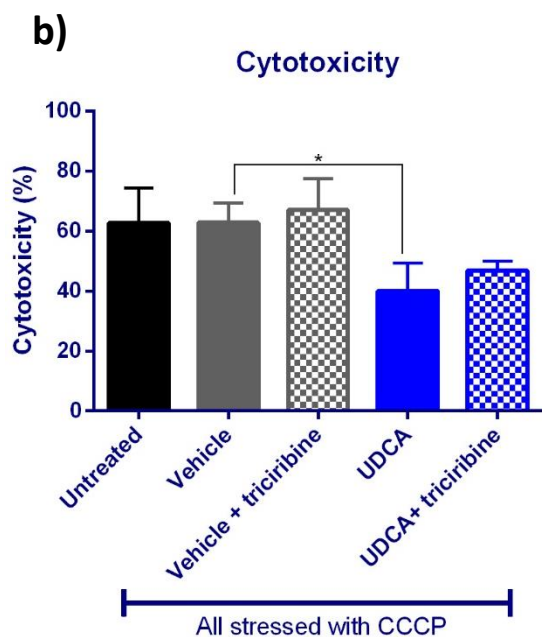
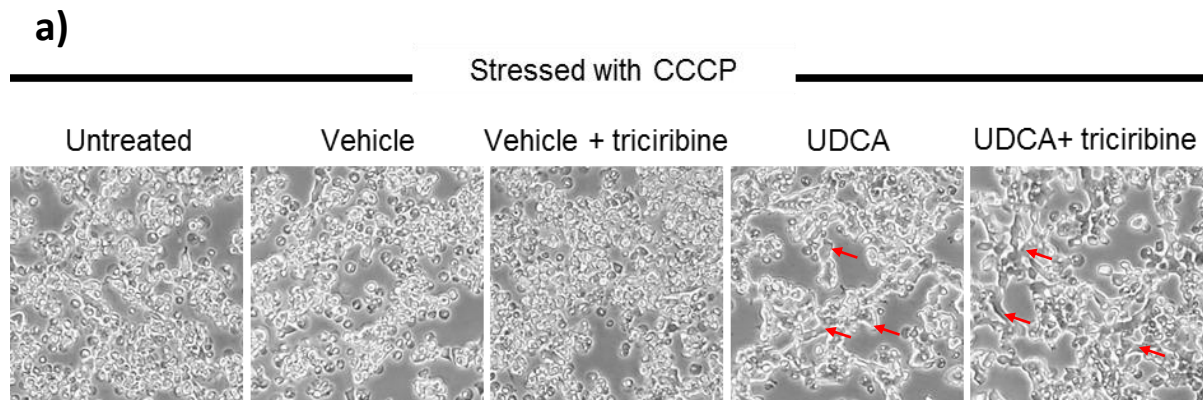


Figure 6.9 AKT inhibition abolished the UDCA-mediated rescue effect on ATP level in CCCP-stressed SH-SY5Y cells.

(a) Optic microscopy images of treated SH-SY5Y cells with and without triciribine (all stressed with CCCP). Red arrows point to some healthy-looking cells, which were not present under the untreated/vehicle conditions. The healthy-looking cells were seen under UDCA conditions regardless of the presence or absence of triciribine. The cells were pre-treated with 300 μ M UDCA and 0.5 μ M triciribine for 12 hours before the addition of 50 μ M CCCP, which was applied for 24 hours. (b), (c) Cytotoxicity and ATP levels under different treatment conditions. Triciribine did not affect the cytotoxicity level of UDCA-treated cells (a). However, it abolished the UDCA-mediated effect on ATP level (b). The error bars represent the SD of three independent experiments. * $p < 0.05$, *** $p < 0.001$, one-way ANOVA test.

6.5 Investigating AKT translocation into the mitochondria in UDCA-treated SH-SY5Y cells

6.5.1 Cellular fractionation

To assess the efficiency of the fractionation protocol that was used to extract the mitochondrion-enriched fraction, an untreated sample was fractionated and probed with various mitochondrial and cytoplasmic markers. The results demonstrated significant enrichment of the mitochondrial fraction with mitochondrion-specific proteins (Tom20, Tim23 and NDUFS2) [Figure 6.10 a].

While equal amounts of protein were loaded into the gel for WB (12 μ g), the mitochondrial fraction, in comparison to the total lysate, displayed an increase of approximately 400% in the amount of Tom20, 650% for Tim23, and 7000% for NDUFS2 [Figure 6.10 (b), (c) and (d)]. On the other hand, the obtained cytoplasmic fraction showed an approximately 90% decrease in its amount of Tom20 in comparison to the total lysate, 50% less Tim23, and 30% less NDUFS2 [Figure 6.10 (b), (c) and (d)].

As expected, this picture was inverted upon probing the membranes for cytoplasmic proteins (β -actin, α -tubulin and GAPDH). The mitochondrial fraction showed an approximately 60% decrease in its amount of β -actin relative to the total lysate, 60% less α -tubulin, and 45% less GAPDH [Figure 6.10 (e), (f) and (g)]. Conversely, in comparison to the total lysate, the extracted cytoplasmic fraction had an approximately 55% increased amount of β -actin, 25% more α -tubulin, and 20% more GAPDH [Figure 6.10 (e), (f) and (g)].

Collectively, these data indicate that the fractionation protocol is efficient in producing mitochondrion-enriched fractions.

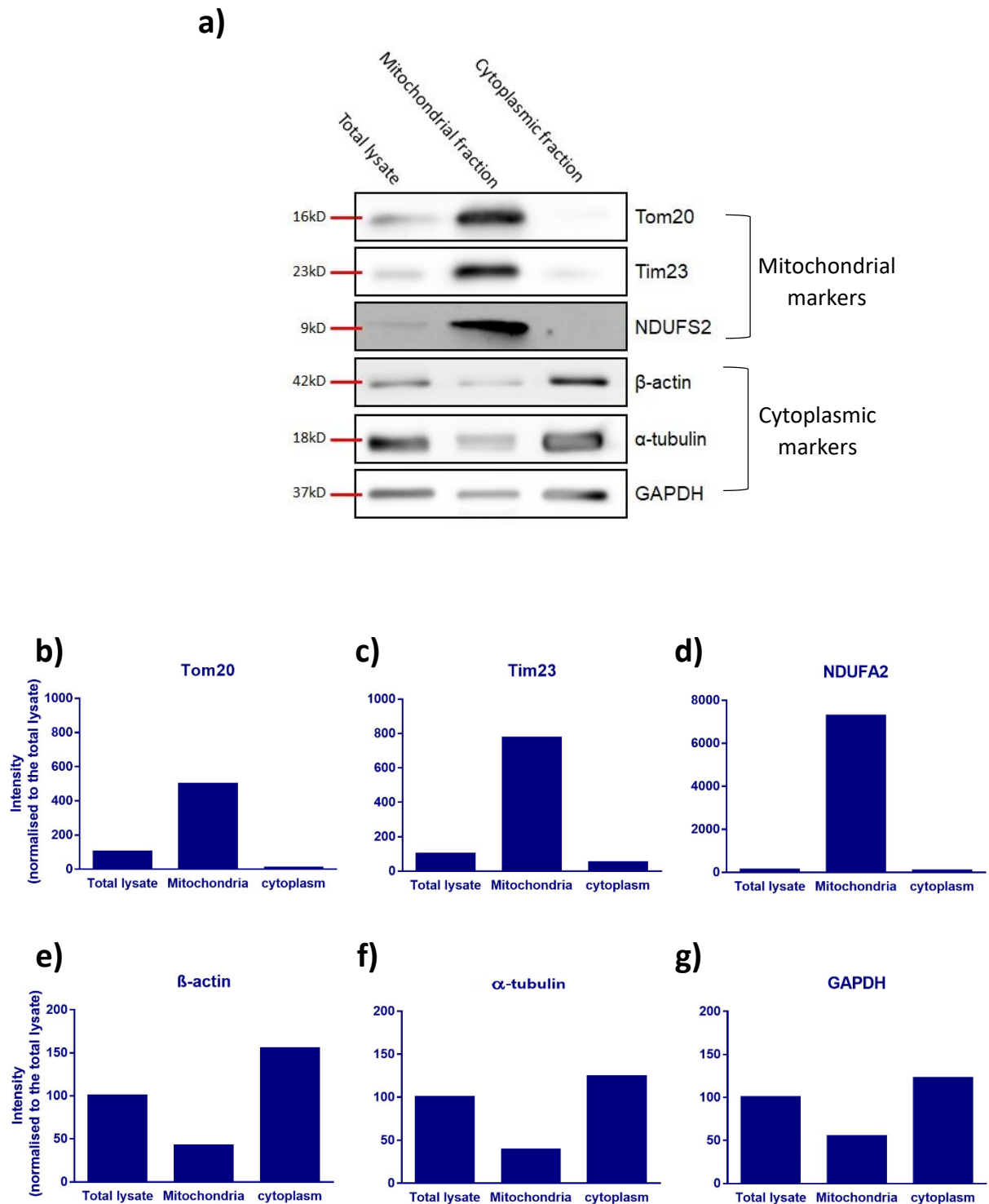


Figure 6.10 The fractionation protocol proved to be efficient in producing mitochondrial enriched extracts.

(a) WB images of fractionated untreated samples probed with various mitochondrial and cytoplasmic markers. Following the BSA assay, equal protein quantities (12µg) from the total lysate, mitochondrial fraction and cytoplasmic fraction were loaded into the gel to allow direct comparison. WB and imaging were performed as described in the methods section. The images show significant enrichment of mitochondrial proteins in the extracted mitochondrial fraction. The lower panel shows the results of WB image quantification of (b) Tom20, (c) Tim23, (d) NDUFA2, (e) β-actin, (f) α-tubulin, and (g) GAPDH. The graphs represent the data from a pilot WB experiment.

6.5.2 The effect of UDCA on AKT translocation into the mitochondria in SH-SY5Y cells

As performed in the previous chapter [Figure 5.4], the SH-SY5Y cells were pre-treated with 300 μ M UDCA for 12 hours before the addition of 50 μ M CCCP, which was applied for 24 hours. IGF (100 nM) was applied as a positive control for 10 minutes before collecting the cells for the fractionation process. Prior to probing the blotted fractionated samples with AKT antibodies, Tom20 and β -actin antibodies were applied to confirm that the fractionation was successful [Figure 6.11, Figure 6.12]. WB images of the total lysate showed that the cells responded to IGF treatment, with a significant increase in AKT phosphorylation [Figure 6.11]. WB images reveal that the expression of AKT in the mitochondrial fraction was remarkably low relative to the other compartments.

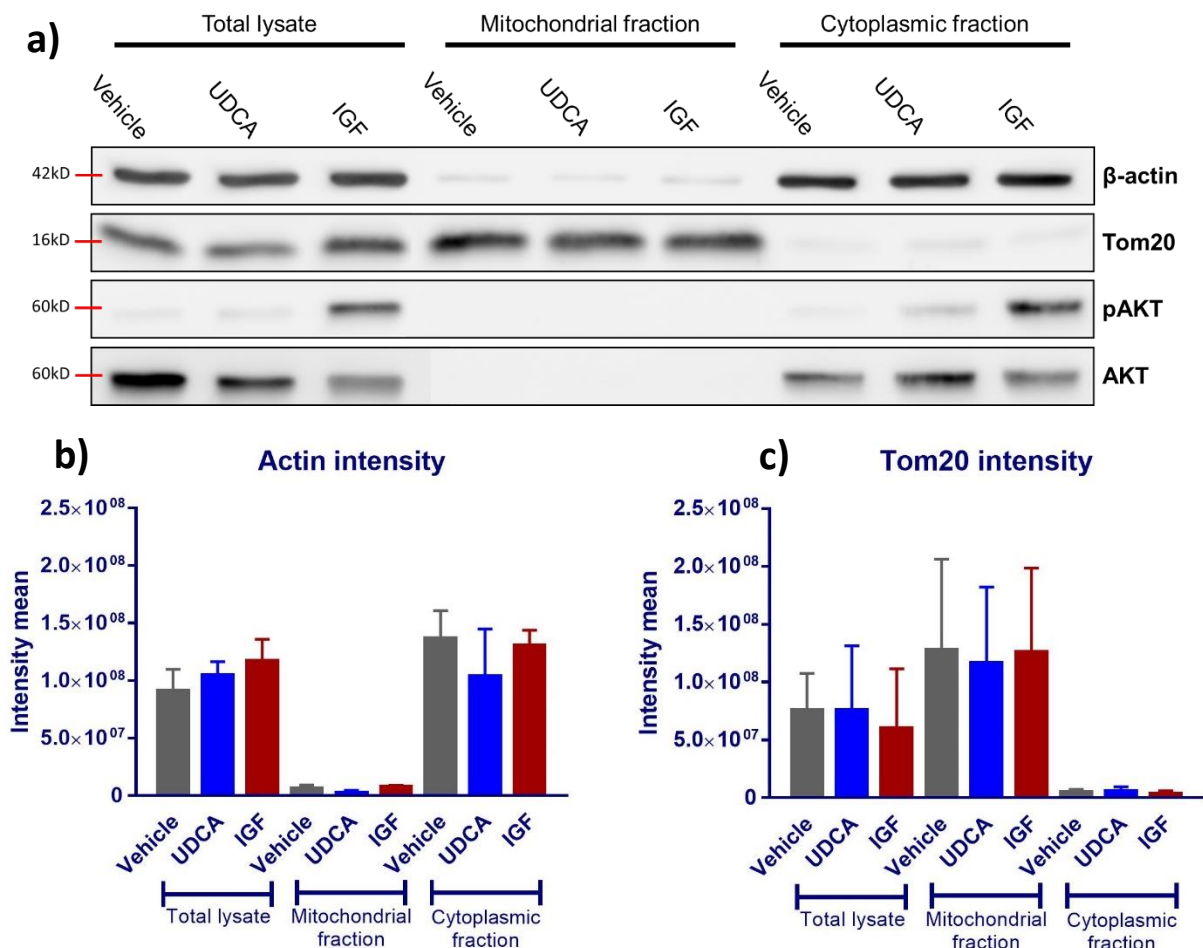


Figure 6.11 Fractionation of treated SH-SY5Y cells (unstressed).

(a) WB images of treated samples probed with β -actin, Tom20, (phos) AKT and (total) AKT (all unstressed). The images show no increase in mitochondrial (phos) AKT or (total) AKT upon UDCA treatment. WB and imaging were performed as described in the methods section. (b), (c) WB image quantification of β -actin and Tom20 confirm successful fractionation of all treated conditions. The graphs represent the data from three independent experiments.

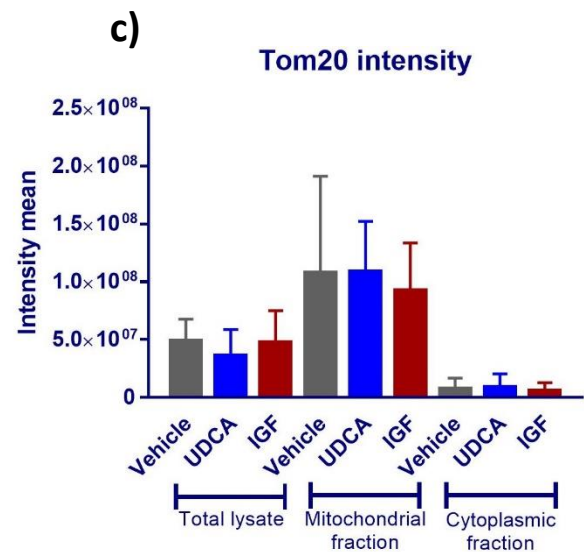
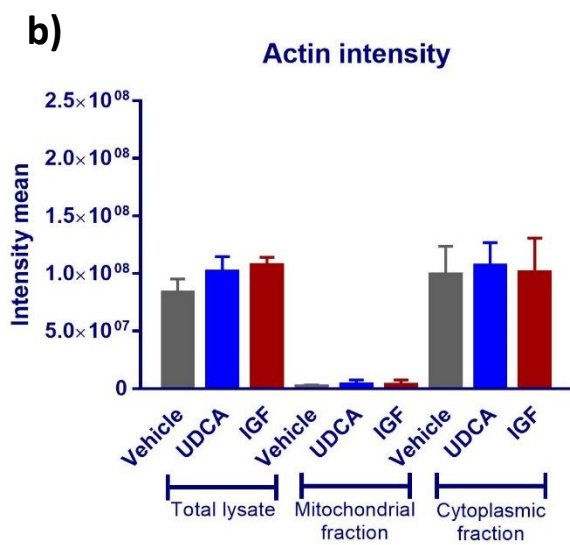
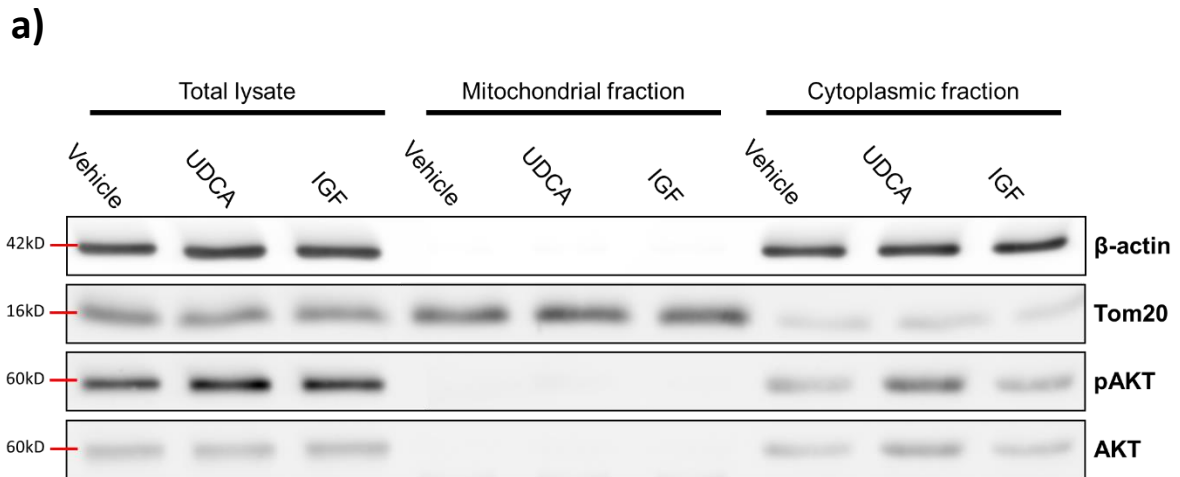


Figure 6.12 Fractionation of treated SH-SY5Y cells (CCCP-stressed).

WB images of treated samples probed with β -actin, Tom20, (phos) AKT and (total) AKT (all stressed with CCCP). The images show no increase in mitochondrial (phos) AKT or (total) AKT upon UDCA treatment. WB and imaging were performed as described in the methods section. (b), (c) WB image quantification for β -actin and Tom20 confirmed successful fractionation of all treated conditions. The graphs represent the data from three independent experiments.

Quantification of WB images of the mitochondrial fractions reveals that UDCA treatment increased the amount of (total) AKT and (phos) AKT in CCCP-stressed cells [Figure 6.13]. However, the increase was not significant due to the variability between the replicates.

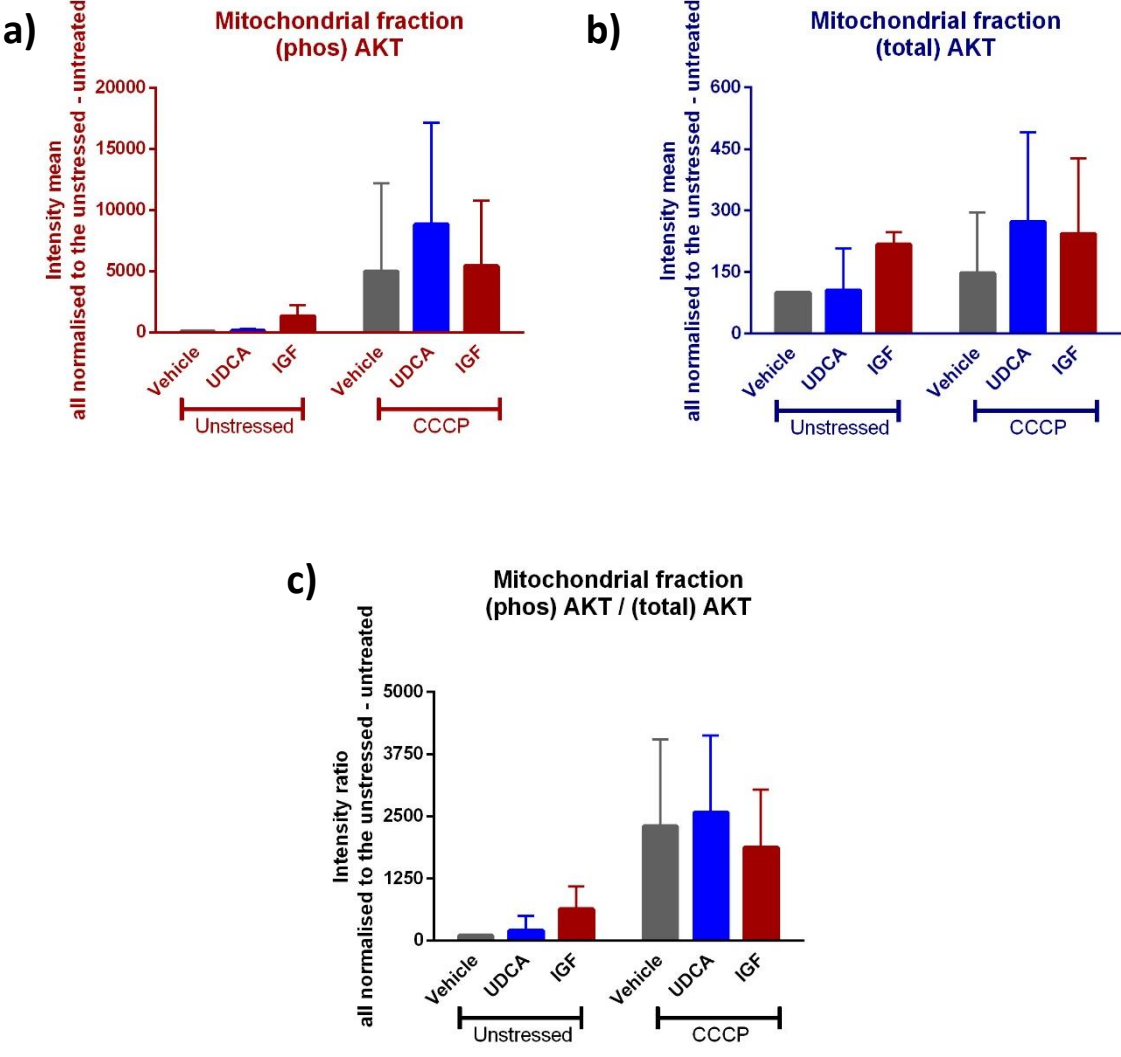


Figure 6.13 UDCA treatment did not induce a significant change in the expression of AKT in the mitochondrial fraction of SH-SY5Y cells.

(a) and (b) show the results of WB image quantification for (phos) AKT and (total) AKT in mitochondrial fractions of unstressed and CCCP-stressed cells. Raw intensity readings for (phos) AKT and (total) AKT were normalised against the corresponding Tom20 readings. UDCA increased mitochondrial (phos) AKT and (total) AKT but this increase was associated with significant variability between the replicates. (c) AKT activation levels calculated as the ratio between (phos) AKT and (total) AKT. The graphs represent the data from three independent experiments.

In the cytoplasm, UDCA treatment increased (phos) AKT level but had no effect on (total) AKT level [Figure 6.14]. Again, the increase was not significant due the variability between the replicates. Taken together, it is difficult to conclude that AKT translocates into mitochondria as a result of UDCA treatment in CCCP-stressed SH-SY5Y.

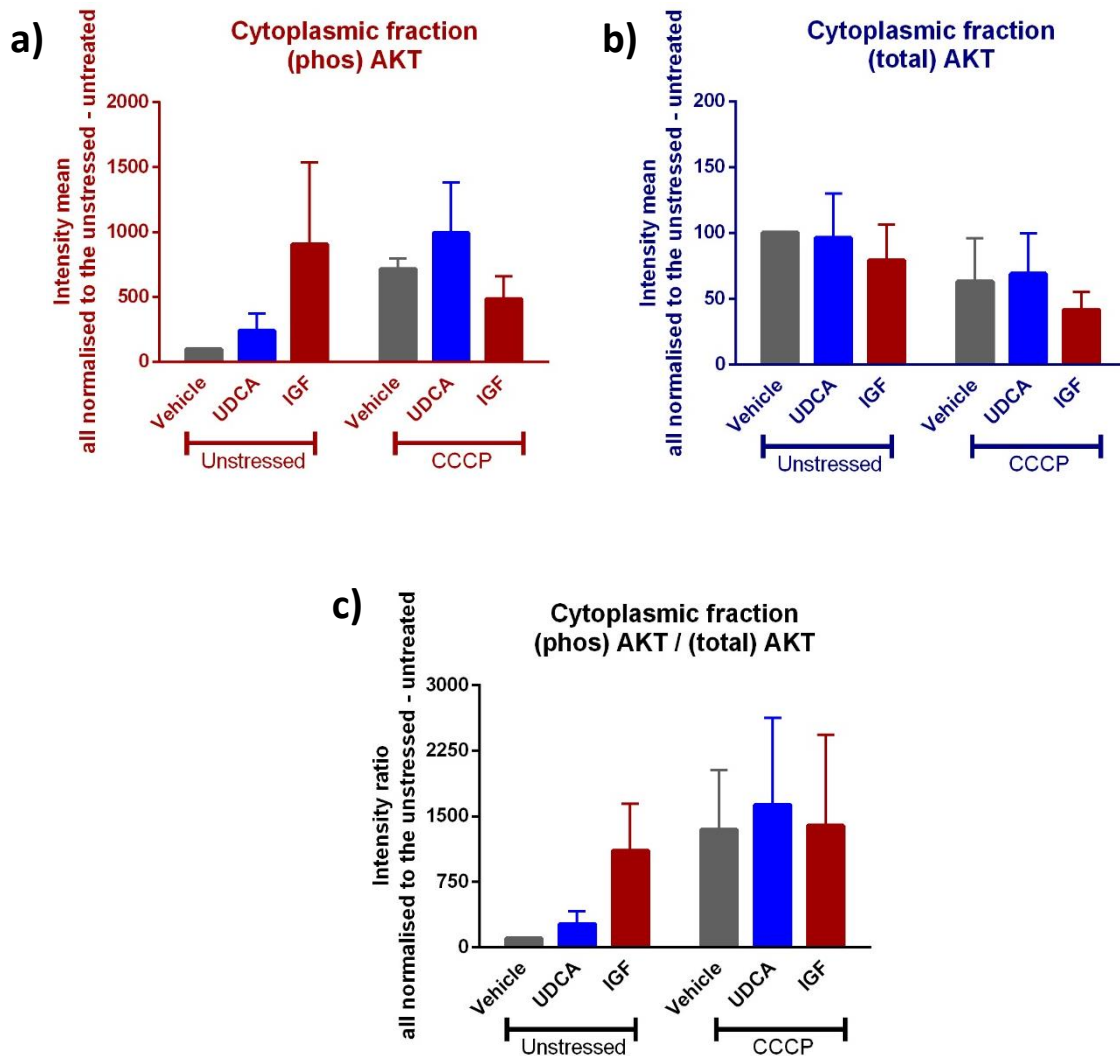


Figure 6.14 UDCA treatment did not induce a significant change in the expression of AKT in the cytoplasmic fraction of SH-SY5Y cells.

(a) and (b) show the results of WB image quantification for (phos) AKT and (total) AKT in the cytoplasmic fractions of unstressed and CCCP-stressed cells. Raw intensity readings for (phos) AKT and (total) AKT were normalised against the corresponding Tom20 readings. UDCA increased cytoplasmic (phos) AKT but this increase was associated with significant variability between the replicates. (c) AKT activation levels calculated as the ratio between (phos) AKT and (total) AKT. The graphs represent the data from three independent experiments.

Investigating the effect of UDCA on AKT downstream targets in SH-SY5Y cells

In this set of experiments, UDCA treatment was performed on SH-SY5Y cells following the previously used protocol that was associated with significant rescue effect (pre-treatment with 300 μ M for 12 hours followed by 24 hours' treatment with 50 μ M CCCP) [Figure 5.4]. The assessment was performed using two techniques, WB and ICC. The application of CCCP was reduced to six hours in plates for ICC to prevent the detachment of cells during the washing steps. The cells were probed with antibodies against the total and phosphorylated forms of the targets simultaneously because the antibodies were raised in different species (mouse, rabbit). In WB, the membrane was probed with the (phos) antibody, stripped and then probed with the (total) antibody. WB and ICC were conducted as described in the methods section.

6.6.1 Assessing the effect of UDCA on CREB phosphorylation

WB results show that the phosphorylation of CREB was significantly lower in CCCP-stressed SH-SY5Y cells (an 85% decrease) [Figure 6.15]. However, various treatment conditions with UDCA failed to increase CREB phosphorylation in either unstressed or stressed cells [Figure 6.15]. Equally, WB results showed that IGF treatment was not associated with an increase in CREB phosphorylation. The 85% decrease in CREB phosphorylation in the untreated stressed cells was not observed in the ICC results [Figure 6.17]. The response of the cells to UDCA and IGF treatments was also absent in the ICC results [Figure 6.16] [Figure 6.17].

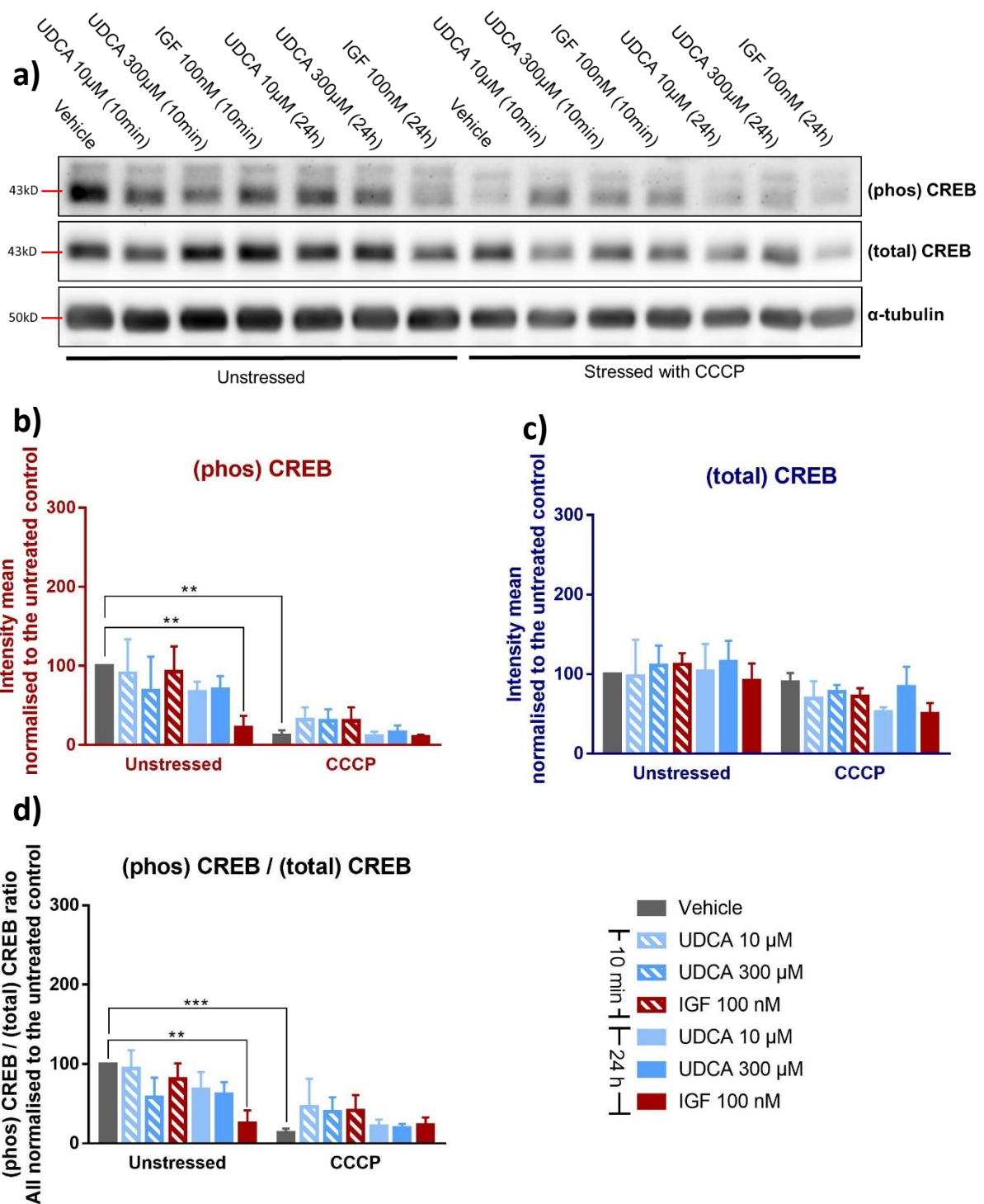


Figure 6.15 UDCA treatment had no significant effect on CREB phosphorylation in CCCP-stressed SH-SY5Y cells (via western blotting).

(a) WB images showing the expression levels of (phos) CREB and (total) CREB under different treatment conditions. The cells were pre-treated with UDCA for 12 hours before the addition of 50 μ M CCCP, which was applied for 24 hours. For the 10-minute treatment conditions, the cells were pre-treated with the vehicle for 12 hours before the addition of 50 μ M CCCP, which was applied for 24 hours, while the drugs were applied 10 minutes prior to collecting the cells for WB. WB and imaging were performed as described in the methods section. The cells were probed with (phos) CREB antibody (rabbit) and then the membrane was striped and re-probed with (total) CREB (mouse) antibody. The lower panel shows the results of WB image analysis for (b) (phos) CREB and (c) (total) CREB. (d) CREB activation levels calculated as the ratio between (phos) CREB and (total) CREB. The graphs show that all UDCA treatment conditions had no effect on CREB phosphorylation. The graphs represent the data from three independent experiments. ** $p < 0.01$, *** $p < 0.001$, two-way ANOVA test.

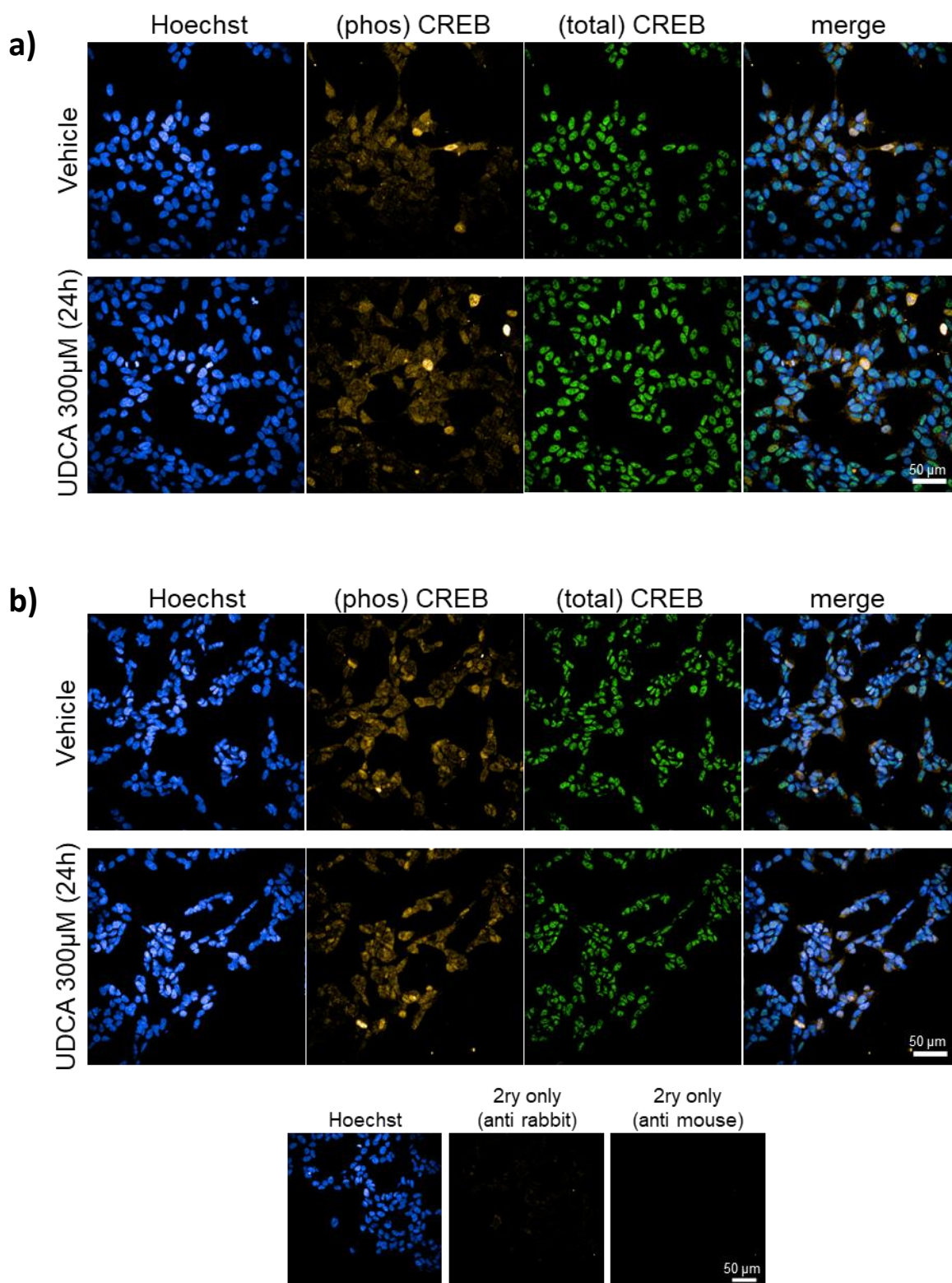


Figure 6.16 Immunocytochemistry images of UDCA-treated SH-SY5Y cells probed with phosphorylated and total CREB antibodies.

These are representative images obtained via confocal microscopy showing CREB staining in unstressed (a) and CCCP-stressed cells (b). The images show no difference between the vehicle and UDCA-treated conditions. The cells were probed with Hoechst (in blue (I, V)), (phos) CREB (in yellow (II, VI)) and (total) CREB (in green (III, VII)). (c) shows background signalling in cells that were probed with only the secondary antibodies. Scale bar = 50µm.

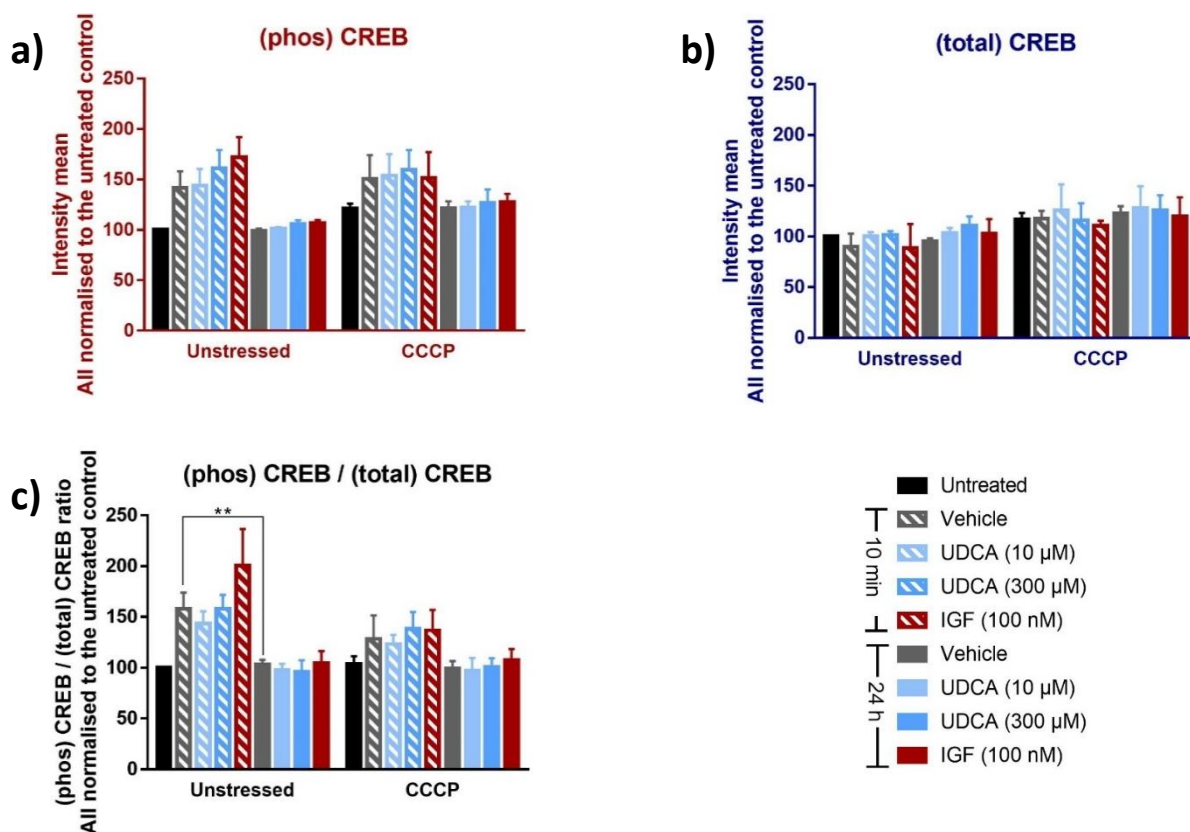


Figure 6.17 UDCA treatment had no significant effect on CREB phosphorylation in CCCP-stressed SH-SY5Y cells (via immunocytochemistry).

Analysis of (phos) CREB (a) and (total) CREB (b) images obtained via confocal microscopy. (c) AKT activation levels calculated as the ratio between (phos) AKT and (total) AKT. The cells were pre-treated with UDCA for 12 hours before the addition of 50 μM CCCP, which was applied for 6 hours. For the 10-minute treatment conditions, the cells were pre-treated with the vehicle for 12 hours before the addition of 50 μM CCCP, which was applied for 6 hours, while the drug was applied 10 minutes prior to the fixation process. The graphs show that all UDCA treatment conditions had no effect on CREB phosphorylation. ICC and imaging were performed as described in the methods section. The error bars represent the SD of three independent experiments. In each experiment, at least 20 fields per condition were captured, and the average of the intensity readings was used as a readout. ** $p < 0.01$, two-way ANOVA test.

6.6.2 Assessing the effect of UDCA on mTOR phosphorylation

Analysis of WB images of (phos) mTOR and (total) mTOR showed no significant difference between the unstressed and stressed conditions [Figure 6.18]. No treatment condition had any significant effect on (total) mTOR levels or mTOR phosphorylation [Figure 6.18]. Similar findings were observed in ICC results [Figure 6.19, Figure 6.20], except for a minor – but statistically significant – decrease in the mTOR phosphorylation ratio in stressed cells in comparison to unstressed ones [Figure 6.20 c]. However, this decrease was due to an increase in the intensity of (total) mTOR rather than a decrease in the intensity of (phos) mTOR.

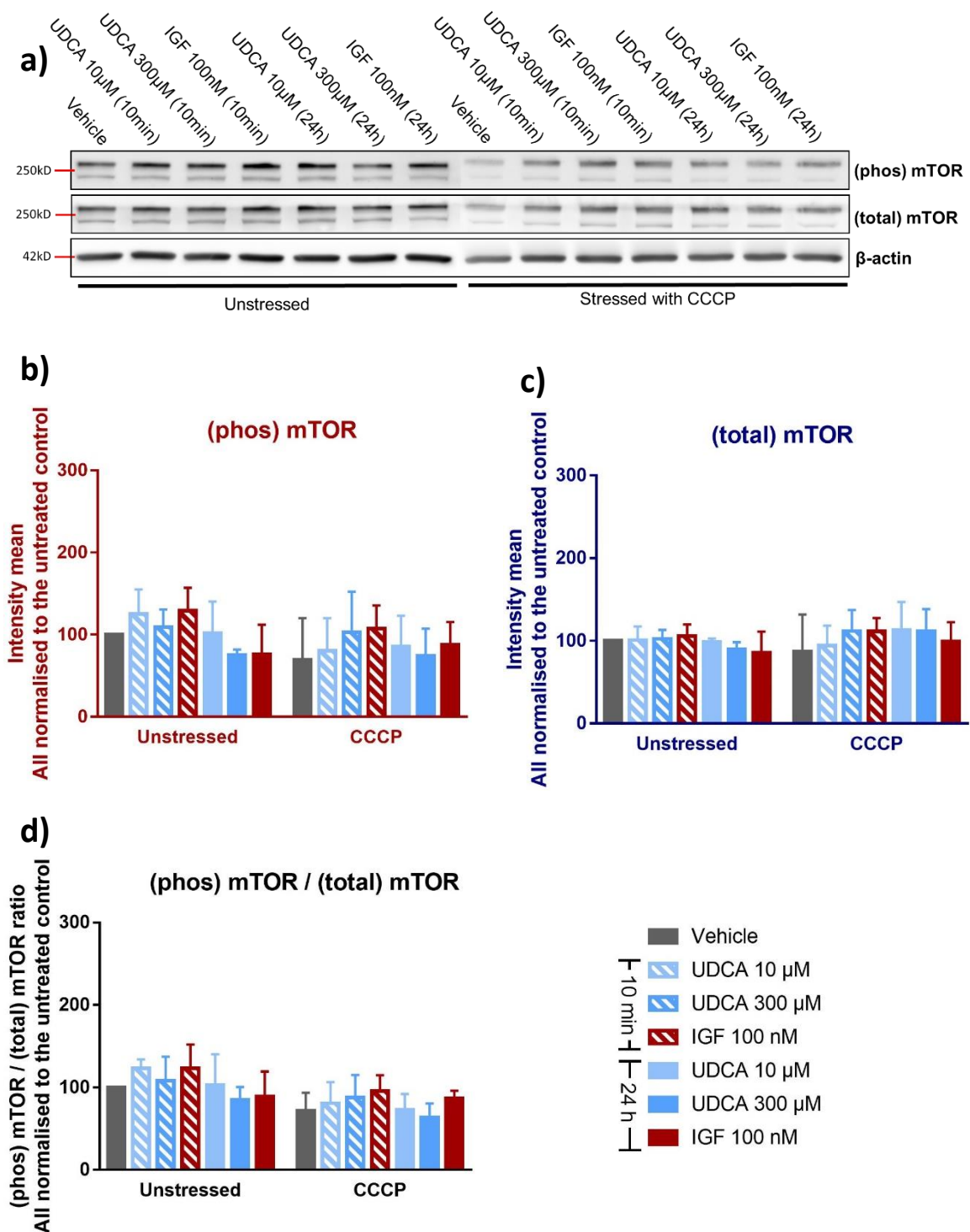


Figure 6.18 UDCA treatment had no significant effect on mTOR phosphorylation in CCCP-stressed SH-SY5Y cells (via western blotting).

(a) WB images showing the expression levels of (phos) mTOR and (total) mTOR under different treatment conditions. The cells were pre-treated with UDCA for 12 hours before the addition of 50 μ M CCCP, which was applied for 24 hours. For the 10-minute treatment conditions, the cells were pre-treated with the vehicle for 12 hours before the addition of 50 μ M CCCP, which was applied for 24 hours, while the drugs were applied 10 minutes prior to collection of the cells for WB. WB and imaging were performed as described in the methods section. The cells were probed with (phos) mTOR antibody (rabbit) and then the membrane was striped and re-probed with (total) mTOR (mouse) antibody. The lower panel shows the results of WB image analysis for (b) (phos) mTOR and (c) (total) mTOR. (d) mTOR activation levels calculated as the ratio between (phos) mTOR and (total) mTOR. The graphs show that all UDCA treatment conditions had no effect on mTOR phosphorylation. The graphs represent the data from three independent experiments.

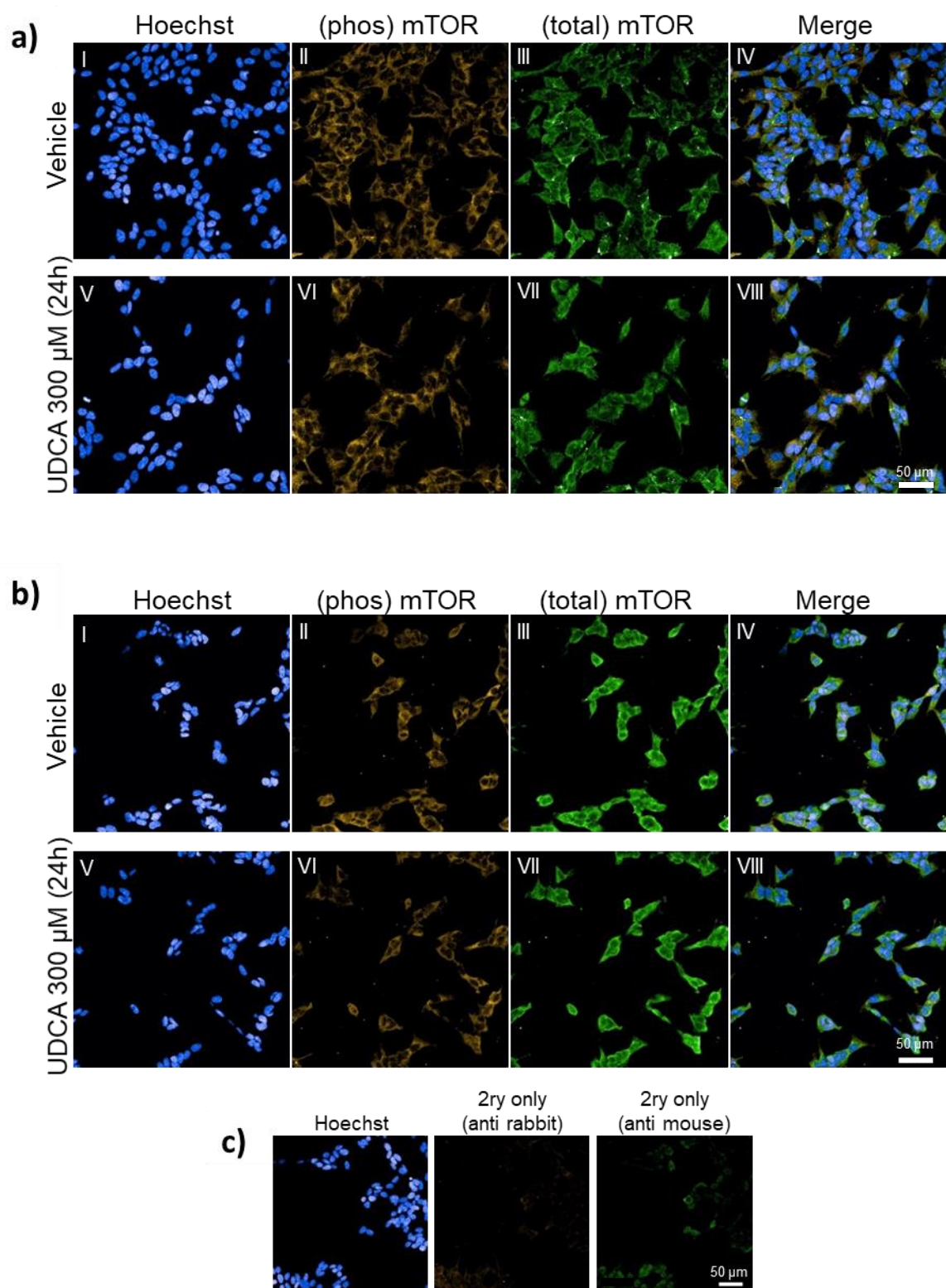


Figure 6.19 Immunocytochemistry images of UDCA-treated SH-SY5Y cells probed with phosphorylated and total mTOR antibodies.

Representative images obtained via confocal microscopy showing mTOR staining in unstressed (a) and CCCP-stressed cells (b). The images show no difference between the vehicle and the UDCA-treated conditions. The cells were probed with Hoechst (in blue (I, V)), (phos) mTOR (in yellow (II, VI)) and (total) mTOR (in green (III, VII)). (c) shows background signalling in cells that were probed only with the secondary antibodies. Scale bar = 50μm.

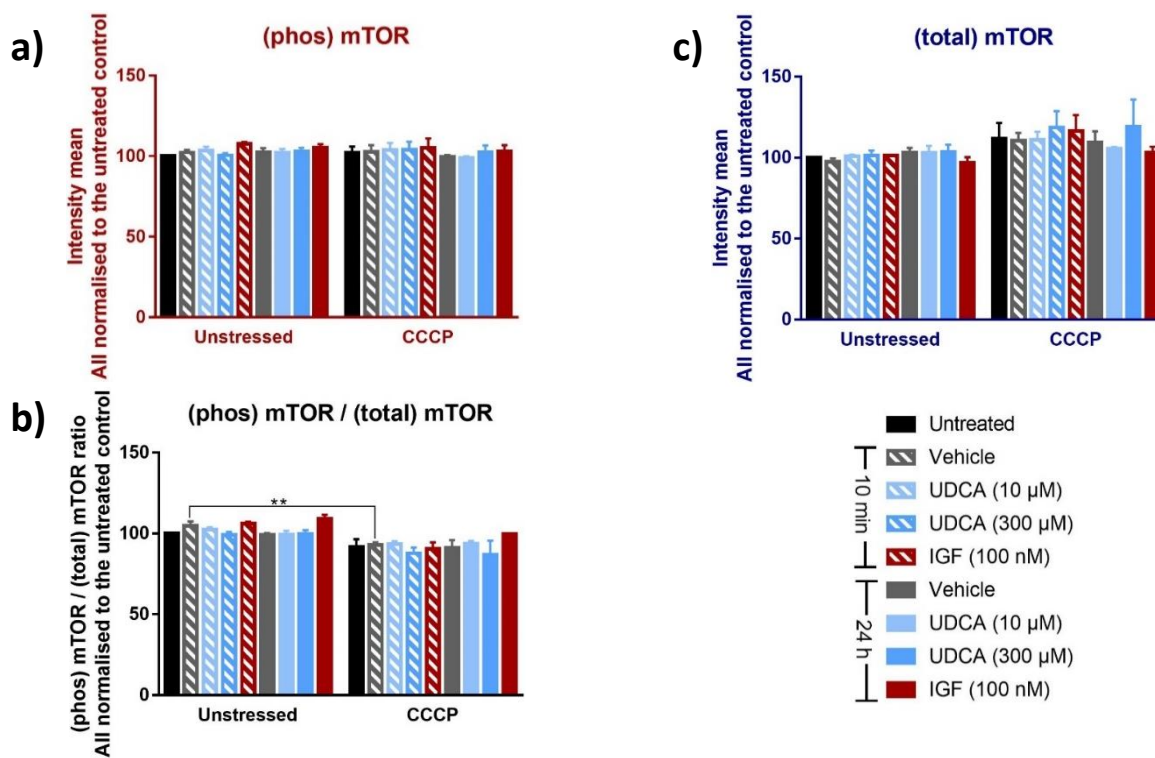


Figure 6.20 UDCA treatment had no significant effect on mTOR phosphorylation in CCCP-stressed SH-SY5Y cells (via immunocytochemistry).

Analysis of (phos) mTOR (a) and (total) mTOR (b) images obtained via confocal microscopy. (c) mTOR activation levels calculated as the ratio between (phos) mTOR and (total) mTOR. The cells were pre-treated with UDCA for 12 hours before the addition of 50 μM CCCP, which was applied for 6 hours. For the 10-minute treatment conditions, the cells were pre-treated with the vehicle for 12 hours before the addition of 50 μM CCCP, which was applied for 6 hours, while the drug was applied 10 minutes prior to the fixation process. The graphs show that all UDCA treatment conditions had no effect on mTOR phosphorylation. ICC and imaging were performed as described in the methods section. The error bars represent the SD of three independent experiments. In each experiment, at least 20 fields per condition were captured, and the average of the intensity readings was used as a readout. ** p < 0.01, two-way ANOVA test.

6.6.3 Assessing the effect of UDCA on FOXO1 phosphorylation

In initial testing experiments, no bands were observed upon probing WB membranes with (total) FOXO1 antibody. (total) FOXO1 bands were only observed when the WB protocol was optimised by doubling both the loading quantity of the sample (40μg/lane) and the concentration of the applied (total) FOXO1 antibody (1:500 titre) [Figure 6.21].

In ICC, (total) FOXO1 signals (unlike (phos) FOXO1) were remarkably weak, close to the level of the background, despite trials of various concentrations [Figure 6.22]. Therefore, it was decided to omit ICC for drug treatment experiment for FOXO1. The assessment of the drug treatment experiment by WB showed variable results and it was difficult to establish any significant difference between the untreated and treated conditions [Figure 6.21].

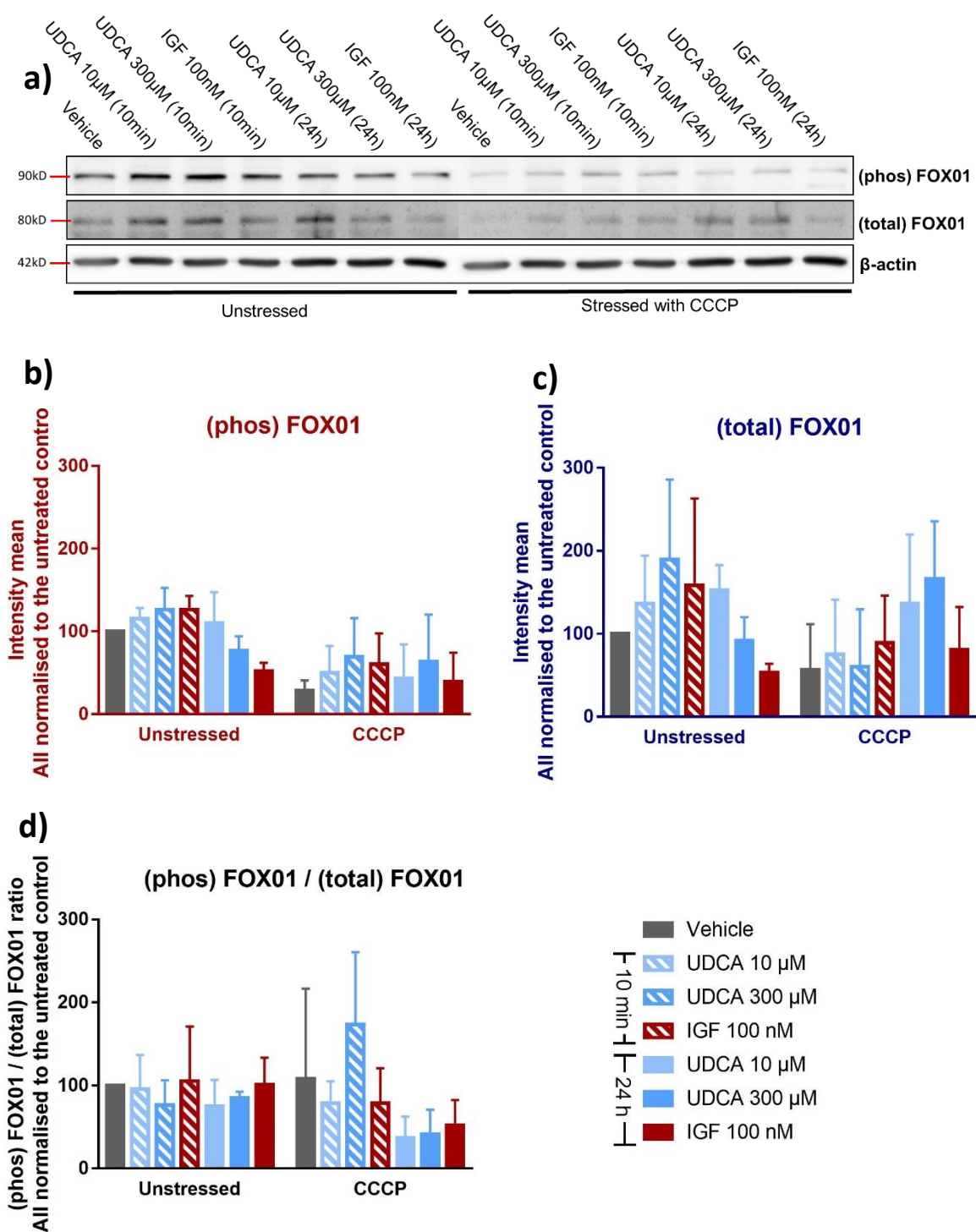


Figure 6.21 UDCA treatment had no significant effect on FOXO1 phosphorylation in CCCP-stressed SH-SY5Y cells (via western blotting) .

(a) WB images showing the expression levels of (phos) FOXO1 and (total) FOXO1 under different treatment conditions. Cells were pre-treated with UDCA for 12 hours before the addition of 50 μ M CCCP, which was applied for 24 hours. For the 10-minute treatment conditions, the cells were pre-treated with the vehicle for 12 hours before the addition of 50 μ M CCCP, which was applied for 24 hours, while the drugs were applied 10 minutes prior to collection of the cells for WB. WB and imaging were performed as described in the methods section. The cells were probed with (phos) FOXO1 antibody (rabbit) and then the membrane was striped and re-probed with (total) FOXO1 (mouse) antibody. The lower panel shows the results of WB image analysis for (b) (phos) FOXO1 and (c) (total) FOXO1. (d) FOXO1 inhibition levels calculated as the ratio between (phos) FOXO1 and (total) FOXO1. The graphs show variable results and it is difficult to assert if UDCA treatment had an effect on FOXO1 phosphorylation. The graphs represent the data from three independent experiments.

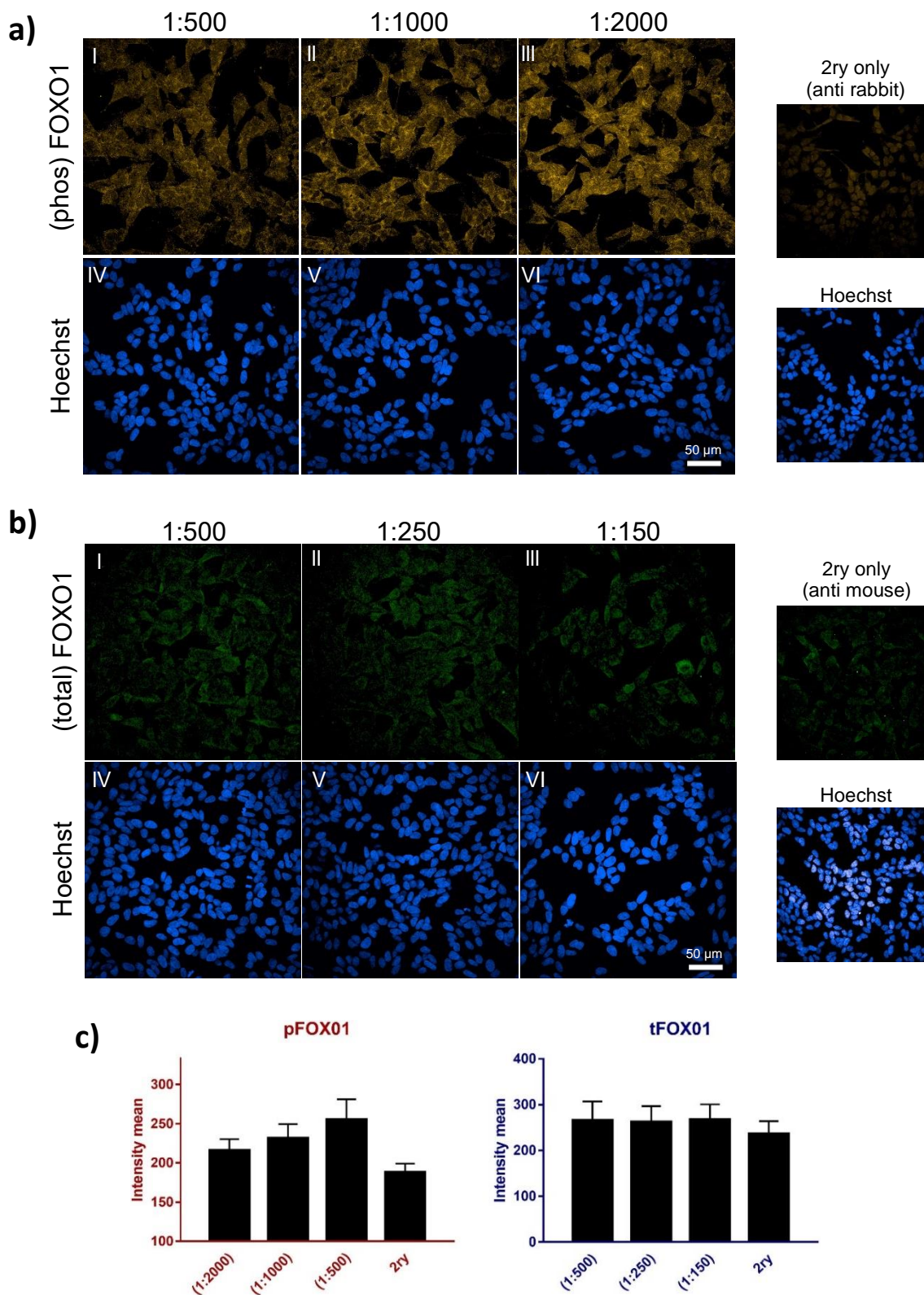


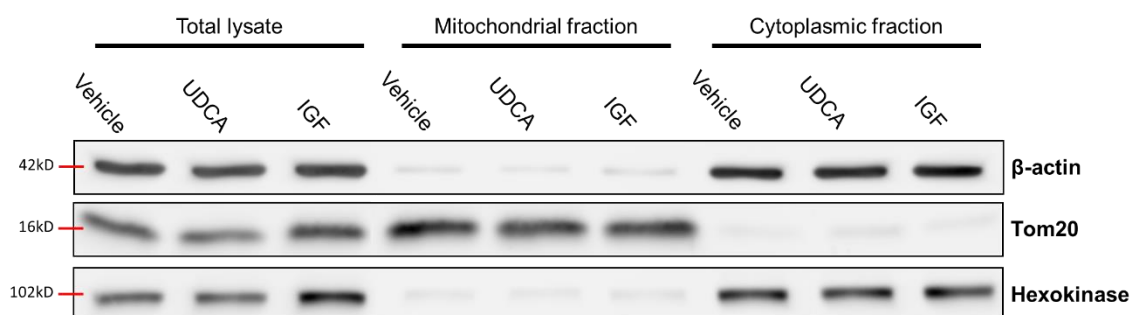
Figure 6.22 Total FOXO1 antibody is not effective in immunocytochemistry experiments.

(a) ICC images of various dilutions of (phos) FOXO1 antibody (in yellow, I–III) and corresponding Hoechst staining (in blue, IV–VI). (b) ICC images of various dilutions of (total) FOXO1 antibody (in green, I–III) and corresponding Hoechst staining (in blue, IV–VI). (c) Analysis of (phos) FOXO1 and (total) FOXO1 images obtained by confocal microscopy. The images and the graphs indicate that the (total) FOXO1 antibody is not reliable for detecting (total) FOXO1 in cells. The right panels show background signalling in cells that were probed only with the secondary antibodies. The graphs represent the data from a single pilot experiment. Scale bar = 50 μ m.

6.6.4 Assessing the effect of UDCA on the mitochondrial hexokinase level

Following drug treatment, mitochondrion-enriched fractions were obtained using the fractionation protocol described in the methods chapter [Heading 2.11]. Evaluation of this protocol was previously performed [Heading 6.5.1]. Figure 6.23 shows WB membranes of treated fractionated samples probed with hexokinase as well as mitochondrial and cytoplasmic markers.

a) Unstressed



b) CCCP-stressed

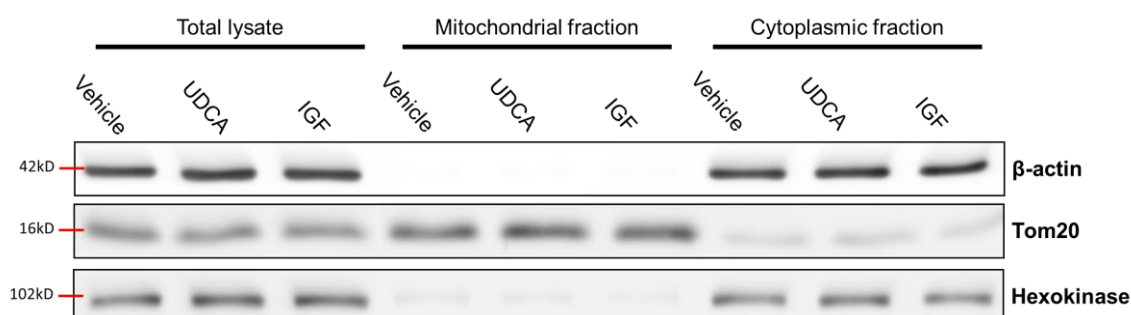


Figure 6.23 Assessing the effect of UDCA on mitochondrial hexokinase content in CCCP-stressed SH-SY5Y cells by western blotting.

WB images of fractionated unstressed (a) and CCCP-stressed (b) samples probed with mitochondrial markers, cytoplasmic markers and hexokinase. The cells were pre-treated with 300 μ M UDCA for 12 hours before the addition of 50 μ M CCCP, which was applied for 24 hours. IGF (100 nM) was applied as a positive control for 10 minutes before collection of the cells for the fractionation process. Equal quantities of protein (12 μ g) from the total lysate, mitochondrial fraction and cytoplasmic fraction were loaded in WB to allow direct comparison. The images show successful fractionation of the mitochondrial compartment but UDCA treatment did not increase the hexokinase content in the mitochondria fraction. Cellular fractionation, WB and imaging were performed as described in the methods section.

Analysis of WB images revealed that the amount of hexokinase was approximately three times higher in the mitochondrial fraction of stressed cells in comparison to the unstressed cells [Figure 6.24]. However, neither UDCA nor IGF increased hexokinase levels in the mitochondrial fraction.

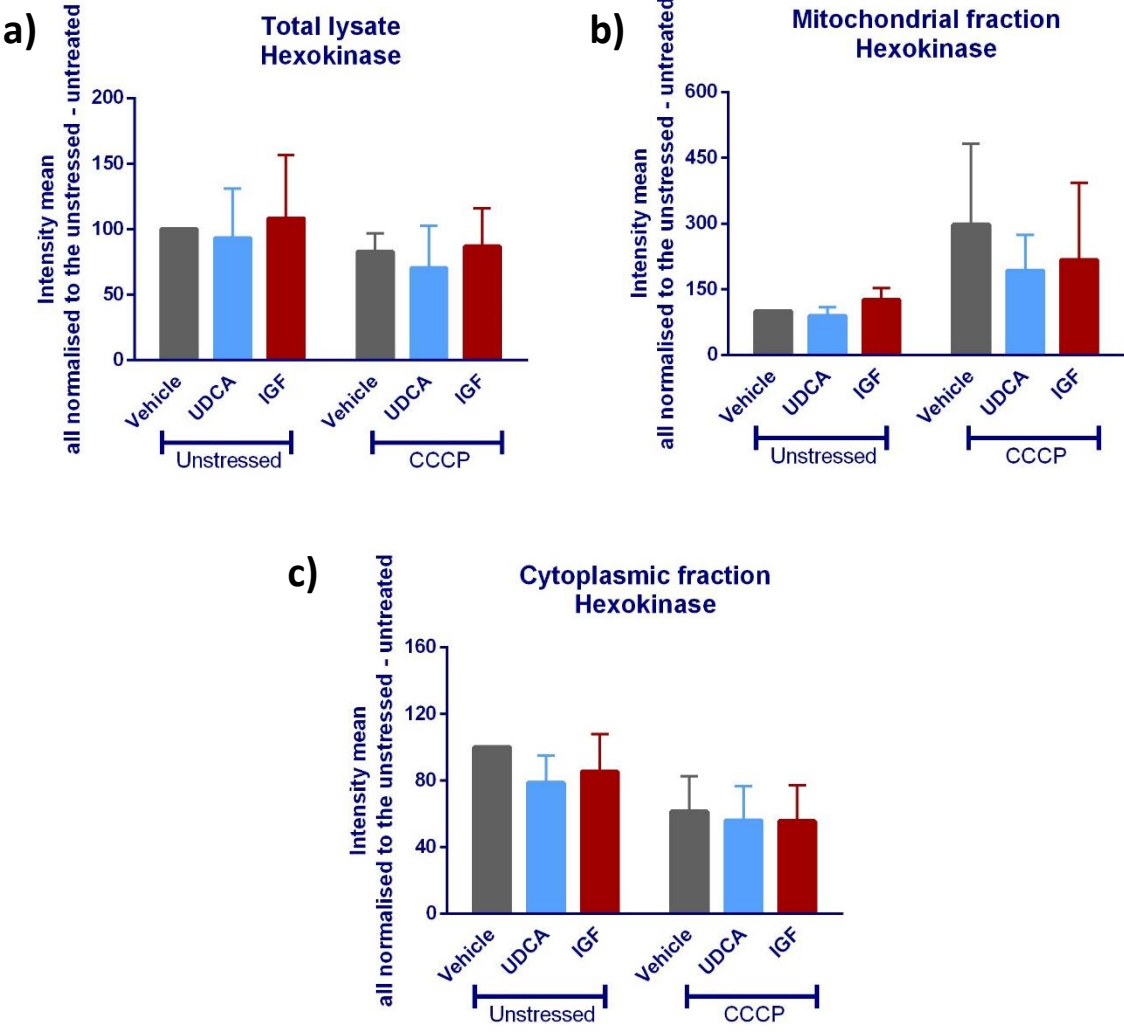


Figure 6.24 UDCA treatment did not induce a significant change in the expression of hexokinase in the mitochondrial fraction of SH-SY5Y cells.

The results of WB image analysis for various treatment conditions. UDCA treatment had no effect on hexokinase content in the mitochondrial fraction. The error bars represent the SD of three independent experiments.

To assess mitochondrial hexokinase via ICC, cells were co-stained with Tom20 to determine their mitochondrial regions. An image analysis protocol was set to calculate hexokinase intensity both within the area occupied by mitochondria and in the remaining area of the cell. Consequently, the ratio between the hexokinase intensities in the mitochondrial and cytoplasmic regions was used as a measure of hexokinase localisation to the mitochondria.

Analysis of ICC images revealed an increase of approximately 10% in mitochondrial hexokinase in stressed cells in comparison to unstressed cells [Figure 6.25, Figure 6.26]. Both WB and ICC results suggest that the different treatment conditions had no effect on mitochondrial hexokinase.

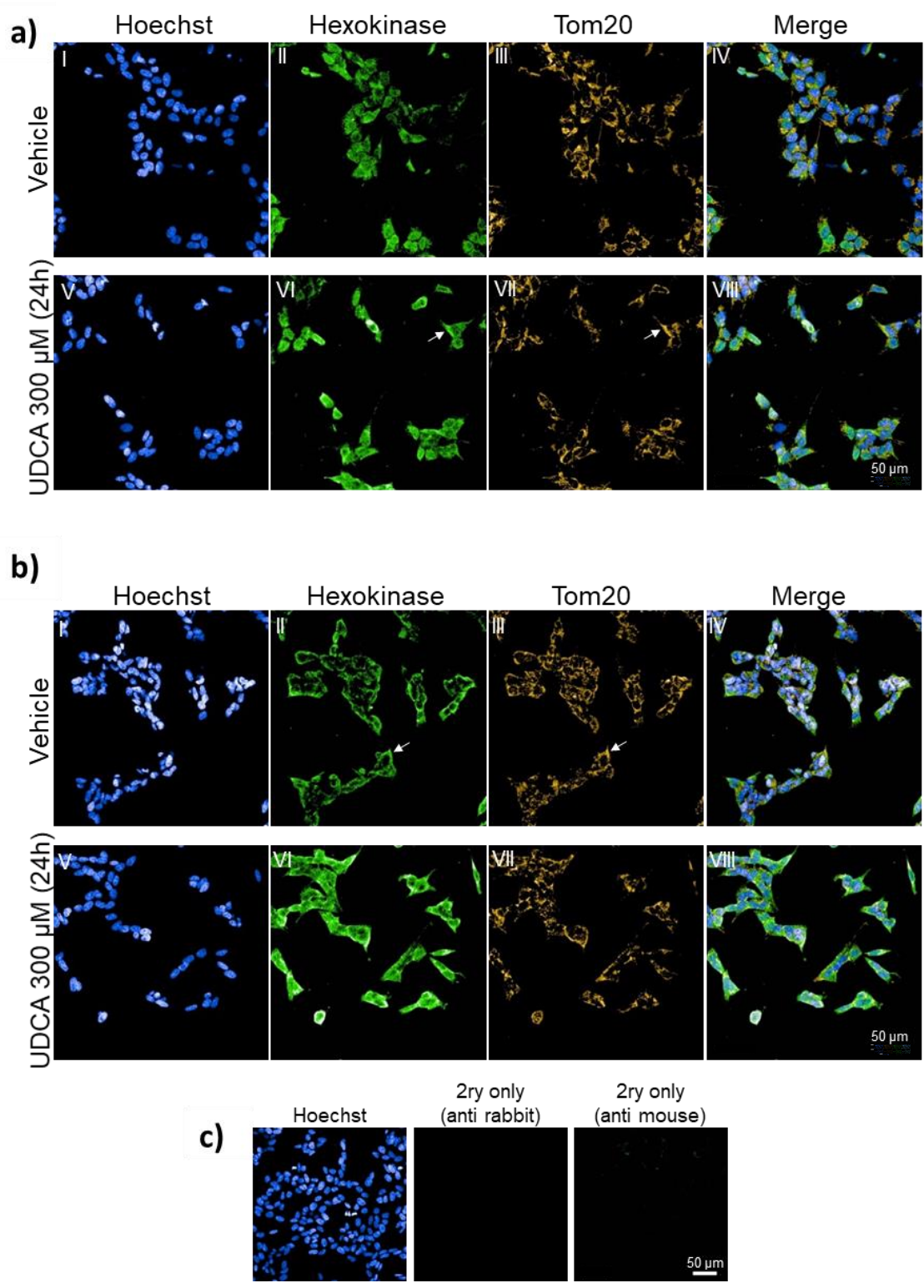


Figure 6.25 Immunocytochemistry images of UDCA-treated SH-SY5Y cells probed with hexokinase and Tom20 antibodies.

These are representative images obtained via confocal microscopy showing hexokinase staining (in green (I, V)) in unstressed (a) and CCCP-stressed (b) cells. The cells were also co-stained with Tom20 (in yellow (III, VII)) to determine mitochondrial regions and Hoechst (in blue (I, V)) to show nuclei. The images show that hexokinase areas of high intensities colocalise with mitochondrial areas as indicated by the white arrows. (c) shows background signalling in cells that were probed with only the secondary antibodies. Scale bar = 50 μ m.

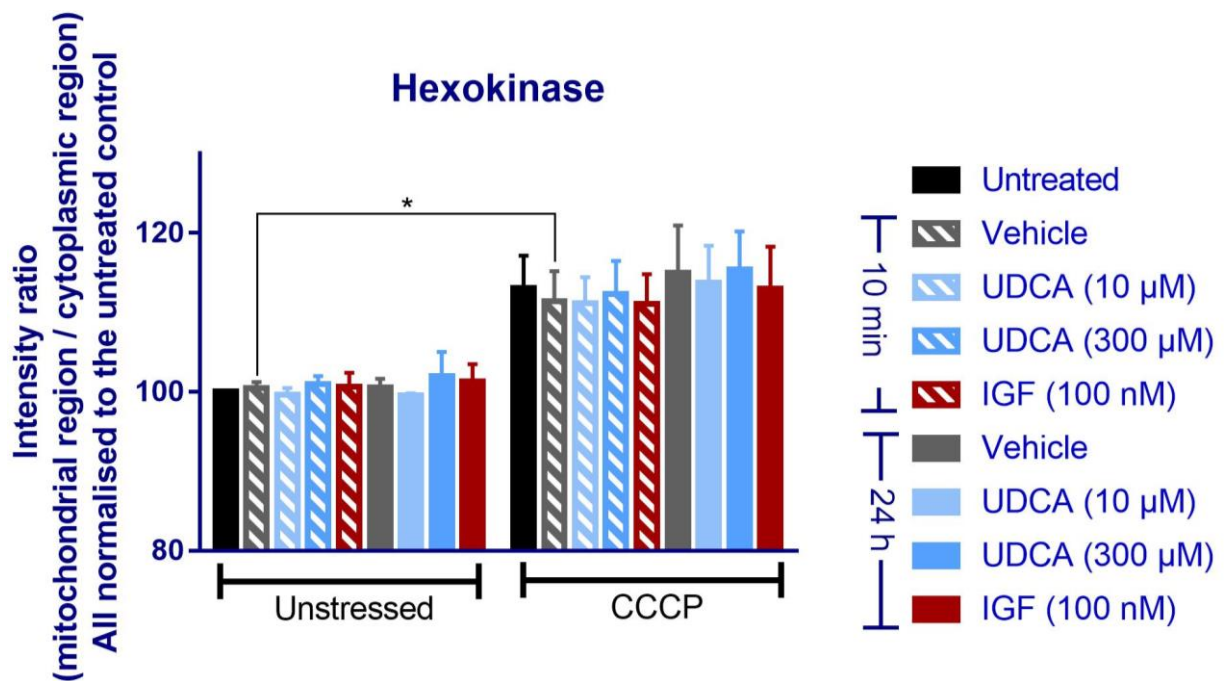


Figure 6.26 UDCA treatment had no significant effect on mitochondrial hexokinase content in CCCP-stressed SH-SY5Y cells (via immunocytochemistry) .

Analysis of hexokinase images obtained via confocal microscopy. The intensity of hexokinase in the mitochondrial region is expressed relative to hexokinase intensity in the cytoplasmic region. The graph show that mitochondrial hexokinase was significantly increased after the application of CCCP but UDCA treatment did not affect its levels. The cells were pre-treated with UDCA for 12 hours before the addition of 50 μM CCCP, which was applied for 6 hours. For the 10-minute treatment conditions, the cells were pre-treated with the vehicle for 12 hours before the addition of 50 μM CCCP, which was kept for 6 hours, while the drug was applied 10 minutes prior to the fixation process. ICC and imaging were performed as described in the methods section. The error bars represent the SD of three independent experiments. In each experiment, at least 20 fields per condition were captured, and the average of the intensity readings was used as a readout. * $p < 0.05$, two-way ANOVA test.

6.7 Discussion

As mentioned in the introduction chapter [Heading 1.6], AKT and Nrf2 are putative pathways through which UDCA exerts its beneficial effects. These two pathways are not considered separate entities since AKT regulates Nrf2 activity via one of its downstream targets, GSK3 β (Manning and Toker, 2017). The suppression of AKT activity is sufficient to abolish Nrf2 activation and the subsequent antioxidant effects (Wu et al., 2013, Cui et al., 2016, Ryu et al., 2014). Although UDCA and UCA treatments did not rescue mitochondrial function in toxin-stressed CHO cells in Chapter 4 [Heading 4.4], they were associated with a small but significant induction of ARE expression. Therefore, we planned to determine whether that increase was associated with AKT activation. The results in this chapter [Figure 6.3] demonstrated that neither UDCA nor UCA were able to activate AKT in CHO cells, even though the treatment protocol was identical to the one used in ARE experiments.

There are several possible explanations for this outcome. First, the observed ARE induction was small and it is possible that the AKT activation required to induce this effect is small and beyond the detectable level in the experiment performed. Second, AKT activation may have occurred transiently following the application of the drugs and become undetectable by the time of ICC. Third, it is possible that Nrf2 activation was achieved via AKT-independent mechanisms, since GSK3 β is a downstream target of other kinases including MAPK (Bryan et al., 2013). Additionally, ROS can directly modify subsets of the cysteine residues in Keap1, resulting in a conformational change that disturbs the Keap1-Nrf2 interaction and consequently increases the level of Nrf2 in the nucleus (Taguchi et al., 2011). The activation mechanism of Nrf2 was discussed in detail in Chapter 4 [Heading 4.1.3].

Because the CHO cell line is not relevant to PD, we decided to conduct the subsequent experiments using SH-SY5Y cells. As predicted, the UDCA-mediated rescue effect observed in CCCP-stressed cells was associated with a significant increase in AKT activation. Since UDCA was used in high doses (300 μ M) in the SH-SY5Y cells, it is possible that the doses applied in the CHO experiments (10 μ M) were insufficient to activate AKT. Further, the discrepancy between the results in CHO and SH-SY5Y cells might be attributed to the differences in type and origin of

these cells. In addition, the effect of UDCA on AKT activation in CHO cells was only tested in unstressed conditions since no rescue effect was observed in toxin-stressed cells. On the other hand, AKT activation was triggered in SH-SY5Y cells in association with the rescue effect observed in CCCP-stressed cells, suggesting that UDCA-mediated AKT activation might only occur as a response to abnormal biological states. In line with this notion, the results in the study previously undertaken in the Bandmann group showed clearly that UCA was able to increase AKT phosphorylation only in *parkin* patient fibroblasts and not in healthy control fibroblasts (Mortiboys et al., 2013).

The role of AKT activation in the UDCA-mediated rescue effect was investigated further via the use of the AKT inhibitor triciribine. This is a tricyclic nucleoside originally developed as a potential anticancer therapy, though it has been also investigated as an antiviral agent against HIV. Although initial clinical trials were not promising (Hoffman et al., 1995, Feun et al., 1993), further investigation suggested that triciribine could be beneficial against tumours with hyperactivated AKT, such as cancers of the breast, ovary and pancreas (Yang et al., 2004, Garrett et al., 2011). Within cells, triciribine is phosphorylated into a monophosphate active analogue. This is the active form of the compound that interacts with the PH domain of AKT and interferes with its localisation to the membrane, consequently preventing AKT phosphorylation and activation (Sampath et al., 2013). Triciribine is superior to other commonly used AKT inhibitors (for instance LY294002), as it directly inhibits AKT phosphorylation (Nitulescu et al., 2016). In contrast, LY294002 is an indirect AKT inhibitor that blocks PI3K, which is an upstream of AKT. Moreover, LY294002 mediates PI3K-independent events, such as inhibition of NF- κ B and Ca²⁺ signalling (Gharbi et al., 2007), which might negatively affect the interpretation of data.

Unexpectedly, our results uncovered a discrepancy between the cytotoxicity and ATP findings when the AKT pathway was inhibited. Triciribine inhibited the UDCA-mediated increase in ATP but did not affect cytotoxicity [Figure 6.9]. This observation has not been reported before. In a previously published study, the application of triciribine inhibited a UDCA-mediated increase in viability in sodium nitroprusside-stressed SH-SY5Y cells (Chun and Low, 2012). However, that assessment of viability was performed using the MTT assay, which primarily reflects mitochondrial

activity (van Meerloo et al., 2011). Our results suggest that the observed UDCA-mediated rescue effect is not entirely dependent on the AKT pathway.

The mechanism by which UDCA mediates its AKT-independent rescue effect might involve direct interaction between UDCA and AKT downstream targets. For example, it has been reported that UDCA has high affinity for BAX (a pro-apoptotic protein), and that its binding prevents BAX translocation within cells, allowing anti-apoptotic proteins to prevail (Sousa et al., 2015).

Further, it is possible that UDCA exerts its rescue effect in part via alternative pathways. Hepatobiliary system-related study has found that the anti-apoptotic effect of TUDCA involves the activation of protein kinase A (PKA) and consequent phosphorylation and inhibition of CD95 (a receptor that leads to programmed cell death via the extrinsic pathway of apoptosis (Le Gallo et al., 2017, Sommerfeld et al., 2015). Arguably, the mechanism of cell death in the study could be irrelevant due to the use of hydrophobic bile acid as an inducer of apoptosis. Nonetheless, reports have shown previously that treating cells with a mitochondrial uncoupler such as CCCP also enhances the activity of CD95 (Vier et al., 2004).

Our results show that activation of AKT was associated with an increase in ATP level in CCCP-stressed SH-SY5Y cells [Figure 6.9]. Therefore, we decided to investigate whether UDCA treatment was associated with spatial translocation of AKT into mitochondria. Although this had never been assessed in UDCA-treated cells, a previously published study demonstrated that a fraction of AKT is inherently present in the mitochondria of SH-SY5Y cells (Bijur and Jope, 2003). Specifically, AKT was associated with the inner and outer mitochondrial membranes, while only a negligible amount was found in the matrix. More importantly, IGF treatment induced a rapid increase in the mitochondrial AKT level, which occurred synchronously with AKT phosphorylation in the cytoplasm (Bijur and Jope, 2003). Likewise, our results reveal an increased (total) AKT level in the mitochondrial fraction following IGF treatment [Figure 6.13 b]. Although UDCA increased (total) AKT content in the mitochondrial fractions of CCCP-stressed cells [Figure 6.13 b], it is difficult to draw conclusions from this because of the considerable variability between replicates. Further research is needed to verify the significance of this increase.

The presented work in this chapter supports the assumption that AKT activation plays a significant role in the UDCA-mediated rescue effect. Accordingly, the effect of UDCA on AKT downstream targets was investigated. The results indicate that UDCA treatment did not affect the phosphorylation level of CREB in either unstressed or CCCP-stressed SH-SY5Y cells. The effect of UDCA on CREB in CCCP-stressed cells had never been assessed before. However, in biliary epithelial cells, TUDCA treatment has previously been reported to activate CREB and protect cells from the toxicity of CCI-779 (a specific inhibitor of mTOR) (Wang et al., 2005).

Notably, the application of CCCP was associated with a significant decrease in CREB phosphorylation [Figure 6.15]. Since AKT is significantly activated in CCCP-stressed SH-SY5Y cells [Figure 6.5], CREB phosphorylation was expected to increase. In addition, research has indicated that CREB can be phosphorylated via the action of AMP-activated protein kinase (AMPK) under such conditions (Thomson et al., 2008). Therefore, the decrease in CREB phosphorylation reported in this chapter should be interpreted with caution, especially as it was observed in WB results and not in ICC results. Further research is needed to verify these findings and to investigate the underlying mechanism. Decreased CREB phosphorylation may be attributed to several protein phosphatases that are known to dephosphorylate CREB, such as serine/threonine protein phosphatase 2A (PP2A) and calcineurin (PP2B) (Johannessen et al., 2004).

Similarly, the application of CCCP decreased the level of phosphorylated mTOR in SH-SY5Y cells. This decrease was smaller but it was statistically significant and was observed in ICC results [Figure 6.20]. Reduced mTOR phosphorylation as a result of CCCP treatment has been assessed before, in HEK293 cells, and displayed a similar trend (Park et al., 2014). The mitigation of mTORC1 activity is known to be a part of the survival response under stressful conditions via AMPK (Kang et al., 2011). By inhibiting mTORC1, AMPK restricts anabolic mechanisms (RNA translation and protein synthesis), increases mitophagy and promotes cell survival by enhancing the production of ATP via glycolysis (Kang et al., 2011). Of note, the previous study showed that complete inhibition of mTOR was associated with increased cell death, indicating that basal mTOR activity is equally important to protect cells (Park et al., 2014). Other PD-related toxins

(such as 6-OHDA, MPP+ and rotenone) have also been found to decrease mTOR phosphorylation in primary neurons (Xu et al., 2014). Therefore, it is plausible that the mechanism of the effect observed is relevant to PD as well.

With regard to FOXO1, it has been reported previously that CCCP and rotenone treatment increase FOXO1 expression in the nuclear compartment in adipocytes (Barbato et al., 2014). The phosphorylation of FOXO1 is expected to rise in CCCP-stressed cells due to the action of activated AKT and AMPK (Eijkelenboom and Burgering, 2013). Nonetheless, in this study, it was difficult to assess the effect of CCCP and UDCA on FOXO1 expression and phosphorylation due to variability in the results [Figure 6.21].

Several lines of evidence suggest that mitochondrial hexokinase opposes apoptosis by interfering with BAX-mitochondrion interaction and consequent mitochondrial outer membrane permeabilisation (Robey and Hay, 2006). Evidence also indicates that the activation of AKT not only increases hexokinase-mitochondrion association but also increases hexokinase expression (Roberts and Miyamoto, 2015).

As mentioned above, the activation of AMPK in stressed cells with reduced ATP levels increases their reliance on glycolysis to compensate for energy loss. Since hexokinase catalyses the first step of glucose metabolism, its availability becomes more crucial in these conditions. As predicted, our results reveal a significant increase in hexokinase content in the mitochondrial compartment of CCCP-stressed cells through both WB and ICC results [Figure 6.24, Figure 6.26]. This was also previously reported in CCCP-stressed Hela cells (McCoy et al., 2013). The effect of UDCA on hexokinase had never been investigated before. The results showed that UDCA treatment had no effect on hexokinase expression or localisation [Figure 6.24, Figure 6.26].

In conclusion, we could not demonstrate that AKT activation was associated with any significant effect on the selected AKT targets. This implies that there are other targets and pathways by which UDCA exerts its rescue effect, which will be addressed in the next chapter.

Chapter 7. Discussion

7 Discussion

7.1 Mitochondrial biogenesis in *parkin* patients' fibroblasts

As aforementioned, previous work in our research group demonstrated a beneficial effect of UDCA on *parkin* and *LRRK2* patient fibroblasts; it was plausible to assume that this effect was due to enhanced mitochondrial biogenesis. Accordingly, we assessed the effect of UDCA treatment on mitochondrial protein expression and mtDNA copy numbers in *parkin* patient fibroblasts. The results obtained in this project did not show evidence of increased mitochondrial biogenesis with UDCA treatment [Heading 3.5, 3.7]. However, it is difficult to draw a firm conclusion since the tested positive control, resveratrol, did not induce a positive effect, although it has been previously reported to increase mitochondrial biogenesis in *parkin* patients fibroblasts (Ferretta et al., 2014).

In Ferretta and colleague's study, resveratrol significantly increased mtDNA copy numbers, as well as the mRNA level of PGC-1 α target genes, such as TFAM, in the fibroblasts of both controls' and patients' (*parkin*) fibroblasts (Ferretta et al., 2014). In contrast to Ferretta and colleague's study, where the cells were grown in a regular glucose-containing culture medium, the cells in this project were forced to rely on OXPHOS, via the use of a galactose-containing medium [Heading 3.2]. In a recent study, in which healthy fibroblasts were cultured in a galactose-containing medium, resveratrol treatment did not increase the expression of PGC-1 α (Sgarbi et al., 2018). This suggests that culturing cells in a galactose-containing medium might obscure the effects of resveratrol (and possibly UDCA) on mitochondrial biogenesis.

Several groups have reported that mitophagy is inhibited when cells are grown in a galactose medium (Van Laar et al., 2010, MacVicar and Lane, 2014, Allen et al., 2013). One study reported that the reliance on OXPHOS prevents Parkin translocation in uncoupled mitochondria (Van Laar et al., 2010). In contrast, another study, which was conducted afterward, demonstrated that Parkin translocation occurs, but mitophagy is still inhibited, suggesting that a Parkin-independent pathway is involved in this inhibition (MacVicar and Lane, 2014). Since mitophagy and mitochondrial biogenesis are tightly coupled (Palikaras and Tavernarakis, 2014), it is possible that blocking mitophagy would downregulate the mitochondrial biogenesis programme, consequently

decreasing the response to mitochondrial biogenesis enhancers, such as resveratrol. Nonetheless, UDCA treatment in a galactose-containing medium significantly rescues mitochondrial function in *parkin* patient fibroblasts (Mortiboys et al., 2013). Therefore, the results in this project suggest that mitochondrial biogenesis does not play a significant role in the mechanism of action of UDCA.

7.2 Activation of the Nrf2 pathway in ARE reporter cell lines

The mechanism of action of UDCA has been extensively investigated in the context of hepatobiliary diseases. The activation of the Nrf2 pathway is one of the most important mechanisms by which UDCA stimulates hepatocellular transport, detoxification and antioxidative stress systems (Okada et al., 2008). Evidence shows that the activation of Nrf2 is sufficient to stimulate mitochondrial biogenesis via the regulation of Nrf1 and PGC1 α (Dinkova-Kostova and Abramov, 2015). While the results in this project showed no evidence of enhanced mitochondrial biogenesis following UDCA treatment, this does not necessarily mean that Nrf2 was not activated in the treated cells, due to the complex regulatory mechanism of the mitochondrial biogenesis programme. Accumulative evidence of the role of oxidative stress in PD (more details in the introduction chapter [Heading 1.3]) imply that drugs with an antioxidant effect might be a novel treatment for PD. Accordingly, it was decided to investigate the ability of UDCA to activate the Nrf2 pathway.

It is plausible to assume that the beneficial mitochondrial effect observed in *parkin* patient fibroblasts (Mortiboys et al., 2013) was achieved via Nrf2 activation. Evidence shows that Nrf2 is closely linked to mitochondrial function. In a previously published report, the basal mitochondrial membrane potential, oxygen consumption and ATP levels in Nrf2-KO mouse embryonic fibroblasts (MEFs) and cultured primary glioneuronal cells were significantly reduced in comparison to the wild type (Holmström et al., 2013). In contrast, mitochondrial function was enhanced when Nrf2 was genetically constitutively upregulated via *Keap1* knockdown (Holmström et al., 2013). These responses were believed to be prompted via changes in the rate of utilisation of mitochondrial substrates (Holmström et al., 2013). This proposed mechanism

could explain the increase in the activity of mitochondrial respiratory complexes that was previously observed in fibroblasts of *parkin* patients (Mortiboys et al., 2013).

The availability of the ARE-CHO reporter cell line in-house provided a feasible tool to assess the ability of UDCA to activate Nrf2. Our results showed that UDCA treatment was associated with a statistically significant increase in ARE expression [Figure 4.5]. However, this increase (approximately twofold in comparison to the vehicle) was remarkably lower when compared to the positive control, BG12, which increased ARE expression by more than fivefold (at a concentration of 10 μ m) [Figure 4.5]. The effect of UDCA on ARE expression was comparable when the cells were treated either with 10 μ M or 100 μ M of UDCA [Figure 4.5]. The results clearly indicated that the effective UDCA dose in *parkin* patient fibroblasts, 100 nm (Mortiboys et al., 2013), would not increase ARE expression in the CHO reporter cell line. Accordingly, we decided to pursue the 10 μ m UDCA in the subsequent experiments. To confirm that UDCA activated the Nrf2 pathway, the expression of multiple Nrf2 downstream genes (*NQO1*, *GCLC* and *FTH1*) was quantified via RT-qPCR [Figure 4.11]. The positive control, BG12, increased the expression of *NQO1*, but not *GCLC* or *FTH1*. Although there are no studies investigating the effect of BG12 and UDCA on the expression of Nrf2 downstream genes in CHO cells, research shows that the response to BG12 varies across different type of cells. For example, in hippocampal cells, BG12 treatment increased the expression of both *NQO1* and *GCLC*, while it only increased the expression of *NQO1* in cortical neurons and had no effect on the expression of *GCLC* (Albrecht et al., 2012). Notably, our results showed that UDCA increased the expression of *NQO1*, which is the only gene that responded to BG12 [Figure 4.11].

Subsequently, we investigated the ability of UDCA to reduce oxidative stress in CuSO₄-stressed CHO cells using DCF assay, but no positive results were obtained [Heading 4.3]. Neither UDCA nor BG12 were able to reduce DCF readings in CuSO₄-stressed cells. Since the potent antioxidant, Trolox, also failed to decrease DCF readings, despite the trials of different concentrations, it is likely that the method used was not appropriate to assess oxidative stress. This could also explain why the initial trials of toxins known to increase oxidative stress levels, H₂O₂ and rotenone, did not demonstrate an increase in DCF readings. DCF has been widely used

as a probe for measuring oxidative stress. Nonetheless, Kalyanaraman and colleagues have critically evaluated various oxidative stress detecting probes and concluded that DCF cannot be reliably used to detect intracellular reactive oxygen species; however, it may be used as a redox indicator that responds to changes in intracellular iron/copper signalling (Kalyanaraman et al., 2012). Accordingly, the ability of UDCA to ameliorate oxidative stress should be assessed via alternative probes in future experiments, such as hydroethidine (HE) and Mito-SOX. The assessment of oxidative stress can be achieved through measuring the ROS-mediated damage to proteins, lipids, RNA and DNA, which are more stable than ROS, or via quantifying the levels of antioxidant enzymes that neutralise ROS, such as superoxide dismutase.

Further experiments showed that UDCA was unable to increase ATP levels and reduce cytotoxicity in CCCP/rotenone-stressed CHO cells, despite trials of various treatment conditions. Treating CHO cells with UDCA was only reported in one study, which investigated its effect on a glucocorticoid receptor-dependent pathway (Tanaka et al., 1996). In this study, UDCA was applied at a concentration of 100 μ M. This dose was also tested in our CHO–rotenone model, but did not show a beneficial effect. The absence of a UDCA-mediated rescue effect in CHO cells could be attributed to their inherent characteristic as hamster ovarian cells. Yet, it makes it difficult to assert that the increase in ARE expression is relevant to the rescue effect of UDCA.

7.3 Beneficial effects in stressed SH-SY5Y cells

In SH-SY5Y cells, the ability of UDCA to ameliorate toxicity was investigated initially in rotenone-stressed cells, but no positive effect was observed. Then, CCCP was applied as an alternative toxin following a treatment protocol of a recently published paper (Fonseca et al., 2017). While no rescue effect was observed with 10 μ M UDCA, the trial of 100 μ M UDCA resulted in a minor positive effect on ATP and cytotoxicity [Figure 5.3]. Further experiments showed that the application of a higher UDCA dose (300 μ M) significantly increased ATP levels and decreased cytotoxicity in CCCP-stressed cells [Figure 5.4]. Indeed, the response of cells with neuronal features, such as SH-SY5Y, to UDCA treatment is important for supporting the applicability of UDCA as a treatment for PD. However, since the SH-SY5Y cell line is a derivative of neuroblastoma, it inherently has cancerous properties that affect its metabolism and genomic

stability. Therefore, the use of primary neuron cultures would be superior, because they are more likely to represent the properties of neuronal cells. However, it is obviously extremely difficult to obtain, prepare and keep sufficient numbers of primary neurons to perform all experiments described in this project.

To tackle this limitation of the SH-SY5Y cell line, we attempted to reproduce the UDCA-mediated rescue effect in terminally differentiated SH-SY5Y cells. Although the differentiation was successful, and was associated with a significant increase in neuronal and DA markers [Figure 5.7, Figure 5.8], UDCA treatment did not ameliorate the CCCP-induced toxicity [Figure 5.15, Figure 5.16, Figure 5.17]. Possible causes for the absence of a response in differentiated SH-SY5Y cells is discussed in chapter 5.

7.4 Mechanism of action of UDCA in SH-SY5Y cells

Since UDCA increased ARE expression in CHO cells, the effect of UDCA on the Nrf2 pathway in CCCP-stressed SH-SY5Y cells was investigated first. Unlike the previously used CHO cells, the SH-SY5Y cell line in this project was not a reporter cell line and, therefore, we only looked at the expression of Nrf2 downstream genes. However, the RT-PCR results did not show an upregulation in the expression of Nrf2 genes in response to UDCA treatment or to treatment with the positive control, BG12 [Figure 5.23]. With regard to BG12, it is possible that the increase in mRNA levels was transient, and was not detectable 24 hours after the treatment. However, it has been reported that BG12 treatment (2 μm) for 24 hours increased mRNA levels of Nrf2 targets in SH-SY5Y cells (including *GCLC*, which was assessed in this project) (Jing et al., 2015). Notably, in a different study, the effect of BG12 treatment (30 μm , 24 hours) on the mRNA levels of *GCLC* in SH-SY5Y cells was particularly minor (Lin-Holderer et al., 2016), indicating that the upregulation of Nrf2 targets in response to BG12 might not be consistent in SH-SY5Y cells. In the Nrf2 - SH-SY5Y experiments, we increased the number of assessed Nrf2 genes and designed primers for five genes (*FTH1*, *GCLC*, *GST2A*, *HMOX1* and *NQO1*). Unfortunately, only three of them were specific.

Due to the lack of a response to the positive control, it is difficult to conclude that UDCA is not a Nrf2 activator in our SH-SY5Y model. Recently, Fonseca and colleagues found that the rescue

effect of TUDCA on CCCP-stressed SH-SY5Y cells was not associated with an increase in the expression of Nrf2 target genes, and did not increase nuclear translocation of Nrf2 (Fonseca et al., 2017). However, no positive control was used in the study to validate these findings. Unexpectedly, our results showed a decrease in mRNA levels of *GST2A* and *FTH1* with UDCA treatment in CCCP-stressed cells, in comparison to vehicle CCCP-stressed cells [Figure 5.23]. We postulated that UDCA activated an alternative protective pathway that decreased oxidative stress levels and, as a consequence, the expression of the Nrf2 genes. Accordingly, no further experiments related to the Nrf2 pathway were conducted.

AKT kinase is a strong candidate mediator of the UDCA rescue effect. The protective effect of UDCA has been attributed to AKT activation in various cell lines, including HepG2 cells, colon carcinoma-derived cell lines and cardiomyocytes (Arisawa et al., 2009, Hanafi et al., 2016, Im et al., 2005). More importantly, previous work in our group has shown that the UDCA-mediated rescue effect in *parkin* patient fibroblasts is dependent on AKT activation (Mortiboys et al., 2013). Indeed, the results in this project showed that UDCA significantly activated AKT in CCCP-stressed SH-SY5Y cells [Figure 6.7]. Interestingly, further experiments revealed that the inhibition of AKT eliminated the UDCA-mediated increase in ATP levels, but did not affect cytotoxicity. This finding suggests a closer relationship between the AKT and the mitochondria.

It has been previously reported that IGF induces AKT translocation into the mitochondria in SH-SY5Y cells (Bijur and Jope, 2003). Accordingly, we investigated if UDCA treatment in our SH-SY5Y cells would induce a similar response, but the results were negative [Figure 6.13]. If AKT does not directly interact with the mitochondria, this suggests that the effect of AKT on the mitochondria is indirect, via its downstream targets. Consequently, we explored the effect of UDCA treatment on selected AKT downstream targets (CREB, FOXO1, mTOR and hexokinase) to elucidate the mechanism by which UDCA exerts its rescue effect. However, none of them showed a significant response either to UDCA or to the positive control, IGF, regardless of the trail of different techniques and treatment conditions. More work is needed to verify these results and to investigate other potential AKT targets that might be involved in the mechanism of action of UDCA.

7.5 UDCA doses

In this project, the beneficial UDCA dose required in SH-SY5Y cells was higher than the beneficial dose in fibroblasts. A UDCA concentration of 100 nM significantly increased ATP levels in *parkin* fibroblasts, and an even lower concentration (10 nM) was sufficient to increase ATP levels in LRRK2 G2019S fibroblasts of PD patients and non-manifesting carriers (Mortiboys et al., 2013, Mortiboys et al., 2015). On the other hand, the rescue effect of UDCA in SH-SY5Y cells was only significant at doses higher than 100 μ M [Figure 5.4]. The application of UDCA doses in SH-SY5Y cells at micro molar scales was also reported in previous studies. For example, 100 – 200 μ M UDCA significantly increased viability and decreased ROS levels in SH-SY5Y cells stressed with sodium nitroprusside (Chun and Low, 2012). In addition, 100 μ M TUDCA was required to increase viability and ATP levels and to decrease ROS levels in CCCP and MPP⁺ stressed SH-SY5Y cells (Rosa et al., 2017, Fonseca et al., 2017). The difference in UDCA doses between fibroblasts and SH-SY5Y cells is justifiable, given the mismatch in cell type, culturing conditions and the underlying mitochondrial defect. However, it raises the question of whether high UDCA doses would be needed in humans to induce effective protection against neuronal loss.

The implication of this need is that the administration of exceedingly high UDCA doses will induce side effects and cytotoxicity in the human body. Additionally, the ingested UDCA doses and blood UDCA levels are not measures of UDCA concentrations in the CNS, due to the BBB. There is limited knowledge about the bioavailability of UDCA in the CNS. Parry and colleagues have previously reported that UDCA crosses the BBB in a dose-dependent manner (Parry et al., 2010). However, the study showed that the mean concentration in the CSF, at a dose of 15 mg/kg/day, was 86.69 nM. Increasing the dose to 50 mg/kg produced a mean CSF concentration of 191.11 nM (Parry et al., 2010). On the other hand, the UDCA serum concentration ranged between 7 and 30 μ M (Parry et al., 2010). This apparent partial permeability of the BBB implies that the rescue effect of UDCA in *in vitro* studies should be achieved at a low concentration. Only a limited number of studies have assessed the protective effect of UDCA in primary neuronal cells. In mouse cortical neurons, with small interfering RNA-mediated *parkin* knockdown, a UDCA dose of 10 pM was sufficient to restore ATP depletion (Mortiboys et al., 2013). However, in a

different study, where mouse cortical neurons were stressed with MPP+, 100 μ M TUDCA was required to restore ATP to the levels of the unstressed control (Rosa et al., 2017). More work is needed to elucidate the effective UDCA dose in neuronal models of PD.

7.6 Future work

7.6.1 Alternative AKT downstream targets

AKT has a vast number of substrates. Only a few of them were selected to be investigated in this project and did not show a significant response to UDCA treatment. Other AKT substrates that might be involved in the UDCA-mediated rescue effect are briefly reviewed below.

Apoptotic proteins

The pro-apoptotic protein BAD is directly phosphorylated by AKT (Franke et al., 2003). The phosphorylation neutralises BAD activity by facilitating its interaction with 14-3-3 proteins, allowing the anti-apoptotic factors to prevail (Aghazadeh and Papadopoulos, 2016). AKT has also been reported to phosphorylate the mouse double minute 2 homolog (MDM2) and, consequently, increase its activity and nuclear translocation (Downward, 2004). MDM2 is a potent inhibitor of the p53 protein, which is a major regulator of cell death in response to various stress conditions. p53 stimulates the expression of multiple pro-apoptotic proteins, such as BAX, NOXA, PUMA and FAS (Khoo et al., 2014). In addition, AKT phosphorylates and inhibits the pro-apoptotic protein BAX, by preventing its insertion into the mitochondria (Kale et al., 2018).

GSK3 β

GSK3 β has various vital cellular functions other than glucose metabolism, such as the regulation of cellular signalling and the regulation of cell survival and differentiation (Beurel et al., 2015). Activated AKT inhibits GSK3 β via phosphorylation. This inactivation regulates inflammatory pathways, such as the NF- κ B pathway (Zhang et al., 2014a), which has been implicated in the pathogenesis of PD (Herrero et al., 2015). The inhibition of GSK3 β decreases the release of pro-inflammatory cytokines, such as IL-6 and interferons, and increases the release of anti-inflammatory cytokines, such as IL-10 (Martin et al., 2005). Additionally, overexpression of active

GSK3 β in mitochondria has been reported to intensify the apoptotic effects of rotenone and MPP+, and reduce the activity of complex I and overall ATP production (King et al., 2008).

7.6.2 Glucocorticoid receptors

As mentioned in the introduction section, UDCA is a steroid-based molecule. In the drug screening paper published by our group, half of the positive hits in the second stage of the screen were steroids or steroid-related compounds (Mortiboys et al., 2013). Additionally, blocking the GRs (either via the application of Mifepristone or via RNA-mediated knockdown) eliminated the rescue effect of the structurally similar compound, UCA, in *parkin* fibroblasts (Mortiboys et al., 2013). The GRs act as a ligand-dependent transcription factors. When activated, GRs translocate into the nucleus and regulate the transcription of various genes in a highly cell- and context-specific manner (classical glucocorticoid pathway) (Herrero et al., 2015). GRs interact with the pro-inflammatory transcription factor activator protein 1 (AP1) and nuclear factor NF- κ B, and neutralise their activity, which is the main mechanism by which glucocorticoids alleviate inflammation (Moreira et al., 2017). Evidence shows that GRs also act via a non-genomic mechanism (non-classical pathway). This mechanism mediates a relatively more rapid response and involves various signalling pathways, such as PI3K, AKT and MAPK (Oakley and Cidlowski, 2013). The non-classical pathway is triggered by the dissociation of accessory proteins from the GRs complex upon the binding of the glucocorticoid legends. Among the released proteins is the BAG family molecular chaperone regulator 1 (BAG-1), which is involved in the regulation of apoptosis and neuronal differentiation (Shen et al., 2016, Samarasinghe et al., 2012).

7.6.3 Mitophagy pathway

Recently, Fonseca and colleagues showed that the rescue effect of TUDCA was associated with significant upregulation in autophagy and mitophagy in CCCP-stressed SH-SY5Y cells (Fonseca et al., 2017). TUDCA treatment increased the levels of full-length PINK1 in the mitochondria concomitantly with increased expression and translocation of Parkin (Fonseca et al., 2017). Importantly, 50% knockdown of *parkin* via siRNA was sufficient to abolish the positive effect of TUDCA on ATP levels (Fonseca et al., 2017). In the drug screening paper, UDCA restored ATP levels in *parkin* mutant fibroblasts (Mortiboys et al., 2013). These findings suggest that upregulation in mitophagy mediates, at least in part, the cytoprotective effect of UDCA.

7.7 Concluding remarks

The main aim of this project is to investigate the rescue effect of UDCA in the context of PD. Previous work by our group revealed that UDCA rescues mitochondrial function in *parkin* patients' fibroblasts (Mortiboys et al., 2013) [Figure 7.1]. The work presented in this project suggests that this rescue effect is not associated with an increase in mitochondrial biogenesis. Consequently, we investigated the ability of UDCA to activate the Nrf2 pathway, which is one of the most important antioxidant pathways in cells. Using an ARE reporter CHO cells, we found that UDCA induced a small dose-dependent increase in Nrf2 activation. However, this increase was not translated into a reduction in oxidative stress level in copper-stressed CHO cells. Moreover, UDCA treatment did not rescue CHO cells when they were stressed with rotenone/CCCP.

In neuronal-like cells (SH-SY5Y cells) stressed with CCCP, UDCA treatment significantly increased ATP levels and decreased cytotoxicity. This rescue effect was not associated with increased expression of Nrf2 target genes, but it was associated with a significant increase in AKT activation. Inhibition of the AKT pathway abolished the beneficial effect of UDCA on ATP. Notably, the cytotoxicity level remained unchanged, indicating that the rescue effect of UDCA is partially dependent on AKT. The effect of UDCA treatment on the phosphorylation of selected AKT downstream targets was investigated but no positive results were obtained. More work is needed to identify the AKT downstream targets that are activated/inhibited upon UDCA treatment [Figure 7.1].

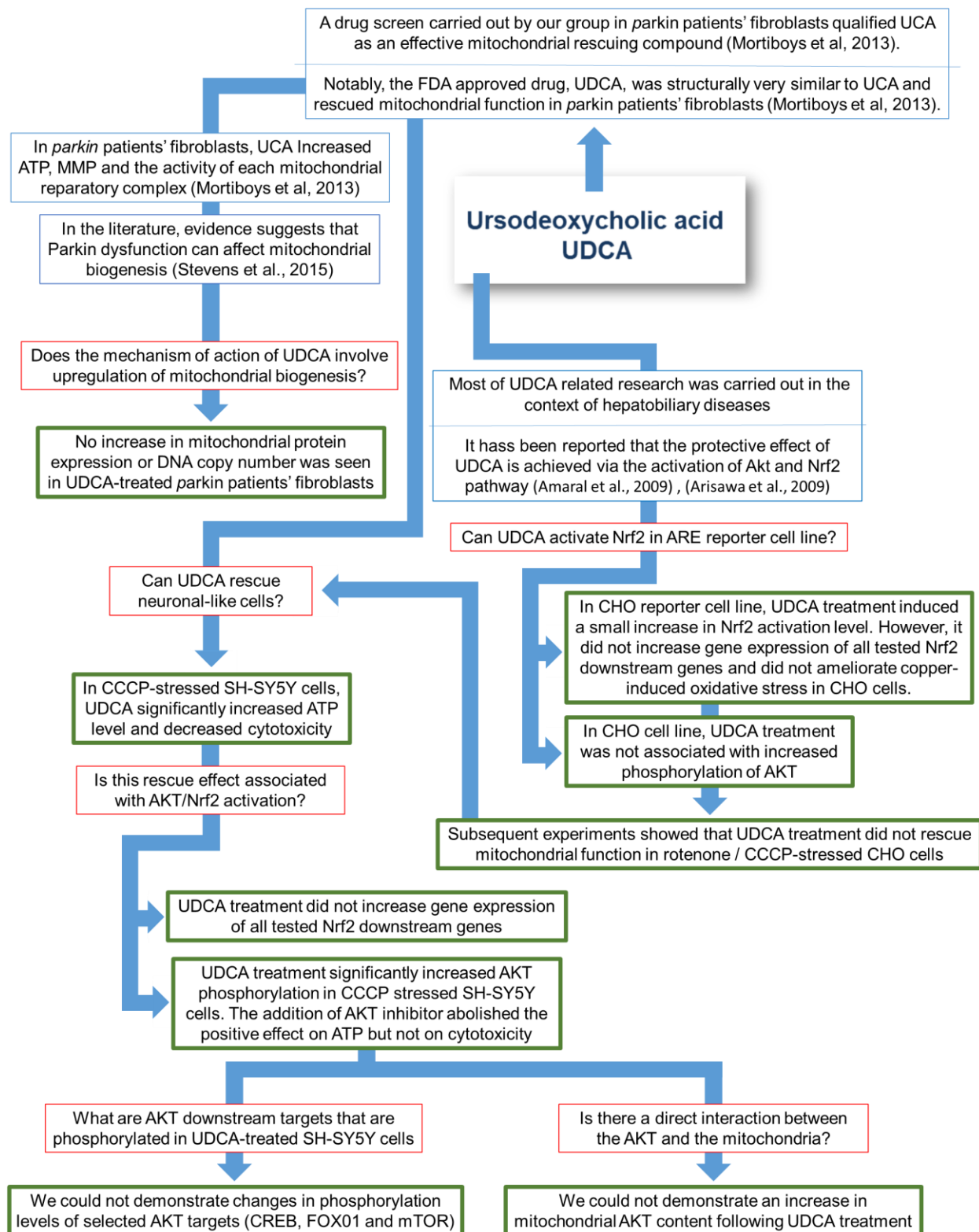


Figure 7.1 A summary of the main research questions and the main findings in this projects

The figure shows the main research questions (in red boxes) and the main findings (in green boxes) in this project. Based on the literature review and a previous work carried out by our group, upregulation in mitochondrial pathogenesis, AKT pathway and Nrf2 pathway are plausible mechanisms that mediate the cytoprotective effect of UDCA in the context of PD. The work presented in this project demonstrated that the rescue effect of UDCA is reproducible in cells of neuronal nature (SH-SY5Y cells), and that the rescue effect is partially dependant on the AKT pathway. More work is needed to identify the AKT downstream targets that are involved in this process as well as other pathways that contribute the rescue mechanism.

References:

- ABDELKADER, N. F., SAFAR, M. M. & SALEM, H. A. 2016. Ursodeoxycholic acid ameliorates apoptotic cascade in the rotenone model of Parkinson's disease: modulation of mitochondrial perturbations. *Molecular neurobiology*, 53, 810-817.
- ABDULLAH, R., BASAK, I., PATIL, K. S., ALVES, G., LARSEN, J. P. & MØLLER, S. G. 2015. Parkinson's disease and age: the obvious but largely unexplored link. *Experimental gerontology*, 68, 33-38.
- ADAM-VIZI, V. & CHINOPOULOS, C. 2006. Bioenergetics and the formation of mitochondrial reactive oxygen species. *Trends in pharmacological sciences*, 27, 639-645.
- AGHAZADEH, Y. & PAPADOPOULOS, V. 2016. The role of the 14-3-3 protein family in health, disease, and drug development. *Drug discovery today*, 21, 278-287.
- AKHMEDOV, A. T. & MARÍN-GARCÍA, J. 2015. Mitochondrial DNA maintenance: an appraisal. *Molecular and cellular biochemistry*, 1-23.
- ALBRECHT, P., BOUCHACHIA, I., GOEBELS, N., HENKE, N., HOFSTETTER, H. H., ISSBERNER, A., KOVACS, Z., LEWERENZ, J., LISAK, D. & MAHER, P. 2012. Effects of dimethyl fumarate on neuroprotection and immunomodulation. *Journal of neuroinflammation*, 9, 163.
- ALLEN, G. F., TOTH, R., JAMES, J. & GANLEY, I. G. 2013. Loss of iron triggers PINK1/Parkin-independent mitophagy. *EMBO reports*, 14, 1127-1135.
- ALMEIDA, R. G. & LYONS, D. A. 2017. On Myelinated Axon Plasticity and Neuronal Circuit Formation and Function. *Journal of Neuroscience*, 37, 10023-10034.
- AMARAL, J. D., VIANA, R. J., RAMALHO, R. M., STEER, C. J. & RODRIGUES, C. M. 2009. Bile acids: regulation of apoptosis by ursodeoxycholic acid. *Journal of lipid research*, 50, 1721-1734.
- AMBROSI, G., GHEZZI, C., SEPE, S., MILANESE, C., PAYAN-GOMEZ, C., BOMBARDIERI, C. R., ARMENTERO, M.-T., ZANGAGLIA, R., PACCHETTI, C. & MASTROBERARDINO, P. G. 2014. Bioenergetic and proteolytic defects in fibroblasts from patients with sporadic Parkinson's disease. *Biochimica et Biophysica Acta (BBA)-Molecular Basis of Disease*, 1842, 1385-1394.
- AMINZADEH, S., VIDALI, S., SPERL, W., KOFLER, B. & FEICHTINGER, R. G. 2015. Energy metabolism in neuroblastoma and Wilms tumor. *Translational pediatrics*, 4, 20.
- AO, H., KO, S. W. & ZHUO, M. J. M. P. 2006. CREB activity maintains the survival of cingulate cortical pyramidal neurons in the adult mouse brain. 2, 15.
- ARISAWA, S., ISHIDA, K., KAMEYAMA, N., UEYAMA, J., HATTORI, A., TATSUMI, Y., HAYASHI, H., YANO, M., HAYASHI, K. & KATANO, Y. 2009. Ursodeoxycholic acid induces glutathione synthesis through activation of PI3K/Akt pathway in HepG2 cells. *Biochemical pharmacology*, 77, 858-866.
- ASCHERIO, A. & SCHWARZSCHILD, M. A. 2016. The epidemiology of Parkinson's disease: risk factors and prevention. *The Lancet Neurology*, 15, 1257-1272.
- AUBURGER, G., KLINKENBERG, M., DROST, J., MARCUS, K., MORALES-GORDO, B., KUNZ, W. S., BRANDT, U., BROCCOLI, V., REICHMANN, H. & GISPERT, S. 2012. Primary skin fibroblasts as a model of Parkinson's disease. *Molecular neurobiology*, 46, 20-27.
- BABA, M., NAKAJO, S., TU, P.-H., TOMITA, T., NAKAYA, K., LEE, V., TROJANOWSKI, J. Q. & IWATSUBO, T. 1998. Aggregation of alpha-synuclein in Lewy bodies of sporadic Parkinson's disease and dementia with Lewy bodies. *The American journal of pathology*, 152, 879.
- BAE, E.-J., HO, D.-H., PARK, E., JUNG, J. W., CHO, K., HONG, J. H., LEE, H.-J., KIM, K. P. & LEE, S.-J. 2013. Lipid peroxidation product 4-hydroxy-2-nonenal promotes seeding-capable oligomer formation and cell-to-cell transfer of α -synuclein. *Antioxidants & redox signaling*, 18, 770-783.
- BARBATO, D. L., AQUILANO, K., BALDELLI, S., CANNATA, S., BERNARDINI, S., ROTILIO, G. & CIRIOLO, M. J. C. D. A. D. 2014. Proline oxidase–adipose triglyceride lipase pathway restrains adipose cell death and tissue inflammation. 21, 113.
- BARCO, A. & MARIE, H. J. M. N. 2011. Genetic approaches to investigate the role of CREB in neuronal plasticity and memory. 44, 330-349.
- BARONE, M. C., SYKIOTIS, G. P. & BOHMANN, D. 2011. Genetic activation of Nrf2 signaling is sufficient to ameliorate neurodegenerative phenotypes in a Drosophila model of Parkinson's disease. *Disease models & mechanisms*, 4, 701-707.
- BAUER, G. 2014. Targeting extracellular ROS signaling of tumor cells. *Anticancer research*, 34, 1467-1482.

- BEUREL, E., GRIECO, S. F. & JOPE, R. S. 2015. Glycogen synthase kinase-3 (GSK3): regulation, actions, and diseases. *Pharmacology & therapeutics*, 148, 114-131.
- BIEDLER, J. L., HELSON, L. & SPENGLER, B. A. 1973. Morphology and growth, tumorigenicity, and cytogenetics of human neuroblastoma cells in continuous culture. *Cancer research*, 33, 2643-2652.
- BIEDLER, J. L., ROFFLER-TARLOV, S., SCHACHNER, M. & FREEDMAN, L. S. 1978. Multiple neurotransmitter synthesis by human neuroblastoma cell lines and clones. *Cancer research*, 38, 3751-3757.
- BIJUR, G. N. & JOPE, R. S. 2003. Rapid accumulation of Akt in mitochondria following phosphatidylinositol 3-kinase activation. *Journal of neurochemistry*, 87, 1427-1435.
- BINGOL, B. & SHENG, M. 2016. Mechanisms of mitophagy: PINK1, Parkin, USP30 and beyond. *Free Radical Biology and Medicine*, 100, 210-222.
- BLAUWENDRAAT, C., KIA, D. A., PIHLSTRØM, L., GAN-OR, Z., LESAGE, S., GIBBS, J. R., DING, J., ALCALAY, R. N., HASSIN-BAER, S. & PITTMAN, A. M. 2018. Insufficient evidence for pathogenicity of SNCA His50Gln (H50Q) in Parkinson's disease. *Neurobiology of aging*, 64, 159. e5-159. e8.
- BLESA, J., TRIGO-DAMAS, I., QUIROGA-VARELA, A. & JACKSON-LEWIS, V. R. 2015. Oxidative stress and Parkinson's disease. *Frontiers in neuroanatomy*, 9.
- BLESA, J., TRIGO-DAMAS, I., QUIROGA-VARELA, A. & DEL REY, N. L. G. 2016. Animal Models of Parkinson's Disease. *Challenges in Parkinson's Disease*. InTech.
- BO, T., YAMAMORI, T., SUZUKI, M., SAKAI, Y., YAMAMOTO, K. & INANAMI, O. 2018. Calmodulin-dependent protein kinase II (CaMKII) mediates radiation-induced mitochondrial fission by regulating the phosphorylation of dynamin-related protein 1 (Drp1) at serine 616. *Biochemical and biophysical research communications*, 495, 1601-1607.
- BOCKAERT, J. & MARIN, P. J. P. R. 2015. mTOR in brain physiology and pathologies. 95, 1157-1187.
- BOLAÑOS, J. P., ALMEIDA, A. & MONCADA, S. 2010. Glycolysis: a bioenergetic or a survival pathway? *Trends in biochemical sciences*, 35, 145-149.
- BONIFATI, V., RIZZU, P., SQUITIERI, F., KRIEGER, E., VANACORE, N., VAN SWIETEN, J., BRICE, A., VAN DUJIN, C., OOSTRA, B. & MECO, G. 2003. DJ-1 (PARK7), a novel gene for autosomal recessive, early onset parkinsonism. *Neurological sciences*, 24, 159-160.
- BOSE, A. & BEAL, M. F. 2016. Mitochondrial dysfunction in Parkinson's disease. *Journal of neurochemistry*, 139, 216-231.
- BOVERIS, A. & NAVARRO, A. 2008. Brain mitochondrial dysfunction in aging. *IUBMB life*, 60, 308-314.
- BOVOLENTA, T. M., DE AZEVEDO SILVA, S. M. C., ARB SABA, R., BORGES, V., FERRAZ, H. B. & FELICIO, A. C. 2017. Systematic review and critical analysis of cost studies associated with Parkinson's disease. *Parkinson's Disease*, 2017.
- BROOKS, W., JARVIS, M. & WAGNER, G. 1989. Astrocytes as a primary locus for the conversion MPTP into MPP+. *Journal of neural transmission*, 76, 1-12.
- BRYAN, H. K., OLAYANJU, A., GOLDRING, C. E. & PARK, B. K. 2013. The Nrf2 cell defence pathway: Keap1-dependent and-independent mechanisms of regulation. *Biochemical pharmacology*, 85, 705-717.
- BUENDIA, I., MICHALSKA, P., NAVARRO, E., GAMEIRO, I., EGEA, J. & LEÓN, R. 2016. Nrf2-ARE pathway: an emerging target against oxidative stress and neuroinflammation in neurodegenerative diseases. *Pharmacology & therapeutics*, 157, 84-104.
- BURBULLA, L. F. & KRÜGER, R. 2012. The use of primary human fibroblasts for monitoring mitochondrial phenotypes in the field of Parkinson's disease. *Journal of visualized experiments: JoVE*.
- BÉLANGER, M., ALLAMAN, I. & MAGISTRETTI, P. J. 2011. Brain energy metabolism: focus on astrocyte-neuron metabolic cooperation. *Cell metabolism*, 14, 724-738.
- CABRERA-VALLADARES, G., MATSCHINSKY, F. M., WANG, J. & FERNANDEZ-MEJIA, C. 2001. Effect of retinoic acid on glucokinase activity and gene expression in neonatal and adult cultured hepatocytes. *Life sciences*, 68, 2813-2824.
- CALVO, S. E. & MOOTHA, V. K. 2010. The mitochondrial proteome and human disease. *Annual review of genomics and human genetics*, 11, 25.
- CAMILLERI, M. & GORES, G. J. 2015. Therapeutic targeting of bile acids. *American Journal of Physiology-Gastrointestinal and Liver Physiology*, 309, G209-G215.

- CAMPOLO, M., CASILI, G., BIUNDO, F., CRUPI, R., CORDARO, M., CUZZOCREA, S. & ESPOSITO, E. 2017. The neuroprotective effect of dimethyl fumarate in an MPTP-mouse model of Parkinson's disease: involvement of reactive oxygen species/nuclear factor- κ B/nuclear transcription factor related to NF-E2. *Antioxidants & redox signaling*, 27, 453-471.
- CANNING, P., SORRELL, F. J. & BULLOCK, A. N. 2015. Structural basis of Keap1 interactions with Nrf2. *Free Radical Biology and Medicine*, 88, 101-107.
- CARTELLI, D., GOLDWURM, S., CASAGRANDE, F., PEZZOLI, G. & CAPPELLETTI, G. 2012. Microtubule destabilization is shared by genetic and idiopathic Parkinson's disease patient fibroblasts. *PLoS One*, 7, e37467.
- CASTRO-CALDAS, M., CARVALHO, A. N., RODRIGUES, E., HENDERSON, C., WOLF, C., RODRIGUES, C. & GAMA, M. 2012. Tauroursodeoxycholic acid prevents MPTP-induced dopaminergic cell death in a mouse model of Parkinson's disease. *Molecular neurobiology*, 46, 475-486.
- CEDIKOVA, M., KRIPNEROVÁ, M., DVORAKOVA, J., PITULE, P., GRUNDMANOVA, M., BABUSKA, V., MULLEROVA, D. & KUNCOVA, J. 2016. Mitochondria in white, brown, and beige adipocytes. *Stem cells international*, 2016.
- CELARDO, I., MARTINS, L. & GANDHI, S. 2014. Unravelling mitochondrial pathways to Parkinson's disease. *British journal of pharmacology*, 171, 1943-1957.
- CEREGHETTI, G., STANGHERLIN, A., DE BRITO, O. M., CHANG, C., BLACKSTONE, C., BERNARDI, P. & SCORRANO, L. 2008. Dephosphorylation by calcineurin regulates translocation of Drp1 to mitochondria. *Proceedings of the National Academy of Sciences*, 105, 15803-15808.
- CHABAN, Y., BOEKEMA, E. J. & DUDKINA, N. V. 2014. Structures of mitochondrial oxidative phosphorylation supercomplexes and mechanisms for their stabilisation. *Biochimica et Biophysica Acta (BBA)-Bioenergetics*, 1837, 418-426.
- CHANG, C.-R. & BLACKSTONE, C. 2007. Cyclic AMP-dependent protein kinase phosphorylation of Drp1 regulates its GTPase activity and mitochondrial morphology. *Journal of Biological Chemistry*, 282, 21583-21587.
- CHANG, C. R. & BLACKSTONE, C. 2010. Dynamic regulation of mitochondrial fission through modification of the dynamin-related protein Drp1. *Annals of the New York Academy of Sciences*, 1201, 34-39.
- CHARTIER-HARLIN, M.-C., DACHSEL, J. C., VILARIÑO-GÜELL, C., LINCOLN, S. J., LEPRÊTRE, F., HULIHAN, M. M., KACHERGUS, J., MILNERWOOD, A. J., TAPIA, L. & SONG, M.-S. 2011. Translation initiator EIF4G1 mutations in familial Parkinson disease. *The American Journal of Human Genetics*, 89, 398-406.
- CHARTIER-HARLIN, M.-C., KACHERGUS, J., ROUMIER, C., MOUROUX, V., DOUAY, X., LINCOLN, S., LEVEQUE, C., LARVOR, L., ANDRIEUX, J. & HULIHAN, M. 2004. α -Synuclein locus duplication as a cause of familial Parkinson's disease. *The Lancet*, 364, 1167-1169.
- CHASCSA, D., CAREY, E. J. & LINDOR, K. D. 2017. Old and new treatments for primary biliary cholangitis. *Liver International*, 37, 490-499.
- CHEN, H., MCCAFFERY, J. M. & CHAN, D. C. 2007a. Mitochondrial fusion protects against neurodegeneration in the cerebellum. *Cell*, 130, 548-562.
- CHEN, H., O'REILLY, E., MCCULLOUGH, M. L., RODRIGUEZ, C., SCHWARZSCHILD, M. A., CALLE, E. E., THUN, M. J. & ASCHERIO, A. 2007b. Consumption of dairy products and risk of Parkinson's disease. *American journal of epidemiology*, 165, 998-1006.
- CHEUNG, Y.-T., LAU, W. K.-W., YU, M.-S., LAI, C. S.-W., YEUNG, S.-C., SO, K.-F. & CHANG, R. C.-C. 2009. Effects of all-trans-retinoic acid on human SH-SY5Y neuroblastoma as in vitro model in neurotoxicity research. *Neurotoxicology*, 30, 127-135.
- CHIANG, G. G. & ABRAHAM, R. T. J. J. O. B. C. 2005. Phosphorylation of mammalian target of rapamycin (mTOR) at Ser-2448 is mediated by p70S6 kinase. 280, 25485-25490.
- CHOI, K. C., KIM, S. H., HA, J. Y., KIM, S. T. & SON, J. H. J. J. O. N. 2010. A novel mTOR activating protein protects dopamine neurons against oxidative stress by repressing autophagy related cell death. 112, 366-376.
- CHOI, M. S., KIM, Y., JUNG, J. Y., YANG, S. H., LEE, T. R. & SHIN, D. W. 2013. Resveratrol induces autophagy through death-associated protein kinase 1 (DAPK1) in human dermal fibroblasts under normal culture conditions. *Experimental dermatology*, 22, 491-494.

- CHOUDHURY, J. D., KUMAR, S., MAYANK, V., MEHTA, J. & BARDALAI, D. 2012. A review on apoptosis and its different pathway. *International Journal of Biological and Pharmaceutical Research*, 3, 848-861.
- CHOWDHRY, S., ZHANG, Y., MCMAHON, M., SUTHERLAND, C., CUADRADO, A. & HAYES, J. D. 2013. Nrf2 is controlled by two distinct β -TrCP recognition motifs in its Neh6 domain, one of which can be modulated by GSK-3 activity. *Oncogene*, 32, 3765.
- CHUN, H. S. & LOW, W. C. 2012. Ursodeoxycholic acid suppresses mitochondria-dependent programmed cell death induced by sodium nitroprusside in SH-SY5Y cells. *Toxicology*, 292, 105-112.
- CIOCIOLA, A. A., COHEN, L. B., KULKARNI, P., KEFALAS, C., BUCHMAN, A., BURKE, C., CAIN, T., CONNOR, J., EHRENPREIS, E. D. & FANG, J. 2014. How drugs are developed and approved by the FDA: current process and future directions. *The American journal of gastroenterology*, 109, 620.
- CLEETER, M. W., CHAU, K.-Y., GLUCK, C., MEHTA, A., HUGHES, D. A., DUCHEN, M., WOOD, N. W., HARDY, J., COOPER, J. M. & SCHAPIRA, A. H. 2013. Glucocerebrosidase inhibition causes mitochondrial dysfunction and free radical damage. *Neurochemistry international*, 62, 1-7.
- COGLIATI, S., ENRIQUEZ, J. A. & SCORRANO, L. 2016. Mitochondrial cristae: where beauty meets functionality. *Trends in biochemical sciences*, 41, 261-273.
- COGLIATI, S., FREZZA, C., SORIANO, M. E., VARANITA, T., QUINTANA-CABRERA, R., CORRADO, M., CIPOLAT, S., COSTA, V., CASARIN, A. & GOMES, L. C. 2013. Mitochondrial cristae shape determines respiratory chain supercomplexes assembly and respiratory efficiency. *Cell*, 155, 160-171.
- COLLIER, T. J., KANAAN, N. M. & KORDOWER, J. H. 2011. Ageing as a primary risk factor for Parkinson's disease: evidence from studies of non-human primates. *Nature Reviews Neuroscience*, 12, 359.
- CONSTANTINESCU, R., ELM, J., AUINGER, P., SHARMA, S., AUGUSTINE, E. F., KHADIM, L. & KIEBURTZ, K. 2014. Malignant melanoma in early-treated Parkinson's disease: The NET-PD trial. *Movement Disorders*, 29, 263-265.
- COOKSON, M. R. 2015. LRRK2 pathways leading to neurodegeneration. *Current Neurology and neuroscience reports*, 15, 42.
- COSTA, A. L., LE BACHELIER, C., MATHIEU, L., ROTIG, A., BONEH, A., DE LONLAY, P., TARNOPOLSKY, M. A., THORBURN, D. R., BASTIN, J. & DJOUADI, F. 2014. Beneficial effects of resveratrol on respiratory chain defects in patients' fibroblasts involve estrogen receptor and estrogen-related receptor alpha signaling. *Human molecular genetics*, 23, 2106-2119.
- COUVILLION, M. T., SOTO, I. C., SHIPKOVENSKA, G. & CHURCHMAN, L. S. 2016. Synchronized mitochondrial and cytosolic translation programs. *Nature*, 533, 499.
- CREE, L., PATEL, S., PYLE, A., LYNN, S., TURNBULL, D., CHINNERY, P. & WALKER, M. 2008. Age-related decline in mitochondrial DNA copy number in isolated human pancreatic islets. *Diabetologia*, 51, 1440-1443.
- CUI, Q., LI, X. & ZHU, H. 2016. Curcumin ameliorates dopaminergic neuronal oxidative damage via activation of the Akt/Nrf2 pathway. *Molecular medicine reports*, 13, 1381-1388.
- DAS, B. C., THAPA, P., KARKI, R., DAS, S., MAHAPATRA, S., LIU, T.-C., TORREGROZA, I., WALLACE, D. P., KAMBHAMPATI, S. & VAN VELDHUIZEN, P. 2014. Retinoic acid signaling pathways in development and diseases. *Bioorganic & medicinal chemistry*, 22, 673-683.
- DAS, K., GHOSH, M., NAG, C., NANDY, S. P., BANERJEE, M., DATTA, M., DEVI, G. & CHATERJEE, G. 2010. Role of familial, environmental and occupational factors in the development of Parkinson's disease. *Neuro-degenerative diseases*, 8, 345-351.
- DASURI, K., ZHANG, L. & KELLER, J. N. 2013. Oxidative stress, neurodegeneration, and the balance of protein degradation and protein synthesis. *Free Radical Biology and Medicine*, 62, 170-185.
- DAWSON, T. M. & DAWSON, V. L. 2014. Parkin plays a role in sporadic Parkinson's disease. *Neurodegenerative Diseases*, 13, 69-71.
- DE OLIVEIRA, M. R., NABAVI, S. F., MANAYI, A., DAGLIA, M., HAJHEYDARI, Z. & NABAVI, S. M. 2016. Resveratrol and the mitochondria: from triggering the intrinsic apoptotic pathway to inducing mitochondrial biogenesis, a mechanistic view. *Biochimica et Biophysica Acta (BBA)-General Subjects*, 1860, 727-745.
- DE PAEPE, B., VANDEMEULEBROECKE, K., SMET, J., VANLANDER, A., SENECA, S., LISSENS, W., VAN HOVE, J. L., DESCHEPPER, E., BRIONES, P. & VAN COSTER, R. 2014. Effect of resveratrol on cultured skin

- fibroblasts from patients with oxidative phosphorylation defects. *Phytotherapy Research*, 28, 312-316.
- DE VOS, K. J., MOROTZ, G. M., STOICA, R., TUDOR, E. L., LAU, K.-F., ACKERLEY, S., WARLEY, A., SHAW, C. E. & MILLER, C. C. 2011. VAPB interacts with the mitochondrial protein PTPIP51 to regulate calcium homeostasis. *Human molecular genetics*, 21, 1299-1311.
- DEHAY, B., BOURDENX, M., GORRY, P., PRZEDBORSKI, S., VILA, M., HUNOT, S., SINGLETON, A., OLANOW, C. W., MERCHANT, K. M. & BEZARD, E. 2015. Targeting α -synuclein for treatment of Parkinson's disease: mechanistic and therapeutic considerations. *The Lancet Neurology*, 14, 855-866.
- DENNERLEIN, S., WANG, C. & REHLING, P. 2017. Plasticity of mitochondrial translation. *Trends in cell biology*, 27, 712-721.
- DI FONZO, A., DEKKER, M., MONTAGNA, P., BARUZZI, A., YONOVA, E., GUEDES, L. C., SZCZERBINSKA, A., ZHAO, T., DUBBEL-HULSMAN, L. & WOUTERS, C. 2009. FBXO7 mutations cause autosomal recessive, early-onset parkinsonian-pyramidal syndrome. *Neurology*, 72, 240-245.
- DI MAIO, R., BARRETT, P. J., HOFFMAN, E. K., BARRETT, C. W., ZHARIKOV, A., BORAH, A., HU, X., MCCOY, J., CHU, C. T. & BURTON, E. A. α -Synuclein binds to TOM20 and inhibits mitochondrial protein import in Parkinson's disease.
- DICKEY, A. S. & STRACK, S. 2011. PKA/AKAP1 and PP2A/B β 2 regulate neuronal morphogenesis via Drp1 phosphorylation and mitochondrial bioenergetics. *Journal of Neuroscience*, 31, 15716-15726.
- DIJKSTRA, A. A., VOORN, P., BERENDSE, H. W., GROENEWEGEN, H. J., ROZEMULLER, A. J. & BERG, W. D. 2014. Stage-dependent nigral neuronal loss in incidental Lewy body and Parkinson's disease. *Movement Disorders*, 29, 1244-1251.
- DINKOVA-KOSTOVA, A. T. & ABRAMOV, A. Y. 2015. The emerging role of Nrf2 in mitochondrial function. *Free Radical Biology and Medicine*, 88, 179-188.
- DOWNWARD, J. PI 3-kinase, Akt and cell survival. *Seminars in cell & developmental biology*, 2004. Elsevier, 177-182.
- DU, T.-T., WANG, L., DUAN, C.-L., LU, L.-L., ZHANG, J.-L., GAO, G., QIU, X.-B., WANG, X.-M. & YANG, H. 2015. GBA deficiency promotes SNCA/ α -synuclein accumulation through autophagic inhibition by inactivated PPP2A. *Autophagy*, 11, 1803-1820.
- DUVOISIN, R. 1987. History of parkinsonism. *Pharmacology & therapeutics*, 32, 1-17.
- EDVARDSON, S., CINNAMON, Y., TA-SHMA, A., SHAAG, A., YIM, Y.-I., ZENVIRT, S., JALAS, C., LESAGE, S., BRICE, A. & TARABOULOS, A. 2012. A deleterious mutation in DNAJC6 encoding the neuronal-specific clathrin-uncoating co-chaperone auxilin, is associated with juvenile parkinsonism. *PloS one*, 7, e36458.
- EFREMOV, R. G., BARADARAN, R. & SAZANOV, L. A. 2010. The architecture of respiratory complex I. *Nature*, 465, 441.
- EIJKELENBOOM, A. & BURGERING, B. M. J. N. R. M. C. B. 2013. FOXOs: signalling integrators for homeostasis maintenance. 14, 83.
- ERNSTER, L. & SCHATZ, G. 1981. Mitochondria: a historical review. *J Cell Biol*, 91, 227s-255s.
- ESPINOSA-DIEZ, C., MIGUEL, V., MENNERICH, D., KIETZMANN, T., SÁNCHEZ-PÉREZ, P., CADENAS, S. & LAMAS, S. 2015. Antioxidant responses and cellular adjustments to oxidative stress. *Redox biology*, 6, 183-197.
- ETTEMA, T. J. 2016. Evolution: mitochondria in the second act. *Nature*, 531, 39.
- FAHN, S. & COHEN, G. 1992. The oxidant stress hypothesis in Parkinson's disease: evidence supporting it. *Annals of neurology*, 32, 804-812.
- FDA. 2009. *URSO 250® / URSO Forte® (ursodiol) TABLETS* [Online]. Food and Drug Administration (FDA). Available: https://www.accessdata.fda.gov/drugsatfda_docs/label/2009/020675s017lbl.pdf [Accessed may 25, 2017].
- FERNÁNDEZ-MILLÁN, P., LÁZARO, M., CANSIZ-ARDA, Ş., GERHOLD, J. M., RAJALA, N., SCHMITZ, C.-A., SILVA-ESPIÑA, C., GIL, D., BERNADÓ, P. & VALLE, M. 2015. The hexameric structure of the human mitochondrial replicative helicase Twinkle. *Nucleic acids research*, 43, 4284-4295.
- FERREIRA, M. & MASSANO, J. 2017. An updated review of Parkinson's disease genetics and clinicopathological correlations. *Acta Neurologica Scandinavica*, 135, 273-284.

- FERRETTA, A., GABALLO, A., TANZARELLA, P., PICCOLI, C., CAPITANIO, N., NICO, B., ANNESE, T., DI PAOLA, M., DELL'AQUILA, C. & DE MARI, M. 2014. Effect of resveratrol on mitochondrial function: implications in parkin-associated familial Parkinson's disease. *Biochimica et Biophysica Acta (BBA)-Molecular Basis of Disease*, 1842, 902-915.
- FEUN, L. G., BLESSING, J. A., BARRETT, R. J. & HANJANI, P. 1993. A phase II trial of tricyclic nucleoside phosphate in patients with advanced squamous cell carcinoma of the cervix. A Gynecologic Oncology Group Study. *American journal of clinical oncology*, 16, 506-508.
- FONSECA, I., GORDINO, G., MOREIRA, S., NUNES, M. J., AZEVEDO, C., GAMA, M. J., RODRIGUES, E., RODRIGUES, C. M. P. & CASTRO-CALDAS, M. 2017. Tauroursodeoxycholic acid protects against mitochondrial dysfunction and cell death via mitophagy in human neuroblastoma cells. *Molecular neurobiology*, 54, 6107-6119.
- FORSTER, J., KÖGLSBERGER, S., TREFOIS, C., BOYD, O., BAUMURATOV, A., BUCK, L., BALLING, R. & ANTONY, P. 2016. Characterization of differentiated SH-SY5Y as neuronal screening model reveals increased oxidative vulnerability. *Journal of biomolecular screening*, 21, 496-509.
- FRANKE, T. F., HORNIK, C. P., SEGEV, L., SHOSTAK, G. A. & SUGIMOTO, C. 2003. PI3K/Akt and apoptosis: size matters. *Oncogene*, 22, 8983.
- GANDHI, S. & ABRAMOV, A. Y. 2012. Mechanism of oxidative stress in neurodegeneration. *Oxidative medicine and cellular longevity*, 2012.
- GARCIA-GIMÉNEZ, J., GIMENO, A., GONZALEZ-CABO, P., DASÍ, F., BOLINCHES-AMORÓS, A., MOLLA, B., PALAU, F. & PALLARDO, F. 2011. Differential expression of PGC-1 α and metabolic sensors suggest age-dependent induction of mitochondrial biogenesis in Friedreich ataxia fibroblasts. *PLoS One*, 6, e20666.
- GARRETT, C. R., COPPOLA, D., WENHAM, R. M., CUBITT, C. L., NEUGER, A. M., FROST, T. J., LUSH, R. M., SULLIVAN, D. M., CHENG, J. Q. & SEBTI, S. M. 2011. Phase I pharmacokinetic and pharmacodynamic study of triciribine phosphate monohydrate, a small-molecule inhibitor of AKT phosphorylation, in adult subjects with solid tumors containing activated AKT. *Investigational new drugs*, 29, 1381-1389.
- GASSER, T., MÜLLER-MYHSOK, B., WSZOLEK, Z. K., OEHLMANN, R., CALNE, D. B., BONIFATI, V., BEREZNAI, B., FABRIZIO, E., VIEREGGE, P. & HORSTMANN, R. D. 1998. A susceptibility locus for Parkinson's disease maps to chromosome 2p13. *Nature genetics*, 18, 262.
- GHARBI, S. I., ZVELEBIL, M. J., SHUTTLEWORTH, S. J., HANCOX, T., SAGHIR, N., TIMMS, J. F. & WATERFIELD, M. D. 2007. Exploring the specificity of the PI3K family inhibitor LY294002. *Biochemical Journal*, 404, 15-21.
- GLOVER, J. M. & HARRISON, S. C. 1995. Crystal structure of the heterodimeric bZIP transcription factor c-Fos-c-Jun bound to DNA. *Nature*, 373, 257.
- GOLDIE, B. J., BARNETT, M. M. & CAIRNS, M. J. 2014. BDNF and the maturation of posttranscriptional regulatory networks in human SH-SY5Y neuroblast differentiation. *Frontiers in cellular neuroscience*, 8.
- GOLDMAN, S. M. 2014. Environmental toxins and Parkinson's disease. *Annual review of pharmacology and toxicology*, 54, 141-164.
- GOLDSTEIN, D. S., SULLIVAN, P., HOLMES, C., MILLER, G. W., ALTER, S., STRONG, R., MASH, D. C., KOPIN, I. J. & SHARABI, Y. 2013. Determinants of buildup of the toxic dopamine metabolite DOPAL in Parkinson's disease. *Journal of neurochemistry*, 126, 591-603.
- GOLSON, M. L. & KAESTNER, K. H. J. D. 2016. Fox transcription factors: from development to disease. 143, 4558-4570.
- GOMES, L. C., DI BENEDETTO, G. & SCORRANO, L. 2011. During autophagy mitochondria elongate, are spared from degradation and sustain cell viability. *Nature cell biology*, 13, 589.
- GONG, L., ZHANG, Q. L., ZHANG, N., HUA, W. Y., HUANG, Y. X., DI, P. W., HUANG, T., XU, X. S., LIU, C. F. & HU, L. F. 2012. Neuroprotection by urate on 6-OHDA-lesioned rat model of Parkinson's disease: linking to Akt/GSK 3 β signaling pathway. *Journal of neurochemistry*, 123, 876-885.
- GORELL, J. M., PETERSON, E. L., RYBICKI, B. A. & JOHNSON, C. C. 2004. Multiple risk factors for Parkinson's disease. *Journal of the neurological sciences*, 217, 169-174.

- GREENE, L. A., LEVY, O. & MALAGELADA, C. 2011. Akt as a victim, villain and potential hero in Parkinson's disease pathophysiology and treatment. *Cellular and molecular neurobiology*, 31, 969-978.
- GRÜNEWALD, A., ARNS, B., MEIER, B., BROCKMANN, K., TADIC, V. & KLEIN, C. 2014a. Does uncoupling protein 2 expression qualify as marker of disease status in LRRK2-associated Parkinson's disease? *Antioxidants & redox signaling*, 20, 1955-1960.
- GRÜNEWALD, A., ARNS, B., MEIER, B., BROCKMANN, K., TADIC, V. & KLEIN, C. 2014b. Does uncoupling protein 2 expression qualify as marker of disease status in LRRK2-associated Parkinson's disease? : Mary Ann Liebert, Inc. 140 Huguenot Street, 3rd Floor New Rochelle, NY 10801 USA.
- GUINEY, S. J., ADLARD, P. A., BUSH, A. I., FINKELSTEIN, D. I. & AYTON, S. 2017. Ferroptosis and cell death mechanisms in Parkinson's disease. *Neurochemistry international*, 104, 34-48.
- GUSTAFSSON, C. M., FALKENBERG, M. & LARSSON, N.-G. 2016. Maintenance and expression of mammalian mitochondrial DNA. *Annual review of biochemistry*, 85, 133-160.
- HADDAD, D. & NAKAMURA, K. 2015. Understanding the susceptibility of dopamine neurons to mitochondrial stressors in Parkinson's disease. *FEBS letters*, 589, 3702-3713.
- HALLIDAY, G., LEES, A. & STERN, M. 2011. Milestones in Parkinson's disease—clinical and pathologic features. *Movement Disorders*, 26, 1015-1021.
- HAM, S., LEE, Y.-I., JO, M., KIM, H., KANG, H., JO, A., LEE, G. H., MO, Y. J., PARK, S. C. & LEE, Y. S. J. S. R. 2017. Hydrocortisone-induced parkin prevents dopaminergic cell death via CREB pathway in Parkinson's disease model. 7, 525.
- HAMANAKA, R. B. & CHANDEL, N. S. 2010. Mitochondrial reactive oxygen species regulate cellular signaling and dictate biological outcomes. *Trends in biochemical sciences*, 35, 505-513.
- HANADA, M., FENG, J. & HEMMING, B. A. 2004. Structure, regulation and function of PKB/AKT—a major therapeutic target. *Biochimica et Biophysica Acta (BBA)-Proteins and Proteomics*, 1697, 3-16.
- HANAFI, N., MOHAMED, A., MD NOOR, J., ABDUL HAMID HASANI, N., SIRAN, R., OSMAN, N., AB RAHIM, S. & KADIR, S. H. S. A. 2016. Ursodeoxycholic acid upregulates ERK and Akt in the protection of cardiomyocytes against CoCl₂. *Genetics and Molecular Research*, 15.
- HAPGOOD, J. P., AVENANT, C. & MOLIKI, J. M. 2016. Glucocorticoid-independent modulation of GR activity: Implications for immunotherapy. *Pharmacology & therapeutics*, 165, 93-113.
- HARBAUER, A. B., ZAHEDI, R. P., SICKMANN, A., PFANNER, N. & MEISINGER, C. 2014. The protein import machinery of mitochondria—a regulatory hub in metabolism, stress, and disease. *Cell metabolism*, 19, 357-372.
- HARTMANN, A., HUNOT, S., MICHEL, P. P., MURIEL, M.-P., VYAS, S., FAUCHEUX, B. A., MOUATT-PRIGENT, A., TURMEL, H., SRINIVASAN, A. & RUBERG, M. 2000. Caspase-3: a vulnerability factor and final effector in apoptotic death of dopaminergic neurons in Parkinson's disease. *Proceedings of the National Academy of Sciences*, 97, 2875-2880.
- HASEGAWA, E., TAKESHIGE, K., OISHI, T., MURAI, Y. & MINAKAMI, S. 1990. 1-Methyl-4-phenylpyridinium (MPP+) induces NADH-dependent superoxide formation and enhances NADH-dependent lipid peroxidation in bovine heart submitochondrial particles. *Biochemical and biophysical research communications*, 170, 1049-1055.
- HASHEMI, S. H., LI, J.-Y., AHLMAN, H. & DAHLSTRÖM, A. 2003. SSR 2 (a) Receptor Expression and Adrenergic/Cholinergic Characteristics in Differentiated SH-SY5Y Cells. *Neurochemical research*, 28, 449-460.
- HASS, D. T. & BARNSTABLE, C. J. 2016. Uncoupling protein 2 in the glial response to stress: implications for neuroprotection. *Neural regeneration research*, 11, 1197.
- HATTORI, M. & GOUAUX, E. 2012. Molecular mechanism of ATP binding and ion channel activation in P2X receptors. *Nature*, 485, 207.
- HAYLETT, W., SWART, C., VAN DER WESTHUIZEN, F., VAN DYK, H., VAN DER MERWE, L., VAN DER MERWE, C., LOOS, B., CARR, J., KINNEAR, C. & BARDIEN, S. 2016. Altered mitochondrial respiration and other features of mitochondrial function in Parkin-mutant fibroblasts from Parkinson's disease patients. *Parkinson's Disease*, 2016.
- HEALY, D. G., FALCHI, M., O'SULLIVAN, S. S., BONIFATI, V., DURR, A., BRESSMAN, S., BRICE, A., AASLY, J., ZABETIAN, C. P. & GOLDWURM, S. 2008. Phenotype, genotype, and worldwide genetic

- penetrance of LRRK2-associated Parkinson's disease: a case-control study. *The Lancet Neurology*, 7, 583-590.
- HELLEY, M. P., PINNELL, J., SPORTELLI, C. & TIEU, K. 2017. Mitochondria: a common target for genetic mutations and environmental toxicants in Parkinson's disease. *Frontiers in genetics*, 8.
- HERRERO, M.-T., ESTRADA, C., MAATOUK, L. & VYAS, S. 2015. Inflammation in Parkinson's disease: role of glucocorticoids. *Frontiers in neuroanatomy*, 9, 32.
- HERS, I., VINCENT, E. E. & TAVARÉ, J. M. 2011. Akt signalling in health and disease. *Cellular signalling*, 23, 1515-1527.
- HICKS, A. A., PÉTURSSON, H., JÓNSSON, T., STEFÁNSSON, H., JÓHANNSDÓTTIR, H. S., SAINZ, J., FRIGGE, M. L., KONG, A., GULCHER, J. R. & STEFANSSON, K. 2002. A susceptibility gene for late-onset idiopathic Parkinson's disease. *Annals of Neurology: Official Journal of the American Neurological Association and the Child Neurology Society*, 52, 549-555.
- HIKIAMI, R., YAMASHITA, H., KOITA, N., JINGAMI, N., SAWAMOTO, N., FURUKAWA, K., KAWAI, H., TERASHIMA, T., OKA, N. & HASHIGUCHI, A. 2018. Charcot-Marie-Tooth disease type 2A with an autosomal-recessive inheritance: the first report of an adult-onset disease. *Journal of human genetics*, 63, 89.
- HINDLE, J. V. 2010. Ageing, neurodegeneration and Parkinson's disease. *Age and ageing*, 39, 156-161.
- HOFFMAN, K., HOLMES, F. A., FRASCHINI, G., ESPARZA, L., FRYE, D., RABER, M. N., NEWMAN, R. A. & HORTOBAGYI, G. N. 1995. Phase I-II study: tricyclic nucleoside phosphate for metastatic breast cancer. *Cancer chemotherapy and pharmacology*, 37, 254-258.
- HOFMANN, A. F. & HAGEY, L. R. 2014. Key discoveries in bile acid chemistry and biology and their clinical applications: history of the last eight decades. *Journal of lipid research*, 55, 1553-1595.
- HOLMSTRÖM, K. M., BAIRD, L., ZHANG, Y., HARGREAVES, I., CHALASANI, A., LAND, J. M., STANYER, L., YAMAMOTO, M., DINKOVA-KOSTOVA, A. T. & ABRAMOV, A. Y. 2013. Nrf2 impacts cellular bioenergetics by controlling substrate availability for mitochondrial respiration. *Biology open*, 2, 761-770.
- HUANG, Y., LI, W., SU, Z.-Y. & KONG, A.-N. T. 2015. The complexity of the Nrf2 pathway: beyond the antioxidant response. *The Journal of nutritional biochemistry*, 26, 1401-1413.
- HWANG, I., OH, H., SANTO, E., KIM, D. Y., CHEN, J. W., BRONSON, R. T., LOCASALE, J. W., NA, Y., LEE, J. & REED, S. J. A. C. 2018. FOXO protects against age-progressive axonal degeneration. 17, e12701.
- IKEGAMI, T. & MATSUZAKI, Y. 2008. Ursodeoxycholic acid: mechanism of action and novel clinical applications. *Hepatology Research*, 38, 123-131.
- IKEMOTO, S., YANG, C. & TAN, A. 2015. Basal ganglia circuit loops, dopamine and motivation: a review and enquiry. *Behavioural brain research*, 290, 17-31.
- IM, E., AKARE, S., POWELL, A. & MARTINEZ, J. D. 2005. Ursodeoxycholic acid can suppress deoxycholic acid-induced apoptosis by stimulating Akt/PKB-dependent survival signaling. *Nutrition and cancer*, 51, 110-116.
- INOKI, K., LI, Y., ZHU, T., WU, J. & GUAN, K.-L. J. N. C. B. 2002. TSC2 is phosphorylated and inhibited by Akt and suppresses mTOR signalling. 4, 648.
- IRWIN, D. M. & TAN, H. J. M. P. A. E. 2014. Evolution of glucose utilization: glucokinase and glucokinase regulator protein. 70, 195-203.
- ITOH, K., WAKABAYASHI, N., KATOH, Y., ISHII, T., IGARASHI, K., ENGEL, J. D. & YAMAMOTO, M. 1999. Keap1 represses nuclear activation of antioxidant responsive elements by Nrf2 through binding to the amino-terminal Neh2 domain. *Genes & development*, 13, 76-86.
- JAGMAG, S. A., TRIPATHI, N., SHUKLA, S. D., MAITI, S. & KHURANA, S. 2016. Evaluation of models of Parkinson's disease. *Frontiers in neuroscience*, 9, 503.
- JAKEL, R. J., TOWNSEND, J. A., KRAFT, A. D. & JOHNSON, J. A. 2007. Nrf2-mediated protection against 6-hydroxydopamine. *Brain research*, 1144, 192-201.
- JANG, Y. & JUNG, J. H. 2017. Direct conversion from skin fibroblasts to functional dopaminergic neurons for biomedical application. *Biomedical Dermatology*, 1, 4.
- JAVITCH, J. A., D'AMATO, R. J., STRITTMATTER, S. M. & SNYDER, S. H. 1985. Parkinsonism-inducing neurotoxin, N-methyl-4-phenyl-1, 2, 3, 6-tetrahydropyridine: uptake of the metabolite N-methyl-

- 4-phenylpyridine by dopamine neurons explains selective toxicity. *Proceedings of the National Academy of Sciences*, 82, 2173-2177.
- JIANG, W., JU, C., JIANG, H. & ZHANG, D. 2014. Dairy foods intake and risk of Parkinson's disease: a dose-response meta-analysis of prospective cohort studies. Springer.
- JING, X., SHI, H., ZHANG, C., REN, M., HAN, M., WEI, X., ZHANG, X. & LOU, H. 2015. Dimethyl fumarate attenuates 6-OHDA-induced neurotoxicity in SH-SY5Y cells and in animal model of Parkinson's disease by enhancing Nrf2 activity. *Neuroscience*, 286, 131-140.
- JOHANNESSEN, M., DELGHANDI, M. P. & MOENS, U. J. C. S. 2004. What turns CREB on? 16, 1211-1227.
- JOMOVA, K., BAROS, S. & VALKO, M. 2012. Redox active metal-induced oxidative stress in biological systems. *Transition Metal Chemistry*, 37, 127-134.
- JOZEFCAK, M., REMANS, T., VANGRONSVELD, J. & CUYPERS, A. 2012. Glutathione is a key player in metal-induced oxidative stress defenses. *International journal of molecular sciences*, 13, 3145-3175.
- KALE, J., KUTUK, O., BRITO, G. C., ANDREWS, T. S., LEBER, B., LETAI, A. & ANDREWS, D. W. 2018. Phosphorylation switches Bax from promoting to inhibiting apoptosis thereby increasing drug resistance. *EMBO reports*, e45235.
- KALINDERI, K., BOSTANTJOPOULOU, S. & FIDANI, L. 2016. The genetic background of Parkinson's disease: current progress and future prospects. *Acta Neurologica Scandinavica*, 134, 314-326.
- KALYANARAMAN, B., DARLEY-USMAR, V., DAVIES, K. J., DENNERY, P. A., FORMAN, H. J., GRISHAM, M. B., MANN, G. E., MOORE, K., ROBERTS II, L. J. & ISCHIROPOULOS, H. 2012. Measuring reactive oxygen and nitrogen species with fluorescent probes: challenges and limitations. *Free Radical Biology and Medicine*, 52, 1-6.
- KANDEL, E. R. J. M. B. 2012. The molecular biology of memory: cAMP, PKA, CRE, CREB-1, CREB-2, and CPEB. 5, 14.
- KANE, M. S., PARIS, A., CODRON, P., CASSEREAU, J., PROCACCIO, V., LENAERS, G., REYNIER, P. & CHEVROLLIER, A. 2017. Current mechanistic insights into the CCCP-induced cell survival response. *Biochemical pharmacology*.
- KANG, K. A., LEE, K. H., CHAE, S., ZHANG, R., JUNG, M. S., HAM, Y. M., BAIK, J. S., LEE, N. H. & HYUN, J. W. 2006. Cytoprotective effect of phloroglucinol on oxidative stress induced cell damage via catalase activation. *Journal of cellular biochemistry*, 97, 609-620.
- KANG, U. B. & MARTO, J. A. 2017. Leucine-rich repeat kinase 2 and Parkinson's disease. *Proteomics*, 17.
- KANG, Y., LU, M. & GUAN, K. J. C. D. A. D. 2011. The TSC1 and TSC2 tumor suppressors are required for proper ER stress response and protect cells from ER stress-induced apoptosis. 18, 133.
- KARIN, M., TAKAHASHI, T., KAPAH, P., DELHASE, M., CHEN, Y., MAKRI, C., ROTHWART, D., BAUD, V., NATOLI, G. & GUIDO, F. 2001. Oxidative stress and gene expression: The AP-1 and NF- κ B connections. *Biofactors*, 15, 87-89.
- KARLSSON, M., KURZ, T., BRUNK, U. T., NILSSON, S. E. & FRENNESSON, C. I. 2010. What does the commonly used DCF test for oxidative stress really show? *Biochemical Journal*, 428, 183-190.
- KASHATUS, J. A., NASCIMENTO, A., MYERS, L. J., SHER, A., BYRNE, F. L., HOEHN, K. L., COUNTER, C. M. & KASHATUS, D. F. 2015. Erk2 phosphorylation of Drp1 promotes mitochondrial fission and MAPK-driven tumor growth. *Molecular cell*, 57, 537-551.
- KASPAR, J. W. & JAISWAL, A. K. 2010. An autoregulatory loop between Nrf2 and Cul3-Rbx1 controls their cellular abundance. *Journal of Biological Chemistry*, 285, 21349-21358.
- KATOH, Y., ITOH, K., YOSHIDA, E., MIYAGISHI, M., FUKAMIZU, A. & YAMAMOTO, M. 2001. Two domains of Nrf2 cooperatively bind CBP, a CREB binding protein, and synergistically activate transcription. *Genes to Cells*, 6, 857-868.
- KERINS, M. J. & OOI, A. 2017. The roles of NRF2 in modulating cellular iron homeostasis. *Antioxidants & redox signaling*.
- KEUM, Y.-S., YU, S., CHANG, P. P.-J., YUAN, X., KIM, J.-H., XU, C., HAN, J., AGARWAL, A. & KONG, A.-N. T. 2006. Mechanism of action of sulforaphane: inhibition of p38 mitogen-activated protein kinase isoforms contributing to the induction of antioxidant response element-mediated heme oxygenase-1 in human hepatoma HepG2 cells. *Cancer research*, 66, 8804-8813.
- KHOO, K. H., VERMA, C. S. & LANE, D. P. 2014. Drugging the p53 pathway: understanding the route to clinical efficacy. *Nature reviews Drug discovery*, 13, 217-236.

- KIM, G. H., KIM, J. E., RHIE, S. J. & YOON, S. 2015. The role of oxidative stress in neurodegenerative diseases. *Experimental neurobiology*, 24, 325-340.
- KIM, I., RODRIGUEZ-ENRIQUEZ, S. & LEMASTERS, J. J. 2007. Selective degradation of mitochondria by mitophagy. *Archives of biochemistry and biophysics*, 462, 245-253.
- KIM, S. R., CHEN, X., OO, T. F., KAREVA, T., YARYGINA, O., WANG, C., DURING, M., KHOLODILOV, N. & BURKE, R. E. 2011. Dopaminergic pathway reconstruction by Akt/Rheb-induced axon regeneration. *Annals of neurology*, 70, 110-120.
- KIM, S. R., KAREVA, T., YARYGINA, O., KHOLODILOV, N. & BURKE, R. E. J. M. T. 2012. AAV transduction of dopamine neurons with constitutively active Rheb protects from neurodegeneration and mediates axon regrowth. 20, 275-286.
- KING, T. D., CLODFELDER-MILLER, B., BARKSDALE, K. A. & BIJUR, G. N. 2008. Unregulated mitochondrial GSK3 β activity results in NADH: Ubiquinone oxidoreductase deficiency. *Neurotoxicity research*, 14, 367-382.
- KIRAZ, Y., ADAN, A., YANDIM, M. K. & BARAN, Y. 2016. Major apoptotic mechanisms and genes involved in apoptosis. *Tumor Biology*, 37, 8471-8486.
- KITADA, T., ASAKAWA, S., HATTORI, N., MATSUMINE, H., YAMAMURA, Y., MINOSHIMA, S., YOKOCHI, M., MIZUNO, Y. & SHIMIZU, N. 1998. Mutations in the parkin gene cause autosomal recessive juvenile parkinsonism. *Nature*, 392, 605.
- KOOPMAN, W. J., DISTELMAIER, F., SMEITINK, J. A. & WILLEMS, P. H. 2013. OXPHOS mutations and neurodegeneration. *The EMBO journal*, 32, 9-29.
- KORECKA, J. A., VAN KESTEREN, R. E., BLAAS, E., SPITZER, S. O., KAMSTRA, J. H., SMIT, A. B., SWAAB, D. F., VERHAAGEN, J. & BOSSERS, K. 2013. Phenotypic characterization of retinoic acid differentiated SH-SY5Y cells by transcriptional profiling. *PloS one*, 8, e63862.
- KREBS, C. E., KARKHEIRAN, S., POWELL, J. C., CAO, M., MAKAROV, V., DARVISH, H., DI PAOLO, G., WALKER, R. H., SHAHIDI, G. A. & BUXBAUM, J. D. 2013. The Sac1 domain of SYNJ1 identified mutated in a family with early-onset progressive Parkinsonism with generalized seizures. *Human mutation*, 34, 1200-1207.
- KRIGE, D., CARROLL, M. T., COOPER, J. M., MARSDEN, C. D., SCHAPIRA, A. H. & GROUP), R. K. Q. P. D. R. 1992. Platelet mitochondria function in Parkinson's disease. *Annals of neurology*, 32, 782-788.
- KRISHNA, A., BIRYUKOV, M., TREFOIS, C., ANTONY, P. M., HUSSONG, R., LIN, J., HEINÄNIEMI, M., GLUSMAN, G., KÖGLSBERGER, S. & BOYD, O. 2014. Systems genomics evaluation of the SH-SY5Y neuroblastoma cell line as a model for Parkinson's disease. *BMC genomics*, 15, 1154.
- KUKAT, C. & LARSSON, N.-G. 2013. mtDNA makes a U-turn for the mitochondrial nucleoid. *Trends in cell biology*, 23, 457-463.
- KUMARAN, R. & COOKSON, M. R. 2015. Pathways to Parkinsonism Redux: convergent pathobiological mechanisms in genetics of Parkinson's disease. *Human molecular genetics*, ddv236.
- KUNZLER, A., ZEIDÁN-CHULIÁ, F., GASPAROTTO, J., GIRARDI, C. S., KLAFKE, K., PETIZ, L. L., BORTOLIN, R. C., ROSTIROLLA, D. C., ZANOTTO-FILHO, A. & DE BITTENCOURT PASQUALI, M. A. 2017. Changes in cell cycle and up-regulation of neuronal markers during SH-SY5Y neurodifferentiation by retinoic acid are mediated by reactive species production and oxidative stress. *Molecular neurobiology*, 54, 6903-6916.
- KURODA, Y., MITSUI, T., KUNISHIGE, M., SHONO, M., AKAIKE, M., AZUMA, H. & MATSUMOTO, T. 2006. Parkin enhances mitochondrial biogenesis in proliferating cells. *Human molecular genetics*, 15, 883-895.
- KÖSEL, S., EGENSPERGER, R., VON EITZEN, U., MEHRAEIN, P. & GRAEBER, M. B. 1997. On the question of apoptosis in the parkinsonian substantia nigra. *Acta neuropathologica*, 93, 105-108.
- KÜHLBRANDT, W. 2015. Structure and function of mitochondrial membrane protein complexes. *BMC biology*, 13, 89.
- LANGSTON, J. W., BALLARD, P., TETRUD, J. W. & IRWIN, I. 1983. Chronic Parkinsonism in humans due to a product of meperidine-analog synthesis. *Science*, 219, 979-980.
- LASTRES-BECKER, I., GARCÍA-YAGÜE, A. J., SCANNEVIN, R. H., CASAREJOS, M. J., KÜGLER, S., RÁBANO, A. & CUADRADO, A. 2016. Repurposing the NRF2 Activator Dimethyl Fumarate as Therapy Against Synucleinopathy in Parkinson's Disease. *Antioxidants & redox signaling*.

- LE GALLO, M., POISSONNIER, A., BLANCO, P. & LEGEMBRE, P. 2017. CD95/Fas, non-apoptotic signaling pathways, and kinases. *Frontiers in immunology*, 8, 1216.
- LEE, B., CAO, R., CHOI, Y. S., CHO, H. Y., RHEE, A. D., HAH, C. K., HOYT, K. R. & OBRIETAN, K. J. J. O. N. 2009. The CREB/CRE transcriptional pathway: protection against oxidative stress-mediated neuronal cell death. 108, 1251-1265.
- LEE, L.-S., CHOI, E.-J., KIM, C.-H., SUNG, J.-M., KIM, Y.-B., SEO, D.-H., CHOI, H.-W., CHOI, Y.-S., KUM, J.-S. & PARK, J.-D. 2016. Contribution of flavonoids to the antioxidant properties of common and tartary buckwheat. *Journal of Cereal Science*, 68, 181-186.
- LEMARIE, A. & GRIMM, S. 2011. Mitochondrial respiratory chain complexes: apoptosis sensors mutated in cancer? *Oncogene*, 30, 3985.
- LEROY, E., BOYER, R., AUBURGER, G., LEUBE, B., ULM, G., MEZEY, E., HARTA, G., BROWNSTEIN, M. J., JONNALAGADA, S. & CHERNOVA, T. 1998. The ubiquitin pathway in Parkinson's disease. *Nature*, 395, 451.
- LESAGE, S., DÜRR, A., TAZIR, M., LOHMANN, E., LEUTENEGGER, A.-L., JANIN, S., POLLAK, P. & BRICE, A. 2006. LRRK2 G2019S as a cause of Parkinson's disease in North African Arabs. *New England Journal of Medicine*, 354, 422-423.
- LEV, N., MELAMED, E. & OFFEN, D. 2003. Apoptosis and Parkinson's disease. *Progress in Neuro-Psychopharmacology and Biological Psychiatry*, 27, 245-250.
- LI, N., RAGHEB, K., LAWLER, G., STURGIS, J., RAJWA, B., MELENDEZ, J. A. & ROBINSON, J. P. 2003. Mitochondrial complex I inhibitor rotenone induces apoptosis through enhancing mitochondrial reactive oxygen species production. *Journal of Biological Chemistry*, 278, 8516-8525.
- LI, X., LI, W., LIU, G., SHEN, X. & TANG, Y. 2015. Association between cigarette smoking and Parkinson's disease: a meta-analysis. *Archives of gerontology and geriatrics*, 61, 510-516.
- LIESA, M. & SHIRIHAI, O. S. 2013. Mitochondrial dynamics in the regulation of nutrient utilization and energy expenditure. *Cell metabolism*, 17, 491-506.
- LIN, M. T. & BEAL, M. F. 2006. Mitochondrial dysfunction and oxidative stress in neurodegenerative diseases. *Nature*, 443, 787-795.
- LIN-HOLDERER, J., LI, L., GRUNEBERG, D., MARTI, H. H. & KUNZE, R. 2016. Fumaric acid esters promote neuronal survival upon ischemic stress through activation of the Nrf2 but not HIF-1 signaling pathway. *Neuropharmacology*, 105, 228-240.
- LINKER, R. A., LEE, D.-H., RYAN, S., VAN DAM, A. M., CONRAD, R., BISTA, P., ZENG, W., HRONOWSKY, X., BUKO, A. & CHOLLATE, S. 2011. Fumaric acid esters exert neuroprotective effects in neuroinflammation via activation of the Nrf2 antioxidant pathway. *Brain*, 134, 678-692.
- LIOCHEV, S. I. 2013. Reactive oxygen species and the free radical theory of aging. *Free Radical Biology and Medicine*, 60, 1-4.
- LIU, P., BEGLEY, M., MICHOWSKI, W., INUZUKA, H., GINZBERG, M., GAO, D., TSOU, P., GAN, W., PAPA, A. & KIM, B. M. 2014. Cell-cycle-regulated activation of Akt kinase by phosphorylation at its carboxyl terminus. *Nature*, 508, 541.
- LIU, W., WANG, B., WANG, T., LIU, X., HE, X., LIU, Y., LI, Z. & ZENG, H. 2016. Ursodeoxycholic Acid Attenuates Acute Aortic Dissection Formation in Angiotensin II-Infused Apolipoprotein E-Deficient Mice Associated with Reduced ROS and Increased Nrf2 Levels. *Cellular Physiology and Biochemistry*, 38, 1391-1405.
- LOFRUMENTO, D. D., NICOLARDI, G., CIANCIULLI, A., NUCCIO, F. D., PESA, V. L., CAROFIGLIO, V., DRAGONE, T., CALVELLO, R. & PANARO, M. A. 2014. Neuroprotective effects of resveratrol in an MPTP mouse model of Parkinson's-like disease: possible role of SOCS-1 in reducing pro-inflammatory responses. *Innate immunity*, 20, 249-260.
- LOPES, F. M., DA MOTTA, L. L., DE BASTIANI, M. A., PFAFFENSELLER, B., AGUIAR, B. W., DE SOUZA, L. F., ZANATTA, G., VARGAS, D. M., SCHÖNHOFEN, P. & LONDERO, G. F. 2017. RA differentiation enhances dopaminergic features, changes redox parameters, and increases dopamine transporter dependency in 6-hydroxydopamine-induced neurotoxicity in SH-SY5Y cells. *Neurotoxicity research*, 31, 545-559.
- LOPES, F. M., SCHRÖDER, R., DA FROTA JÚNIOR, M. L. C., ZANOTTO-FILHO, A., MÜLLER, C. B., PIRES, A. S., MEURER, R. T., COLPO, G. D., GELAIN, D. P. & KAPCZINSKI, F. 2010. Comparison between

- proliferative and neuron-like SH-SY5Y cells as an in vitro model for Parkinson disease studies. *Brain research*, 1337, 85-94.
- LOPEZ, J. & TAIT, S. 2015. Mitochondrial apoptosis: killing cancer using the enemy within. *British journal of cancer*, 112, 957.
- LOW, V., BEN-SHLOMO, Y., COWARD, E., FLETCHER, S., WALKER, R. & CLARKE, C. E. 2015. Measuring the burden and mortality of hospitalisation in Parkinson's disease: a cross-sectional analysis of the English Hospital Episodes Statistics database 2009–2013. *Parkinsonism & related disorders*, 21, 449-454.
- LUSHCHAK, V. 2015. Free radicals, reactive oxygen species, oxidative stresses and their classifications. *The Ukrainian Biochemical Journal*, 11-18.
- MACLEOD, A. D., TAYLOR, K. S. & COUNSELL, C. E. 2014. Mortality in Parkinson's disease: A systematic review and meta-analysis. *Movement Disorders*, 29, 1615-1622.
- MACVICAR, T. & LANGER, T. 2016. OPA1 processing in cell death and disease—the long and short of it. *J Cell Sci*, 129, 2297-2306.
- MACVICAR, T. D. & LANE, J. D. 2014. Impaired OMA1 dependent OPA1 cleavage and reduced DRP1 fission activity combine to prevent mitophagy in OXPHOS dependent cells. *J Cell Sci*, jcs. 144337.
- MAES, M., VANHAECKE, T., COGLIATI, B., YANGUAS, S. C., WILLEBRORDS, J., ROGIERS, V. & VINKEN, M. 2015. Measurement of apoptotic and necrotic cell death in primary hepatocyte cultures. *Protocols in In Vitro Hepatocyte Research*. Springer.
- MAK, Y. T., LAM, W. P., LÜ, L., WONG, Y. W. & YEWE, D. T. 2010. The toxic effect of ketamine on SH-SY5Y neuroblastoma cell line and human neuron. *Microscopy research and technique*, 73, 195-201.
- MALAGELADA, C., JIN, Z. H. & GREENE, L. A. 2008. RTP801 is induced in Parkinson's disease and mediates neuron death by inhibiting Akt phosphorylation/activation. *Journal of Neuroscience*, 28, 14363-14371.
- MANN, V., COOPER, J., KRIGE, D., DANIEL, S., SCHAPIRA, A. & MARSDEN, C. 1992. Brain, skeletal muscle and platelet homogenate mitochondrial function in Parkinson's disease. *Brain*, 115, 333-342.
- MANNING, B. D. & TOKER, A. 2017. AKT/PKB signaling: navigating the network. *Cell*, 169, 381-405.
- MARAGANORE, D. M., DE ANDRADE, M., ELBAZ, A., FARRER, M. J., IOANNIDIS, J. P., KRÜGER, R., ROCCA, W. A., SCHNEIDER, N. K., LESNICK, T. G. & LINCOLN, S. J. 2006. Collaborative analysis of α -synuclein gene promoter variability and Parkinson disease. *Jama*, 296, 661-670.
- MARK, M., BROUWER, M., KROMHOUT, H., NIJSSEN, P., HUSS, A. & VERMEULEN, R. 2012. Is pesticide use related to Parkinson disease? Some clues to heterogeneity in study results. *Environmental health perspectives*, 120, 340-347.
- MARTIN, M., REHANI, K., JOPE, R. S. & MICHALEK, S. M. 2005. Toll-like receptor-mediated cytokine production is differentially regulated by glycogen synthase kinase 3. *Nature immunology*, 6, 777.
- MARTINOT, E., SEDÈS, L., BAPTISSART, M., LOBACCARO, J.-M., CAIRA, F., BEAUDOIN, C. & VOLLE, D. H. 2017. Bile acids and their receptors. *Molecular Aspects of Medicine*.
- MARTINS, R., LITHGOW, G. J. & LINK, W. J. A. C. 2016. Long live FOXO: unraveling the role of FOXO proteins in aging and longevity. 15, 196-207.
- MASTROENI, D., GROVER, A., LEONARD, B., JOYCE, J. N., COLEMAN, P. D., KOZIK, B., BELLINGER, D. L. & ROGERS, J. 2009. Microglial responses to dopamine in a cell culture model of Parkinson's disease. *Neurobiology of aging*, 30, 1805-1817.
- MATA, I. F., SHI, M., AGARWAL, P., CHUNG, K. A., EDWARDS, K. L., FACTOR, S. A., GALASKO, D. R., GINGHINA, C., GRIFFITH, A. & HIGGINS, D. S. 2010. SNCA variant associated with Parkinson disease and plasma α -synuclein level. *Archives of neurology*, 67, 1350-1356.
- MAYR, J. A., ZIMMERMANN, F. A., FAUTH, C., BERGHEIM, C., MEIERHOFER, D., RADMAYR, D., ZSCHOCKE, J., KOCH, J. & SPERL, W. 2011. Lipoic acid synthetase deficiency causes neonatal-onset epilepsy, defective mitochondrial energy metabolism, and glycine elevation. *The American Journal of Human Genetics*, 89, 792-797.
- MCCOY, M. K., KAGANOVICH, A., RUDENKO, I. N., DING, J. & COOKSON, M. R. J. H. M. G. 2013. Hexokinase activity is required for recruitment of parkin to depolarized mitochondria. 23, 145-156.
- MCMILLIN, M. & DEMORROW, S. 2016a. Effects of bile acids on neurological function and disease. *The FASEB Journal*, fj. 201600275R.

- MCMILLIN, M. & DEMORROW, S. 2016b. Effects of bile acids on neurological function and disease. *The FASEB Journal*, 30, 3658-3668.
- MCWILLIAMS, T. G., PRESCOTT, A. R., MONTAVA-GARRIGA, L., BALL, G., SINGH, F., BARINI, E., MUQIT, M. M., BROOKS, S. P. & GANLEY, I. G. 2018. Basal Mitophagy Occurs Independently of PINK1 in Mouse Tissues of High Metabolic Demand. *Cell metabolism*.
- MEAD, R. J., HIGGINBOTTOM, A., ALLEN, S. P., KIRBY, J., BENNETT, E., BARBER, S. C., HEATH, P. R., COLUCCIA, A., PATEL, N. & GARDNER, I. 2013. S [+] Apomorphine is a CNS penetrating activator of the Nrf2-ARE pathway with activity in mouse and patient fibroblast models of amyotrophic lateral sclerosis. *Free Radical Biology and Medicine*, 61, 438-452.
- MERTENS, J., MARCHETTO, M. C., BARDY, C. & GAGE, F. H. 2016. Evaluating cell reprogramming, differentiation and conversion technologies in neuroscience. *Nature Reviews Neuroscience*, 17, 424.
- MERTENS, J., PAQUOLA, A. C., KU, M., HATCH, E., BÖHNKE, L., LADJEVARDI, S., MCGRATH, S., CAMPBELL, B., LEE, H. & HERDY, J. R. 2015. Directly reprogrammed human neurons retain aging-associated transcriptomic signatures and reveal age-related nucleocytoplasmic defects. *Cell stem cell*, 17, 705-718.
- MILLET, A., BERTHOLET, A. M., DALOYAU, M., REYNIER, P., GALINIER, A., DEVIN, A., WISSINGUER, B., BELENGUER, P. & DAVEZAC, N. 2016. Loss of functional OPA1 unbalances redox state: implications in dominant optic atrophy pathogenesis. *Annals of clinical and translational neurology*, 3, 408-421.
- MISHRA, P. & CHAN, D. C. 2016. Metabolic regulation of mitochondrial dynamics. *J Cell Biol*, jcb.201511036.
- MOISAN, F., SPINOSI, J., DUPUPET, J. L., DELABRE, L., MAZURIE, J. L., GOLDBERG, M., IMBERNON, E., TZOURIO, C. & ELBAZ, A. 2011. The relation between type of farming and prevalence of Parkinson's disease among agricultural workers in five French districts. *Movement disorders*, 26, 271-279.
- MOREIRA, S., FONSECA, I., NUNES, M. J., ROSA, A., LEMOS, L., RODRIGUES, E., CARVALHO, A. N., OUTEIRO, T. F., RODRIGUES, C. M. P. & GAMA, M. J. 2017. Nrf2 activation by tauroursodeoxycholic acid in experimental models of Parkinson's disease. *Experimental neurology*, 295, 77-87.
- MORTIBOYS, H., AASLY, J. & BANDMANN, O. 2013. Ursocholic acid rescues mitochondrial function in common forms of familial Parkinson's disease. *Brain*, 136, 3038-3050.
- MORTIBOYS, H., FURMSTON, R., BRONSTAD, G., AASLY, J., ELLIOTT, C. & BANDMANN, O. 2015. UDCA exerts beneficial effect on mitochondrial dysfunction in LRRK2G2019S carriers and in vivo. *Neurology*, 85, 846-852.
- MORTIBOYS, H., JOHANSEN, K. K., AASLY, J. O. & BANDMANN, O. 2010. Mitochondrial impairment in patients with Parkinson disease with the G2019S mutation in LRRK2. *Neurology*, 75, 2017-2020.
- MORTIBOYS, H., THOMAS, K. J., KOOPMAN, W. J., KLAFFKE, S., ABOU-SLEIMAN, P., OLPIN, S., WOOD, N. W., WILLEMS, P. H., SMEITINK, J. A. & COOKSON, M. R. 2008. Mitochondrial function and morphology are impaired in parkin-mutant fibroblasts. *Annals of neurology*, 64, 555-565.
- MUSTI, A. M., TREIER, M. & BOHMANN, D. 1997. Reduced ubiquitin-dependent degradation of c-Jun after phosphorylation by MAP kinases. *Science*, 275, 400-402.
- MYTILINEOU, C., WERNER, P., MOLINARI, S., DI ROCCO, A., COHEN, G. & YAHR, M. 1994. Impaired oxidative decarboxylation of pyruvate in fibroblasts from patients with Parkinson's disease. *Journal of Neural Transmission-Parkinson's Disease and Dementia Section*, 8, 223-228.
- NAKASO, K., YANO, H., FUKUHARA, Y., TAKESHIMA, T., WADA-ISOE, K. & NAKASHIMA, K. 2003. PI3K is a key molecule in the Nrf2-mediated regulation of antioxidative proteins by hemin in human neuroblastoma cells. *FEBS letters*, 546, 181-184.
- NALLS, M. A., PANKRATZ, N., LILL, C. M., DO, C. B., HERNANDEZ, D. G., SAAD, M., DESTEFANO, A. L., KARA, E., BRAS, J. & SHARMA, M. 2014. Large-scale meta-analysis of genome-wide association data identifies six new risk loci for Parkinson's disease. *Nature genetics*, 46, 989.
- NAVARRO, A. & BOVERIS, A. 2010. Brain mitochondrial dysfunction in aging, neurodegeneration, and Parkinson's disease. *Frontiers in aging neuroscience*, 2, 34.

- NIOI, P., NGUYEN, T., SHERRATT, P. J. & PICKETT, C. B. 2005. The carboxy-terminal Neh3 domain of Nrf2 is required for transcriptional activation. *Molecular and cellular biology*, 25, 10895-10906.
- NITULESCU, G. M., MARGINA, D., JUZENAS, P., PENG, Q., OLARU, O. T., SALOUSTROS, E., FENGA, C., SPANDIDOS, D. A., LIBRA, M. & TSATSAKIS, A. M. 2016. Akt inhibitors in cancer treatment: The long journey from drug discovery to clinical use. *International journal of oncology*, 48, 869-885.
- NUMAZAWA, S., ISHIKAWA, M., YOSHIDA, A., TANAKA, S. & YOSHIDA, T. 2003. Atypical protein kinase C mediates activation of NF-E2-related factor 2 in response to oxidative stress. *American Journal of Physiology-Cell Physiology*.
- NUNNARI, J. & SUOMALAINEN, A. 2012. Mitochondria: in sickness and in health. *Cell*, 148, 1145-1159.
- OAKLEY, R. H. & CIDLOWSKI, J. A. 2013. The biology of the glucocorticoid receptor: new signaling mechanisms in health and disease. *Journal of Allergy and Clinical Immunology*, 132, 1033-1044.
- OKADA, K., SHODA, J., TAGUCHI, K., MAHER, J. M., ISHIZAKI, K., INOUE, Y., OHTSUKI, M., GOTO, N., TAKEDA, K. & UTSUNOMIYA, H. 2008. Ursodeoxycholic acid stimulates Nrf2-mediated hepatocellular transport, detoxification, and antioxidative stress systems in mice. *American Journal of Physiology-Gastrointestinal and Liver Physiology*, 295, G735-G747.
- ORHAN, H., GURER-ORHAN, H., VRIESE, E., VERMEULEN, N. & MEERMAN, J. 2006. Application of lipid peroxidation and protein oxidation biomarkers for oxidative damage in mammalian cells. A comparison with two fluorescent probes. *Toxicology in vitro*, 20, 1005-1013.
- ORRENIUS, S. 2007. Reactive oxygen species in mitochondria-mediated cell death. *Drug metabolism reviews*, 39, 443-455.
- OZELIUS, L. J., SENTHIL, G., SAUNDERS-PULLMAN, R., OHMANN, E., DELIGTISCH, A., TAGLIATI, M., HUNT, A. L., KLEIN, C., HENICK, B. & HAILPERN, S. M. 2006. LRRK2 G2019S as a cause of Parkinson's disease in Ashkenazi Jews. *New England Journal of Medicine*, 354, 424-425.
- PACELLI, C., DE RASMO, D., SIGNORILE, A., GRATAGLIANO, I., DI TULLIO, G., D'ORAZIO, A., NICO, B., COMI, G. P., RONCHI, D. & FERRANINI, E. 2011. Mitochondrial defect and PGC-1 α dysfunction in parkin-associated familial Parkinson's disease. *Biochimica et Biophysica Acta (BBA)-Molecular Basis of Disease*, 1812, 1041-1053.
- PAISAN-RUIZ, C., BHATIA, K. P., LI, A., HERNANDEZ, D., DAVIS, M., WOOD, N. W., HARDY, J., HOULDEN, H., SINGLETON, A. & SCHNEIDER, S. A. 2009. Characterization of PLA2G6 as a locus for dystonia-parkinsonism. *Annals of neurology*, 65, 19-23.
- PAISÁN-RUÍZ, C., JAIN, S., EVANS, E. W., GILKS, W. P., SIMÓN, J., VAN DER BRUG, M., DE MUNAIN, A. L., APARICIO, S., GIL, A. M. N. & KHAN, N. 2004. Cloning of the gene containing mutations that cause PARK8-linked Parkinson's disease. *Neuron*, 44, 595-600.
- PALACINO, J. J., SAGI, D., GOLDBERG, M. S., KRAUSS, S., MOTZ, C., WACKER, M., KLOSE, J. & SHEN, J. 2004. Mitochondrial dysfunction and oxidative damage in parkin-deficient mice. *Journal of Biological Chemistry*, 279, 18614-18622.
- PALIKARAS, K. & TAVERNARAKIS, N. 2014. Mitochondrial homeostasis: the interplay between mitophagy and mitochondrial biogenesis. *Experimental gerontology*, 56, 182-188.
- PANKRATZ, N., NICHOLS, W. C., UNIACKE, S. K., HALTER, C., MURRELL, J., RUDOLPH, A., SHULTS, C. W., CONNEALLY, P. M. & FOROUD, T. 2003a. Genome-wide linkage analysis and evidence of gene-by-gene interactions in a sample of 362 multiplex Parkinson disease families. *Human molecular genetics*, 12, 2599-2608.
- PANKRATZ, N., NICHOLS, W. C., UNIACKE, S. K., HALTER, C., RUDOLPH, A., SHULTS, C., CONNEALLY, P. M., FOROUD, T. & GROUP, P. S. 2003b. Significant linkage of Parkinson disease to chromosome 2q36-37. *The American Journal of Human Genetics*, 72, 1053-1057.
- PAPKOVSKAIA, T. D., CHAU, K.-Y., INESTA-VAQUERA, F., PAPKOVSKY, D. B., HEALY, D. G., NISHIO, K., STADDON, J., DUCHEN, M. R., HARDY, J. & SCHAPIRA, A. H. 2012. G2019S leucine-rich repeat kinase 2 causes uncoupling protein-mediated mitochondrial depolarization. *Human molecular genetics*, 21, 4201-4213.
- PARK, D., LEE, M. N., JEONG, H., KOH, A., YANG, Y. R., SUH, P.-G. & RYU, S. H. J. C. S. 2014. Parkin ubiquitinates mTOR to regulate mTORC1 activity under mitochondrial stress. 26, 2122-2130.
- PARK, J.-W., CHOI, J.-Y., HONG, S. A., KIM, N. Y., DO, K.-T., SONG, K.-D. & CHO, B.-W. 2017. Exercise induced upregulation of glutamate-cysteine ligase catalytic subunit and glutamate-cysteine ligase modifier

- subunit gene expression in Thoroughbred horses. *Asian-Australasian journal of animal sciences*, 30, 728.
- PARRY, G. J., RODRIGUES, C. M., ARANHA, M. M., HILBERT, S. J., DAVEY, C., KELKAR, P., LOW, W. C. & STEER, C. J. 2010. Safety, tolerability, and cerebrospinal fluid penetration of ursodeoxycholic acid in patients with amyotrophic lateral sclerosis. *Clinical neuropharmacology*, 33, 17-21.
- PASTORINO, J. G. & HOEK, J. B. J. O. B. A. B. 2008. Regulation of hexokinase binding to VDAC. 40, 171-182.
- PENG, K., TAO, Y., ZHANG, J., WANG, J., YE, F., DAN, G., ZHAO, Y., CAI, Y., ZHAO, J. & WU, Q. 2016. Resveratrol regulates mitochondrial biogenesis and fission/fusion to attenuate rotenone-induced neurotoxicity. *Oxidative medicine and cellular longevity*, 2016.
- PEREZ, M. J. & BRIZ, O. 2009. Bile-acid-induced cell injury and protection. *World journal of gastroenterology: WJG*, 15, 1677.
- PEREZ, M. J., VELASCO, E., MONTE, M. J., GONZALEZ-BUITRAGO, J. M. & MARIN, J. J. 2006. Maternal ethanol consumption during pregnancy enhances bile acid-induced oxidative stress and apoptosis in fetal rat liver. *Toxicology*, 225, 183-194.
- PERKINS, G. & FREY, T. 2000. Recent structural insight into mitochondria gained by microscopy. *Micron*, 31, 97-111.
- PI, J., BAI, Y., REECE, J. M., WILLIAMS, J., LIU, D., FREEMAN, M. L., FAHL, W. E., SHUGAR, D., LIU, J. & QU, W. 2007. Molecular mechanism of human Nrf2 activation and degradation: role of sequential phosphorylation by protein kinase CK2. *Free Radical Biology and Medicine*, 42, 1797-1806.
- PIRAS, S., FURFARO, A. L., BRONDOLO, L., PASSALACQUA, M., MARINARI, U. M., PRONZATO, M. A. & NITTI, M. 2017. Differentiation impairs Bach1 dependent HO-1 activation and increases sensitivity to oxidative stress in SH-SY5Y neuroblastoma cells. *Scientific reports*, 7, 7568.
- PLOUMI, C., DASKALAKI, I. & TAVERNARAKIS, N. 2017. Mitochondrial biogenesis and clearance: a balancing act. *The FEBS journal*, 284, 183-195.
- POEWE, W., SEPPI, K., TANNER, C. M., HALLIDAY, G. M., BRUNDIN, P., VOLKMANN, J., SCHRAG, A.-E. & LANG, A. E. 2017. Parkinson disease. *Nature reviews Disease primers*, 3, 17013.
- POLYMERPOULOS, M. H., LAVEDAN, C., LEROY, E., IDE, S. E., DEHEJIA, A., DUTRA, A., PIKE, B., ROOT, H., RUBENSTEIN, J. & BOYER, R. 1997. Mutation in the α -synuclein gene identified in families with Parkinson's disease. *science*, 276, 2045-2047.
- PONT-SUNYER, C., HOTTER, A., GAIG, C., SEPPI, K., COMPTA, Y., KATZENSCHLAGER, R., MAS, N., HOFENEDER, D., BRÜCKE, T. & BAYÉS, A. 2015. The onset of nonmotor symptoms in Parkinson's disease (the ONSET PD study). *Movement Disorders*, 30, 229-237.
- POPOVA, D., KARLSSON, J. & JACOBSSON, S. O. 2017. Comparison of neurons derived from mouse P19, rat PC12 and human SH-SY5Y cells in the assessment of chemical-and toxin-induced neurotoxicity. *BMC Pharmacology and Toxicology*, 18, 42.
- POULAIN, F. E. & SOBEL, A. 2010. The microtubule network and neuronal morphogenesis: Dynamic and coordinated orchestration through multiple players. *Molecular and Cellular Neuroscience*, 43, 15-32.
- POUPON, R. 2012. Ursodeoxycholic acid and bile-acid mimetics as therapeutic agents for cholestatic liver diseases: an overview of their mechanisms of action. *Clinics and research in hepatology and gastroenterology*, 36, S3-S12.
- PRASAI, K. 2017. Regulation of mitochondrial structure and function by protein import: a current review. *Pathophysiology*, 24, 107-122.
- PRINGSHEIM, T., JETTE, N., FROLKIS, A. & STEEVES, T. D. 2014. The prevalence of Parkinson's disease: A systematic review and meta-analysis. *Movement Disorders*, 29, 1583-1590.
- PUSPITA, L., CHUNG, S. Y. & SHIM, J.-W. 2017. Oxidative stress and cellular pathologies in Parkinson's disease. *Molecular brain*, 10, 53.
- PÅHLMAN, S., RUUSALA, A.-I., ABRAHAMSSON, L., MATTSSON, M. E. & ESSCHER, T. 1984. Retinoic acid-induced differentiation of cultured human neuroblastoma cells: a comparison with phorbol ester-induced differentiation. *Cell differentiation*, 14, 135-144.
- QUIRÓS, P. M., LANGER, T. & LÓPEZ-OTÍN, C. 2015. New roles for mitochondrial proteases in health, ageing and disease. *Nature reviews Molecular cell biology*, 16, 345.

- RAEFSKY, S. M. & MATTSON, M. P. 2017. Adaptive responses of neuronal mitochondria to bioenergetic challenges: roles in neuroplasticity and disease resistance. *Free Radical Biology and Medicine*, 102, 203-216.
- RAMIREZ, A., HEIMBACH, A., GRÜNDEMANN, J., STILLER, B., HAMPSHIRE, D., CID, L. P., GOEBEL, I., MUBAIDIN, A. F., WRIEKAT, A.-L. & ROEPER, J. 2006. Hereditary parkinsonism with dementia is caused by mutations in ATP13A2, encoding a lysosomal type 5 P-type ATPase. *Nature genetics*, 38, 1184.
- RAMSAY, R. & SINGER, T. 1986. Energy-dependent uptake of N-methyl-4-phenylpyridinium, the neurotoxic metabolite of 1-methyl-4-phenyl-1, 2, 3, 6-tetrahydropyridine, by mitochondria. *Journal of Biological Chemistry*, 261, 7585-7587.
- RECASENS, A., DEHAY, B., BOVÉ, J., CARBALLO-CARBAJAL, I., DOVERO, S., PÉREZ-VILLALBA, A., FERNAGUT, P. O., BLESA, J., PARENT, A. & PERIER, C. 2014. Lewy body extracts from Parkinson disease brains trigger α -synuclein pathology and neurodegeneration in mice and monkeys. *Annals of neurology*, 75, 351-362.
- REN, X., CHEN, L., XIE, J., ZHANG, Z., DONG, G., LIANG, J., LIU, L., ZHOU, H. & LUO, P. 2017. Resveratrol Ameliorates Mitochondrial Elongation via Drp1/Parkin/PINK1 Signaling in Senescent-Like Cardiomyocytes. *Oxidative medicine and cellular longevity*, 2017.
- RIEKER, C., ENGBLOM, D., KREINER, G., DOMANSKYI, A., SCHOBER, A., STOTZ, S., NEUMANN, M., YUAN, X., GRUMMT, I. & SCHÜTZ, G. 2011. Nucleolar disruption in dopaminergic neurons leads to oxidative damage and parkinsonism through repression of mammalian target of rapamycin signaling. *Journal of Neuroscience*, 31, 453-460.
- RISSO, G., BLAUSTEIN, M., POZZI, B., MAMMI, P. & SREBROW, A. 2015. Akt/PKB: one kinase, many modifications. *Biochemical Journal*, 468, 203-214.
- ROBERTS, D. & MIYAMOTO, S. J. C. D. A. D. 2015. Hexokinase II integrates energy metabolism and cellular protection: Akt acting on mitochondria and TORCing to autophagy. 22, 248.
- ROBERTS, D. J., TAN-SAH, V. P., SMITH, J. M. & MIYAMOTO, S. J. J. O. B. C. 2013. Akt phosphorylates HK-II at Thr473 and increases mitochondrial HK-II association to protect cardiomyocytes. *jbc*. M113. 482026.
- ROBEY, R. A. & HAY, N. J. O. 2006. Mitochondrial hexokinases, novel mediators of the antiapoptotic effects of growth factors and Akt. 25, 4683.
- RODRIGUEZ, M., RODRIGUEZ-SABATE, C., MORALES, I., SANCHEZ, A. & SABATE, M. 2015. Parkinson's disease as a result of aging. *Aging cell*, 14, 293-308.
- ROHAN, M., FAIRWEATHER, A. & GRAINGER, N. 2015. Using gamma distribution to determine half-life of rotenone, applied in freshwater. *Science of the Total Environment*, 527, 246-251.
- ROSA, A. I., DUARTE-SILVA, S., SILVA-FERNANDES, A., NUNES, M. J., CARVALHO, A. N., RODRIGUES, E., GAMA, M. J., RODRIGUES, C. M. P., MACIEL, P. & CASTRO-CALDAS, M. 2018. Tauroursodeoxycholic Acid Improves Motor Symptoms in a Mouse Model of Parkinson's Disease. *Molecular neurobiology*, 1-17.
- ROSA, A. I., FONSECA, I., NUNES, M. J., MOREIRA, S., RODRIGUES, E., CARVALHO, A. N., RODRIGUES, C. M., GAMA, M. J. & CASTRO-CALDAS, M. 2017. Novel insights into the antioxidant role of tauroursodeoxycholic acid in experimental models of Parkinson's disease. *Biochimica et Biophysica Acta (BBA)-Molecular Basis of Disease*, 1863, 2171-2181.
- ROSS, R. A. & BIEDLER, J. L. 1985. Presence and regulation of tyrosinase activity in human neuroblastoma cell variants in vitro. *Cancer research*, 45, 1628-1632.
- ROSTOVTSEVA, T. K., GURNEV, P. A., PROTCHENKO, O., HOOGERHEIDE, D. P., YAP, T. L., PHILPOTT, C. C., LEE, J. C. & BEZRUKOV, S. M. 2015. α -Synuclein shows high affinity interaction with voltage-dependent anion channel, suggesting mechanisms of mitochondrial regulation and toxicity in Parkinson disease. *Journal of Biological Chemistry*, 290, 18467-18477.
- RYU, M. J., KANG, K. A., PIAO, M. J., KIM, K. C., ZHENG, J., YAO, C. W., CHA, J. W., CHUNG, H. S., KIM, S. C. & JUNG, E. 2014. 7, 8-Dihydroxyflavone protects human keratinocytes against oxidative stress-induced cell damage via the ERK and PI3K/Akt-mediated Nrf2/HO-1 signaling pathways. *International journal of molecular medicine*, 33, 964-970.

- RÜB, C., WILKENING, A. & VOOS, W. 2017. Mitochondrial quality control by the Pink1/Parkin system. *Cell and tissue research*, 367, 111-123.
- SAKAMOTO, K., KARELINA, K. & OBRIETAN, K. J. J. O. N. 2011. CREB: a multifaceted regulator of neuronal plasticity and protection. 116, 1-9.
- SAMARASINGHE, R. A., WITCHELL, S. F. & DEFRANCO, D. B. 2012. Cooperativity and complementarity: synergies in non-classical and classical glucocorticoid signaling. *Cell Cycle*, 11, 2819-2827.
- SAMPATH, D., MALIK, A., PLUNKETT, W., NOWAK, B., WILLIAMS, B., BURTON, M., VERSTOVSEK, S., FADERL, S., GARCIA-MANERO, G. & LIST, A. F. 2013. Phase I clinical, pharmacokinetic, and pharmacodynamic study of the Akt-inhibitor triciribine phosphate monohydrate in patients with advanced hematologic malignancies. *Leukemia research*, 37, 1461-1467.
- SAMUELS, R., BAYERRI, C. R., SAYER, J. A., PRICE, D. A. & PAYNE, B. A. 2017. Tenofovir disoproxil fumarate-associated renal tubular dysfunction: noninvasive assessment of mitochondrial injury. *AIDS (London, England)*, 31, 1297.
- SARKAR, A., YE, A. & SINGH, H. 2016. On the role of bile salts in the digestion of emulsified lipids. *Food Hydrocolloids*, 60, 77-84.
- SARRAF, S. A., RAMAN, M., GUARANI-PEREIRA, V., SOWA, M. E., HUTTLIN, E. L., GYGI, S. P. & HARPER, J. W. 2013. Landscape of the PARKIN-dependent ubiquitylome in response to mitochondrial depolarization. *Nature*, 496, 372-376.
- SATAKE, W., NAKABAYASHI, Y., MIZUTA, I., HIROTA, Y., ITO, C., KUBO, M., KAWAGUCHI, T., TSUNODA, T., WATANABE, M. & TAKEDA, A. 2009. Genome-wide association study identifies common variants at four loci as genetic risk factors for Parkinson's disease. *Nature genetics*, 41, 1303-1307.
- SAXTON, R. A. & SABATINI, D. M. J. C. 2017. mTOR signaling in growth, metabolism, and disease. 168, 960-976.
- SCARPULLA, R. C., VEGA, R. B. & KELLY, D. P. 2012. Transcriptional integration of mitochondrial biogenesis. *Trends in Endocrinology & Metabolism*, 23, 459-466.
- SCHAPIRA, A., COOPER, J., DEXTER, D., CLARK, J., JENNER, P. & MARSDEN, C. 1990. Mitochondrial complex I deficiency in Parkinson's disease. *Journal of neurochemistry*, 54, 823-827.
- SCHAPIRA, A. H., CHAUDHURI, K. R. & JENNER, P. 2017. Non-motor features of Parkinson disease. *Nature Reviews Neuroscience*, 18, 435.
- SCHEIBER, I. F., MERCER, J. F. & DRINGEN, R. 2014. Metabolism and functions of copper in brain. *Progress in neurobiology*, 116, 33-57.
- SCHIEBER, M. & CHANDEL, N. S. 2014. ROS function in redox signaling and oxidative stress. *Current Biology*, 24, R453-R462.
- SCHÜLE, B., PERA, R. A. R. & LANGSTON, J. W. 2009. Can cellular models revolutionize drug discovery in Parkinson's disease? *Biochimica et Biophysica Acta (BBA)-Molecular Basis of Disease*, 1792, 1043-1051.
- SENA, L. A. & CHANDEL, N. S. 2012. Physiological roles of mitochondrial reactive oxygen species. *Molecular cell*, 48, 158-167.
- SGARBI, G., LIUZZI, F., BARACCA, A. & SOLAINI, G. 2018. Resveratrol preserves mitochondrial function in a human post-mitotic cell model. *The Journal of nutritional biochemistry*, 62, 9-17.
- SHAULIAN, E. & KARIN, M. 2001. AP-1 in cell proliferation and survival. *Oncogene*, 20, 2390.
- SHEN, X., WANG, W., LIU, Y., LEI, L., WU, H., XU, S., FENG, S.-W. & WANG, F. 2016. Receptor Accessory Proteins and Glucocorticoid Receptor Activation.
- SHIN, J.-H., KO, H. S., KANG, H., LEE, Y., LEE, Y.-I., PLETINKOVA, O., TROCONSO, J. C., DAWSON, V. L. & DAWSON, T. M. 2011. PARIS (ZNF746) repression of PGC-1 α contributes to neurodegeneration in Parkinson's disease. *Cell*, 144, 689-702.
- SHIN, S. M., YANG, J. H. & KI, S. H. 2013. Role of the Nrf2-ARE pathway in liver diseases. *Oxidative medicine and cellular longevity*, 2013.
- SHIPLEY, M. M., MANGOLD, C. A. & SZPARA, M. L. 2016. Differentiation of the SH-SY5Y human neuroblastoma cell line. *Journal of visualized experiments: JoVE*, 53193.
- SHULMAN, J. M., DE JAGER, P. L. & FEANY, M. B. 2011. Parkinson's disease: genetics and pathogenesis. *Annual Review of Pathology: Mechanisms of Disease*, 6, 193-222.

- SIDRANSKY, E., NALLS, M. A., AASLY, J. O., AHARON-PERETZ, J., ANNESI, G., BARBOSA, E. R., BAR-SHIRA, A., BERG, D., BRAS, J. & BRICE, A. 2009. Multicenter analysis of glucocerebrosidase mutations in Parkinson's disease. *New England Journal of Medicine*, 361, 1651-1661.
- SILVERS, A. L., BACHELOR, M. A. & BOWDEN, G. T. 2003. The role of JNK and p38 MAPK activities in UVA-induced signaling pathways leading to AP-1 activation and c-Fos expression. *Neoplasia*, 5, 319-329.
- SINGLETON, A., FARRER, M., JOHNSON, J., SINGLETON, A., HAGUE, S., KACHERGUS, J., HULIHAN, M., PEURALINNA, T., DUTRA, A. & NUSSBAUM, R. 2003. α -Synuclein locus triplication causes Parkinson's disease. *Science*, 302, 841-841.
- SOHN, Y., GANJU, N. & WANDS, J. 1998. P53-and CD95-associated apoptosis in neurodegenerative diseases. *Laboratory investigation; a journal of technical methods and pathology*, 78, 401-411.
- SOMMERFELD, A., REINEHR, R. & HÄUSSINGER, D. 2015. Tauroursodeoxycholate protects rat hepatocytes from bile acid-induced apoptosis via β 1-integrin-and protein kinase A-dependent mechanisms. *Cellular Physiology and Biochemistry*, 36, 866-883.
- SONG, G., OUYANG, G. & BAO, S. 2005. The activation of Akt/PKB signaling pathway and cell survival. *Journal of cellular and molecular medicine*, 9, 59-71.
- SONG, P. & ZOU, M. H. 2015. Roles of reactive oxygen species in physiology and pathology. *Atherosclerosis: Risks, Mechanisms, and Therapies*, 379-392.
- SOUSA, T., COUTINHO, A., BANERJEE, S., CASTRO, R., YOULE, R., RODRIGUES, C., PRIETO, M. & FERNANDES, F. 2015. Binding of Pro-Apoptotic Protein Bax to Cytoprotective UDCA and TUDCA. *Biophysical Journal*, 108, 608a-609a.
- SPATARO, N., CALAFELL, F., CERVERA-CARLES, L., CASALS, F., PAGONABARRAGA, J., PASCUAL-SEDANO, B., CAMPOLONGO, A., KULISEVSKY, J., LLEÓ, A. & NAVARRO, A. 2015. Mendelian genes for Parkinson's disease contribute to the sporadic forms of the disease. *Human molecular genetics*, 24, 2023-2034.
- SPRENGER, A., KÜTTNER, V., BINIOSSEK, M. L., GRETZMEIER, C., BOERRIES, M., MACK, C., HAS, C., BRUCKNER-TUDERMAN, L. & DENGJEL, J. 2010. Comparative quantitation of proteome alterations induced by aging or immortalization in primary human fibroblasts and keratinocytes for clinical applications. *Molecular BioSystems*, 6, 1579-1582.
- STAAL, S. P. 1987. Molecular cloning of the akt oncogene and its human homologues AKT1 and AKT2: amplification of AKT1 in a primary human gastric adenocarcinoma. *Proceedings of the National Academy of Sciences*, 84, 5034-5037.
- STARK, A. & PAKKENBERG, B. 2004. Histological changes of the dopaminergic nigrostriatal system in aging. *Cell and tissue research*, 318, 81-92.
- STEVENS, D. A., LEE, Y., KANG, H. C., LEE, B. D., LEE, Y.-I., BOWER, A., JIANG, H., KANG, S.-U., ANDRABI, S. A. & DAWSON, V. L. 2015. Parkin loss leads to PARIS-dependent declines in mitochondrial mass and respiration. *Proceedings of the National Academy of Sciences*, 112, 11696-11701.
- STEWART, J. B. & CHINNERY, P. F. 2015. The dynamics of mitochondrial DNA heteroplasmy: implications for human health and disease. *Nature Reviews Genetics*, 16, 530-542.
- STORZ, P. J. A. & SIGNALING, R. 2011. Forkhead homeobox type O transcription factors in the responses to oxidative stress. 14, 593-605.
- STOTT, S. R., METZAKOPIAN, E., LIN, W., KAESTNER, K. H., HEN, R. & ANG, S.-L. 2013. Foxa1 and foxa2 are required for the maintenance of dopaminergic properties in ventral midbrain neurons at late embryonic stages. *Journal of Neuroscience*, 33, 8022-8034.
- STRAUSS, K. M., MARTINS, L. M., PLUN-FAVREAU, H., MARX, F. P., KAUTZMANN, S., BERG, D., GASSER, T., WSZOLEK, Z., MÜLLER, T. & BORNEMANN, A. 2005. Loss of function mutations in the gene encoding Omi/HtrA2 in Parkinson's disease. *Human molecular genetics*, 14, 2099-2111.
- SU, Y.-C. & QI, X. 2013. Inhibition of excessive mitochondrial fission reduced aberrant autophagy and neuronal damage caused by LRRK2 G2019S mutation. *Human molecular genetics*, 22, 4545-4561.
- SUN, Z., HUANG, Z. & ZHANG, D. D. 2009. Phosphorylation of Nrf2 at multiple sites by MAP kinases has a limited contribution in modulating the Nrf2-dependent antioxidant response. *PloS one*, 4, e5888.
- SUTHERLAND, C. J. I. J. O. A. S. D. 2011. What are the bona fide GSK3 substrates? 2011.

- SUZUKI, T. & YAMAMOTO, M. 2015. Molecular basis of the Keap1–Nrf2 system. *Free Radical Biology and Medicine*, 88, 93-100.
- TAGUCHI, K., MOTOHASHI, H. & YAMAMOTO, M. 2011. Molecular mechanisms of the Keap1–Nrf2 pathway in stress response and cancer evolution. *Genes to cells*, 16, 123-140.
- TAI, H.-C. & SCHUMAN, E. M. 2008. Ubiquitin, the proteasome and protein degradation in neuronal function and dysfunction. *Nature Reviews Neuroscience*, 9, 826.
- TAIT, S. W., ICHIM, G. & GREEN, D. R. 2014. Die another way–non-apoptotic mechanisms of cell death. *J Cell Sci*, 127, 2135-2144.
- TANAKA, H., MAKINO, Y., MIURA, T., HIRANO, F., OKAMOTO, K., KOMURA, K., SATO, Y. & MAKINO, I. 1996. Ligand-independent activation of the glucocorticoid receptor by ursodeoxycholic acid. Repression of IFN-gamma-induced MHC class II gene expression via a glucocorticoid receptor-dependent pathway. *The Journal of Immunology*, 156, 1601-1608.
- TEBAY, L. E., ROBERTSON, H., DURANT, S. T., VITALE, S. R., PENNING, T. M., DINKOVA-KOSTOVA, A. T. & HAYES, J. D. 2015. Mechanisms of activation of the transcription factor Nrf2 by redox stressors, nutrient cues, and energy status and the pathways through which it attenuates degenerative disease. *Free Radical Biology and Medicine*, 88, 108-146.
- TESTA, J. R. & TSICHLIS, P. N. 2005. AKT signaling in normal and malignant cells. *Oncogene*, 24, 7391-7393.
- THACKER, E., O'REILLY, E., WEISSKOPF, M., CHEN, H., SCHWARZSCHILD, M., MCCULLOUGH, M., CALLE, E., THUN, M. & ASCHERIO, A. 2007. Temporal relationship between cigarette smoking and risk of Parkinson disease. *Neurology*, 68, 764-768.
- THOMSON, D. M., HERWAY, S. T., FILLMORE, N., KIM, H., BROWN, J. D., BARROW, J. R. & WINDER, W. W. J. J. O. A. P. 2008. AMP-activated protein kinase phosphorylates transcription factors of the CREB family. 104, 429-438.
- TODOROVIC, M., WOOD, S. A. & MELLICK, G. D. 2016. Nrf2: a modulator of Parkinson's disease? *Journal of Neural Transmission*, 123, 611-619.
- TOKER, A. & MARMIROLI, S. 2014. Signaling specificity in the Akt pathway in biology and disease. *Advances in biological regulation*, 55, 28-38.
- TUFEKCI, K. U., CIVI BAYIN, E., GENÇ, S. & GENÇ, K. 2011. The Nrf2/ARE pathway: a promising target to counteract mitochondrial dysfunction in Parkinson's disease. *Parkinson's disease*, 2011.
- TYSNES, O.-B. & STORSTEIN, A. 2017. Epidemiology of Parkinson's disease. *Journal of Neural Transmission*, 124, 901-905.
- VALENTE, E. M., ABOU-SLEIMAN, P. M., CAPUTO, V., MUQIT, M. M., HARVEY, K., GISPERT, S., ALI, Z., DEL TURCO, D., BENTIVOGLIO, A. R. & HEALY, D. G. 2004. Hereditary early-onset Parkinson's disease caused by mutations in PINK1. *Science*, 304, 1158-1160.
- VAN DER BLIEK, A. M., SHEN, Q. & KAWAJIRI, S. 2013. Mechanisms of mitochondrial fission and fusion. *Cold Spring Harbor perspectives in biology*, 5, a011072.
- VAN LAAR, V. S., ARNOLD, B., CASSADY, S. J., CHU, C. T., BURTON, E. A. & BERMAN, S. B. 2010. Bioenergetics of neurons inhibit the translocation response of Parkin following rapid mitochondrial depolarization. *Human molecular genetics*, 20, 927-940.
- VAN MEERLOO, J., KASPERS, G. J. & CLOOS, J. 2011. Cell sensitivity assays: the MTT assay. *Cancer cell culture*. Springer.
- VANSTONE, J. R., SMITH, A. M., MCBRIDE, S., NAAS, T., HOLCIK, M., ANTOUN, G., HARPER, M.-E., MICHAUD, J., SELL, E. & CHAKRABORTY, P. 2016. DNMT1-related mitochondrial fission defect presenting as refractory epilepsy. *European Journal of Human Genetics*, 24, 1084.
- VIER, J., GERHARD, M., WAGNER, H. & HÄCKER, G. 2004. Enhancement of death-receptor induced caspase-8-activation in the death-inducing signalling complex by uncoupling of oxidative phosphorylation. *Molecular immunology*, 40, 661-670.
- VILARIÑO-GÜELL, C., RAJPUT, A., MILNERWOOD, A. J., SHAH, B., SZU-TU, C., TRINH, J., YU, I., ENCARNACION, M., MUNSIE, L. N. & TAPIA, L. 2013. DNAJC13 mutations in Parkinson disease. *Human molecular genetics*, 23, 1794-1801.
- WANG, C.-C., CHANG, C.-H., CHANG, S.-C., FAN, G.-J., LIN, M.-J., YU, B. & LEE, T.-T. 2016. In vitro free radicals scavenging activity and antioxidant capacity of solid-state fermented wheat bran and its

- potential modulation of antioxidative molecular targets in chicken PBMC. *Revista Brasileira de Zootecnia*, 45, 451-457.
- WANG, D. Q. & CAREY, M. C. 2014. Therapeutic uses of animal biles in traditional Chinese medicine: an ethnopharmacological, biophysical chemical and medicinal review. *World Journal of Gastroenterology: WJG*, 20, 9952.
- WANG, H., LIU, K., GENG, M., GAO, P., WU, X., HAI, Y., LI, Y., LI, Y., LUO, L. & HAYES, J. D. 2013. RXR α inhibits the NRF2-ARE signaling pathway through a direct interaction with the Neh7 domain of NRF2. *Cancer research*, 73, 3097-3108.
- WANG, L., PIGUET, A. C., SCHMIDT, K., TORDJMANN, T. & DUFOUR, J. F. J. H. 2005. Activation of CREB by tauroursodeoxycholic acid protects cholangiocytes from apoptosis induced by mTOR inhibition. 41, 1241-1251.
- WANG, Q., CHUIKOV, S., TAITANO, S., WU, Q., RASTOGI, A., TUCK, S. J., COREY, J. M., LUNDY, S. K. & MAO-DRAAYER, Y. 2015. Dimethyl fumarate protects neural stem/progenitor cells and neurons from oxidative damage through Nrf2-ERK1/2 MAPK pathway. *International journal of molecular sciences*, 16, 13885-13907.
- WANG, X. & MICHAELIS, E. K. 2010. Selective neuronal vulnerability to oxidative stress in the brain. *Frontiers in aging neuroscience*, 2, 12.
- WATERHAM, H. R., KOSTER, J., VAN ROERMUND, C. W., MOOYER, P. A., WANDERS, R. J. & LEONARD, J. V. 2007. A lethal defect of mitochondrial and peroxisomal fission. *New England Journal of Medicine*, 356, 1736-1741.
- WEN, A. Y., SAKAMOTO, K. M. & MILLER, L. S. J. T. J. O. I. 2010. The role of the transcription factor CREB in immune function. 185, 6413-6419.
- WESTERMANN, B. 2012. Bioenergetic role of mitochondrial fusion and fission. *Biochimica et Biophysica Acta (BBA)-Bioenergetics*, 1817, 1833-1838.
- WICHMANN, T., DELONG, M. R., GURIDI, J. & OBESO, J. A. 2011. Milestones in research on the pathophysiology of Parkinson's disease. *Movement Disorders*, 26, 1032-1041.
- WINNER, B., JAPPELLI, R., MAJI, S. K., DESPLATS, P. A., BOYER, L., AIGNER, S., HETZER, C., LOHER, T., VILAR, M. & CAMPIONI, S. 2011. In vivo demonstration that α -synuclein oligomers are toxic. *Proceedings of the National Academy of Sciences*, 108, 4194-4199.
- WIRDEFELDT, K., WEIBULL, C. E., CHEN, H., KAMEL, F., LUNDHOLM, C., FANG, F. & YE, W. 2013. Parkinson's disease and cancer: a register-based family study. *American journal of epidemiology*, 179, 85-94.
- WU, J., LI, Q., WANG, X., YU, S., LI, L., WU, X., CHEN, Y., ZHAO, J. & ZHAO, Y. 2013. Neuroprotection by curcumin in ischemic brain injury involves the Akt/Nrf2 pathway. *PloS one*, 8, e59843.
- XIANGSHAN, Z., LIXIA, G., HAIYUN, P., DONGHUI, K., MAJESKI, M. & UNTERMAN, T. G. J. B. J. 2004. Multiple elements regulate nuclear/cytoplasmic shuttling of FOXO1: characterization of phosphorylation- and 14-3-3-dependent and-independent mechanisms. 378, 839-849.
- XICOY, H., WIERINGA, B. & MARTENS, G. J. 2017. The SH-SY5Y cell line in Parkinson's disease research: a systematic review. *Molecular neurodegeneration*, 12, 10.
- XIE, Q., KHAOUSTOV, V. I., CHUNG, C. C., SOHN, J., KRISHNAN, B., LEWIS, D. E. & YOFFE, B. 2002. Effect of tauroursodeoxycholic acid on endoplasmic reticulum stress-induced caspase-12 activation. *Hepatology*, 36, 592-601.
- XU, Y., LIU, C., CHEN, S., YE, Y., GUO, M., REN, Q., LIU, L., ZHANG, H., XU, C. & ZHOU, Q. J. C. S. 2014. Activation of AMPK and inactivation of Akt result in suppression of mTOR-mediated S6K1 and 4E-BP1 pathways leading to neuronal cell death in in vitro models of Parkinson's disease. 26, 1680-1689.
- XUN, Z., LEE, D.-Y., LIM, J., CANARIA, C. A., BARNEBEY, A., YANONNE, S. M. & MCMURRAY, C. T. 2012. Retinoic acid-induced differentiation increases the rate of oxygen consumption and enhances the spare respiratory capacity of mitochondria in SH-SY5Y cells. *Mechanisms of ageing and development*, 133, 176-185.
- YANG, J., HERTZ, E., ZHANG, X., LEINARTAITÉ, L., LUNDIUS, E. G., LI, J. & SVENNINGSSON, P. 2016. Overexpression of α -synuclein simultaneously increases glutamate NMDA receptor phosphorylation and reduces glucocerebrosidase activity. *Neuroscience letters*, 611, 51-58.

- YANG, L., DAN, H. C., SUN, M., LIU, Q., SUN, X.-M., FELDMAN, R. I., HAMILTON, A. D., POLOKOFF, M., NICOSIA, S. V. & HERLYN, M. 2004. Akt/protein kinase B signaling inhibitor-2, a selective small molecule inhibitor of Akt signaling with antitumor activity in cancer cells overexpressing Akt. *Cancer research*, 64, 4394-4399.
- YANG, Y., JIANG, S., YAN, J., LI, Y., XIN, Z., LIN, Y. & QU, Y. 2015. An overview of the molecular mechanisms and novel roles of Nrf2 in neurodegenerative disorders. *Cytokine & growth factor reviews*, 26, 47-57.
- YOSHINO, H., NAKAGAWA-HATTORI, Y., KONDO, T. & MIZUNO, Y. 1992. Mitochondrial complex I and II activities of lymphocytes and platelets in Parkinson's disease. *Journal of Neural Transmission-Parkinson's Disease and Dementia Section*, 4, 27-34.
- YOULE, R. J. & VAN DER BLIEK, A. M. 2012. Mitochondrial fission, fusion, and stress. *Science*, 337, 1062-1065.
- ZANELLATI, M. C., MONTI, V., BARZAGHI, C., REALE, C., NARDOCCI, N., ALBANESE, A., VALENTE, E. M., GHEZZI, D. & GARAVAGLIA, B. 2015. Mitochondrial dysfunction in Parkinson disease: evidence in mutant PARK2 fibroblasts. *Frontiers in genetics*, 6.
- ZHANG, H., WANG, W., FANG, H., YANG, Y., LI, X., HE, J., JIANG, X., WANG, W., LIU, S. & HU, J. 2014a. GSK-3 β inhibition attenuates CLP-induced liver injury by reducing inflammation and hepatic cell apoptosis. *Mediators of inflammation*, 2014.
- ZHANG, L., HUANG, L., CHEN, L., HAO, D. & CHEN, J. 2013a. Neuroprotection by tetrahydroxystilbene glucoside in the MPTP mouse model of Parkinson's disease. *Toxicology Letters*, 222, 155-163.
- ZHANG, L. N., SHI, T. Y., SHI, X. H., WANG, L., YANG, Y. J., LIU, B., GAO, L. X., SHUAI, Z. W., KONG, F. & CHEN, H. 2013b. Early biochemical response to ursodeoxycholic acid and long-term prognosis of primary biliary cirrhosis: Results of a 14-year cohort study. *Hepatology*, 58, 264-272.
- ZHANG, T., SU, J., GUO, B., ZHU, T., WANG, K. & LI, X. 2014b. Ursolic acid alleviates early brain injury after experimental subarachnoid hemorrhage by suppressing TLR4-mediated inflammatory pathway. *International immunopharmacology*, 23, 585-591.
- ZHOU, M., LI, Y., HU, Q., BAI, X.-C., HUANG, W., YAN, C., SCHERES, S. H. & SHI, Y. 2015. Atomic structure of the apoptosome: mechanism of cytochrome c-and dATP-mediated activation of Apaf-1. *Genes & development*, 29, 2349-2361.
- ZHU, J., VINOTHKUMAR, K. R. & HIRST, J. 2016. Structure of mammalian respiratory complex I. *Nature*, 536, 354.
- ZIMPRICH, A., BENET-PAGÈS, A., STRUHAL, W., GRAF, E., ECK, S. H., OFFMAN, M. N., HAUBENBERGER, D., SPIELBERGER, S., SCHULTE, E. C. & LICHTNER, P. 2011. A mutation in VPS35, encoding a subunit of the retromer complex, causes late-onset Parkinson disease. *The American Journal of Human Genetics*, 89, 168-175.